Durham University

Durham E-Theses

Perturbed conformal field theory, nonlinear integral equations and spectral problems

Tania Clare Dunning

How to cite:

Dunning, Tania Clare (2000) Perturbed conformal field theory, nonlinear integral equations and spectral problems. Doctoral thesis, Durham University.

Use policy

The full-text may be used and/or reproduced, and given to third parties in any format or medium, without prior permission or charge, for personal research or study, educational, or not-for-profit purposes provided that:

- a full bibliographic reference is made to the original source
- a https://etheses.durham.ac.uk/id/eprint/4329/ is made to the metadata record in Durham E-Theses
- the full-text is not changed in any way

The full-text must not be sold in any format or medium without the formal permission of the copyright holders.

Please consult the full Durham E-Theses policy for further details.

Academic Support Office, The Palatine Centre, Durham University, Stockton Road, Durham, DH1 3LE
e-mail: e-theses.admin@durham.ac.uk Tel: +44 0191 334 6107
https://etheses.durham.ac.uk

Perturbed conformal field theory, nonlinear integral equations and spectral problems

Tania Clare Dunning

The copyright of this thesis rests with the author. No quotation from it should be published in any form, including Electronic and the Internet, without the author's prior written consent. All information derived from this thesis must be acknowledged appropriately.

A thesis presented for the degree of Doctor of Philosophy

Department of Mathematical Sciences
University of Durham

December 2000

13 JUL 2001

Perturbed conformal field theory, nonlinear integral equations and spectral problems

Tania Clare Dunning

This thesis is concerned with various aspects of perturbed conformal field theory and the methods used to calculate finite-size effects of integrable quantum field theories.

Nonlinear integral equations are the main tools to find the exact ground-state energy of a quantum field theory. The thermodyamic Bethe ansatz (TBA) equations are a set of examples and are known for a large number of models. However, it is also an interesting question to find exact equations describing the excited states of integrable models. The first part of this thesis uses analytical continuation in a continuous parameter to find TBA like equations describing the spin-zero excited states of the sine-Gordon model at coupling $\beta^2 = 16\pi/3$. Comparisons are then made with a further type of nonlinear integral equation which also predicts the excited state energies. Relations between the two types of equation are studied using a set of functional relations recently introduced in integrable quantum field theory.

A relevant perturbation of a conformal field theory results in either a massive quantum field theory such as the sine-Gordon model, or a different massless conformal field theory. The second part of this thesis investigates flows between conformal field theories using a nonlinear integral equation. New families of flows are found which exhibit a rather unexpected behaviour.

The final part of this thesis begins with a review of a connection between integrable quantum field theory and properties of certain ordinary differential equations of second- and third-order. The connection is based on functional relations which appear on both sides of the correspondence; for the second-order case these are exactly the functional relations mentioned above. The results are extended to include a correspondence between n^{th} order differential equations and Bethe ansatz system of $SU(n)$ type. A set of nonlinear integral equations are derived to check the results.

Contents

List of Figures

List of Tables

Declaration

This thesis is the result of research carried out by the author between October 1997 and September 2000 in the Department of Mathematical Sciences at the University of Durham. No part of this thesis has been submitted for a degree at this or any other university.

Chapter 1 and Sections 2.0.1,2.1.5,3.1,3.2 and 4.1 all contain necessary background material and no claim of originality is made. The remaining work is believed to be original, unless otherwise stated.

Chapter 2 has been done in collaboration with Patrick Dorey. This, and further work with Gabor Takacs and Francesco Ravanini, will form part of a paper currently in preparation [1]. Chapters 3 and 4 are based on joint work with Patrick Dorey and Roberto Tateo. The results have been published and can be found in [2], [3] and [4].

The copyright of this thesis rests with the author. No quotation from it should be published without their prior written consent and information derived from it should be acknowledged.

Acknowledgements

I wish to thank Patrick Dorey for his patience and encouragement as well as many interesting discussions over the past few years. It all began with my naive question "What's interesting about 1+1 dimensions?"... I'm also grateful to Roberto Tateo for many explanations, discussions and suggestions. Thanks also to Gabor Takacs and Francesco Ravanini.

I thank the Engineering and Physical Sciences Research Council, the Department of Mathematics, Durham and TMR grant ERBFMRXCT960012 for providing financial support and enabling me to attend various schools and conferences. I also thank Saclay, Paris for hospitality during January and February 2000 and the University of Bologna, Italy for hospitality during July 1999. Thanks to Ed Corrigan and the University of York, where the writing up of this thesis was completed.

Thanks to the many members of staff, including the ladies in the office, of the Maths department who have encouraged me throughout the past three years. I'm grateful to my friends in Durham, particularly my office mates without whom I might have drunk less coffee and done more work.

Thanks to my friends outside Durham who keep me sane and remind me that the real world has more dimensions than one of time and one of space. Thank you to Chris, Jean and David for more than you may realise. I am also grateful to my family for their interest, encouragement and puzzlement when I explain what I do!

Finally, I wish to dedicate this thesis to my mom and dad: in appreciation of your continuous support, encouragement and love throughout the last 26 years.

Chapter 1

Introduction

One of the most interesting developments in mathematical physics during the last few decades has been in the study and application of conformal field theory. String theory provides one example, since the fields living on the world sheet swept out by a string are governed by conformal field theory. Another motivation, more relevant to this thesis, comes from statistical mechanics since the critical behaviour of a statistical system at a second order (continuous) phase transition can be described by a conformally invariant theory. We introducesome of the relevant concepts of statistical mechanics in the next section; more details can be found for example in [5].

1.1 Statistical mechanics

One of the most famous examples of a statistical model is the two-dimensional Ising model. The model is defined on a square lattice with lattice spacing a by assigning to each site a spin σ_i taking the value $+1$ or -1. The energy of a given configuration is given by the Hamiltonian

$$H = -J_1 \sum_{\langle ij \rangle} \sigma_i \sigma_j - h \sum_i \sigma_i \tag{1.1}$$

where the sum should be taken over pairs of nearest-neighbour lattice sites, denoted $\langle ij \rangle$. Since we are discussing a theoretical model we may take the lattice to be of infinite size, or think of it as having N^2 sites and then take $N \to \infty$. The coupling J_1 represents the ferromagnetic interaction between neighbouring sites, and h, an external magnetic field which we set equal to zero. The probability of a configuration with energy E_i at temperature T is given by the Boltzmann distribution

$$P_i = \frac{1}{Z} e^{-E_i/k_B T}, \tag{1.2}$$

where k_B is the Boltzmann constant. The normalisation factor Z is known as the partition function and, as we shall see later, it encodes many interesting thermody-

namic quantities. It is given by the sum over all possible configurations

$$Z = \sum_i e^{-E_i/k_B T} \ . \tag{1.3}$$

At zero temperature the spins will align so as to minimise the energy. This is achieved by all of them aligning in the same direction - either up or down depending upon how the external magnetic field was taken to zero. The material is said to be spontaneously magnetised and in the following we assume that all spins initially point in the up direction. When the temperature increases, some of the spins use the additional energy to change direction and small domains appear in which the spins are all pointing down. However, if we consider the overall behaviour of the material we find the dominating spin direction is still upwards, although the value of the spontaneous magnetisation will have decreased. Domains of downward spin exist in all sizes up to some maximum value; this maximum length is known as the correlation length ξ.

As the temperature increases the domains of downward spin, and hence the correlation length, continue to grow. When the temperature reaches its critical temperature T_c the correlation length becomes (theoretically) infinite and the system is in a unique phase with domains of similar spin existing in all sizes, including one infinite size domain. If the temperature is increased further, the correlation length returns to finite values and there are now domains of down spin and also ones of up spin. In contrast to the behaviour at $T < T_c$, we find that overall neither up nor down spin dominates and the material has lost its spontaneous magnetisation. It has gone through a phase transition and the critical point at $T = T_c$ separates the two distinct phases of the material.

The free energy of a statistical model is defined in terms of the partition function as

$$f = -k_B T \lim_{N\to\infty} N^{-1} \ln Z \ , \tag{1.4}$$

whereas the magnetisation, the mean value of a single spin, is given by

$$M = -\frac{1}{N}\frac{\partial f}{\partial h} \ . \tag{1.5}$$

Other interesting quantities are the magnetic susceptibility - the response of the magnetisation to a small magnetic field - given by

$$\chi = \frac{\partial M}{\partial h}\Big|_{h=0} \ , \tag{1.6}$$

and the specific heat capacity:

$$C = -T\frac{\partial^2 f}{\partial T^2} \ . \tag{1.7}$$

The specific heat capacity per unit volume is known as the specific heat.

Close to the critical point many of the properties of the model greatly simplify and no longer depend upon the microscopic behaviour of the material. Quantities such as the magnetisation, specific heat and susceptibility have a power law dependence upon the distance away from T_c, whereas the pair correlation function $\Gamma(i-j) = \langle \sigma_i \sigma_j \rangle$ at $T = T_c$ has a power law dependence upon the distance between each pair of spins. Moreover, in all cases the powers, which are known as critical exponents, turn out to be pure numbers. The theoretical values of the critical exponents of the Ising model are shown in Table 1.1. The constants of proportionality for each of the thermodynamic quantities in Table 1.1 are not necessarily the same for $T < T_c$ and $T > T_c$.

Critical Exponent	Behaviour	Exponent value
α	$C \propto (T - T_c)^{-\alpha}$	0
β	$M \propto (T_c - T)^{\beta}$	1/8
γ	$\chi \propto (T - T_c)^{-\gamma}$	7/4
δ	$M \propto h^{1/\delta}$	15
ν	$\xi \propto (T - T_c)^{\nu}$	1
η	$\Gamma \propto \lvert i - j \rvert^{-\eta}$	1/4

Table 1.1: Critical exponents for the two-dimensional Ising model.

One of the remarkable facts of statistical mechanics is that all models fall into a small number of classes, where each class is essentially characterised by the critical exponents. This is the concept of universality and one of the main goals of statistical mechanics is to classify all possible universality classes. Wilson [6] made great progress towards this goal by applying the ideas of the renormalisation group method to obtain the values of the critical exponents.

1.1.1 Renormalisation group

The renormalisation group (RG) provides a method of exploring a statistical mechanical model in the vicinity of a critical point. As we mentioned above, the main goal is to extract the values of the critical exponents and thus determine the universality class.

We demonstrate the idea behind the renormalisation group by considering real-space renormalisation of the Ising model. The system is described by the partition function

$$Z = \mathrm{Tr}_\sigma \, e^{-\frac{1}{k_B T} H} = \mathrm{Tr}_\sigma \, e^{-\mathcal{H}}. \tag{1.8}$$

We use the 'reduced Hamiltonian' $\mathcal{H}$ found from the Hamiltonian (1.1) by dividing by $k_B T$.

One of the common aspects of the functions in Table 1.1 is that they characterise large-length-scale trends, rather than the actual microscopic behaviour of the spins at each site. If we look at the model sightly out of focus, so that we no longer see the very small-scale structure, the long-distance effects should remain unchanged. This defocusing can be carried out by a procedure known as block spin renormalisation.

We divide the lattice into 3×3 blocks, and assign each block an overall spin by taking the majority rule of the nine constituent spins. We now rescale the new lattice by a factor of three so that the lattice spacing becomes the same as before. Figure 1.1 demonstrates this block spin transformation on a small part of the lattice.

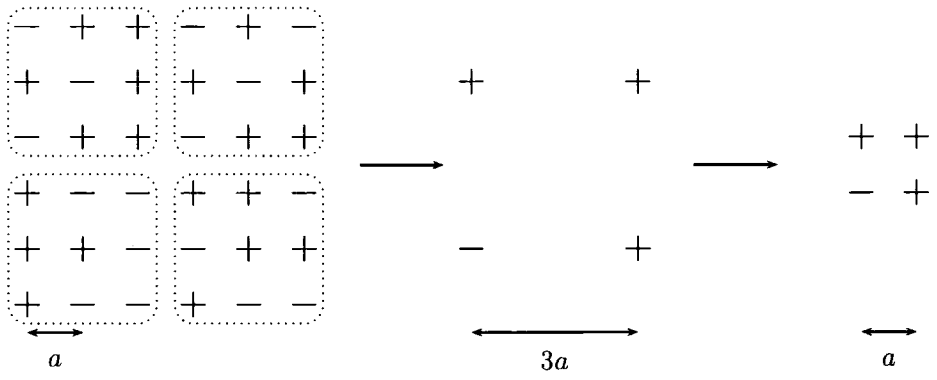

Figure 1.1: Real-space renormalisation of four blocks of the Ising lattice.

Note that the correlation length reduces by a factor of the lattice spacing a each time we repeat this procedure. If we began exactly at the critical point, then, no matter how many times we repeat the transformation, the system will always look the same due to the infinite correlation length. Thus the model at the critical point is invariant under changes of scale. As we shall see later this is an extremely important property of the model at criticality.

If we begin just below the critical point, the renormalisation group transformation causes the domains of downward spin to decrease in size; thus the system becomes more ordered and approaches the completely ordered picture at zero temperature. Above the critical point, the correlation length again decreases under the RG transformation. All of the domains of down and up spin become smaller while overall neither spin dominates. Thus the system approaches the completely disordered picture found at infinite temperature.

We can simulate the blocking procedure by including a projection operator in the partition function. Define for each block

$$T(\sigma', \sigma_1, \ldots, \sigma_9) = \begin{cases} 1 & \text{if } \sigma' \sum_{i=1}^{9} \sigma_i > 0 \\ 0 & \text{otherwise}, \end{cases} \tag{1.9}$$

then the Hamiltonian describing the blocked lattice is

$$e^{-\mathcal{H}'(\sigma')} = \mathrm{Tr}_\sigma \prod_{\text{blocks}} T(\sigma', \sigma_1, \ldots, \sigma_9)\, e^{-\mathcal{H}(\sigma)}\,. \tag{1.10}$$

Since $\sum_{\sigma'} T(\sigma', \sigma_1, \ldots, \sigma_9) = 1$, the renormalisation group transformation leaves the partition function invariant:

$$\mathrm{Tr}_{\sigma'}\, e^{-\mathcal{H}'(\sigma')} = \mathrm{Tr}_\sigma\, e^{-\mathcal{H}(\sigma)}\,. \tag{1.11}$$

The new Hamiltonian can be expressed in a form similar to (1.1), but we must also include a next-to-nearest neighbour term, denoted with the symbol $\sum^{(2)}_{\langle ij\rangle}$, and so on. In principle, these terms could also have been included in the original Hamiltonian with couplings $J_2, J_3, \ldots$. We write the new Hamiltonian as follows

$$\mathcal{H}'(\sigma') = -J_1' \sum_{\langle ij\rangle} \sigma_i\sigma_j - J_2' \sum^{(2)}_{\langle ij\rangle} \sigma_i\sigma_j - J_3' \sum^{(3)}_{\langle ij\rangle} \sigma_i\sigma_j \ldots - h' \sum_i \sigma_i\,. \tag{1.12}$$

Since the partitions functions encoded by the Hamiltonians $\mathcal{H}$ and $\mathcal{H}'$ are equal, there must be a relation between the coupling constants $\mathbf{J} = (J_1, J_2, \ldots)$ and $\mathbf{J}' = (J_1', J_2', \ldots)$. The map between them generates the renormalisation group

$$\mathbf{J}' = \mathbf{T}(\mathbf{J})\,. \tag{1.13}$$

By repeating the renormalisation procedure described above, we generate a sequence of points in the space of all possible couplings. This is known as a renormalisation group trajectory. As mentioned above, if we start close to the critical point, then the renormalisation group trajectory moves away from it since the correlation length decreases at each step. However, if we start at exactly the critical point, then we always remain there, since the correlation length remains infinite under each transformation. Thus, critical points are associated to fixed points of the renormalisation group transformation.

The critical exponents of the model can be found by linearising the RG transformation at the fixed point. We begin by assuming the space of all couplings has a fixed point at $\mathbf{J}^*$, and that $\mathbf{T}$ is differentiable at that point. Then dropping higher order terms we can write

$$J_a' - J_a^* = \sum_b R_{ab}(J_b - J_b^*)\,, \tag{1.14}$$

where $R_{ab} = \partial J_a'/\partial J_b|_{\mathbf{J}=\mathbf{J}^*}$. We suppose R can be diagonalised with eigenvalues λ_i and corresponding eigenvectors ν_a^i:

$$\sum_a \nu_a^i R_{ab} = \lambda^i \nu_b^i\,. \tag{1.15}$$

The scaling variables, defined by $u_i = \sum_a \nu_a^i (J_a - J_a^*)$, transform in a simple way under $\mathbf{T}$:

$$\begin{aligned} u_i' &= \sum_a \nu_a^i (J_a' - J_a^*) \\ &= \sum_{a,b} \nu_a^i R_{ab} (J_b - J_b^*) \\ &= \sum_b \lambda^i \nu_b^i (J_b - J_b^*) \\ &= \lambda^i u_i \,. \end{aligned} \tag{1.16}$$

We set $\lambda^i = a^{y_i}$, where a is the lattice spacing. Then the behaviour of a scaling variable under the RG transformation depends upon the sign of the y_i:

• If $y_i > 0$, then u_i is *relevant* and the renormalisation group trajectory moves away from the critical point,

• If $y_i < 0$, then u_i is *irrelevant* and the renormalisation group trajectory moves towards the critical point,

• If $y_i = 0$, then u_i is *marginal.* In this case the linear approximation about $\mathbf{J}^*$ is no longer valid.

We will see later how a relevant operator can be used to explore the renormalisation group space away from the critical point.

1.1.2 Scaling behaviour of the free energy

The two-dimensional Ising model has two free parameters that we may vary to explore the renormalisation group space: the reduced temperature $t = (T - T_c)/T_c$ and the external magnetic field h. They correspond to two relevant scaling variables u_1 and u_2 with RG eigenvalues y_t and y_h respectively. Close to the critical point, u_1 and u_2 can be taken to be proportional to t and h.

The free energy of the model (1.4) remains constant under a RG transformation since the partition function is itself invariant. However, for this to be true the free energy per unit site must increase

$$f(t', h') = a^2 f(t, h) \,. \tag{1.17}$$

Using (1.16), we arrive at what is known as the scaling hypothesis

$$f(t, h) = a^{-2} f(a^{y_t} t, a^{y_h} h) \,. \tag{1.18}$$

Note that the function $t^{-2/y_t} f(t, h)$ is invariant under $t \to a^{y_t} t$ and $h \to a^{y_h} h$ so must depend only on the scale-invariant variable $h/t^{h_h/y_t}$. So we can write

$$f(t, h) = t^{2/y^t} g(h/t^{y_h/y_t}) \tag{1.19}$$

for some function g. The spontaneous magnetisation M can be found by taking the derivative of f with respect to the external field:

$$M = -\frac{\partial f}{\partial h}|_{h=0} = t^{2/y_t - y_h/y_t} g'(0) \,. \tag{1.20}$$

Comparing with Table 1.1, we can relate the renormalisation group eigenvalues to the critical exponent β:

$$\beta = (2 - y_h)/y_t \,. \tag{1.21}$$

The remaining critical exponents can be found in a similar manner.

1.1.3 Statistical mechanics and quantum field theory

In Euclidean quantum field theory (QFT) the generating function is given by the functional integral of the action $\mathcal{A}$ over all local fields $\phi(x)$:

$$Z = \int \mathcal{D}\phi \; e^{-\beta \mathcal{A}[\phi]} \tag{1.22}$$

where β is the coupling. A convenient way of regularising the theory is to consider it defined on a lattice. Note the similarity between the generating function and the central object of statistical mechanics, that is the partition function:

$$Z = \mathrm{Tr}\, e^{-H/k_B T}, \tag{1.23}$$

where the trace is over all possible configurations encoded by the Hamiltonian H. In fact at a critical point, the correlation functions have a universal behaviour which is independent of whether the underlying Hamiltonian or action describes a lattice quantum field theory or a statistical model. Thus we can use the methods of quantum field theory to solve statistical mechanical problems.

1.1.4 Conformal invariance

We have seen that at the critical point a statistical model is invariant under changes of scale. Polyakov demonstrated in 1970 [7] that for a system with local interactions the model is not only invariant under changes of scale, but is also invariant under conformal transformations. A transformation of the coordinates $\mathbf{x} \to \mathbf{x}'$ is said to be conformal if it leaves the d-dimensional space-time metric tensor invariant up to a scale factor:

$$g'_{\mu\nu}(\mathbf{x}') = \Lambda(\mathbf{x}) g_{\mu\nu}(\mathbf{x}) \,. \tag{1.24}$$

In $d > 3$ dimensions the allowed possible transformations are the Poincaré group of translations and Lorentz transformations:

$$x'^{\mu} = x^{\mu} + a^{\mu} \,, \tag{1.25}$$

$$x'^{\mu} = M^{\mu}_{\nu} x^{\nu} \,, \tag{1.26}$$

the dilatations

$$x'^{\mu} = \lambda x^{\mu} \ , \tag{1.27}$$

and the special conformal transformations which behave as

$$x'^{\mu} = \frac{x^{\mu} + b^{\mu}\mathbf{x}^2}{1 - 2\mathbf{b}.\mathbf{x} + b^2\mathbf{x}^2} \ . \tag{1.28}$$

The two-dimensional case is somewhat special; more details can be found in Section 1.2.

A conformal field theory is a quantum field theory whose action is invariant under conformal transformations. Therefore a statistical mechanical model at a critical point can be given a description in terms of a conformal field theory. Why is this alternative description useful? The hope is that all possible universality classes can be explored by considering all possible conformal field theories. This seems to be a more tractable approach to the problem because conformal invariance strongly constrains the model. Furthermore, it is possible to investigate away from the critical points by considering a perturbation of a conformal field theory. The idea is to use a relevant operator so that the renormalisation group trajectory is driven away from the critical point. This will be discussed in more detail in Section 1.2.1.

It was not until fourteen years later, in the paper by Belavin, Polyakov and A.B. Zamolodchikov [8], that the power of conformal invariance in two-dimensions was fully demonstrated. They constructed a set of exactly solvable conformal field theories by classifying all of the fields in the operator algebra using the representation theory of the Virasoro algebra. In this context, solvable means that the field content consists of a *finite* number of families whose fields have known scaling dimensions. In addition, because the number of fields is finite it is possible to compute all of the correlation functions of these fields. The resulting conformal field theories were called the minimal models, and many have been shown to describe second order phase transitions at the critical points of two-dimensional statistical systems.

1.2 Conformal field theory

Before turning to the main ideas of perturbed conformal field theory, and to fix our notation, we introduce some of the concepts of conformal field theory (CFT). A more complete review can be found, for example, in the book [9].

Let (z^0, z^1) label the coordinates of the plane, and $g_{\mu\nu} = \eta_{\mu\nu}$ be the Euclidean metric tensor. Under a coordinate transformation $z^{\mu} \to z^{\mu} + w^{\mu}$ the metric tensor transforms as

$$g_{\mu\nu} \to g_{\mu\nu} - (\partial_{\mu} w_{\nu} + \partial_{\nu} w_{\mu}) \tag{1.29}$$

where $\partial_\mu = \frac{\partial}{\partial z^\mu}$. The transformation is conformal provided $(\partial_\mu w_\nu + \partial_\nu w_\mu)$ is proportional to $g_{\mu\nu}$. Imposing this conditions yields the Cauchy-Riemann equations

$$\partial_0 w_0 = \partial_1 w_1 \tag{1.30}$$

$$\partial_1 w_0 = -\partial_0 w_1 \ . \tag{1.31}$$

We therefore use complex coordinates $z = z^0 + iz^1$ and $\bar{z} = z^0 - iz^1$. In this notation the partial derivatives are $\partial_z = \frac{1}{2}(\partial_0 - i\partial_1)$ and $\partial_{\bar{z}} = \frac{1}{2}(\partial_0 + i\partial_1)$ and the metric tensor becomes

$$g_{\mu\nu} = \begin{pmatrix} 0 & \frac{1}{2} \\ \frac{1}{2} & 0 \end{pmatrix} \ . \tag{1.32}$$

Then (1.31) implies that conformal transformations coincide with holomorphic and antiholomorphic mappings respectively

$$z \to w(z) \quad , \quad \bar{z} \to \bar{w}(\bar{z}) \ . \tag{1.33}$$

So the conformal group in two dimensions is infinite dimensional. Furthermore, this factorisation into independent holomorphic and antiholomorphic parts means that if we consider z^0 and z^1 to themselves take complex values, then z and $\bar{z}$ can be considered as independent variables. The physical space, $(z^0, z^1) \in R^2$, corresponds to taking $z^* = \bar{z}$.

The conformal symmetry is generated by the energy-momentum tensor $T_{\mu\nu}$. Requiring $T_{\mu\nu}$ to be invariant under conformal transformations means that it must be traceless. Since it is also symmetric, it follows that there are only two nonzero components: T^{zz} and $T^{\bar{z}\bar{z}}$. Furthermore T^{zz} depends only on z and $\overline{T}(\bar{z}\bar{z})$ only on $\bar{z}$. We write

$$T(z) = -2\pi T_{zz} \quad , \quad \overline{T}(\bar{z}) = -2\pi T_{\bar{z}\bar{z}} \ , \tag{1.34}$$

and just concentrate on $T(z)$.

An important concept is that of a *primary* field. These are fields in the theory which transform under a conformal transformation $z \to f(z), \bar{z} \to \bar{f}(\bar{z})$ as

$$\varphi(z, \bar{z}) = \left(\frac{df(z)}{dz}\right)^h \left(\frac{d\bar{f}(\bar{z})}{d\bar{z}}\right)^{\bar{h}} \varphi(f(z), \bar{f}(\bar{z})) \, , \tag{1.35}$$

where $(h, \bar{h})$ are known as the conformal dimensions (or weights). As we will mention below, all other fields in the theory are descendents of the primary fields. Under a conformal transformation T behaves as

$$T'(f(z)) = \left(\frac{df(z)}{dz}\right)^{-2} \left(T(z) - \frac{c}{12}\{f(z), z\}\right) \ , \tag{1.36}$$

where c is a constant and the Schwarzian derivative is

$$\{f(z), z\} = \frac{f'''(z)}{f'(z)} - \frac{3}{2}\left(\frac{f''(z)}{f'(z)}\right)^2 \ . \tag{1.37}$$

Therefore T is not itself a primary field, but is a descendent of the simplest primary field: the identity.

The component T can be expanded in modes as

$$T(z) = \sum_{n\in\mathbb{Z}} z^{-n-2} L_n \quad : \quad L_n = \frac{1}{2\pi i}\int dz\; z^{n+1} T(z)\;. \tag{1.38}$$

An analogous expression exists for the antiholmorphic component $\overline{T}(\bar{z})$ of the stress-energy tensor. The L_n and $\bar{L}_n$ are the generators of the local conformal transformations; in particular the combination $L_0 + \bar{L}_0$ generates scale transformations (dilatations) as well as being proportional to the Hamiltonian of the model. The operators L_n satisfy the Virasoro algebra

$$[L_n, L_m] = (n-m)L_{n+m} + \frac{c}{12} n(n^2-1)\delta_{n+m,0} \tag{1.39}$$

where the constant c, introduced in (1.36), is an important characteristic of the theory and is known as the central charge. Similarly the operators $\bar{L}_n$ satisfy

$$[\bar{L}_n, \bar{L}_m] = (n-m)\bar{L}_{n+m} + \frac{c}{12} n(n^2-1)\delta_{n+m,0}\;, \tag{1.40}$$

and

$$[L_n, \bar{L}_m] = 0\;. \tag{1.41}$$

The vacuum state $|0\rangle$ in the theory must be invariant under global conformal transformations and so is defined by

$$L_n|0\rangle = 0 \quad n \geq -1\,. \tag{1.42}$$

Note that this combined with (1.38) implies the vacuum expectation value of the energy-momentum tensor is zero:

$$\langle 0|T(z)|0\rangle = \langle 0|\overline{T}(\bar{z})|0\rangle = 0\;. \tag{1.43}$$

Representations of the Virasoro algebra are built from highest weight states $|h, \bar{h}\rangle$. These states are defined by the action of a primary field on the vacuum state

$$|h, \bar{h}\rangle \equiv \varphi(0,0)|0\rangle\,. \tag{1.44}$$

The highest weight states have scaling dimension $h + \bar{h}$ and spin $h - \bar{h}$. Since

$$L_o|h, \bar{h}\rangle = h|h, \bar{h}\rangle \quad , \quad \bar{L}_o|h, \bar{h}\rangle = \bar{h}|h, \bar{h}\rangle \tag{1.45}$$

the highest weight states are eigenstates of the Hamitonian. Further states are built by application of the operators L_n

$$L_{-k_1} L_{-k_2} \ldots L_{-k_n}|h\rangle \qquad (1 \leq k_1 \leq \ldots \leq k_n)\;. \tag{1.46}$$

These are eigenstates of L_0 with eigenvalue $h' = h + k_1 + k_2 + \ldots + k_n$, and are the descendent states of the primary field. The subset of the Hilbert space generated by the primary state $|h\rangle$ and its descendents is closed under the action of the Virasoro generators, and so forms a representation of the Virasoro algebra known as a Verma module. The set of a primary field and all its descendents is known as a conformal family.

The minimal models

The first conformal field theories to be classified were the minimal models [8]. They have a finite number of conformal families with well defined scaling dimensions, and are denoted $\mathcal{M}_{p,q}$. The central charge is then expressed in terms of the coprime integers p and q with $p < q$ as

$$c = 1 - 6\frac{(p-q)^2}{pq}\,. \tag{1.47}$$

The conformal dimensions of the primary fields can be organised in a $(p-1)\times(q-1)$ table known as the Kac table. Let $1 \leq a < p$ and $1 \leq b < q$. Then the conformal dimensions are given by the Kac formula

$$h_{ab} = \frac{(bp-aq)^2 - (p-q)^2}{4pq}, \tag{1.48}$$

and the symmetry $h_{a,b} = h_{p-a,q-b}$ implies there are $(p-1)(q-1)/2$ distinct primary fields. Whenever $q = p+1$ the field of smallest conformal dimension is $h_{1,1} = 0$, and the corresponding primary field is the identity. The remaining fields all have positive conformal dimensions which means that there are no states of negative norm and the corresponding model is unitary. Accordingly, these models are known as the unitary minimal models and often denoted $\mathcal{M}_m \equiv \mathcal{M}_{m,m+1}$. In a unitary minimal model the two-point correlation function of a primary field with itself behaves as

$$\langle \phi_{h,\bar{h}}(z,\bar{z})\, \phi_{h,\bar{h}}(0,0)\rangle = \frac{1}{z^{2h}\bar{z}^{2\bar{h}}}\,. \tag{1.49}$$

The critical Ising model

We now make contact with the statistical mechanical model introduced at the beginning of this chapter. The critical Ising model in the continuum has two nontrivial scaling operators: the spin σ and the energy density ε. There is also the trivial operator $\mathbb{1}$ with conformal dimensions $(0,0)$. The correlation functions at the critical point behave as

$$\langle \sigma_i\, \sigma_{i+n}\rangle = \frac{1}{|n|^{\eta}} \quad , \quad \langle \varepsilon_i\, \varepsilon_{i+n}\rangle = \frac{1}{|n|^{4-2/\nu}}\,. \tag{1.50}$$

Table 1.1 indicates $\eta = 1/4$ and $\nu = 1$ so comparing (1.50) with (1.49) and assuming that $h = \bar{h}$ the conformal dimensions of the spin and energy density operators are

$$(h,\bar{h})_\sigma = (1/16, 1/16) \quad , \quad (h,\bar{h})_\varepsilon = (1/2, 1/2)\,. \tag{1.51}$$

The critical Ising model is identified with the simplest nontrivial unitary minimal model $\mathcal{M}_{3,4}$. Figure 1.2 depicts the relevant Kac table. It shows that the minimal model has three primary fields with conformal weights $(0,0), (1/16, 1/16)$ and $(1/2, 1/2)$ so these are identified with the identity, spin and thermal operators $\mathbb{1}, \sigma$ and ε respectively.

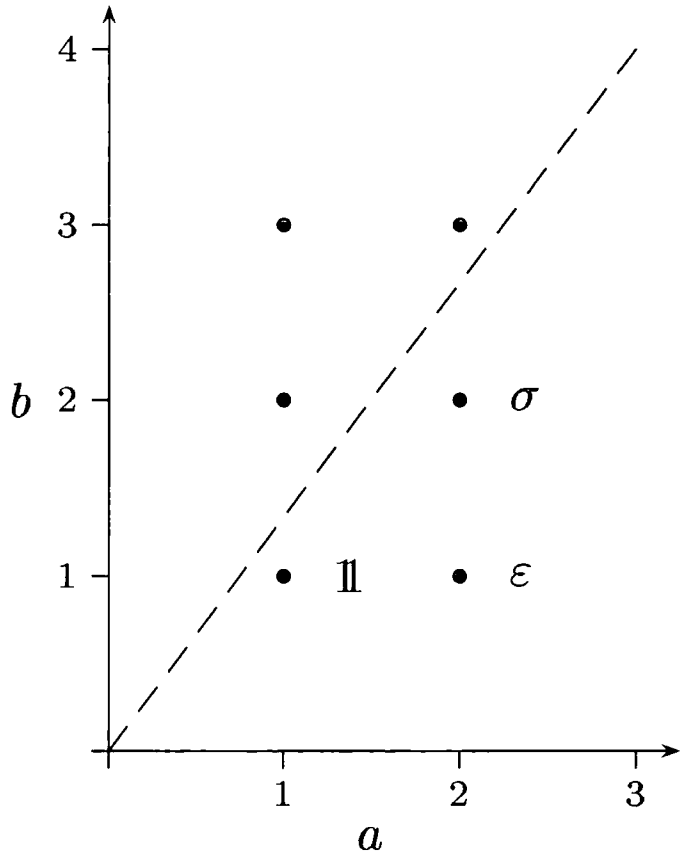

Figure 1.2: Kac table of allowed values of a and b for the weights h_{ab} of the Ising model $\mathcal{M}_{3,4}$. Also shown are the associated primary fields.

Finite-size effects

Throughout the rest of this thesis we will be interested in statistical theories defined on the finite geometry of a cylinder rather than the infinite plane. The following conformal transformation maps the infinite z-plane to a cylinder of circumference R:

$$f(z) = \frac{R}{2\pi} \ln z \ . \tag{1.52}$$

We use (1.36) to find the behaviour of the holomorphic component of the stress energy tensor under this mapping. Since the Schwarzian derivative is $1/2z^2$ we have

$$T_{cylinder}(f(z)) = \left(\frac{2\pi}{R}\right)^2 \left(z^2 T_{plane}(z) - \frac{c}{24}\right) \tag{1.53}$$

Since the vacuum energy density on the plane vanishes (1.43), it follows from (1.53) that the corresponding vacuum energy density on the cylinder is nonzero

$$\langle T_{cylinder}(f(z))\rangle = -\frac{\pi^2 c}{6R^2} \ . \tag{1.54}$$

The difference in energy between an infinite and finite geometry is known as the Casimir energy. We see that in this case it is related to the central charge of the conformal field theory. We will use this result to show that the central charge is also related to the free energy. The variation of the free energy is given by

$$\delta F = -\frac{1}{2}\int d^2x \sqrt{\det g_{\mu\nu}}\, \delta g_{\mu\nu}\langle T_{\mu\nu}\rangle \ . \tag{1.55}$$

We scale the circumference of the cylinder so that $\delta R = \varepsilon R$. This corresponds to $\delta z^0 = \varepsilon z^0$ and $\delta z^1 = 0$ where z^0 runs around the cylinder and z^1 along the length of it. The corresponding variation (1.29) in the metric tensor is $\delta g_{\mu\nu} = -2\varepsilon\delta_{\mu 0}\delta_{\nu 0}$. Now using (1.54) we have

$$\langle T^{00}\rangle = \langle T_{zz}\rangle + \langle T_{\bar{z}\bar{z}}\rangle = -\frac{1}{\pi}\langle T(z)\rangle = \frac{\pi c}{6R^2} \ . \tag{1.56}$$

Plugging everything into (1.55) we find

$$\delta F = \int dz^0 dz^1 \frac{\pi c}{R^2}\frac{\delta R}{R} \ . \tag{1.57}$$

The integration around the cylinder results in an extra factor of R. If we use the free energy F_R per unit length then its variation is

$$\delta F_R = \frac{\pi c}{6R^2}\delta R \ , \tag{1.58}$$

then upon integrating we have [10, 11]

$$F_R = -\frac{\pi c}{6R} \ . \tag{1.59}$$

This quantity is equal to the ground-state energy E_0 of the corresponding conformal field theory.

1.2.1 Perturbed conformal field theory

The notion of solvability or integrability is a central concept in 1+1 dimensions. Its roots lie in classical mechanics where the number of conserved quantities is equal to the number of degrees of freedom, thereby allowing the equations of motion to be solved by integration. A field in quantum field theory has an infinite number of degrees of freedom, and so the notion of integrability requires modification. Instead, if there are sufficiently many conservation laws to identify the infinite number of states, then the theory is said to be integrable.

The integrability of a conformal field theory is assured by the conserved charges provided by the holomorphic and antiholomorphic components of the stress energy tensor and other descendents of the identity. But what happens when we move away from the conformal point? In general, we would expect the charges to no longer be conserved and integrability lost. However, in [12], A.B. Zamolodchikov showed that it is possible to break the conformal symmetry in such a way that some of the integrals of motion (although deformed) survive the perturbation. In most cases the correlation length becomes finite and the result is a massive integrable quantum field theory. This idea of considering a massive integrable quantum field theory as a perturbed conformal field theory provoked an intense amount of research activity which is still ongoing today and finding new applications.

We denote the action of the unperturbed CFT as $\mathcal{A}_{\mathrm{CFT}}$. The perturbed action is given by

$$\mathcal{A} = \mathcal{A}_{\mathrm{CFT}} + \lambda \int \varphi(z, \bar{z})\, d^2 z \tag{1.60}$$

where $\varphi(z, \bar{z})$ is a field belonging to the unperturbed CFT with left and right conformal weights (h, h). The coupling constant λ has scale dimension $y = 2(1-h)$ and so has conformal dimensions $(1-h, 1-h)$. The CFT is a fixed point of the renormalisation group; so provided $2(1-h) > 0$ a RG transformation moves the model away from the critical point. Thus φ is called a relevant operator if $h < 1$, and an irrelevant one if $h > 1$.

At short distances the perturbing term in (1.60) becomes insignificant and we expect that the fields in the theory can be classified by the short distance scaling behaviour, just as in the CFT case. To demonstrate the integrability of a perturbed CFT we review Zamolodchikov's counting argument [12] for the unitary minimal models. The argument easily extends to nonunitary models and we will comment further on this in Section 1.6.

The identity operator I of the unperturbed CFT is the unique primary field with scaling dimension $(0, 0)$. Its conformal family splits into holomorphic and antiholomorphic sectors and can be written

$$[I] = \Lambda \otimes \bar{\Lambda}\,. \tag{1.61}$$

We denote the space Λ to be the left descendents of the identity I. This can be decomposed into subspaces Λ_s, labelled by spin, using the operator L_0:

$$\begin{aligned} L_0 \Lambda_s &= s\Lambda_s\,, \\ \bar{L}_0 \Lambda_s &= 0\,. \end{aligned} \tag{1.62}$$

The decomposition is

$$\Lambda = \bigoplus_{s=0}^{\infty} \Lambda_s\,. \tag{1.63}$$

Each of the fields $T_s \in \Lambda_s$ have conformal dimension $(s,0)$ and therefore spin s. Furthermore, since each T_s is holomorphic it follows that

$$\partial_{\bar{z}} T_s = 0\,, \tag{1.64}$$

and we can define an infinite number of integrals of motion (conserved charges) by

$$\oint T_s(\zeta)(\zeta - z)^{n+s-1} d\zeta \quad , \quad n = 0, \pm 1, \pm 2, \ldots \tag{1.65}$$

Some of the fields T_s may be total derivatives so these conserved charges are not all linearly independent. A linearly independent set follows from considering the factor space $\hat{\Lambda} = \Lambda / L_{-1}\Lambda$, which is found by removing all of the total derivatives. This is again decomposable by spin

$$\hat{\Lambda} = \bigoplus_{s=0}^{\infty} \hat{\Lambda}_s\,. \tag{1.66}$$

In the perturbed theory T_s no longer satisfies (1.64). Instead we expect the following Taylor expansion in powers of the coupling constant

$$\partial_{\bar{z}} T_s = \lambda R^{(1)}_{s-1} + \lambda^2 R^{(2)}_{s-1} + \ldots \tag{1.67}$$

where the $R^{(n)}_{s-1}$ are assumed to be fields belonging to the CFT. The dimensions of λ and $\partial_{\bar{z}} T_s$ are $(1-h, 1-h)$ and $(s,1)$ respectively. By comparing dimensions, the fields $R^{(n)}_{s-1}$ must be of dimension

$$(s - n(1-h), 1 - n(1-h))\,. \tag{1.68}$$

For large enough n, the right dimension of (1.68) will eventually be negative. But all of the fields of the unitary minimal models have positive dimensions, and so the sum in (1.67) must truncate and actually be finite. Of the terms which remain, it follows that $R^{(n)}_{s-1}$ must vanish unless there is a field belonging to the CFT with dimension

$$1 - n(1-h) = \Delta\,. \tag{1.69}$$

This can be easily established since the scaling dimensions of the fields in the conformal theory are all known. For many models it so happens that the only possible term is the one with $n = 1$, and so we have

$$\partial_{\bar{z}} T_s = \lambda R^{(1)}_{s-1}\,. \tag{1.70}$$

The field $R^{(1)}_{s-1}$ has dimension $(s - 1 + h, h)$ and so we assume on dimensional grounds that this is a left descendent of the perturbing field φ. The space Φ of all left descendents of φ has the decomposition

$$\Phi = \bigoplus_{s=0}^{\infty} \Phi_s \tag{1.71}$$

where

$$L_0\Phi_s = (\Delta + s)\Phi_s \quad , \quad \bar{L}_0\Phi_s = \Delta\Phi_s \,. \tag{1.72}$$

This means we can think of $\partial_{\bar{z}}$ as a linear map

$$\partial_{\bar{z}} : \hat{\Lambda}_s \to \hat{\Phi}_{s-1} \tag{1.73}$$

where $\hat{\Phi} = \Phi / L_{-1}\Phi$. In order for T_s to be a non-trivial conserved charge R_{s-1} must be a z-derivative and belong to $L_{-1}\Phi$. Its projection onto $\hat{\Phi}$ must therefore be zero, and it also must lie in the kernel of the linear mapping $\partial_{\bar{z}}$. Conversely, if the kernel is nonzero then there exists a conserved charge. Since (1.73) is a linear map it has non-empty kernel if the dimension of $\hat{\Lambda}_s$ is greater than that of $\hat{\Phi}_{s-1}$. This is the crux of Zamolodchikov's counting argument [12]: the existence of conserved charges follows from a simple comparison of the dimensions of these spaces. In the original paper [12], Zamolodchikov demonstrated the existence of whole series of conserved charges for the minimal models perturbed by the operators ϕ_{13}, ϕ_{12} and ϕ_{21}. On the basis of this, he conjectured that these models are integrable.

1.2.2 Scaling Lee-Yang model

We introduce the scaling Lee-Yang model as an example of a perturbed conformal field theory.

The simplest nonunitary conformal field theory is the Lee-Yang model, denoted $\mathcal{M}_{2,5}$. It has central charge $c = -22/5$ and Kac table as shown in Figure 1.3.

There are two primary fields: the identity $\mathbb{1}$ and the scalar field φ. Since φ has conformal dimensions $(-1/5, -1/5)$ its scaling dimension $(h + \bar{h})$ is $-2/5$ and it is therefore a relevant operator. So φ is a suitable operator to perturb the minimal model $\mathcal{M}_{2,5}$. The result of the perturbation is the scaling Lee-Yang model (SLYM) with action

$$\mathcal{A}_{SLYM} = \mathcal{A}_{\mathcal{M}_{2,5}} + i\lambda \int d^2x\, \varphi(x) \,. \tag{1.74}$$

Cardy and Mussardo [13] conjectured that for $\lambda \in \mathbb{R}^+$ this model has a single particle of mass M, which on dimensional grounds must be related to the perturbation parameter $\lambda^{5/12}$. The exact relation is [14]

$$M = (2.642944662\ldots)\lambda^{5/12} \,. \tag{1.75}$$

Zamolodchikov's counting argument was employed in [13] to demonstrate the existence of conserved charges for the SLYM with spins $1, 5, 7, 11, 13, 17, 19, \ldots$. These higher spin conserved charges strongly constrain the allowed scattering process: in 1+1 dimensions the existence of just two non-trivial conserved charges of higher spin is sufficient to ensure the scattering is purely elastic [15]. This means that there can be no particle production and the individual particle momenta are

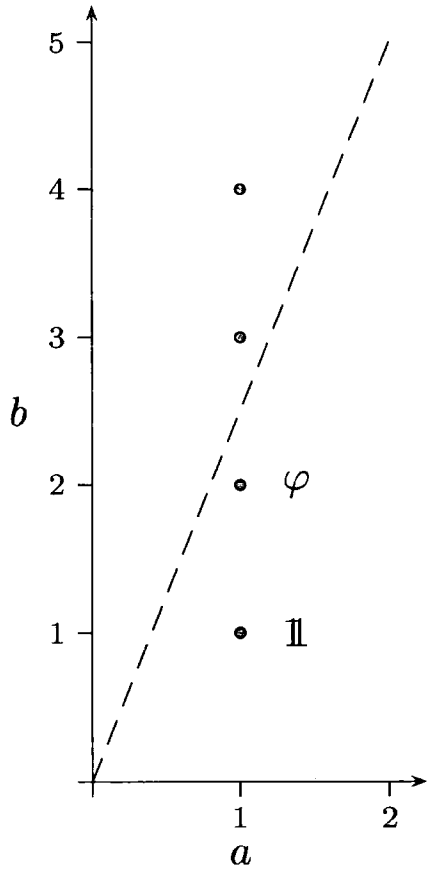

Figure 1.3: Kac table of allowed values of a and b for the weights h_{ab} of the Lee-Yang model $\mathcal{M}_{2,5}$. Also shown are the associated primary fields.

also conserved. Furthermore, all n-particle scattering processes can always be decomposed into products of two-particle scattering amplitudes [16]. The S-matrix describing the two-particle scattering amplitude is then conjectured using the values of the Lorentz spins of the conserved charges. All of these ideas are explained in, for example, [17] and will now be discussed in a little more detail.

We briefly introduce the concept of an S-matrix for the scattering of two particles, of possibly different types, with masses m_a. It is convenient to parameterise the energy and momenta of a particle in terms of the rapidity θ

$$p_a^0 = m_a \cosh\theta \quad , \quad p_a^1 = m_a \sinh\theta \,. \tag{1.76}$$

Then the on-mass shell constraint $(p_a^0)^2 - (p_a^1)^2 = m_a^2$ is satisfied for all values of θ. An in-state, denoted

$$|A_{a_1}(\theta_1)A_{a_2}(\theta_2)\rangle_{IN} \tag{1.77}$$

with $\theta_1 > \theta_2$, is defined such that as time goes to $-\infty$ there are no further interactions between the particles A_{a_1} and A_{a_2}. Analogously, an out-state is defined to be such that there are no further interactions as time tends to $+\infty$. It is denoted

$$|A_{b_1}(\theta_1)A_{b_2}(\theta_2)\rangle_{OUT} \tag{1.78}$$

where $\theta_1 < \theta_2$. The S-matrix $S(\theta)$ provides the map between the in- and out-states, each state being represented by a string of non-commuting symbols A_a. Since we are in $1+1$ dimensions we allow the order of the symbols A_a on the page to indicate the spatial order of the particles that they represent. In terms of this notation, the S-matrix is defined via

$$A_{a_1}(\theta_1)A_{a_2}(\theta_2) = S_{a_1 a_2}(\theta_1 - \theta_2)A_{a_1}(\theta_1)A_{a_2}(\theta_2) \ , \tag{1.79}$$

and due to Lorentz invariance depends only on the rapidity difference of the particles.

The two-particle S-matrix describing the scattering for the scaling Lee-Yang model is conjectured to be [13]

$$S(\theta) = \frac{\sinh(\theta) + i\sin(\pi/3)}{\sinh(\theta) - i\sin(\pi/3)} \ . \tag{1.80}$$

The S-matrix describes the infrared data of the model. However it is important to check that the ultraviolet limit of the model coincides with the conformal field theory that was originally perturbed. One tool that provides such a check is known as the thermodynamic Bethe ansatz (TBA) [18], and was first applied in the context of perturbed conformal field theory in [19]. A set of coupled nonlinear integral equations (the TBA equations) were derived using the two-particle S-matrix of the model. The exact ground-state energy of the theory, defined on a cylinder of circumference R, was then given in terms of the solution of the TBA equation.

The ground-state energy of a conformal field theory defined on a cylinder is given by (1.59) and depends upon the only scale available - the circumference R. A perturbed conformal field theory has an extra scale M, the lightest mass in the theory. However, for small R the effect of the perturbing term is negligible and the ground-state energy is once again given by (1.59). When R is nonzero, the dimensionless quantity c depends on both M and R via the dimensionless combination $r = MR$. Therefore the ground-state energy of the perturbed conformal field theory behaves like

$$E_0(R) = R\,B(\lambda) - \frac{\pi c_{\text{eff}}(r)}{6R} \ . \tag{1.81}$$

On dimensional grounds the term $B(\lambda)$ is proportional to $\lambda^{1/(1-h)}$ and represents the infinite volume vacuum energy; for this reason it is also known as the bulk term. The term $c_{\text{eff}}(r)$ is known as the finite size scaling function, and in the limit $r \to 0$ behaves as [10]

$$\lim_{r\to 0} c_{\text{eff}}(r) = c - 12\Delta_0 \tag{1.82}$$

where Δ_0 is the lowest scaling dimension of a field belonging to the CFT and c the central charge. Recovering the central charge of the expected unperturbed conformal field theory using the TBA equations is one way of checking the validity of the conjectured S-matrix.

1.3 The thermodynamic Bethe ansatz

The thermodynamic Bethe ansatz is an efficient method of calculating the finite-size ground-state energy of a theory entirely from the conjectured scattering amplitudes. In this short section we present the derivation of the TBA equation describing the ground-state energy of the scaling Lee-Yang model.

We start by considering a relativistic quantum field theory defined on a torus, and label the two periods by L and R as shown in Figure 1.4.

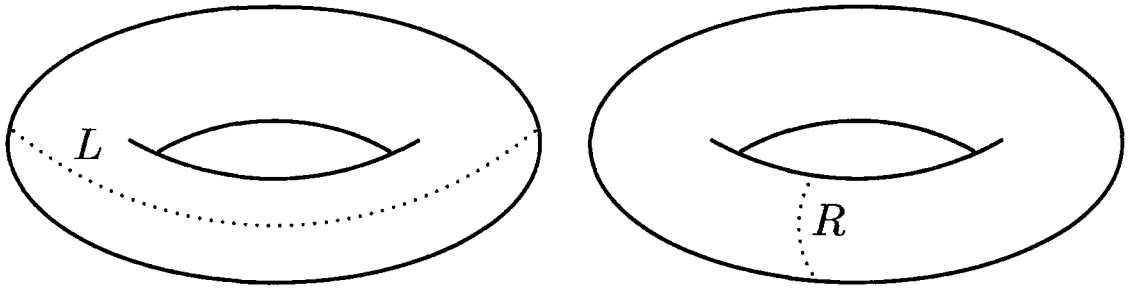

Figure 1.4: The two periods of a torus.

Ultimately we will consider the limit $L \to \infty$ and so the torus will become an infinitely long cylinder of circumference R. There are two ways of passing to the Hamiltonian description on a toroidal geometry corresponding to time being chosen in either the L or the R direction. Starting with the former option the periodicity requires the states to be quantised with momenta $\frac{2\pi m}{L}$ for some integer m. These states evolve in the time-like direction R under the influence of the Hamiltonian H_L. The partition function is $Z(R,L) = Tr(e^{-RH_L})$ and in the limit $L \to \infty$ it behaves as

$$\ln Z(R,L) \sim -LRf(R) \tag{1.83}$$

where $f(R)$ is the free energy per unit length of the quantum field theory at finite temperature $T = 1/R$. Alternatively we can choose to quantise along the L direction where now the momenta will be $\frac{2\pi n}{R}$ (n integer). The states will evolve along the L direction under the Hamiltonian H_R. From this viewpoint the partition function will be dominated by the ground-state energy $E_0(R)$ as $L \to \infty$:

$$Z(R,L) \sim e^{-LE_0(R)}\,. \tag{1.84}$$

Equating (1.83) and (1.84) gives the simple relation

$$E_0(R) = Rf(R)\,. \tag{1.85}$$

Thus if we can calculate the free energy per unit length using the TBA method we will have access to $c_{\text{eff}}(r)$ via the relation (1.81).

We derive the TBA equations for a theory of N identical particles with two-particle amplitude $S(\theta)$. We consider regions of the configuration space where all of the relativistic particles are spatially well separated, $|x_k - x_j| \gg 1/M$, and act like free particles with on-shell energy and momenta $E_k = M\cosh\theta_k$ and $p_k = M\sinh\theta_k$. Ignoring any off-mass shell effects (this is valid provided $L \gg M^{-1}$) the N-particle state can be described by a Bethe wave function $\Phi(x_1,\ldots,x_N) = A(Q)\exp(i\sum_j p_j x_j)$ with $A(Q)$ a configuration dependent function which does not affect the argument below.

If two particles with initial positions $x_k \ll x_{k+1}$ approach each other, interact and then move apart such that the final positions are described by $x_k \gg x_{k+1}$, then we expect the new configuration to be described by a Bethe wave function. We make the assumption that the two wave functions are related by a simple multiplication of the scattering amplitude $S(\theta_k - \theta_{k+1})$.

If the particle x_k is allowed to travel all the way around the cylinder in the L direction, then the wave function will pick up S-matrix contributions each time it scatters with the other particles. When it has returned to its original position the periodicity requirement leads to a quantisation condition for the momentum p_k. Thus we have N (one for each particle) quantisation conditions

$$e^{ip_kL}\prod_{j\neq k} S(\theta_k - \theta_j) = 1\,. \tag{1.86}$$

The logarithm of this equation gives a set of conditions for the possible values of the rapidities θ_k

$$ML\sinh\theta_k - i\sum_{j\neq k}\ln S(\theta_k - \theta_j) = 2\pi n_k\,. \tag{1.87}$$

with N integers n_k.

These transcendental equations are not very tractable in this form, but they can be treated in the thermodynamic limit $L\to\infty$. The number of particles N also tends to infinity, but the ratio is L/N remains finite. In this limit the spectrum condenses and we may introduce a continuous density $\rho^r(\theta)$ to better describe the particles. This is defined to be the number of particles d with rapidity in the interval $(\theta, \theta+\Delta\theta)$

$$\rho^r(\theta) = d/L\Delta(\theta)\,. \tag{1.88}$$

Then we can replace the sum in (1.87) with an integral over the densities

$$ML\sinh\theta_k - iL\int d\theta' \ln S(\theta_k - \theta')\rho^r(\theta') = 2\pi n_k \tag{1.89}$$

There may be values of θ where equation (1.89) holds with an integer n that does not equal any of the n_k. In this case θ is known as a hole whereas the θ_k are called roots. In the Lee-Yang model the particles are considered to be of 'fermionic' type: this

means that each allowed state can only be occupied by one particle. The integers $\{n_k\}$ (once ordered as $n_k < n_{k+1}$) form a monotonically increasing sequence. We can now integrate (1.89) to give an integral equation relating the root density $\rho^r(\theta)$ to the density $\rho(\theta)$ describing all of the allowed states (roots plus holes)

$$M\cosh\theta + \int d\theta' \varphi(\theta-\theta')\rho^r(\theta') = 2\pi\rho(\theta)\,. \tag{1.90}$$

The kernel function $\varphi(\theta)$ is related to the S-matrix via $\varphi(\theta) = -i\frac{d}{d\theta}\ln S(\theta)$.

The rapidity density $\rho(\theta)$ corresponds to every integer being present in the sequence $\{n_k\}$. We define the maximum number of rapidities in the interval $(\theta, \theta+\Delta\theta)$ to be $D = \rho(\theta)L\Delta\theta$. If we fix the number of roots d in a rapidity interval $\Delta\theta$ with density $\rho^r(\theta)$, then the number of ways of obtaining such a configuration from all possible configurations is given by

$$\frac{D!}{d!(D-d)!}\,. \tag{1.91}$$

In the thermodynamic limit the logarithm of this quantity gives the contribution of the rapidity interval $\Delta\theta$ to the entropy $\mathcal{S}$. We can use Stirling's formula to replace the factorials in (1.91) by $\ln\Gamma(z) \sim z\ln z - z + \ldots$ and so find the entropy is

$$\mathcal{S}(\rho,\rho^r) = \int d\theta\,[\rho\ln\rho - \rho^r\ln\rho^r - (\rho-\rho^r)\ln(\rho-\rho^r)]\,. \tag{1.92}$$

The general thermodynamic relation $F = E - T\mathcal{S}$ connects the free energy to the energy, temperature and the entropy of a system. For rapidity densities this becomes a functional in both ρ and ρ^r:

$$RLf(\rho,\rho^r) = RH(\rho^r) - \mathcal{S}(\rho,\rho^r) \tag{1.93}$$

where the total energy of the system is

$$H(\rho^r) = \int d\theta M\cosh\theta\rho^r(\theta)\,. \tag{1.94}$$

To find the thermal equilibrium configuration we need to minimise the free energy per unit length in (1.93) with respect to ρ and ρ^r. The extremum conditions turns out to depend only on the ratio $\rho^r(\theta)/\rho(\theta)$, and so we introduce the pseudoenergy $\varepsilon(\theta)$ and related function $L(\theta)$ via

$$\frac{\rho^r(\theta)}{\rho(\theta)} = \frac{e^{-\varepsilon(\theta)}}{1+e^{-\varepsilon(\theta)}} \quad , \quad L(\theta) = \ln(1+e^{-\varepsilon(\theta)})\,. \tag{1.95}$$

The extremal condition $df = 0$ can be manipulated using the constraint (1.90) to yield a nonlinear integral equation known as the TBA equation

$$\varepsilon(\theta) = MR\cosh\theta - \frac{1}{2\pi}\int d\theta'\varphi(\theta-\theta')L(\theta')\,. \tag{1.96}$$

The extremal free energy per unit length follows from substituting (1.90), (1.94) and (1.96) into (1.93):

$$E_0(R) = Rf(R) = -\frac{1}{2\pi}\int d\theta M \cosh\theta L(\theta)\,. \tag{1.97}$$

The regularisation implicit in the TBA derivation gives the bulk free energy $B(\lambda)$ to be zero so that plugging the solution of (1.96) into (1.97) will allow us to calculate $E_0(R) = -\pi c_{\text{eff}}(r)/6R$. But the ultraviolet central charge is not the only information that can be extracted using the TBA equation. The small r expansion of $c_{\text{eff}}(r)$ allows the scaling dimension of the perturbing field to be extracted, and a comparison can be made with results from conformal perturbation theory. We mention a little more about this at the end of the next section.

1.3.1 The ADE related TBA and the Y-system

Al.B. Zamolodchikov's work [19] provoked a series of papers [20–23] in which the TBA method was extended to cover other diagonal purely elastic scattering theories. The theories in these papers can all be identified with simply laced affine Lie algebras of the ADE type. The number of particles in the scattering theory corresponds to the rank r of the algebra and the mass spectrum is proportional to the positive eigenvalue of the Cartan matrix. For each Lie algebra the related TBA system consists of r pseudoenergies each associated with a particle of mass m_a and satisfying

$$\varepsilon_a(\theta) = m_a R\cosh\theta - \frac{1}{2\pi}\sum_{b=1}^{r}\int d\theta'\,\phi_{ab}(\theta-\theta')\ln(1+e^{-\varepsilon_b(\theta')})\,, \tag{1.98}$$

where the kernel function $\phi_{ab}(\theta)$ is related to the scattering amplitude $S_{ab}(\theta)$ between particle species a and b via

$$\phi_{ab}(\theta) = -i\frac{d}{d\theta}S_{ab}(\theta)\,. \tag{1.99}$$

The S-matrix elements for the A series of models were first conjectured in [24]. The authors of [25] found those for the D and E series as well as proposing a particularly neat notation for all three series of S-matrix elements. This 'block' notation will be explained in more detail in Section 1.4. The authors of [26] independently also found some of the results.

The finite-size energy of the model is determined in terms of the pseudoenergies using

$$E(R) = -\frac{1}{2\pi}\sum_{a=1}^{r} m_a \int d\theta\cosh\theta\ln(1+e^{-\varepsilon(\theta)})\,. \tag{1.100}$$

Al.B Zamolodochikov unified the TBA equations into a consistent form [27] using the incidence matrix l_{ab} of the associated Lie algebra. Each pseudoenergy is

thought of as being 'attached' to a node on the Dynkin diagram of the algebra. The pseudoenergies satisfy the following coupled equations

$$\varepsilon_a(\theta) = m_a R\cosh\theta - \frac{1}{\pi}\sum_{b=1}^{r}\int d\theta'\, l_{ab}\varphi_b(\theta-\theta')\left(m_b R\cosh\theta' - \ln(1+e^{\varepsilon_b(\theta')})\right) . \tag{1.101}$$

Writing the TBA equations in this forms allows the use of a universal kernel which depends only on the Coxeter number h of the Lie algebra

$$\varphi_a(\theta) = \frac{h}{2\cosh\frac{1}{2}h\theta} . \tag{1.102}$$

The term $m_a R\cosh\theta$ is commonly called either the driving or energy term.

Al.B. Zamolodchikov remarked in [27] that the TBA equations encode one particular solution of a set of functional relations. These relations are defined in terms of the functions $Y_a(\theta) = \exp(\varepsilon_a(\theta))$ and they form the so called Y-system:

$$Y_a(\theta - i\pi/h)Y_a(\theta + i\pi/h) = \prod_{b=1}^{r}(1+Y_b(\theta))^{l_{ab}} . \tag{1.103}$$

A curious property of the Y functions, found by successive substitutions of (1.103) into itself by Zamolodchikov [27], is the periodicity

$$Y_a\left(\theta + i\pi(h+2)/h\right) = Y_a(\theta) . \tag{1.104}$$

It follows that the TBA functions $\varepsilon_a(\theta)$ also have this property, and both sets of functions therefore have Laurent expansions

$$\varepsilon_a(\theta) = \sum_{k=-\infty}^{\infty}\varepsilon_a^{(k)}e^{\frac{2h\theta}{h+2}k} \quad , \quad Y_a(\theta) = \sum_{k=-\infty}^{\infty}Y_a^{(k)}e^{\frac{2h\theta}{h+2}k} . \tag{1.105}$$

This information is important because it implies [19]

$$R\Big(E(R)-RB(\lambda)\Big)/2\pi = -c_{\text{eff}}(r)/12 \tag{1.106}$$

will expand in a regular series as $R^{4h/(h+2)}$. The relation between the periodicity and the small r expansion of $c_{\text{eff}}(r)$ will be used in Chapter 3 when we make a comparison with conformal perturbation theory.

1.4 The sine-Gordon model

Another example of a perturbed conformal field theory is provided by the sine-Gordon model. It has been extensively studied in the literature both at the classical and quantum level, and has found applications in many areas of mathematics and physics ranging from partial differential equations to condensed matter physics. At the classical level, the equations of motion have been completely solved via the

inverse scattering method, and the model has been shown to be integrable by the explicit construction of an infinite number of conserved charges, which continue to exist when the model is quantised.

The sine-Gordon action is given by

$$\mathcal{A} = \int dx \frac{1}{2}\partial_\mu\varphi\,\partial^\mu\varphi + \frac{\mu^2}{\beta^2} : \cos\beta\varphi : \tag{1.107}$$

where φ is a real scalar field. The dimensionful parameter μ sets the mass scale whereas the real dimensionless parameter β determines the particle content. We find it more convenient to use the parameter ξ, which is defined to be

$$\xi = \frac{\beta^2}{8\pi - \beta^2} \,. \tag{1.108}$$

The model has infinitely many classical vacua $\varphi(x) = 2n\pi/\beta$, $n \in Z$ and configurations interpolating between different vacua have a conserved spin-zero topological charge

$$Q_0 = \frac{\beta}{2\pi}\int dx\,\partial_x\varphi \,. \tag{1.109}$$

The classical spectrum consists of a soliton (s) with topological charge $Q_0 = +1$ and an antisoliton ($\bar{s}$) with $Q_0 = -1$ which interpolate between neighbouring vacua and are of mass M. These are the only stable solutions with $|Q_0| \geq 1$; however the soliton and antisoliton mutually attract and they can form a continuous family of breather solutions made up of soliton and antisoliton bound states. Their masses range from 0 to $2M$ and they have zero topological charge.

When the theory is quantised, the breather spectrum becomes discrete with masses given by [28]

$$M_k = 2M\sin(\frac{\pi k p}{2}) \quad , \quad k = 1 \ldots < \frac{1}{\xi} \,. \tag{1.110}$$

The existence of breathers neatly divides the sine-Gordon model into two regimes: the repulsive regime $\xi > 1$, in which the particle content consists only of solitons and antisolitons, and the attractive regime $\xi < 1$, which has in addition breather states.

The potential term can be written as

$$\frac{\mu^2}{2\beta^2} : (e^{i\beta\varphi} + e^{-i\beta\varphi}) : \tag{1.111}$$

so that the sine-Gordon model can be considered as a perturbation of a single free massless boson compactified on a circle of radius $\widetilde{R}$, related to ξ via $\widetilde{R}^2 = (1+\xi)/2\xi$. The field content of this $c = 1$ conformal field theory consists of primary fields created by vertex operators $V_{(n,m)}$ and their descendents. Writing the scalar field

$\varphi(x,t)$ in terms of holomorphic and antiholomorphic parts as $\varphi(x,t) = \phi(z) + \bar{\phi}(\bar{z})$ the vertex operators are of the form

$$V_{n,m}(z,\bar{z}) =: \exp\left(i\left(\frac{n}{\widetilde{R}} + \frac{1}{2}m\widetilde{R}\right)\phi(z) + i\left(\frac{n}{\widetilde{R}} - \frac{1}{2}m\widetilde{R}\right)\bar{\phi}(\bar{z})\right) : . \tag{1.112}$$

The conformal weights of the primary fields are

$$\Delta^{\pm} = \frac{1}{2}\left(\frac{n}{\widetilde{R}} \pm \frac{1}{2}m\,\widetilde{R}\right)^2 \tag{1.113}$$

where $m \in \mathbb{Z}$ is identified with the sine-Gordon topological charge Q_0 and $n \in \mathbb{Z}$. In terms of vertex operators the perturbing potential (1.111) is identified with $\mu^2(V_{(1,0)} + V_{(-1,0)})/2\beta^2$.

The sine-Gordon action (1.107) is invariant under the symmetry

$$\varphi \to \varphi + \frac{2\pi n}{\beta} \tag{1.114}$$

for integer n. So the Hilbert space of states $\mathcal{H}$ can be split up into α-sectors, $\mathcal{H}_\alpha$, where the states in each sector transform as $\Psi \to e^{i\alpha}\Psi$ under (1.114). When the model is defined on an infinite line, the transitions (1.114) are suppressed to zero and the spaces $\mathcal{H}_\alpha$ become degenerate. However, when the spatial direction is compactified into a circle of circumference R (so that space-time becomes an infinite cylinder) the degeneracies are lifted and α becomes an important parameter of the model. The various α-vacua (the state in $\mathcal{H}_\alpha$ with lowest energy) are selected by imposing twisted boundary conditions on the cylinder. The vacuum in the sector with $\alpha = 0$ corresponds to the true ground-state energy. The vertex operators creating the primary fields are now given by $V_{(n+\frac{\alpha}{2\pi},m)}$. The twist α plays a particularly important rôle in relation to the nonlinear integral equation which is to be introduced in Section 1.4.2.

The sine-Gordon S-matrix is the minimal $O(2)$-symmetric solution of the defining relations for an S-matrix. That is it satisfies unitarity and crossing as well as the Yang-Baxter relation; for an explanation of these constraints see [17]. We denote the soliton by A and the antisoliton by $\bar{A}$. The two-particle scatterings are [16]:

$$\begin{aligned}
A(\theta_1)A(\theta_2) &= S(\theta_1-\theta_2,\xi)A(\theta_2)A(\theta_1)\\
\bar{A}(\theta_1)\bar{A}(\theta_2) &= S(\theta_1-\theta_2,\xi)\bar{A}(\theta_2)\bar{A}(\theta_1)\\
A(\theta_1)\bar{A}(\theta_2) &= S_T(\theta_1-\theta_2,\xi)\bar{A}(\theta_2)A(\theta_1) + S_R(\theta_1-\theta_2)A(\theta_2)\bar{A}(\theta_1)\,.
\end{aligned} \tag{1.115}$$

The amplitudes can be written using the non-diagonal scattering matrix $\hat{S}$

$$\hat{S}(\theta,\xi) = \begin{pmatrix} S(\theta,\xi) & & & \\ & S_R(\theta,\xi) & S_T(\theta,\xi) & \\ & S_T(\theta,\xi) & S_R(\theta,\xi) & \\ & & & S(\theta,\xi) \end{pmatrix} = S_0(\theta,\xi)\hat{R}(\theta,\xi) \tag{1.116}$$

where the scalar S_0 is

$$S_0(\theta,\xi) = \frac{1}{\sinh((\theta-i\pi)/\xi)} \exp\Big(-i\int_0^\infty \frac{dk}{k}\frac{\sin(k\theta)\sinh(\frac{\pi(1-\xi)k}{2})}{\cosh(\frac{\pi k}{2})\sinh(\frac{\xi\pi k}{2})}\Big), \tag{1.117}$$

and the matrix $\hat{R}$ is given by

$$\hat{R}(\theta,\xi) = \begin{pmatrix} \sinh((\theta-i\pi)/\xi) & & & \\ & -\sinh(i\pi/\xi) & -\sinh(\theta/\xi) & \\ & -\sinh(\theta/\xi) & -\sinh(i\pi/\xi) & \\ & & & \sinh((\theta-i\pi)/\xi) \end{pmatrix}. \tag{1.118}$$

1.4.1 TBA equations

The TBA technique has been applied to the sine-Gordon model for all rational values of ξ in the attractive regime. (For the repulsive regime see the end of this section.) At these rational points the number of coupled nonlinear integral equations becomes finite and essentially follows from work on the XXZ models [29]. The equations depend on writing ξ as a continued fraction:

$$\xi = \xi(n_1, n_2, \ldots, n_F) = \cfrac{1}{n_1 + \cfrac{1}{n_2 + \cdots \cfrac{1}{n_F - 1}}} \tag{1.119}$$

with $n_1 \neq 0$. This representation also allows the related Y-system to be written in a neat way using a Dynkin-like diagram [30, 31]. The TBA system consists of n_1 breathers, a soliton and a total of $\sum_{i=2}^{F} n_i$ magnons (auxiliary functions in the TBA equations not associated to particles). The Y-system is then depicted as a concatenation of a sequence of A_{n_i} Dynkin diagrams ending with a D_{n_F} diagram [31]. The TBA equations can be reconstructed from the Y-system using Fourier transforms.

At the points in the attractive regime where $\xi = \frac{1}{n}$, the sine-Gordon scattering is reflectionless ($S_R = 0$) and the S-matrix simplifies, up to signs, to that of the minimal D_{n+1} related amplitudes. We define the 'block' notation mentioned in Section 1.3.1, commonly used to describe the scattering amplitudes related to the affine Toda theories [25], as

$$x(\theta) = \frac{\sinh(\frac{\theta}{2} + \frac{i\pi x}{2h})}{\sinh(\frac{\theta}{2} - \frac{i\pi x}{2h})} \quad ; \quad \{x\} = (x-1)(x+1) \tag{1.120}$$

where $h = 2n$ is the D_{n+1} Coxeter number. The S-matrix elements are then compactly written as

$$S_{j,k} = \prod_{\substack{|j-k|+1 \\ \text{step } 2}}^{j+k-1} \{l\}\{h-l\} \quad (j,k = 1 \ldots n-1) \tag{1.121}$$

and

$$S_{k,n} = S_{k,n+1} = (-1)^k \prod_{\substack{l=h/2-k+1 \\ \text{step } 2}}^{h/2+k-1} \{l\} \quad (k = 1 \ldots n-1) \tag{1.122}$$

where the labels n and $n+1$ correspond to the soliton and the antisoliton respectively. The remaining elements split into two cases depending on the value of n:

$$n \text{ even} \; : \; S_{n,n} = S_{n+1,n+1} = \prod_{\substack{l=1 \\ \text{step } 4}}^{2n-3} \{l\} \quad ; \quad S_{n,n+1} = \prod_{\substack{l=3 \\ \text{step } 4}}^{2n-1} \{l\} \, ; \tag{1.123}$$

$$n \text{ odd} \; : \; S_{n,n} = S_{n+1,n+1} = \prod_{\substack{l=1 \\ \text{step } 4}}^{2n-1} \{l\} \quad ; \quad S_{n,n+1} = - \prod_{\substack{l=3 \\ \text{step } 4}}^{2n-3} \{l\} \, . \tag{1.124}$$

The TBA system consists of $n+1$ pseudoenergies solving the nonlinear integral equations

$$\varepsilon_j(\theta) = m_j R \cosh\theta - \sum_{k=1}^{n+1} \int \frac{d\theta'}{2\pi} \, \phi_{jk}(\theta - \theta') L_k(\theta') \; , \tag{1.125}$$

where

$$L_k(\theta) = \ln(1 + e^{-\varepsilon_k(\theta)}) \; , \tag{1.126}$$

and the logarithmic derivatives of the S-matrix elements provide the kernels

$$\phi_{jk}(\theta) = -i \frac{d}{d\theta} \ln S_{jk}(\theta) \; . \tag{1.127}$$

The ground-state energy of the finite-size system is given by

$$E(R) = - \sum_{j=1}^{n+1} \int \frac{d\theta}{2\pi} \, m_j \cosh\theta L_j(\theta) \, . \tag{1.128}$$

The TBA system is more convenient for numerical work when written in this form than the universal form mentioned in Section 1.3.1 for the ADE related systems.

Defining $Y_a(\theta) = \exp(\varepsilon_a(\theta))$ the TBA equations can be transformed into the Y-system, which is neatly written using the incidence matrix l_{ab} of the D_{n+1} Lie algebra:

$$Y_a(\theta + \frac{i\pi}{h}) Y_a(\theta - \frac{i\pi}{h}) = \prod_{b=1}^{n+1} (1 + Y_b(\theta))^{l_{ab}} \; . \tag{1.129}$$

Iterating these equations indicate the functions have the following periodicity

$$Y_a(\theta + i\pi(h+2)/h) = Y_a(\theta) \; . \tag{1.130}$$

We will also need the TBA equations at integer values of ξ. They were first proposed in [32, 33]; however, for our purposes it is more convenient to make use of the duality, mentioned in [30], which exists between the attractive regime and repulsive regime. This relates the TBA equations at integer ξ with those at $1/\xi$. The Y-system at ξ is found from that at $1/\xi$ using the following rules

$$h \to 2, \quad Y(\theta) \to Y^{-1}(\theta), \quad M_i \to 0 \, , \, i = 2, \ldots \quad , \quad M_1 = M \tag{1.131}$$

where M is the mass of the soliton.

1.4.2 An alternative equation

An alternative method of calculating the ground-state energy of the sine-Gordon model was proposed by Destri and De Vega in [34]. In fact, the conformal limit of the equation had already been proposed in the context of integrable lattice models by Klümper, Batchelor and Pearce [35].

Destri and De Vega deduced their nonlinear integral equation [1] from a lattice regularization of the model; the equation for the ground-state energy of the sine-Gordon model followed from taking the continuum limit of this equation. Since the resulting NLIE is not deduced from the scattering theory, it provides an independent check of the energy. In addition, agreement between the TBA and NLIE results provides further support for the conjectured scattering amplitudes.

The lattice model is defined by discretizing Minkowski space time in the light cone directions with N lattice sites in the spatial direction each separated by a distance a. Identifying the edges of the lattice by means of periodic boundary conditions results in a cylindrical space-time configuration of circumference $R = Na$. The inhomogeneous 6-vertex model is defined on the lattice with anisotropy parameter γ and inhomogeneity Θ, and then the time evolution operator is diagonalised via the (algebraic) Bethe ansatz, see for example [36]. The result is the following set of Bethe ansatz equations:

$$\left(\frac{\sinh\frac{\gamma}{\pi}(\theta_j+\Theta+\frac{i\pi}{2})\sinh\frac{\gamma}{\pi}(\theta_j-\Theta+\frac{i\pi}{2})}{\sinh\frac{\gamma}{\pi}(\theta_j+\Theta-\frac{i\pi}{2})\sinh\frac{\gamma}{\pi}(\theta_j-\Theta-\frac{i\pi}{2})}\right)^N = -\prod_{l=1}^{M}\frac{\sinh\frac{\gamma}{\pi}(\theta_j-\theta_l+i\pi)}{\sinh\frac{\gamma}{\pi}(\theta_j-\theta_l-i\pi)}\,, \quad (1.132)$$

satisfied by $M \leq N$ complex numbers θ_j, known as roots, describing the Bethe ansatz state under consideration. The 'counting function' $Z(\theta)$ is defined such that

$$Z(\theta_j) = 2\pi I_j \quad , \quad I_j \in \mathbb{Z} + \frac{1}{2} \quad (1.133)$$

at the positions of the roots. The next step is to turn these quantisation conditions into a single nonlinear integral equation [2] which is defined in terms of $f(\theta) = -iZ(\theta)$, and thus satisfies

$$f(\theta_j) = -2\pi I_j\,. \quad (1.134)$$

The ground-state energy of the lattice model is then defined in terms of the function $f(\theta)$. The relation with the sine-Gordon model follows by considering the continuum limit of the lattice model. The limit is taken by sending the number of sites N to infinity, the lattice spacing a to zero and the inhomogeneity Θ to infinity in such a way that the physical mass scale remains fixed, where

$$\Theta \sim \ln\frac{4N}{MR}\,. \quad (1.135)$$

[1] We will refer to equations of such type as NLIEs

[2] We do not present the derivation here. However, in Section 1.5.2 we describe in greater detail another method of deriving the NLIE

The resulting nonlinear integral equation for $f(\theta)$ is

$$f(\theta) = -i\,r\sinh\theta + i\,\alpha + \int_{\mathcal{C}_1} d\theta'\,\varphi(\theta-\theta')\ln(1+e^{f(\theta')}) - \int_{\mathcal{C}_2} d\theta'\,\varphi(\theta-\theta')\ln(1+e^{-f(\theta')})\,. \tag{1.136}$$

In this equation $r = MR$ is the dimensionless volume parameter and the integration contours $\mathcal{C}_1$ and $\mathcal{C}_2$ run just below and above the real axis, and are shown in Figure 1.5. The NLIE, like the TBA equations, implies a periodicity property for its solutions:

$$f(\theta) = f(\theta + i\pi(\xi+1))\,. \tag{1.137}$$

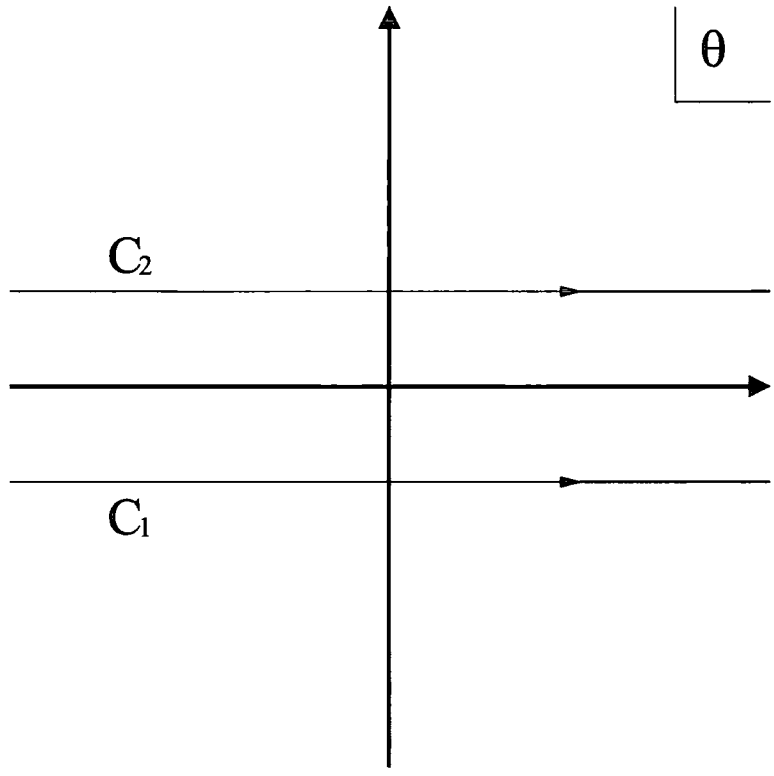

Figure 1.5: The integration contours for the function $f(\theta)$.

The kernel $\varphi(\theta)$ is equal to $\frac{-i}{2\pi}\frac{d}{d\theta}\ln S_0(\theta)$ where $S_0(\theta)$ is related to the scalar factor (1.117) of the sine-Gordon soliton-soliton scattering amplitude:

$$\varphi(\theta) = \int \frac{dk}{2\pi}\,e^{ik\theta}\frac{\sinh(\xi-1)\frac{\pi k}{2}}{2\sinh\frac{\pi\xi k}{2}\cosh\frac{\pi k}{2}}\,. \tag{1.138}$$

The constant α corresponds to allowing general boundary conditions on the lattice rather than periodic ones, and directly corresponds to the twist mentioned in Section 1.4.

Once (1.136) has been solved for $f(\theta)$, the ground-state energy of the model can be calculated using the formula

$$E = -i\,M\left(\int_{\mathcal{C}_1}\frac{d\theta}{2\pi}\sinh\theta\,\ln(1+e^{f(\theta)}) - \int_{\mathcal{C}_2}\frac{d\theta}{2\pi}\sinh\theta\,\ln(1+e^{-f(\theta)})\right)\,. \tag{1.139}$$

One of the advantages of this nonlinear integral equation (NLIE) over the TBA method is that a single NLIE suffices to cover all possible values of ξ. The NLIE (1.136) can be solved iteratively and the energy compared with that found using the TBA method.

1.5 Functional relations in integrable models

So far we have mentioned two types of nonlinear integral equations which independently can be used to calculate the ground-state energy of a quantum field theory. In this section we introduce some work of Bazhanov, Lukyanov and A.B. Zamolodchikov [37,38] in which both types of nonlinear integral equations arose naturally.

The existence of an infinite set of mutually commuting local integrals of motion is a fundamental feature of an integrable quantum field theory and one area of interest has been the diagonalisation of these integrals of motion. Much progress has been made in the theory of solvable lattice models towards this diagonalisation. Baxter introduced a family of commuting transfer matrices, the Ts. They are central in the theory as the spectrum of the quantum problem can be expressed in terms of their eigenvalues. Many powerful algebraic and analytic methods have been developed to diagonalise them, including the method known as quantum inverse scattering.

Baxter defined a further set of matrices, which are known as the Q-matrices. These mutually commute amongst themselves as well as with the Ts and they satisfy Baxter's $T-Q$ functional relation. This relation is extremely restrictive and basically allows the theory to be solved.

A review of solvable lattice models covering the ideas mentioned above can be found in [36]; however this is not the main focus of this thesis. The developed machinery has proven very powerful and it is an interesting avenue of research to find and investigate such structures in the continuum theory; particularly as some quantum field theories can be considered as continuum limits of solvable lattice models. It is for this reason that Bazhanov, Lukyanov and Zamolodchikov have begun to develop the above ideas in the continuous quantum field theory. They began by considering conformal models [37] and later extended the ideas to include a small subset of the massive models [39].

1.5.1 T-operators

Bazhanov, Lukyanov and Zamolodchikov began [37] by considering a conformal field theory with central charge c less than 1. The energy-momentum tensor $T(z)$ can be mode expanded as

$$T(u) = -\frac{c}{24} + \sum_{n\in\mathbb{Z}} L_{-n} e^{inu} . \tag{1.140}$$

The operators L_n satisfy the Virasoro algebra and the space of states splits up into a tensor product of left and right irreducible highest weight representations of this algebra

$$\mathcal{H} = \bigoplus_{h\bar{h}} \mathcal{V}_h \otimes \mathcal{V}_{\bar{h}} \,. \tag{1.141}$$

We define h to be the weight of the highest weight vector $|h\rangle \in \mathcal{V}_h$.

The energy-momentum tensor can equally be defined in terms of the free field operator

$$\varphi(u) = iQ + iPu + \sum_{n\neq 0} \frac{a_{-n}}{n} e^{inu} \tag{1.142}$$

as

$$-\beta^2 T(u) =: \varphi'(u)^2 : + (1-\beta^2)\varphi''(u) + \frac{\beta^2}{24}, \tag{1.143}$$

where β is related to the central charge via

$$\beta = \sqrt{\frac{1-c}{24}} - \sqrt{\frac{25-c}{24}} \,. \tag{1.144}$$

The operators P, Q and a_n satisfy the Heisenberg algebra

$$[Q,P] = \frac{i}{2}\beta^2 \quad ; \quad [a_n, a_m] = \frac{n}{2}\beta^2\, \delta_{n+m,0} \,. \tag{1.145}$$

The vacuum is defined as the vector $|p\rangle$ satisfying

$$a_n|p\rangle = 0 \quad \text{for } n > 0 \quad ; \quad P|p\rangle = p|p\rangle \,. \tag{1.146}$$

A Fock space $\mathcal{F}_p$ can be generated by the action of the operators a_n, with $n < 0$, on the highest weight vector, the vacuum, $|p\rangle$. The space $\mathcal{F}_p$ is then isomorphic to the highest weight Virasoro module $\mathcal{V}_p = \mathcal{V}_h$ provided [40]

$$h = \left(\frac{p}{\beta}\right)^2 + \frac{c-1}{24} \,. \tag{1.147}$$

The continuum analogue of Baxter's quantum transfer matrices is an infinite family of operators $\mathbf{T}_j(\lambda), j = 0, \frac{1}{2}, 1, \frac{3}{2}, \ldots$ defined in terms of $\varphi(u)$ and acting invariantly in each representation space $\mathcal{V}_h \equiv \mathcal{F}_p$. The $\mathbf{T}_j(\lambda)$ mutually commute with each other and both the operators and their eigenvalues are entire functions of λ^2; a proof of these properties can be found in [41].

The precise definition of these operators is not relevant to the following and instead we concentrate on the following functional relations [37]

$$\mathbf{T}_j(q^{\frac{1}{2}}\lambda)\mathbf{T}_j(q^{-\frac{1}{2}}\lambda) = 1 + \mathbf{T}_{j-\frac{1}{2}}(\lambda)\mathbf{T}_{j+\frac{1}{2}}(\lambda) \,. \tag{1.148}$$

The parameter q is related to β^2 via $q = \exp(i\pi\beta^2)$ and the system of equations are known as the fusion relations. Using these equations any operator $\mathbf{T}_j$ can be

expressed in terms of the fundamental operator $\mathbf{T}_{\frac{1}{2}}$. In particular the large λ^2 asymptotic of each operator can be found from that of $\mathbf{T}_{\frac{1}{2}}$

$$\ln \mathbf{T}_{\frac{1}{2}}(\lambda) \sim \lambda^{1+\xi} \quad , \quad |\lambda^2| \to \infty \quad , \quad \arg(\lambda^2) < \pi \; , \tag{1.149}$$

where $\xi = \beta^2/(1-\beta^2)$.

In general the fusions relations do not close, but if β^2 is a rational number then q is a root of unity and the fusion relations truncate within a finite number of operators [37]. Let $N \geq 2$ be the smallest positive integer such that $q^N = \pm 1$. Then truncation occurs because of the relation

$$\mathbf{T}_{\frac{N}{2}+\frac{1}{2}}(\lambda) = 2\cos(2\pi N p) + \mathbf{T}_{\frac{N}{2}-1}(\lambda) \, . \tag{1.150}$$

We can now make a connection with previous sections: we will show that the eigenvalues of these operators are related to the TBA equations of D_N type. To see this let $T_j(\lambda, p)$ (the p dependence will be left implicit in the following) be the eigenvalue of the operator $\mathbf{T}_j(\lambda)$ on the vacuum $|p\rangle$ in $\mathcal{V}_p$. We define a new variable θ by $\theta = \ln(\lambda^{1+\xi})$. The Y functions are then defined as

$$\begin{aligned} Y_j(\theta) &= T_{j+\frac{1}{2}}(\lambda) T_{j-\frac{1}{2}}(\lambda) \quad , \quad j = \tfrac{1}{2}, 1, \ldots, \tfrac{N}{2}-1, \\ Y_0(\theta) &= 0 \\ \overline{Y}(\theta) &= T_{\frac{N}{2}-1}(\lambda) \end{aligned} \tag{1.151}$$

Plugging these into (1.148) results in the Y-system of D_N type, introduced in Section 1.4.1. The functions $Y_j(\theta)$ for $j = \frac{1}{2}, 1, \ldots, \frac{N}{2} - \frac{3}{2}$ are associated with the nodes 1 to $N-2$ of the D_N Dynkin diagram. They satisfy the following equations

$$Y_j\left(\theta + \frac{i\pi\xi}{2}\right) Y_j\left(\theta - \frac{i\pi\xi}{2}\right) = \left(1 + Y_{j-\frac{1}{2}}(\theta)\right)\left(1 + Y_{j+\frac{1}{2}}(\theta)\right) . \tag{1.152}$$

The fork nodes of the Dynkin diagram are associated with $\overline{Y}(\theta)$ and $Y_{\frac{N}{2}-1}(\theta)$ and they satisfy

$$\begin{aligned} Y_{\frac{N}{2}-1}\left(\theta+\frac{i\pi\xi}{2}\right) Y_{\frac{N}{2}-1}\left(\theta-\frac{i\pi\xi}{2}\right) &= \left(1+Y_{\frac{N}{2}-\frac{3}{2}}(\theta)\right)\left(1+e^{2\pi i p N}\,\overline{Y}(\theta)\right)\left(1+e^{-2\pi i p N}\,\overline{Y}(\theta)\right) \\ \overline{Y}\left(\theta + \frac{i\pi\xi}{2}\right)\overline{Y}\left(\theta - \frac{i\pi\xi}{2}\right) &= 1 + Y_{\frac{N}{2}-1}(\theta) \; . \end{aligned} \tag{1.153}$$

These functional equations have an infinite number of solutions. Nevertheless the one we require is picked out uniquely by the pattern of zeros of the vacuum eigenvalues $T_j(\lambda)$. For these eigenvalues all zeros are located along the negative real axis of the complex λ^2-plane [37]. Higher states in $\mathcal{V}_p$ have in addition a finite number of complex zeros and real zeros located along the positive real axis.

The relevant TBA equations, quoted in Section 1.4.1, are those associated to the ground-state energy of the corresponding quantum field theory. However we must

modify the form of the driving terms to match the large λ^2 asymptotics (1.149) of the eigenvalues $T_j(\lambda)$. This has the following effect upon the driving terms

$$m_j R \cosh\theta \to m_j e^{\theta} \ . \tag{1.154}$$

1.5.2 Q-operators

In the context of solvable lattice models Baxter introduced a further family of matrices Q, depending on λ, having the property that they all commute with the Hamiltonian of the model. The eigenvalues of these operators satisfy the Baxter (TQ) equation. This is a finite difference equation of second order and, combined with appropriate boundary conditions, enables the spectrum of the Hamiltonian to be computed exactly. The continuum analogues of the lattice Q-matrix, defined in [38], are two operators $\mathbf{Q}_{\pm}(\lambda)$ that act in the highest weight module $\mathcal{V}_p$ and commute amongst themselves as well as with the $\mathbf{T}$-operators. Again the precise form is unimportant in the following, and we concentrate on the following functional relation known as the $\mathbf{T}-\mathbf{Q}$ relation:

$$\mathbf{T}(\lambda)\mathbf{Q}(\lambda) = \mathbf{Q}(q\lambda) + \mathbf{Q}(q^{-1}\lambda) \, . \tag{1.155}$$

From now on $\mathbf{T}(\lambda) = \mathbf{T}_{\frac{1}{2}}(\lambda)$ and $\mathbf{Q}(\lambda)$ without subscripts means either $\mathbf{Q}_{+}(\lambda)$ or $\mathbf{Q}_{-}(\lambda)$.

The $\mathbf{Q}$-operators also satisfy the "quantum Wronskian" condition [38]

$$\mathbf{Q}_{+}(q^{\frac{1}{2}}\lambda)\mathbf{Q}_{-}(q^{-\frac{1}{2}}\lambda) - \mathbf{Q}_{+}(q^{-\frac{1}{2}}\lambda)\mathbf{Q}_{-}(q^{\frac{1}{2}}\lambda) = 2i\sin(2\pi p) \tag{1.156}$$

which will play an important rôle in Chapter 4.

To make a connection with the second type of nonlinear integral equation we need to define some more notation. Since the $\mathbf{Q}_{\pm}$ operators are in general multi-valued functions of λ^2, we use the single-valued operators $\mathbf{A}_{\pm}(\lambda)$ defined as

$$\mathbf{Q}_{\pm}(\lambda) = \lambda^{\pm 2p/\beta^2}\mathbf{A}_{\pm}(\lambda) \, . \tag{1.157}$$

When $\mathbf{A}_{\pm}(\lambda)$ acts in the space $\mathcal{V}_p$ on the vacuum $|p\rangle$ we denote its eigenvalue $A_{\pm}(\lambda)$. Evaluating the operator equation (1.155) on $|p\rangle \in \mathcal{V}_p$ yields a functional equation between the corresponding vacuum eigenvalues

$$T(\lambda)A(\lambda) = e^{2\pi i p}A(q\lambda) + e^{-2\pi i p}A(q^{-1}\lambda) \ . \tag{1.158}$$

After establishing some necessary analytic properties of these functions, this equation will lead to a nonlinear equation of the type introduced in Section 1.4.2, whose solution will provide the zeros of the (unknown) functions $A_{\pm}(\lambda)$.

The operators $\mathbf{Q}(\lambda)$ are defined in terms of integrals which diverge for some values of β^2. To ensure convergence we restrict β^2 to the semi-classical domain

$$0 < \beta^2 < \frac{1}{2} \tag{1.159}$$

and initially consider $\Im m\, p = 0$. First, some assumptions are made about the analytic properties of the eigenvalue $A(\lambda) \equiv A_+(\lambda)$ [38]: [3]

- $A(\lambda)$ is an entire function of λ^2; a proof of this can be found in [41].
- The zeros of $A(\lambda)$ in the λ^2-plane are either real or occur in complex conjugate pairs. Furthermore, there are only a finite number of complex or real negative zeros, and for the vacuum eigenvalue all the zeros are real and positive if $2p > -\beta^2$. In contrast, recall that the zeros of the vacuum eigenvalue $T(\lambda)$ sit on the negative segment of the real axis of the λ^2-plane. This information will be needed during the derivation of the nonlinear integral equation. More discussion on the positions of zeros can be found in Section 4.3.
- $A(\lambda)$ has the following asymptotic behaviour

$$\ln \mathbf{A}(\lambda) \sim M(-\lambda^2)^{1/(2-2\beta^2)} \quad , \; |\lambda^2| \to \infty \quad , \quad \arg(-\lambda^2) < \pi \; . \tag{1.161}$$

  where the constant M is given by [38]

$$M = \frac{\Gamma(\frac{\xi}{2})\Gamma(\frac{1}{2}-\frac{\xi}{2})}{\sqrt{\pi}} \Gamma(1/(1+\xi))^{1+\xi} \tag{1.162}$$

The order of an entire function $f(z)$ is defined to be equal to the lower bound of all positive numbers B such that $|f(z)| = \mathcal{O}(e^{|z|^B})$ as $|z| \to \infty$. The Hadamard factorisation theorem states that an entire function of order less than 1 with zeros $\{z_k\}$ can be written as a convergent product [42]:

$$f(z) = f(0) \prod_k \left(1 - \frac{z}{z_k}\right) \; . \tag{1.163}$$

The product diverges for functions of order greater than 1, but can be made convergent by introducing extra factors.

The asymptotic behaviour (1.161) indicates $A(\lambda)$ is of order $1/(2-2\beta^2)$ and this is certainly less than 1 for β^2 in the range $0 < \beta^2 < \frac{1}{2}$. The Hadamard factorisation theorem implies $A(\lambda)$ is completely determined by its zeros λ_k^2, $k = 0, 1, \ldots$ and can therefore be written

$$A(\lambda) = \prod_{k=0}^{\infty} \left(1 - \frac{\lambda^2}{\lambda_k^2}\right) \tag{1.164}$$

[3] Similar properties hold for $A_-(\lambda)$ since, restoring the p dependence, the functions are related via

$$A_-(\lambda, p) = A_+(\lambda, -p) \; . \tag{1.160}$$

where the normalisation condition is chosen to be $A(0) = 1$. We rewrite the $T-Q$ relation (1.158)

$$T(\lambda)A_{\pm}(\lambda) = e^{\mp 2i\pi P}A_{\pm}(q^{-1}\lambda)\left(1 + e^{\pm 4\pi i p}\frac{A_{\pm}(\lambda q)}{A_{\pm}(\lambda q^{-1})}\right), \tag{1.165}$$

and set $\lambda^2 = \lambda_k^2$, $k = 0, 1, \ldots$. Since $T(\lambda)$ is entire the left hand side is zero. This implies the following Bethe ansatz type of equations

$$a_{\pm}(\lambda_k) = -1 \tag{1.166}$$

where we have defined a new function

$$a_{\pm}(\lambda) = e^{\pm 4\pi i p}\frac{A_{\pm}(\lambda q)}{A_{\pm}(\lambda q^{-1})}\,. \tag{1.167}$$

The infinite set of equations (1.166) will now be transformed into a single nonlinear integral equation following [38]. First the product representation (1.164) implies

$$\ln a(\lambda) = 4\pi i p + \sum_{k=0}^{\infty} F(\lambda\lambda_k^{-1}) \tag{1.168}$$

where

$$F(\lambda) = \ln\frac{1 - q^2\lambda^2}{1 - q^{-2}\lambda^2}\,. \tag{1.169}$$

If the function $1 + a(\lambda)$ has a zero at $\lambda^2 = \lambda_k^2$, then the logarithmic derivative $\partial_\lambda \ln(1 + a(\lambda))$ has a simple pole at that point. The residue theorem then implies

$$F(\lambda_k) = \int_\Gamma \frac{d\lambda}{2\pi i} F(\lambda/\lambda_k)\ln(1 + a(\lambda)) \tag{1.170}$$

where $F(\lambda)$ is *any* entire function and Γ is a curve encircling λ_k^2 anti-clockwise and avoiding all other singularities. We use this to rewrite the sum in (1.168) as a contour integral where the contour Γ goes from $+\infty$ to zero just above the positive real axis, and then returns to infinity just below the positive real axis of the complex λ^2-plane. This takes into account all of the zeros which are on the positive real axis and we just need to add in a term to account for the finite number of zeros in the complex plane or on the negative real axis. We also assume that the only points within the contour Γ such that $1 + a(\lambda) = 0$ are those at λ_k^2, $\quad k = 1, \ldots$. We now have

$$\ln a(\lambda) = 4\pi i p + f(\lambda) + \int_\lambda \frac{d\lambda'}{2\pi i} F(\lambda/\lambda')\partial_{\lambda'}\ln(1 + a(\lambda'))\,. \tag{1.171}$$

The additional term

$$f(\lambda) = \sum_j F(\lambda/\lambda_j) \tag{1.172}$$

accounts for the zeros not on the positive real axis. We now introduce the parameter θ via $\lambda = \exp(\theta/(1 + \xi))$ and integrate by parts to rewrite this equation as

$$\ln a(\theta) - \int d\theta' R(\theta - \theta')\ln a(\theta - i0) = 4\pi i p + f(\theta) - 2i\int d\theta' R(\theta - \theta')\Im m \ln(1 + a(\theta' - i0)) \tag{1.173}$$

where we have used the property $a(\lambda)^* = a(\lambda^*)^{-1}$, and the function $R(\theta)$ is

$$R(\theta) = \frac{i}{2\pi}\partial_\theta F(e^{2\theta/(\xi+1)}) \,. \tag{1.174}$$

We solve equation (1.173) for $\ln a(\theta)$ by taking the Fourier transform of both sides. Our conventions for the Fourier transform can be found in Appendix A as well as formulae for the transform of $R(\theta)$. Transforming back, we find the solution is

$$\begin{aligned} \ln a_\pm(\theta) &= -2\,i\,M\cos\frac{\pi\xi}{2}\,e^\theta \pm \frac{2i\pi p}{\beta^2} - \sum_j \ln S_0(\theta-\theta_j) \\ &\quad + \int_{\mathcal{C}_1} \varphi(\theta-\theta')\ln(1+a_\pm(\theta)) - \int_{\mathcal{C}_2} \varphi(\theta-\theta')\ln(1+a_\pm^{-1}(\theta)) \,. \end{aligned} \tag{1.175}$$

where we have rewritten the imaginary part in terms of values above and below the real axis, and the integration contours are shown in Figure 1.5. The kernel function

$$\varphi(\theta) = \int \frac{dk}{2\pi}\, e^{ik\theta}\, \frac{\sinh(\xi-1)\frac{\pi k}{2}}{2\sinh\frac{\pi\xi k}{2}\cosh\frac{\pi k}{2}} \,, \tag{1.176}$$

is exactly the logarithmic derivative of the scalar factor used in the description of the sine-Gordon scattering amplitudes (1.138). The asymptotic behaviour (1.161) fixes the coefficient of e^θ, and in-line with earlier notation we now set

$$\alpha_\pm = \pm 2\pi p/\beta^2 \,. \tag{1.177}$$

The points $\lambda_j = \exp(\theta_j/(1+\xi))$ represent the finite number of complex and negative zeros and the nonlinear integral equation must be supplemented with the additional equations

$$a_\pm(\theta_j) = -1 \,. \tag{1.178}$$

Comparing the equations (1.136) and (1.175) we see that this is exactly the nonlinear integral equation for the sine-Gordon model in its conformal limit ($r \to 0$). We must equate $\ln a_+(\theta) = f(\theta)$, and the restriction on β translates to the attractive regime $0 < p < 1$. After solving this equation, we can search for the zeros of $1+a_\pm(\lambda)$ on the positive real axis of the complex λ^2-plane to find the zeros of $A_\pm(\lambda)$.

These equations hold for any value of β^2 within the semi-classical domain (1.159). However, if β^2 is such that $q^N = \exp(i\pi N\beta^2)$ is a root of unity for some integer N, then a further set of relations hold between the $\mathbf{T}$ and $\mathbf{Q}_\pm$-operators [41]:

$$\mathbf{T}_{\frac{N}{2}-\frac{1}{2}}(\lambda) = \frac{\sin(2\pi Np)}{\sin(2\pi p)}\mathbf{Q}_+(\lambda q^{\frac{N}{2}})\mathbf{Q}_-(\lambda q^{\frac{N}{2}}) \,. \tag{1.179}$$

The fusion relations, the $\mathbf{T}$–$\mathbf{Q}$ relation and the functional equations given by (1.179) will be important in Chapter 2, where they will be used to establish connections between the TBA and NLIE functions.

1.6 Interpolating flows

So far we have considered perturbations of conformal field theories that result in massive integrable quantum field theories. However, this behaviour is not the only possibility as there is another class of theories resulting from a perturbation of a conformal field theory: the 'massless flows'. Just as for the massive case, the conformal symmetry is initially broken by perturbing the ultraviolet fixed point with a relevant operator. In contrast to the massive case, the model retains massless excitations during the flow. The model is once again conformally invariant in the infrared (IR) limit, but is now described by a different conformal field theory.

The first examples of such interpolating flows were found independently by A.B. Zamolodchikov [43] and Ludwig and Cardy [44] in 1987. They arose as ϕ_{13} perturbations of the unitary minimal models $\mathcal{M}_{p,p+1}$. We will use the shorthand

$$\mathcal{M}_{p,q} + \phi_{rs} \to \mathcal{M}_{n,m} \tag{1.180}$$

to indicate a perturbation of the model $\mathcal{M}_{p,q}$ by ϕ_{rs} which results in an interpolating flow to $\mathcal{M}_{n,m}$. We also use the convention $p < q$ in the specification of a minimal model$\mathcal{M}_{p,q}$. Perturbative renormalisation group arguments (valid for $p \gg 1$) in [43] (also [44]) were used to show that for one sign of the coupling constant the resulting flow is

$$\mathcal{M}_{p,p+1} + \phi_{13} \to \mathcal{M}_{p-1,p}\,. \tag{1.181}$$

(The other sign of the coupling constant leads to the massive model.)

A.B. Zamolodchikov also observed that the massless perturbations by the operator ϕ_{13} are, like the massive perturbations, integrable. This observation allowed the perturbative calculation to be confirmed by Al.B. Zamolodchikov using ideas from the thermodynamic Bethe ansatz [45]. Exact integral equations were proposed to describe the evolution of the ground-state energy all the way from the UV to the IR. Al.B. Zamolodchikov [45] began by considering the massless flow between the minimal models $M_{4,5}$ and $M_{3,4}$ induced by the operator ϕ_{13}. He proposed S-matrices to describe the massless scattering and from these derived the TBA equations. The resulting equations were based upon the A_2 Dynkin diagram and, apart from the form of the energy terms, coincided with the TBA equations describing the *massive* perturbation of $M_{4,5}$ by the same operator. The similarity between massive and massless TBA systems is described in more detail in Section 3.4.4. In this case it prompted conjectures for the equations describing the models with $p > 4$. The equations were then subjected to analytical and numerical checks confirming their validity. For a large number of models it has subsequently proven possible to make an educated guess for the TBA equations and then check they have the expected features: that is in the UV limit the characteristics of the unperturbed CFT reap-

pear. For TBA equations describing interpolating flows, the effective central charge at large r can also be compared with the expected IR value.

A conformal field theory does not have to be unitary for an integrable perturbation to exist, and A.B. Zamolodchikov's counting argument also works for the nonunitary models. The argument, presented in Section 1.2.1, relied in part on the infinite sum (1.67) truncating. Provided that the dimensions of the fields in the nonunitary minimal model are bounded below the sum will again truncate. The comparison of dimensions then demonstrates the existence of conserved charges, just as before. In [46,47] the renormalisation group arguments of [43] were extended to include ϕ_{13} perturbations of more general minimal models $\mathcal{M}_{p,q}$. The results indicated that there should exist integrable flows

$$\mathcal{M}_{p,q} + \phi_{13} \to \mathcal{M}_{2p-q,p}\,, \tag{1.182}$$

at least in the region $p \gg q-p$ where calculations perturbative in $(q-p)/p$ can be trusted.

The unitary and nonunitary models can be put on a common footing by defining a parameter $\xi = p/(q-p)$. The value of ξ suffices to identify p and q uniquely since they must be coprime. In all cases the predicted flow is from the model specified by ξ to the model specified by $\xi-1$. The TBA approach is not constrained to the region $p \gg q-p$ but so far TBA equations are not known for any of the nonunitary flows. However we have another means of accessing the ground-state energy of the massive models: the single nonlinear integral equation given by (1.136). The real coupled sine-Gordon model is known [48, 49] to also describe the minimal models $M_{p,q}$ perturbed by ϕ_{13} if the parameter ξ is tuned to $\xi = p/(q-p)$. At the level of the massive nonlinear integral equation, the ground-state energy of the massive models is reproduced if, in addition to tuning ξ, the twist is set to $\alpha = 1/p$ [50]. The flows between minimal models perturbed by the operator ϕ_{13} are related to flows within the sine-Gordon model when the coupling λ in the action (1.107) is taken to be imaginary [51]. The massive equation does not describe the interpolating flows. However, the form of the equation enabled Al.B. Zamolodchikov to conjecture two coupled integral equations which do describe such flows between the minimal models [52]. We should mention one problem here: both the TBA equations and the NLIE predict the effective central charge rather than the central charge itself. This means that neither of these methods can uniquely predict which minimal model $M_{p',q'}$ corresponds to the IR point of a flow. The type II conjecture, the details of which can be found in Section 3.3.1, illustrates this problem.

Many massless flows have been discovered and studied mainly using the TBA technique: the papers [32, 53–64] are a sample of this work. We take a slightly different approach and in Chapter 3 we find new families of flows between minimal

models using a single nonlinear integral equation.

1.7 Spectral problems

In this chapter we have introduced two different sets of functional relations: the Y-systems related to the integral equations of TBA type and the $T-Q$ relation which led to a further nonlinear integral equation. These functional relations and related integral equations continue to be of fundamental importance in an unexpected direction of research. Dorey and Tateo [96] have shown how objects normally seen in integrable quantum field theory also arise in the study of the spectra of ordinary differential equations (ODEs). We delay an introduction to these ideas until Section 4.1.

1.8 Layout of thesis

The central theme throughout this thesis is the use of nonlinear integral equations to calculate the finite-size effects of a quantum field theory. In Chapter 2 we study the excited states of the sine-Gordon model using both types of nonlinear integral equations introduced in this chapter. In Chapter 3 we derive a single nonlinear integral equation which describes interpolating flows between nonunitary minimal models.

In Chapter 4 we describe how nonlinear integral equations have been successfully used to numerically solve eigenvalue problems of certain ordinary differential equations. The connection between integrable quantum field theory and spectral problems associated with ordinary differential equations is a new direction of research that is currently under investigation by a number of researchers. In Chapter 5 I suggest some directions for future research.

Chapter 2

The twisted sine-Gordon model

In Chapter 1 we discussed general aspects of finite-size effects and how they have been used to explore perturbed conformal field theories. In particular one of the questions asked was 'what is the energy of the ground-state?'. Due to the discrete nature of the spectrum in a finite geometry the ground state sits at the bottom of a tower of further states. We can therefore ask what are the values of the energies of these excited states? This question can be motivated by a further question: 'what are the corrections to the energy of an n-particle state due to the finite-size geometry?'.

The TBA method has proven to be a powerful tool in the study of integrable quantum field theories, particularly for the calculation of the ground-state energy of a model. However, this method initially does not look very promising as a way of calculating the excited state energies, since taking the thermodynamic limit in the derivation explicitly singles out the ground-state of the theory. Some progress was made by the authors of [65]. They calculated the excited states of the scaling Lee-Yang model using TBA like equations. At about the same time, the authors of [38] proposed similar equations based on a knowledge of the analyticity properties of certain functions within finite strips of the complex plane. The method of [65], which will be rather more relevant in this chapter, relied on a trick of analytic continuation in the complex plane, and we begin with a short review of their ideas.

2.0.1 Excited states in the scaling Lee-Yang model

Bender and Wu [66] first used the idea of analytical continuation in a suitable parameter to move between the energy levels of the quantum anharmonic oscillator. A more relevant example in 1+1 dimensions is provided by the finite-size spectrum of the thermal Ising model. This massive quantum field theory is obtained by taking the scaling limit of the critical Ising model at non-critical temperature. The simplest unitary minimal model $\mathcal{M}_{3,4}$ is identified with the critical Ising model,

and perturbing this model by the operator ϕ_{13} corresponds to the thermal Ising model. It has one free particle: a single massive boson with scattering described by the S-matrix $S(\theta) = -1$. We do not need to use the TBA method to calculate the ground-state energy of a free particle, but for this model the TBA derivation yields a formula which, after some manipulation, explicitly shows the presence of square-root branch points. The TBA equation is trivially solved by

$$\varepsilon(\theta) = r\cosh\theta \tag{2.1}$$

and the ground-state energy on a cylinder of circumference R can be found exactly [23]:

$$\begin{aligned} E_0(R) &= RB(\lambda) - \frac{\pi}{6R}\left(\frac{1}{2} - \frac{3r^2}{2\pi^2}\left[-\ln r + \frac{1}{2} + \ln\pi - \gamma_E\right]\right. \\ &\quad \left. + \frac{6}{\pi}\sum_{k=1}^{\infty}\left(\sqrt{(2k-1)^2\pi^2 + r^2} - (2k-1)\pi - \frac{r^2}{2\,(2k-1)\pi}\right)\right) \end{aligned} \tag{2.2}$$

where $r = MR$, $\gamma_E = 0.57721556...$ is the Euler-Mascheroni constant and $B(\lambda)$ the bulk term. This formula has, in addition to the logarithmic singularity at $r = 0$, a sequence of square-root branch cuts along the imaginary axis. Suppose the first n singularities are at $k_1, k_2, \ldots, k_n$. If R is continued into the complex plane along a path which encloses these singularities, then we find upon return to the real axis that $E_0(R)$ has undergone a nontrivial monodromy and has become [23]

$$E_{k_1,\ldots,k_n}(R) = E_0(R) + \frac{2}{R}\sum_{i=1}^{n}\sqrt{r^2 + (2k_i - 1)^2\pi^2}\,. \tag{2.3}$$

This is exactly the expected form for the energy of an excited state with ultraviolet scaling dimension $\sum_i (2k_i - 1)$.

The authors of [65] adapted the idea of analytical continuation in $r = MR$ to the scaling Lee-Yang model. In contrast to the Ising model, and because an explicit expression for the ground-state energy is not known, the starting point was the basic TBA equation (1.96) and the corresponding equation for the ground-state energy (1.97).

The idea was to consider the ground-state energy as a function of complex r and map out the different sheets of the Riemann surface. The various sheets, each corresponding to a distinct state in the model, are connected by square-root branch points. Once a branch point connecting the ground-state with the first excited state had been located, the plan was to continue r along a suitable path around it in the hope of inducing a monodromy in $E(r)$. Just as for the Ising case, the result would be the conversion of the ground-state into an excited state.

The continuation was first done numerically by solving the TBA equations at a real value of r. Then, with each iteration using the previous solution as the starting

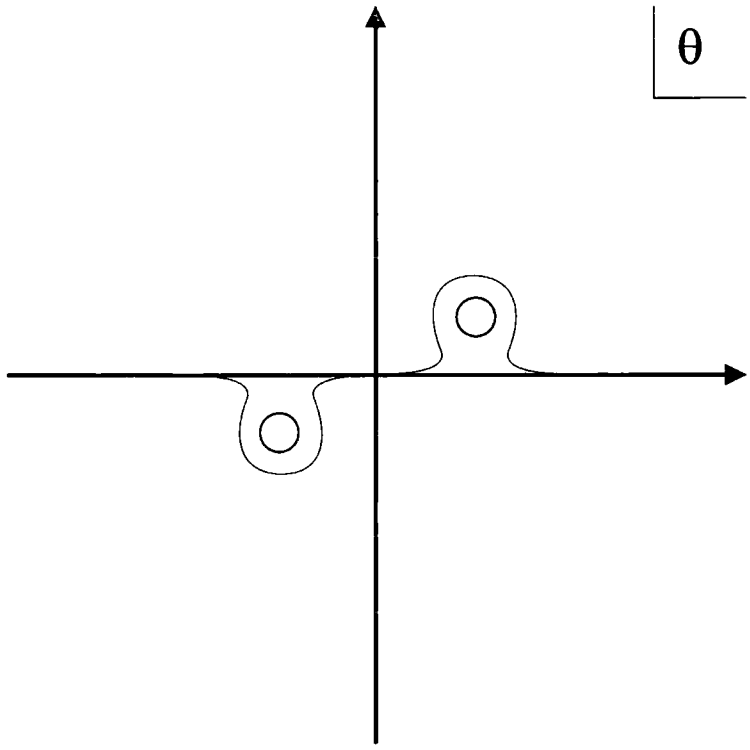

Figure 2.1: The deformed integration contour $\mathcal{C}'$. The positions of the two singularities are both depicted using the symbol ○.

point for the next iteration, r was continued into the complex plane, around the branch point and back to the real axis. During the continuation singularities in the logarithmic term $L(\theta) = \ln(1+e^{-\varepsilon(\theta)})$ were found to approach the integration contour along the real axis forcing the contours to be deformed. The TBA equations are even in θ so singularities are always tied together in pairs at $(\theta_0, -\theta_0)$, and we take $\Im m(\theta_0)$ to be positive after the singularities have crossed the integration contour. The integration contour starts at $-\infty$ and initially follows the real axis, but as it heads towards $-\theta_0$ it must be deformed down and below to avoid the singularity $-\theta_0$ crossing the contour, and then up and above the path of the singularity at θ_0 before returning to the real axis and proceeding to $+\infty$.

The term in the TBA equations containing the logarithmic singularities is

$$-\int_{\mathcal{C}'} \frac{d\theta'}{2\pi}\, \varphi(\theta-\theta') \ln(1+e^{-\varepsilon(\theta')}) \tag{2.4}$$

where $\mathcal{C}'$ is the deformed contour shown in Figure 2.1.

A straightforward integration by parts turns the singularities into simple poles

$$-\int_{\mathcal{C}'} \frac{d\theta'}{2\pi} i\, \ln S(\theta-\theta') \frac{e^{-\varepsilon(\theta')}\, \partial_{\theta'}\varepsilon(\theta')}{1+e^{-\varepsilon(\theta')}}\,. \tag{2.5}$$

Cauchy's Theorem then allows the integration contour to be returned to the real axis with the addition of residue terms containing the explicit positions of the sin-

gularities. The new TBA equation is

$$\varepsilon(\theta) = r\cosh\theta - \int_{-\infty}^{\infty} \frac{d\theta'}{2\pi}\,\varphi(\theta-\theta')\ln(1+e^{-\varepsilon(\theta')}) + \ln\frac{S(\theta-\theta_0)}{S(\theta+\theta_0)}\,. \tag{2.6}$$

The energy equation also depends on $\ln(1+e^{-\varepsilon(\theta)})$ and must be similarly modified. The result is

$$E(r) = -i\,M\sinh\theta_0 - M\int\frac{d\theta}{2\pi}\cosh\theta\ln(1+e^{-\varepsilon(\theta)})\,. \tag{2.7}$$

The TBA equation now seems to have one unknown – the position of the singularity θ_0. However, this is fixed by its definition, that is it must satisfy $1+e^{-\varepsilon(\theta_0)}=0$. Setting $\theta=\theta_0$ in the pseudoenergy equation gives an additional equation

$$(2k+1)i\pi = r\cosh\theta_0 - \ln(2\theta_0) - \int\frac{d\theta}{2\pi}\,\varphi(\theta_0-\theta)\ln(1+e^{-\varepsilon(\theta)}) \tag{2.8}$$

in which the choice of the integer k depends on the branch of the logarithm and should be fixed using continuity. The equations (2.6), (2.8) and (2.7) proposed using numerical continuation are actually exact. The only information required to deduce the equations is whether the singularities have crossed the integration contour or not, and we obtain this using the numerics.

The form of the resulting equations also allowed conjectures to be made for the states with nonzero spin; the ground-state particle has zero spin so analytical continuation from this state can only produce states with a similar spin. In addition, analytical continuation around further square-root branch points of the Riemann surface enabled conjectures to be made for the TBA equations describing multiparticle states.

The method of analytical continuation was used successfully in [67] to find TBA equations describing the massive quantum field theories which correspond to ϕ_{13} perturbations of the minimal models $\mathcal{M}_{2,2N+3}$. Again the parameter used for the analytical continuation was r or equivalently the mass, but any continuous parameter may in principle achieve the same effect. The necessary condition is that the Riemann surface contains branch points connecting the energy levels under consideration. In this chapter we find the excited state TBA equations for the sine-Gordon model at the point $\xi=2$ using a continuation in the twist parameter α rather than r. This material will form part of a paper currently in preparation [1].

The chapter falls into two parts: the first concerns the excited state TBA equations for the sine-Gordon model with parameter ξ=2. The energies are then compared with results from a single nonlinear integral equation which also describes the excited states. We noticed a close link between the zero structure of the functions defining both NLIEs, and we investigate this in the second part of the chapter. Relations found between these functions are partially justified using the functional relations introduced in Section 1.5.

2.1 The sine-Gordon excited states at $\xi = 2$

The twisted TBA equations at the point $\xi = 2$ in the repulsive regime can be encoded on a D_3 (or equivalently an A_3) Dynkin diagram. The central node is associated with the soliton of mass M, and the end (or fork) nodes are related to massless particles (known as magnons). The twists $\pm 2\,\alpha$ are attached to the end nodes. The pseudoenergies associated with the magnons satisfy the same nonlinear integral equation so the TBA system reduces to two equations:

$$\varepsilon_1(\theta) = r\cosh\theta - \int \frac{d\theta'}{2\pi}\frac{L_2(\theta')}{\cosh(\theta-\theta')} \tag{2.9}$$

$$\varepsilon_2(\theta) = -\int \frac{d\theta'}{2\pi}\frac{L_1(\theta')}{\cosh(\theta-\theta')} \tag{2.10}$$

where $r = mR$ and

$$L_1(\theta) = \ln(1+e^{-\varepsilon_1(\theta)}) \tag{2.11}$$

$$L_2(\theta) = \ln(1+e^{2i\alpha-\varepsilon_2(\theta)})(1+e^{-2i\alpha-\varepsilon_2(\theta)})\ . \tag{2.12}$$

To simplify the notation the dependence on α is left implicit. The ground-state energy is given in terms of the pseudoenergy $\varepsilon_1(\theta)$

$$E(r) = -M\int \frac{d\theta}{2\pi}\cosh\theta\, L_1(\theta)\ . \tag{2.13}$$

The D_3 Y-system, which is defined in terms of the pseudoenergies via $X(\theta) = \exp(-\varepsilon_1(\theta))$ and $Y(\theta) = \exp(-\varepsilon_2(\theta))$, is

$$\begin{aligned} X(\theta+i\pi/2)\,X(\theta-i\pi/2) &= 1+2\,\cos(2\,\alpha)\,Y(\theta)+Y^2(\theta)\ , \\ Y(\theta+i\pi/2)\,Y(\theta-i\pi/2) &= 1+X(\theta)\ . \end{aligned} \tag{2.14}$$

These functions and the related pseudoenergies have the following periodicity

$$X(\theta) = X(\theta+3i\pi) \quad , \quad Y(\theta) = Y(\theta+3i\pi) \tag{2.15}$$

which is a (non-trivial) consequence of (2.14) and can be shown by successive substitutions.

2.1.1 Analytic structure of the ground-state energy

As the first step towards finding the excited state equations we map out the analytic structure of the ground-state energy as a function of α. The conformal spectrum indicates the ground and first excited state energy levels cross at $\alpha = \pi$, but if we turn on a small perturbation, by allowing r to be nonzero, the levels move apart. We use arguments from perturbation theory to show there now exists a pair of branch

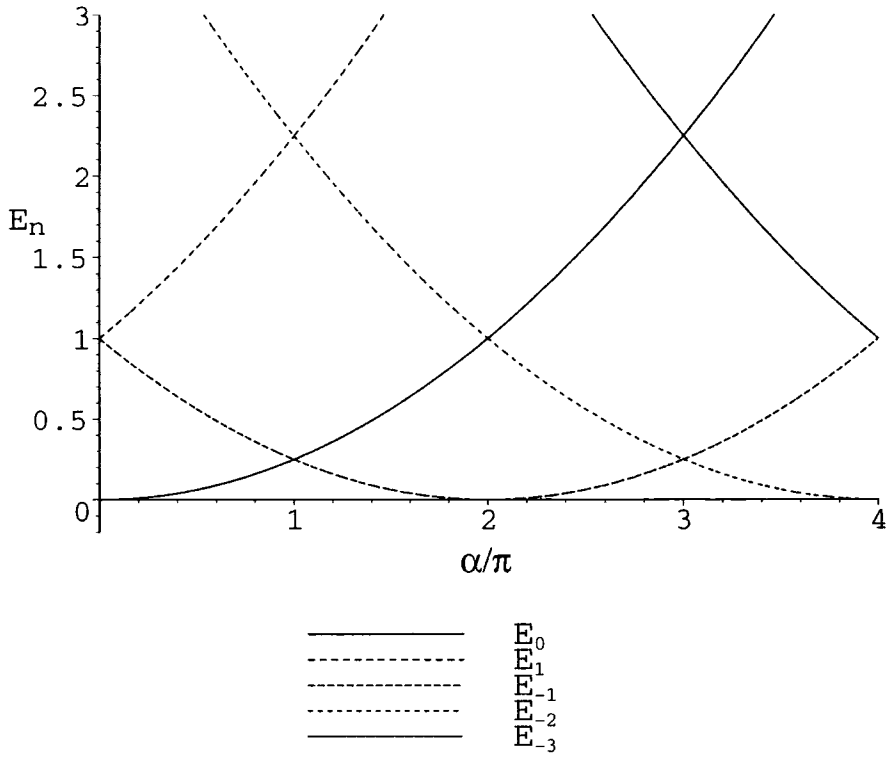

Figure 2.2: Energy levels E_n at the conformal point as a function of α/π.

points in the complex plane near to $\alpha = \pi$, which connect the ground-state with the first excited state.

We consider the zero topological charge sector of the sine-Gordon model corresponding to $m = 0$, since analytical continuation from the spin-zero ground-state can only access states with a similar spin. The conformal spectrum for $E_n \equiv E_{n+\frac{\alpha}{2\pi},0}$ is given by

$$\frac{RE_n}{2\pi} = \Delta_+ + \Delta_- - \frac{c}{12}. \tag{2.16}$$

The ultraviolet central charge is equal to 1 and the conformal weights are given in (1.113). In terms of α and ξ the above relation is equivalent to

$$\frac{RE_n}{2\pi} = \frac{2\xi}{1+\xi}\left(n + \frac{\alpha}{2\pi}\right)^2 - \frac{1}{12}. \tag{2.17}$$

Figure 2.2 shows the first few energy levels and the level crossings between them. We focus on $\alpha = \pi$ where the energy levels denoted E_0 and E_{-1} cross over. These levels correspond to states created by the vertex operators $V_{\frac{\alpha}{2\pi},0}$ and $V_{\frac{-1+\alpha}{2\pi},0}$ respectively. We can approximate the energies of these two levels by combining the truncated conformal space approach (TCSA) [68] with degenerate perturbation theory. The idea of TCSA is to restrict the Hilbert space to only those states whose energy eigenvalue (associated to the unperturbed Hamiltonian) is less than some cutoff energy E_{cut}. Thus we are now dealing with a finite Hilbert space, and the full

Hamiltonian can be described by a matrix $\widehat{H}$:

$$\frac{R\widehat{H}}{2\pi} = \widehat{L}_0 + \widehat{\overline{L}}_0 - \frac{c}{12}\widehat{I} + \kappa\frac{r^{2-h}}{(2\pi)^{1-h}}\widehat{B}\,. \tag{2.18}$$

The entries of the diagonal matrices $\widehat{L}_0$ and $\widehat{\overline{L}}_0$ are the left and right conformal weights and $\widehat{I}$ is the identity matrix. The last term of (2.18) is the result of sandwiching the perturbing term in the action (1.107) between the states $|\Phi\rangle$ and $|\Psi\rangle$. The resulting three-point function is fixed up to a constant using conformal invariance. Integrating then gives the above formula, in which the matrix $\widehat{B}$ is defined by

$$\widehat{B}_{\Phi,\Psi} = \frac{1}{2}\langle\Phi|V_{1,0}(1,1) + V_{-1,0}(1,1)|\Psi\rangle\,. \tag{2.19}$$

We use the rules of degenerate perturbation theory to extract the leading behaviour of (2.18) at $\alpha = \pi$ when $r = 0$. This is given by the 2×2 submatrix of the right hand side of (2.18) acting on the vector space spanned by the states created by the two vertex operators in question. We now set $0 < r \ll 1$ to perturb away from the conformal point and lift the degeneracy between the levels. For small enough r and $\alpha = \pi + \delta\alpha$, with $\delta\alpha$ suitably small, the system is near degenerate and the same matrix dominates. We write this explicitly using the conformal dimensions of the vertex operators given by (1.113) and the three-point function

$$\langle V_{n_1,m_1}|V_{n_2,m_2}|V_{n_3,m_3}\rangle = \delta_{n_1,n_2+n_3}\delta_{m_1,m_2+m_3}\,. \tag{2.20}$$

The result is

$$\frac{\xi}{2(1+\xi)}\left(1+\frac{\delta\alpha^2}{\pi^2}\right)\begin{pmatrix}0&1\\1&0\end{pmatrix} + \frac{\delta\alpha\xi}{\pi(1+\xi)}\begin{pmatrix}1&0\\0&-1\end{pmatrix} + \kappa\frac{r^{2-h}}{2(2\pi)^{1-h}}\begin{pmatrix}0&1\\1&0\end{pmatrix} \tag{2.21}$$

which upon diagonalisation yields the eigenvalues

$$\frac{RE(R)}{2\pi} \sim \frac{\xi}{2(1+\xi)}\left(1+\frac{(\alpha-\pi)^2}{\pi^2}\right) - \frac{1}{12} \pm \sqrt{\frac{\xi^2\,(\alpha-\pi)^2}{\pi^2(1+\xi)^2} + \frac{\kappa^2\, r^{\frac{4}{1+\xi}}}{4\,(2\pi)^{\frac{2(1-\xi)}{1+\xi}}}}\,. \tag{2.22}$$

In the above κ denotes the constant of proportionality relating the soliton mass to the perturbing parameter $\lambda = \mu^2/\beta^2$. The relation is $\lambda = \kappa M^{2/(1+\xi)}$ and the exact value was found by Al.B. Zamolodchikov [69]

$$\kappa = \frac{2\,\Gamma(\frac{\xi}{1+\xi})}{\pi\,\Gamma(\frac{1}{1+\xi})}\left(\frac{\sqrt{\pi}}{2\,\Gamma(\frac{1+\xi}{2})\,\Gamma(\frac{\xi}{2})}\right)^{2/(1+\xi)}\,. \tag{2.23}$$

Figure 2.3 shows the splitting between the energy levels E_{-1} and E_0 at finite r calculated using the formula (2.22). The separation between the energy levels increases as r is increased and it is clear from (2.22) that the levels only cross in the conformal limit.

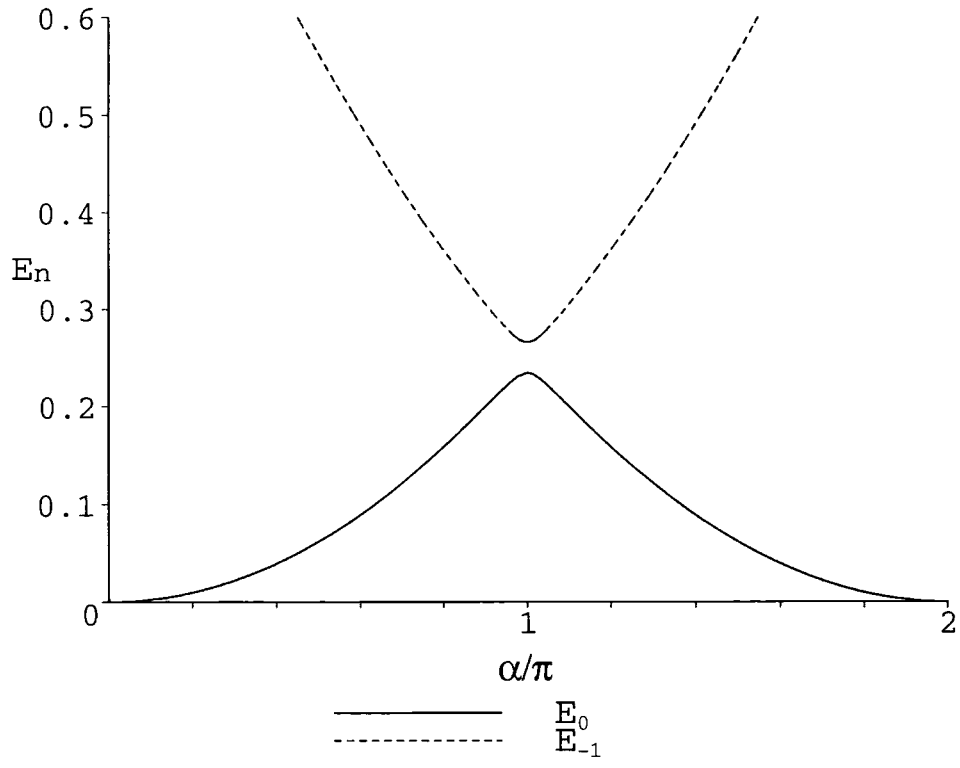

Figure 2.3: The energy level splitting at $r = 0.1$ calculated using the CPT prediction (2.22)

The formula for the energy levels (2.22) indicates a pair of square-root branch points at

$$\alpha = \pi \pm i \frac{\pi\kappa\,(1+\xi)\,r^{\frac{2}{1+\xi}}}{2\,\xi\,(2\,\pi)^{\frac{1-\xi}{1+\xi}}}\,. \tag{2.24}$$

Now we have found a branch point in the complex α-plane we can analytically continue the ground-state energy around it, and convert the ground-state into the first excited state. The continuation automatically provides the modified TBA equations, just as described for the scaling Lee-Yang model.

The plot of the conformal spectrum shown in Figure 2.3 indicates many more level crossings which separate at nonzero r. Again a simple calculation should predict the energy level splitting at each crossing. We can also find complex conjugate pairs of square-root branch points which then provide access to further spin-zero excited states.

2.1.2 The TBA equations

In this section we propose TBA equations describing the energy levels of the excited states of the sine-Gordon model at ξ=2. We start from the ground-state energy at zero twist and continue α around the upper branch point at (2.24). During this process singularities in the logarithmic terms of (2.9) and (2.10) move around and attempt to cross the integration contours along the real axis. After deforming the

contour, and following the method of Section 2.0.1, we can use the residue trick to find the new TBA equations.

First we need to find the values of α at which singularities in the logarithmic terms, $L_1(\theta)$ and $L_2(\theta)$, cross the integration contour. To do this we take a look at [70] in which Fendley proposed TBA equations describing the excited state energies of the $\xi = 2$ sine-Gordon model. A different approach was used to the one given here, and while we agree with the results for large values of α, we are able to clarify and correct the results in certain regions where the equations of [70] are discontinuous.

Fendley considered the limit $r \to 0$ of the TBA equations and proposed excited state equations using a lemma due to Klümper and Pearce [71]. The equations relied on a knowledge of the positions of the zeros of $X(\theta)$ and $Y(\theta)$ within the strip $|\Im m(\theta)| < \pi/2$ of the complex plane. In this chapter we focus on the singularities in the logarithmic terms of (2.9) and (2.10), but the two viewpoints are intrinsically tied together via the Y-system (2.14):

$$\begin{aligned} Y(x \pm i\pi/2) &= -e^{\pm 2i\alpha} \iff X(x) = 0 \\ X(y \pm i\pi/2) &= -1 \iff Y(y) = 0 \end{aligned} \tag{2.25}$$

These equations imply that if a singularity in one of the logarithmic terms crosses the real axis, then at the same time a zero of $X(\theta)$ or $Y(\theta)$ enters the strip $|\Im m(\theta)| < \pi/2$.

Fendley conjectured TBA equations describing the massive energy levels ($r \neq 0$) from the TBA equations for the conformal energy levels using an argument based on continuity in r. The resulting TBA equations whilst continuous in r were discontinuous in α, which was a little surprising. We would expect the equations to be continuous in both r and α.

The discontinuity in the functions $X(\theta)$ and $Y(\theta)$ as α increases past π can be explained by taking a quick look again at Figure 2.3. Fendley's TBA equations for $\alpha < \pi$ correspond to the ground-state energy; whereas for $\alpha > \pi$ the equations (correctly) describe the first excited state. But, as we have seen from Figure 2.3, the levels are no longer connected when r is nonzero. The discontinuity follows from swapping equations at $\alpha = \pi$ and therefore jumping between the levels. If the correct continuation in real α had been carried out, then the TBA equations would still describe the ground-state energy. The only way to vary α and arrive in a continuous fashion at the first excited state is to use the square-root branch point, unless the system size is exactly zero.

The plan is to fix r at some finite value and then send α towards π. We need to keep an eye out for singularities in the logarithmic terms heading towards the integration contour, and, as explained above, this is entirely equivalent to zeros of $X(\theta)$ or $Y(\theta)$ entering the strip $|\Im m(\theta)| < \pi/2$. We begin by establishing at

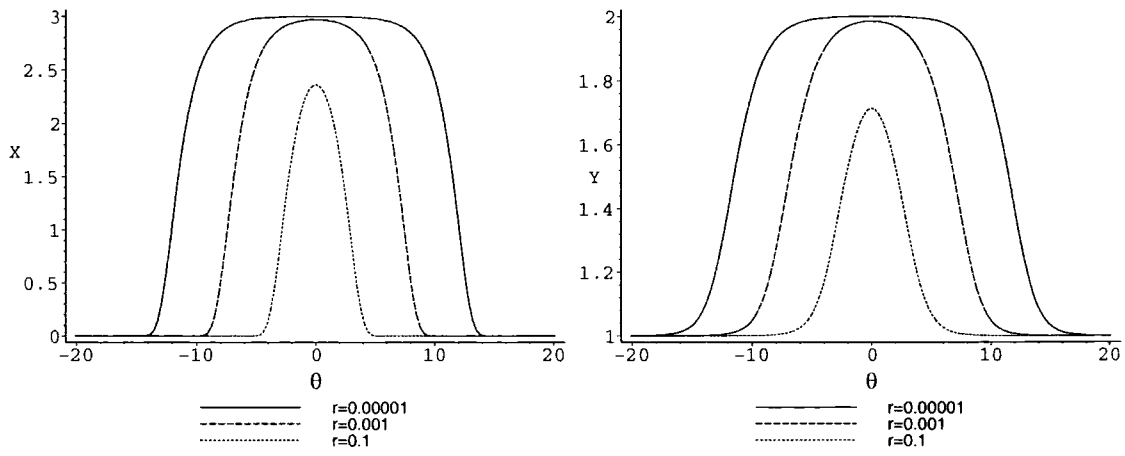

Figure 2.4: $X(\theta)$ and $Y(\theta)$ as r varies.

which values of α a pair of logarithmic singularities hit the integration contour. We can lift this information (almost) directly from [70]: the values of α at which zeros arrive were found by considering the form of the TBA equations in the limit $r \to 0$. Generally these are known as the massless equations, but as we wish to distinguish them from the TBA equations describing massless flows (see Section 1.6) we will refer to them as the kink TBA equations.

2.1.3 The kink TBA equations

As $r \to 0$ the functions $X(\theta)$ and $Y(\theta)$ begin to resemble two 'kinks': a left and a right bolted together in the centre. An example is shown at $\alpha = 0$ in Figure 2.4.

In the limit $r \to 0$ the TBA system splits completely into a pair of 'kink systems' where the nontrivial behaviour is concentrated at approximately $\pm \ln(2/r)$ and the pseudoenergies are constant in the region in between. The symmetry $\theta \to -\theta$ means we may focus on just one of the kink systems. The right kink system is obtained from (2.9) and (2.10) by replacing the driving term $r \cosh\theta$ with $\frac{1}{2} r e^{\theta}$ and then removing the r dependence via a trivial shift of θ to $\theta - \ln r/2$. The resulting kink TBA equations read

$$\varepsilon_1^R(\theta) = e^{\theta} - \int \frac{d\theta'}{2\pi} \frac{L_2^R(\theta')}{\cosh(\theta - \theta')}, \tag{2.26}$$

$$\varepsilon_2^R(\theta) = -\int \frac{d\theta'}{2\pi} \frac{L_1^R(\theta')}{\cosh(\theta - \theta')}, \tag{2.27}$$

where $L_1^R(\theta)$ and $L_2^R(\theta)$ are defined similarly to (2.12). Figure 2.5 shows the form of the functions as they interpolate smoothly between $X^R(-\infty)$ and $X^R(+\infty)$ and $Y^R(-\infty)$ and $Y^R(+\infty)$

Fendley determined the only possible way new zeros can enter the strip $|\Im m(\theta)| < \pi/2$ is at $\theta = -\infty$. When a zero enters one of the plateau values, $X^R(-\infty)$ or $Y^R(-\infty)$, will therefore be equal to zero.

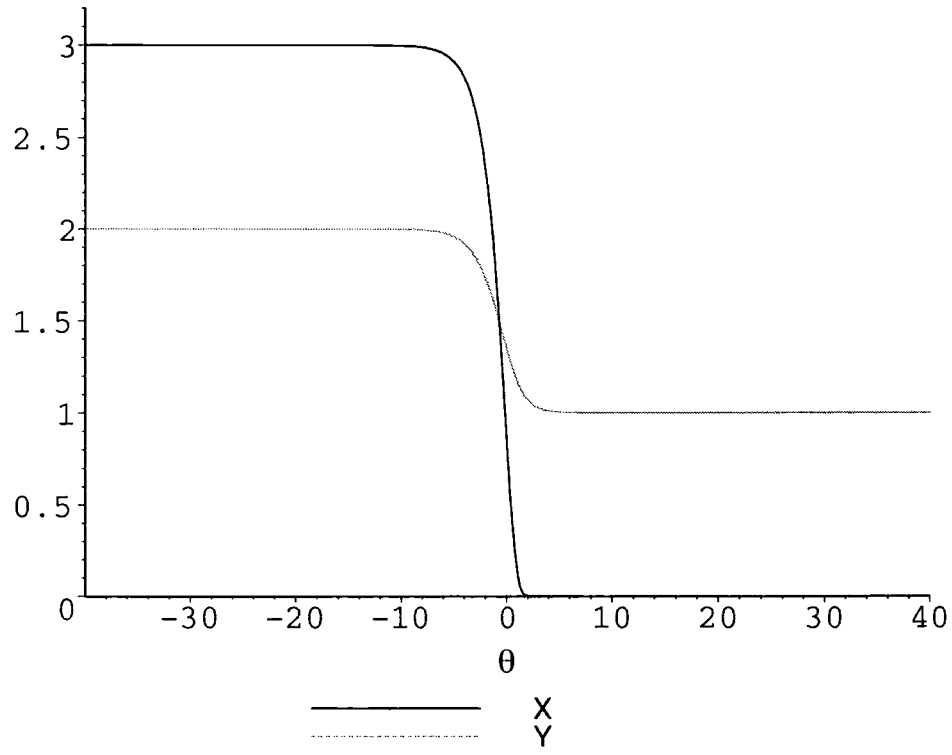

Figure 2.5: $X^R(\theta)$ and $Y^R(\theta)$ at $\alpha = 0$.

To find the plateau values set $\theta = -\infty$ in (2.26) and (2.27). Integration yields a pair of simultaneous equations for $X = X^R(-\infty)$ and $Y = Y^R(-\infty)$:

$$X^2 = 1 + 2\cos(2\alpha)\, Y + Y^2 \,, \tag{2.28}$$

$$Y^2 = 1 + X \,. \tag{2.29}$$

The solution positive at $\alpha = 0$ is

$$X = \frac{\sin(2\,\alpha)}{\sin(2\,\alpha/3)} \,, \tag{2.30}$$

$$Y = 2\,\cos(2\,\alpha/3) \,. \tag{2.31}$$

The plateau values as a function of α, shown in Figure 2.6, indicate the first X zero appears at $\alpha = \pi/2$, and the first Y zero appears at $\alpha = 3\pi/4$.

The opposite limit, $\theta \to \infty$, of the kink TBA equations also provides some useful information. In this limit the functions take the values

$$X(\theta \to \infty) \to 2\cos(\alpha)\, e^{-\exp(\theta)} \quad \text{and} \quad Y(\infty) = 1 \,. \tag{2.32}$$

The first of these can be used to predict the values of α for which the X zeros reach infinity (at this point their contribution to the TBA equations simplifies and we no longer need to explicitly search for them). The driving term in (2.9) prevents the Y zeros from ever reaching infinity; once they have appeared they always contribute to the TBA equations. Table 2.1 contains a summary of the values of α at which zeros enter or leave the strip $|\Im m(\theta)| < \pi/2$ [70].

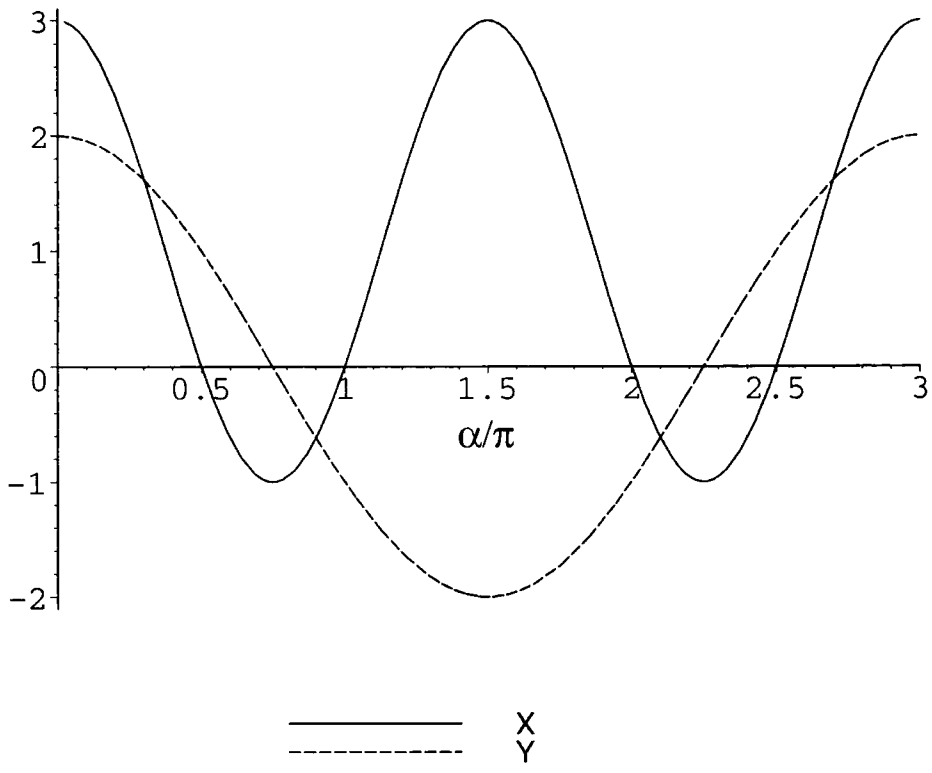

Figure 2.6: Plateau values $X(-\infty)$ and $Y(-\infty)$ as α/π varies.

Zero	α (zero enters)	α (zero leaves)
x_{2i-1}	$\pi(3i-2)/2$	$\pi(4i-3)/2$
x_{2i}	$\pi(3i-1)/2$	$\pi(4i-1)/2$
y_j	$\pi(3j/2-3/4)$	–

Table 2.1: Values of α where zeros of $X^R(\theta)$ and $Y^R(\theta)$ enter or leave the strip $|\Im m(\theta)| < \pi/2$.

2.1.4 The massive TBA equations

We use the results of the last section to predict for which values of α the massive TBA equations require modification due to the appearance of zeros. Since the massive TBA functions are even functions of θ, the zeros are now in pairs $(x_i, -x_i)$ and $(y_j, -y_j)$. These zeros enter the strip $|\Im m(\theta)| < \pi/2$ at $\theta = \pm i\pi/2$ rather than at $\theta = -\infty$. Moreover, the plateau values now correspond to the central region between $-\ln 2/r < \theta < \ln 2/r$ (recall Figure 2.4). So we can still use the plateau values to predict the values of α at which zeros arrive or leave, even though they now depend upon the system size. This means that the zeros no longer arrive or leave at exactly the values given in Table 2.1. However, for small enough values of r zeros will arrive at approximately the predicted values of α.

The first zero, x_1, appears when $\alpha = \pi/2$ according to (2.1). However, this happens to be an atypical case because (as explained in [70]) $X(\theta) = 0$ at this

value of α independent of the value of r. Instead, the pair $(x_1, -x_1)$ immediately shoot all the way to $\pm\infty$ and the TBA equations require a small modification: $\varepsilon_1(\theta) \to \varepsilon_1(\theta) - i\pi$.

The conformal results (2.1) indicate the next zero y_1 appears at $\alpha = 3\pi/4$. To see what actually happens at nonzero r we solved the ground-state TBA equations numerically for a number of values of α tending towards $\alpha = 3\pi/4$. Appendix B shows the movement of the singularities in the logarithmic terms. The contour plots actually show the functions

$$G_1(\theta) = \frac{|1 + X(\theta)|}{1 + |1 + X(\theta)|} \tag{2.33}$$

$$G_2(\theta) = \frac{|1 + 2\cos\alpha\, Y(\theta) + Y^2(\theta)|}{1 + |1 + 2\cos\alpha\, Y(\theta) + Y^2(\theta)|}. \tag{2.34}$$

The centres of the concentric circles indicate the points at which $1 + X(\theta)$ and $1 + 2\cos\alpha\, Y(\theta) + Y^2(\theta)$ are equal to zero.

First singularity of $L_1(\theta)$

First we focus on the function $G_1(\theta)$. As α increases, four zeros of $G_1(\theta)$ are seen to move towards the imaginary axis; this is most clearly seen in Figure B.4. We label the zeros A_1, A_2, B_1 and B_2 and initially take y_1 to be a real positive number. With this convention, and recalling the $3\pi i$ periodicity, the zeros are in the following positions

B_1	A_1
$-y_1 + i\pi$	$y_1 + i\pi$
B_2	A_2
$-y_1 - i\pi$	$y_1 - i\pi$

(2.35)

The notation is chosen such that $Y(\pm y_1 + 3i\pi/2) = 0$.

Only two of these zeros ever come close to the integration contour: A_1 and B_2. As $\alpha \to 3\pi/4$ they move towards the imaginary axis on lines with fixed imaginary part. Upon reaching this axis they take advantage of the extra possibility and A_1 moves down towards the origin whilst B_2 moves up. This can be seen in Figure B.6. Note that the symmetry $\theta \to -\theta$ and the $3\pi i$ periodicity of the TBA functions means that B_2 is not free to move but is in fact the other half of a pair with A_1. These singularities will, eventually, pinch the integration contour. We note here that A_2 and B_1 also form a pair, but constrained by the Y-system they always remain safely away from the integration contour.

The results of the previous section indicate that the Y plateau value is zero at exactly $\alpha = 3\pi/4$ for the conformal model. What happens in the conformal case

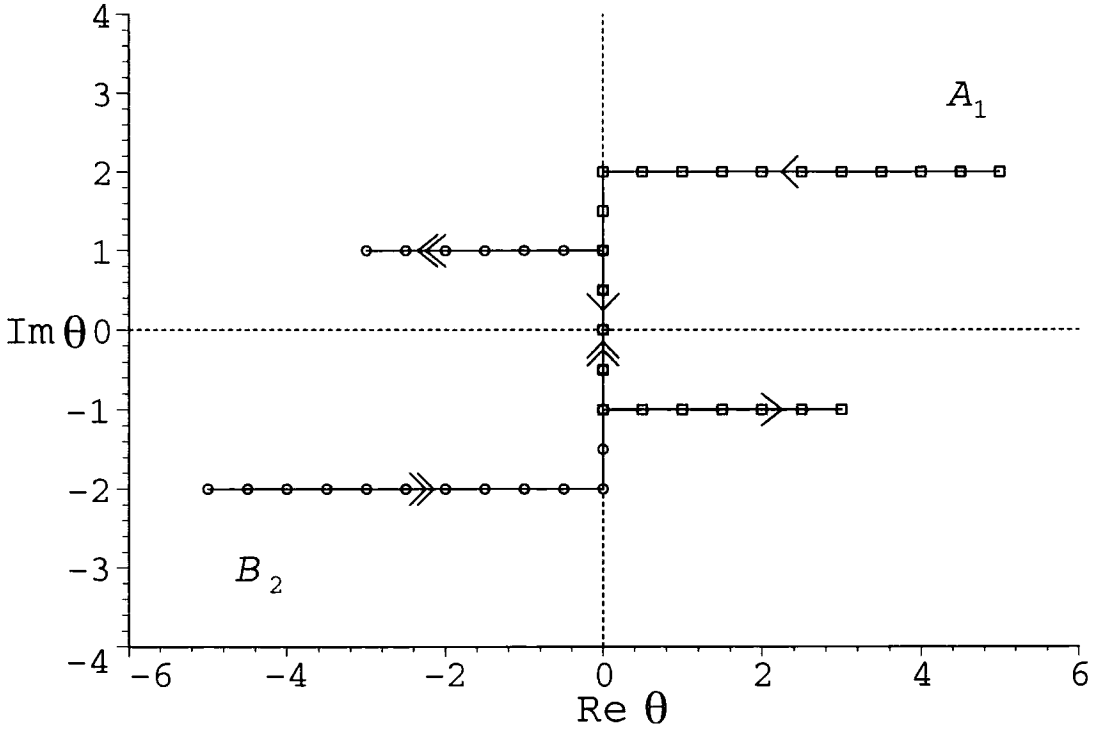

Figure 2.7: The movement of the zeros A_1 and B_2 as α increases from 0 to 0.9995π. The arrows indicate the direction of increasing α.

is that as α tends towards $3\pi/4$, a zero of $Y(\theta)$ moves along the imaginary line at $\Im m 3\pi/2$ towards $-\infty$. At $\alpha = 3\pi/4$ it reaches $-\infty$, slides off the line $\Im m 3\pi/2$ and reappears on the real axis. The integration contour must be deformed to avoid this zero and the resulting modified TBA equations now describe the excited state.

When r is nonzero the Y plateau value reaches zero for some value of α slightly greater than $3\pi/4$. The difference between the conformal and the massive model is that in the latter case the zeros must also move along the imaginary axis before they approach the integration contour. Our numerics confirm this behaviour and the TBA equations continue to hold for a small, r dependent, region after α reaches $3\pi/4$. Eventually A_1 and B_2 cross the real axis and continue onwards until they reach the imaginary lines at $\mp i\pi/2$ respectively. The accompanying Y zeros now sit on the real axis: $Y(\pm y_1) = 0$. The zeros now change direction and begin to move along lines with fixed imaginary part; this is shown in Figure B.8.

Figure 2.7 shows the behaviour of the pair (A_1, B_2) in the complex θ-plane as a function of real α. Both zeros clearly cross the integration contour along the real axis.

During this process we have to deform the integration contour above the singularity (B_2) at $-y_1+i\pi/2$ then below the singularity (A_1) at $y_1-i\pi/2$. Just as described in Section 2.0.1 the logarithmic singularities can be turned into simple poles by integrating by parts. Then, by taking the residue at both poles, the integration contour can be rewritten along the real axis with the addition of the residue

terms. Following this procedure we find the new equations are

$$\varepsilon_1(\theta) = r\cosh\theta - \int \frac{d\theta'}{2\pi}\frac{L_2(\theta')}{\cosh(\theta-\theta')} - i\pi \ , \tag{2.36}$$

$$\varepsilon_2(\theta) = -\int \frac{d\theta'}{2\pi}\frac{L1(\theta')}{\cosh(\theta-\theta')} + 2\,i\left(\arctan(e^{\theta+y_1-\frac{i\pi}{2}}) - \arctan(e^{\theta-y_1+\frac{i\pi}{2}})\right) \tag{2.37}$$

The position of the zeros $(y_1, -y_1)$ are fixed by consistency with the Y-system:

$$\varepsilon_1\Big(\pm y_1 - \frac{i\pi}{2}\Big) = i\pi(2N_1+1) \quad , \quad N_1 \in \mathbb{N} \ . \tag{2.38}$$

Plugging this into (2.36) yields an additional nonlinear integral equation which must be solved in conjunction with (2.36) and (2.37)

$$\pi(2N_1+1) = r\sinh y_1 + \int \frac{d\theta}{2\pi}\frac{L_2(\theta)}{\sinh(y_1-\theta)} - i\pi \ . \tag{2.39}$$

Numerically we find that choosing $N_1 = 1$ is the correct choice of integer; this is again connected with the choice of branch for the logarithm. Once the TBA equations have been solved the energy can be calculated using the following equation

$$E(r) = -M\int \frac{d\theta}{2\,\pi}\cosh\theta L_1(\theta) + 2\,M\cosh y_1 \ . \tag{2.40}$$

So far we are still calculating the ground-state energy; although for $\alpha \gtrsim 3\pi/4$ we must use the new TBA equations (2.36),(2.37) and (2.39). Recall that we need to reach $\alpha \approx \pi$ before we can head off into the complex α-plane and find the first excited state.

Second singularity of $L_2(\theta)$

The conformal results indicate an X zero enters at $\alpha = \pi$ and, by following the plots of $G_2(\theta)$ as $\alpha \to \pi$, we see a further set of zeros, with imaginary part π and 2π, heading towards the imaginary axis. This can be seen in Figure B.12. We take x_2 to be initially real and positive and label the zeros as shown below:

B_1' $-x_2 + i\pi$	A_1' $x_2 + i\pi$
B_2' $-x_2 - i\pi$	A_2' $x_2 - i\pi$

(2.41)

As $\alpha \to \pi$, the pair (A_1', B_2') head towards the integration contour via the imaginary axis (see Figure B.13) in exactly the same way as (A_1, B_2) did. However, in contrast to the behaviour of the zeros (A_1, B_2), when α is increased past π the pair (A_1', B_2') are seen to turn around and retreat along the imaginary axis. Then they

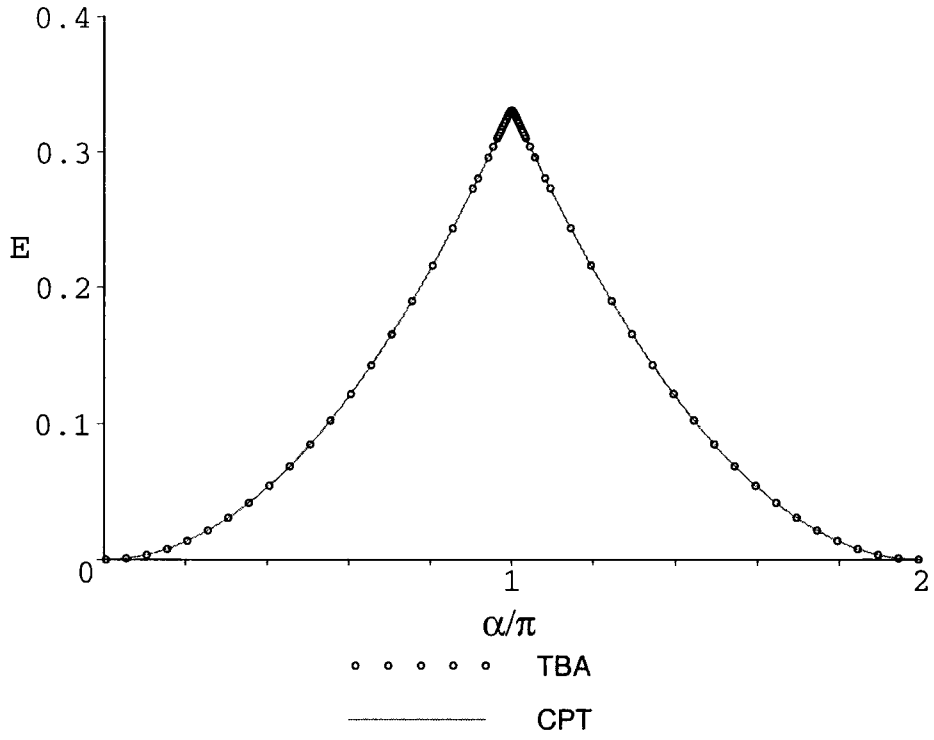

Figure 2.8: The ground-state energy $E(r)$ at $r = 0.001$ calculated using the TBA equations and the conformal perturbation theory prediction.

move back onto the imaginary lines they were on before. This behaviour agrees with the observation that the TBA equations are symmetric, as functions of α, about the point π. As α increases further, the pair (A_1, B_2) also return to the origin, move back along the imaginary axis and then onto their respective imaginary lines. During the continuation the contours must be readjusted and so the TBA equations return to their original form (2.9) and (2.10).

The energy calculated in this way always corresponds to the ground-state energy; as it must since α remained real throughout the continuation. Figure 2.8 compares the energy calculated using the TBA equations (either (2.10) or (2.36),(2.37) and (2.39) depending upon α) with the conformal perturbation theory (CPT) calculation (2.22) for the ground-state. The CPT result is only approximate but the comparison allows us to be confident that the modified TBA equations (2.36),(2.37) and (2.39) are correct.

In order to access the first excited state α must be analytically continued into the complex plane and around one of the branch points given by (2.24). We begin by solving the TBA equations (2.36),(2.37) and (2.39) for small r close to $\alpha = \pi$. Then we send α into the complex plane along the path depicted in Figure 2.9. The movement of the pair (A_1', B_2') in the complex plane as α varies is shown in Figure 2.10.

During the continuation the pair (A_1', B_2') are seen to move off the imaginary

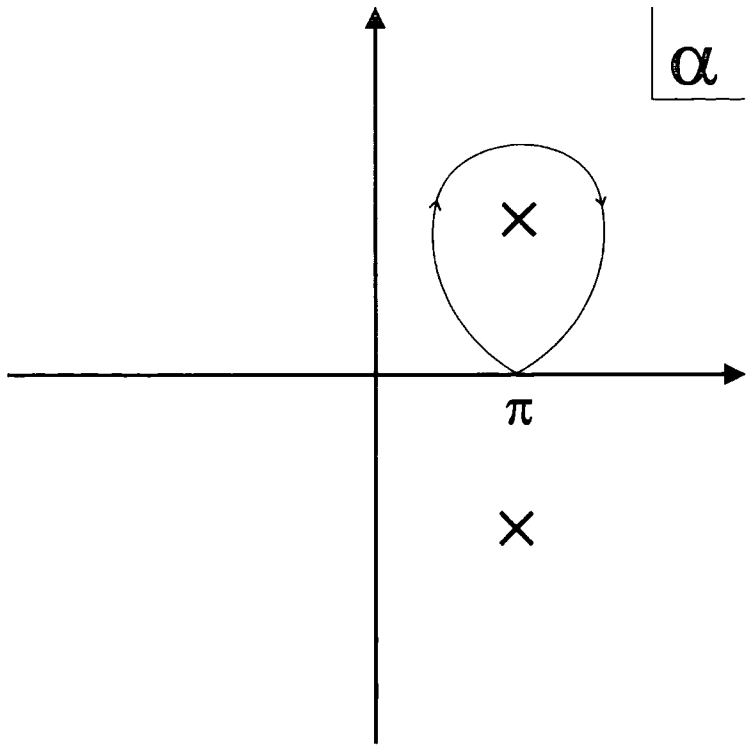

Figure 2.9: A nontrivial path in the complex α-plane. The positions of the branch points are marked by the symbol X.

axis into the complex plane whilst the pair (A_1, B_2) also move away from their fixed imaginary lines. As α continues around the branchpoint, the pair (A_1', B_2') approach the integration contour and attempt to cross it. At this point the contour must be deformed; applying the residue trick yields a further set of TBA equations. Finally we return α to purely real values and (A_1', B_2') take up positions along the imaginary lines $\Im m(\theta) = \mp i\pi/2$. The labelling of the initial zero positions was chosen such that we now have $X(\pm x_2) = 0$ with x_2 purely real. Just as we described for the pair (A_1, B_2), the deformed integration contour goes above B_2' at $-x_2 + i\pi/2$ then below A_1' at $x_2 - i\pi/2$. Finally, the modified TBA equations are:

$$\begin{aligned}\varepsilon_1(\theta) &= r\cosh\theta - \int \frac{d\theta'}{2\pi}\frac{L_2(\theta')}{\cosh(\theta-\theta')} \\ &\qquad +2\,i\left(\arctan(e^{\theta+x_2-\frac{i\pi}{2}}) - \arctan(e^{\theta-x_2+\frac{i\pi}{2}})\right) - i\,\pi \qquad (2.42)\end{aligned}$$

$$\varepsilon_2(\theta) = -\int \frac{d\theta'}{2\pi}\frac{L1(\theta')}{\cosh(\theta-\theta')} + 2\,i\left(\arctan(e^{\theta+y_1-\frac{i\pi}{2}}) - \arctan(e^{\theta-y_1+\frac{i\pi}{2}})\right). \qquad (2.43)$$

There are now two unknowns: y_1 and x_2. The former can be fixed using (2.39) and the Y-system implies the latter must satisfy

$$\varepsilon_2(x_2 - \frac{i\pi}{2}) = i\pi(2N_2+1) \quad , \quad N_2 \in \mathbb{N}\,. \qquad (2.44)$$

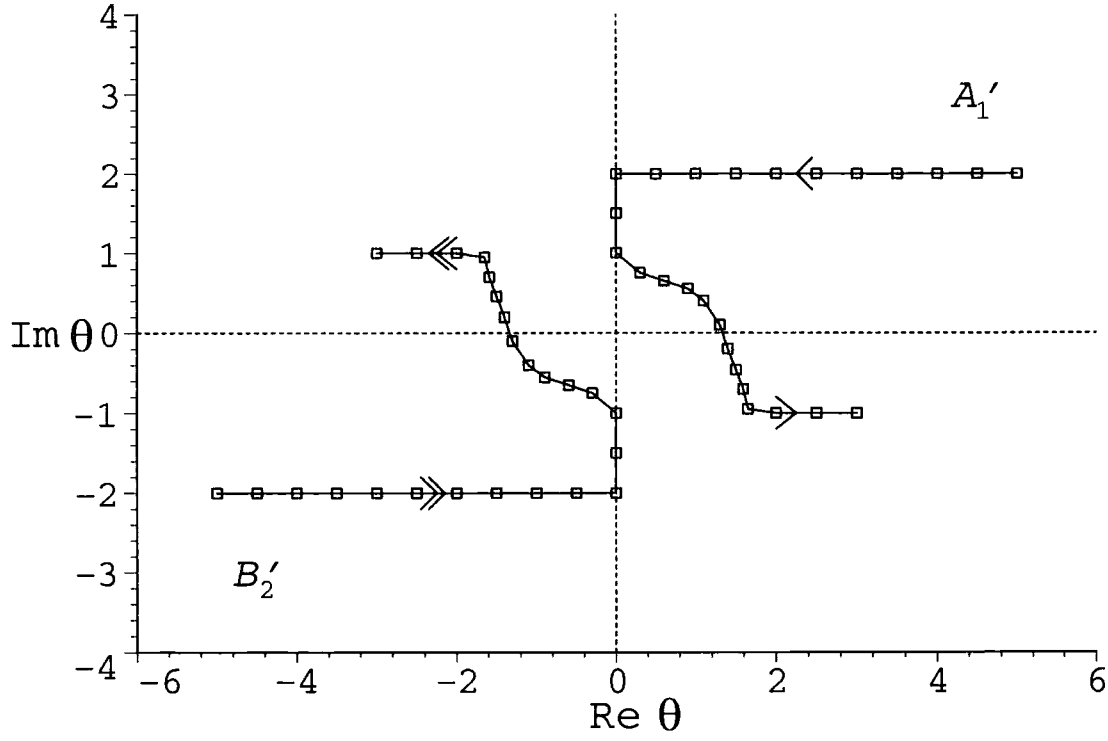

Figure 2.10: The movement of the zeros A_1' and B_2' as α increases from 0 to 1.0025π following a path that goes into the complex plane and around a branch point as depicted in Figure 2.9. The arrows indicate the direction of increasing α.

Writing this condition as a nonlinear integral equation we have

$$\pm 2\alpha + \pi(2N_2 + 1) = \int \frac{d\theta}{2\pi} \frac{L_1(\theta)}{\sinh(x_2 - \theta)} - 2\left(\arctan(e^{x_2+y_1}) + \arctan(e^{x_2-y_1})\right) . \tag{2.45}$$

Numerically we find that the plus sign preceding the twist should be chosen (further arguments for the validity of this can be found in [70]). The form of the energy equation remains unchanged by the addition of this extra pair of zeros and can be calculated using (2.40). The solution to the equations (2.42),(2.43),(2.39) and (2.45) can be input into the formula for the energy (2.40), and then compared with the CPT prediction for the first excited state (2.22). Figure 2.11 shows the comparison and provides strong encouragement that the TBA equations have been correctly continued to described this state.

We can calculate the energy of higher states by increasing α to larger values thus requiring the addition of more zeros x_i and y_j. The ys are a necessary requirement but, as discussed above, we choose to add in x zeros to lever ourselves up onto the next sheet of the Riemann surface.

If we consider the completely general case where there are n_i and n_j zeros of $X(\theta)$ and $Y(\theta)$ at positions x_i and y_j respectively (recall that some of the x_i may have reached $+\infty$), then the residue trick implies the modified TBA equations are

$$\varepsilon_1(\theta) = r\cosh\theta - \int \frac{d\theta'}{2\pi} \frac{L_2(\theta')}{\cosh(\theta - \theta')}$$

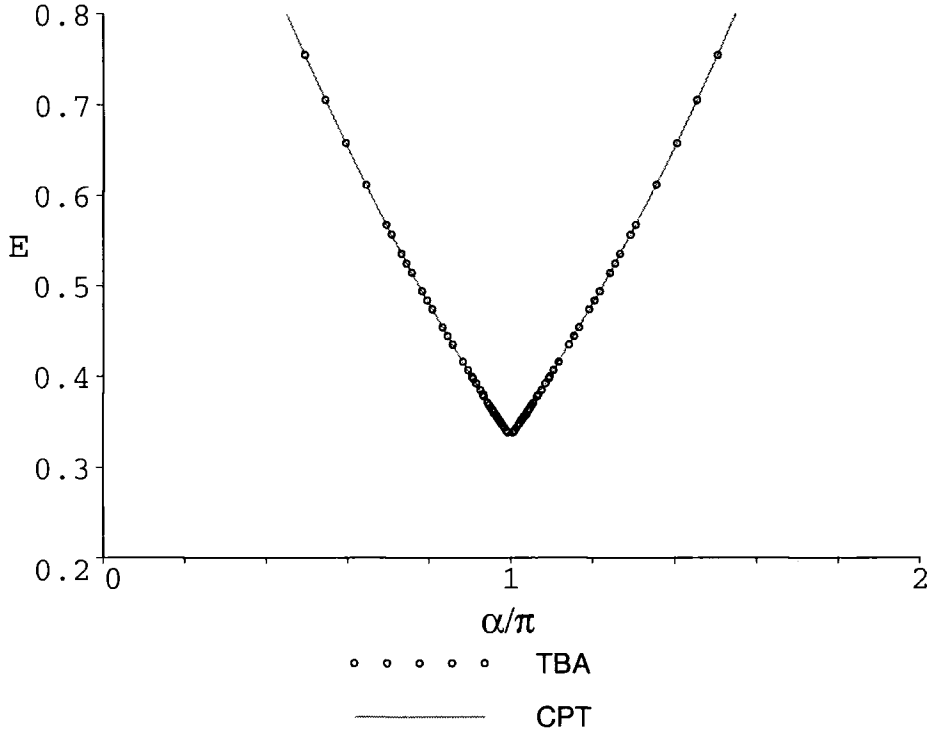

Figure 2.11: The first excited state energy $E(r)$ at $r = 0.001$ calculated using the TBA equations and the conformal perturbation theory prediction.

$$+2\,i\sum_{i=1}^{n_i}\arctan(e^{\theta+x_i-\frac{i\pi}{2}})-\arctan(e^{\theta-x_i+\frac{i\pi}{2}}) \tag{2.46}$$

$$\varepsilon_2(\theta) = -\int\frac{d\theta'}{2\pi}\frac{L_1(\theta')}{\cosh(\theta-\theta')}+2\,i\sum_{j=1}^{n_j}\arctan(e^{\theta+y_j-\frac{i\pi}{2}})-\arctan(e^{\theta-y_j+\frac{i\pi}{2}}). \tag{2.47}$$

The positions x_i and y_j are fixed by their definitions as zeros of X and Y and consistency with the Y-system: they must satisfy $\varepsilon_2(x_i-\frac{i\pi}{2}) = i\pi(2N_i+1)$ and $\varepsilon_1(y_j-\frac{i\pi}{2}) = i\pi(2N_j+1)$ for integers N_i and N_j respectively. Our numerical results indicate the integers should be $N_i = i$ and $N_j = j$. Feeding these requirements into (2.46) and (2.47) yields two further equations

$$\begin{aligned}\pi(2N_j+1) &= r\sinh y_j+\int\frac{d\theta}{2\pi}\frac{L_2(\theta)}{\sinh(y_j-\theta)}\\ &\quad -2\sum_{i=1}^{n_i}\arctan(e^{y_j+x_i})+\arctan(e^{y_j-x_i})\,, \qquad (2.48)\\ \pm2\alpha+\pi(2N_i+1) &= \int\frac{d\theta}{2\pi}\frac{L_1(\theta)}{\sinh(x_i-\theta)}\\ &\quad -2\sum_{j=1}^{n_j}\arctan(e^{x_i+y_j})+\arctan(e^{x_i-y_j})\,, \qquad (2.49)\end{aligned}$$

which must be solved in conjunction with (2.46) and (2.47). In the general case the

energy equation becomes

$$E(r) = -M \int \frac{d\theta}{2\pi} \cosh\theta \, L_1(\theta) + 2M \sum_{j=1}^{n_j} \cosh y_j \, . \tag{2.50}$$

The energy calculated using the modified TBA equations does agree with the CPT predictions for both the ground and first excited state. Nevertheless we would like to make a more accurate check of our equations.

2.1.5 The excited state NLIE

In Section 1.4.2 we introduced an alternative method of calculating the exact ground-state energy of the sine-Gordon model using a single nonlinear integral equation. In its current form (1.136), the equation is only suitable for finding the ground-state energy. However, the extension to include the excited states has recently been attacked in a number of papers [50, 72–76]. The authors of [50] first extended the equation to describe the spectrum of states consisting only of solitons by introducing 'holes' into the Bethe ansatz state. More general excited states of even topological charge were treated in [72–74], while states with odd topological charge were tackled in [75]. The recent paper [76] found the prescription to describe breather states.

In all cases the extension to describe these excited states is achieved simply by adding an extra term to the equation. The so-called source term is

$$\begin{aligned} g(\theta, \theta_k) \;=\; & -\sum_{j=1}^{N_h} \ln S_0(\theta - h_j) + 2\sum_{j=1}^{N_s} \ln S_0(\theta - y_j) \\ & - \sum_{j=1}^{M_c} \ln S_0(\theta - c_j) - \sum_{j=1}^{M_w} (\ln S_0(\theta - w_j))_{II} \, , \end{aligned} \tag{2.51}$$

where $S_0(\theta)$ is the scalar factor in the sine-Gordon S-matrix. The subscript II refers to the 'second determination' of a function [72]. It is defined by

$$f(\theta)_{II} = \begin{cases} f(\theta) + f\left(\theta - i\,\pi\,\mathrm{sign}(\Im m\theta)\right) & \xi > 1 \, , \\ f(\theta) - f\left(\theta - i\,\xi\pi\,\mathrm{sign}(\Im m\theta)\right) & \xi < 1 \, . \end{cases} \tag{2.52}$$

The new term is made up of contributions from the sources: holes at h_k, special objects at y_k and complex roots of close (c_k) and wide (w_k) type denoted collectively by $\{\theta_k\} = \{h_k, y_k, c_k, w_k\}$. All of these satisfy the following quantisation condition

$$f(\theta_k) = 2\pi i \, I_k \quad , \quad I_k \in \mathbb{Z} + \frac{1}{2} \, . \tag{2.53}$$

Note that this also holds for the Bethe ansatz roots. The difference between the roots and the various source objects is that the roots are also solutions of the Bethe ansatz equations (1.132).

The holes are points on the real axis where (2.53) holds; complex roots are those points in the complex plane. Complex roots always come in complex conjugate pairs and are split into two types: if $|\Im m\ c_k| < \min(\pi, \pi\,\xi)$ they are known as close roots, otherwise they are wide. The sole exceptions are the roots with imaginary part $\Im m\ w_k = \pm i\pi(1+\xi)/2$: they are self-conjugate due to the $i\pi(1+\xi)$ periodicity of the equation. The special objects are either holes or roots at y_k that satisfy

$$\Im m\, f'(y_k) > 0; \tag{2.54}$$

the relevance of these objects will become clear later. Normally, $f(\theta)$ is a monotonically decreasing function on the imaginary axis and the special objects are tied up with the branch choice for the logarithm in (1.136).

The full equation describing the excited states is

$$\begin{aligned} f(\theta) = -i\,r\sinh\theta + i\,\alpha + g(\theta,\theta_k) \;+\; & \int_{\mathcal{C}_1} d\theta'\,\varphi(\theta-\theta')\ln(1+e^{f(\theta')}) \\ & - \int_{\mathcal{C}_2} d\theta'\,\varphi(\theta-\theta')\ln(1+e^{-f(\theta')})\,. \end{aligned} \tag{2.55}$$

The equation for calculating the energy of a particular state is given by

$$\begin{aligned} E \;=\; & M\Big(\int_{\mathcal{C}_1}\frac{d\theta}{2\,i\,\pi}\sinh\theta\,\ln(1+e^{f(\theta)}) - \int_{\mathcal{C}_2}\frac{d\theta}{2\,i\,\pi}\sinh\theta\,\ln(1+e^{-f(\theta)}) \\ & + \sum_{j=1}^{N_H}\cosh h_j - 2\sum_{j=1}^{N_s}\cosh y_j - \sum_{j=1}^{M_s}\cosh c_j - \sum_{j=1}^{M_W}(\cosh w_j)_{II}\Big)\,. \end{aligned} \tag{2.56}$$

A particular state is specified by a finite number of holes and complex roots together with their quantum numbers I_k. The energy then follows from solving (2.55) as well as a finite number of equations corresponding to the quantisation conditions (2.53).

To distinguish between the two types of nonlinear integral equation we will refer to either the TBA equation or the NLIE.

2.1.6 Comparison of the results

We solved both the TBA equation and the NLIE using an iterative method, and calculated the ground-state energy. The results at $r = 0.1$ are shown in Figure 2.12.

The energy calculated using both methods agreed to about 15dp until α approached $3\pi/4$. At this point the iteration of the NLIE failed to converge. From our experience with the TBA equation, we expected the lack of convergence to be connected with singularities in the logarithmic terms crossing the integration contours. So we investigated the behaviour of the zeros of the function $1 + e^{f(\theta)}$ as α approached $3\pi/4$. We discovered that there was a pair of zeros moving along the imaginary axis towards the integration contours $\mathcal{C}_1, \mathcal{C}_2$. These zeros can be seen in Figure 2.13.

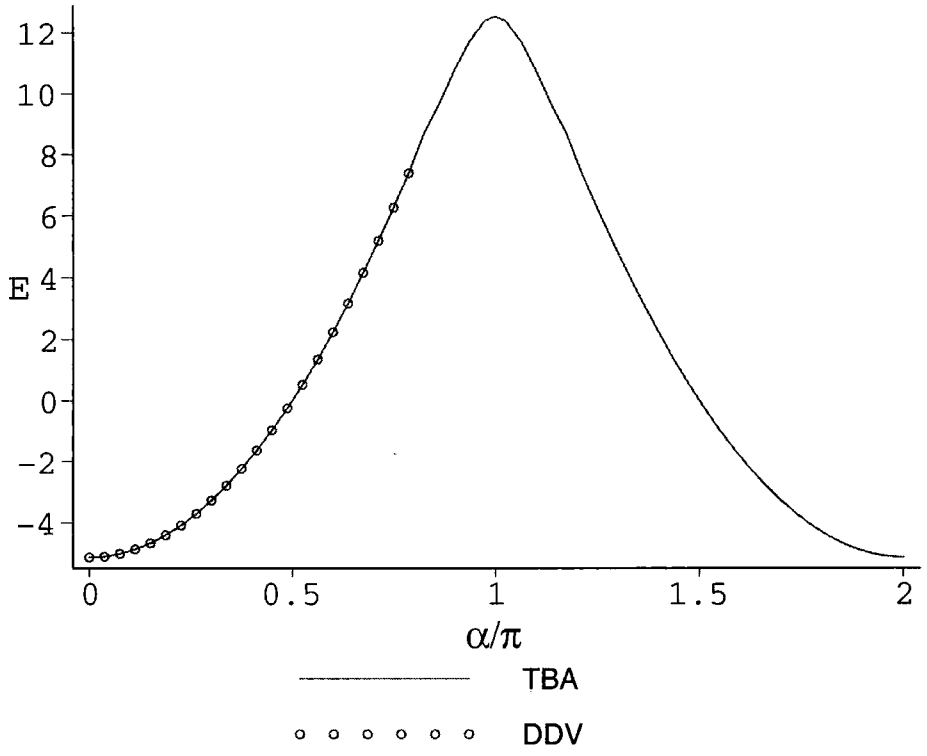

Figure 2.12: Energy calculated using the TBA equations and, when the equation converged, the results from the NLIE.

Following the method successfully used to find the excited state TBA equations, we deform the contours away from the singularities and then use the residue trick. We find the NLIE becomes

$$\begin{aligned} f(\theta) &= -i\,r\sinh\theta + i\,\alpha - \ln S_0(\theta - h_1) - \ln S_0(\theta + h_1) \\ &+ \int_{C_1} d\theta'\,\varphi(\theta-\theta')\ln(1+e^{f(\theta')}) - \int_{C_2} d\theta'\,\varphi(\theta-\theta')\ln(1+e^{-f(\theta')})\ . \end{aligned} \tag{2.57}$$

Numerically we find that once the zeros reach the origin they change direction and move along the real axis at h_1 and $-h_1$ respectively. Their positions are fixed by their definition as singularities of the logarithmic term:

$$1 + e^{f(h_1)} = 0 \quad \Rightarrow \quad f(h_1) = i\pi I_1 \tag{2.58}$$

for some $I_1 \in \mathbb{Z} + \frac{1}{2}$. In the above classification of source objects, these zeros must both be holes. However, we need to be a little careful here. Figure 2.14 shows the form of $\Im m f(\theta)$ as a function of real θ. The roots of the Bethe ansatz equations can be found from this plot by noting where $\Im m f(\theta)/\pi$ crosses the lines marked at odd integers. As $\alpha \to 3\pi/4$ Figure 2.15 shows a plateau moving towards the line $\Im m\theta = \pi$. For values of α greater than $3\pi/4$ the function $\Im m f(\theta)$ resembles the curve shown in Figure 2.16. There are now three points all satisfing

$$\Im m f(\theta) = \pi\,. \tag{2.59}$$

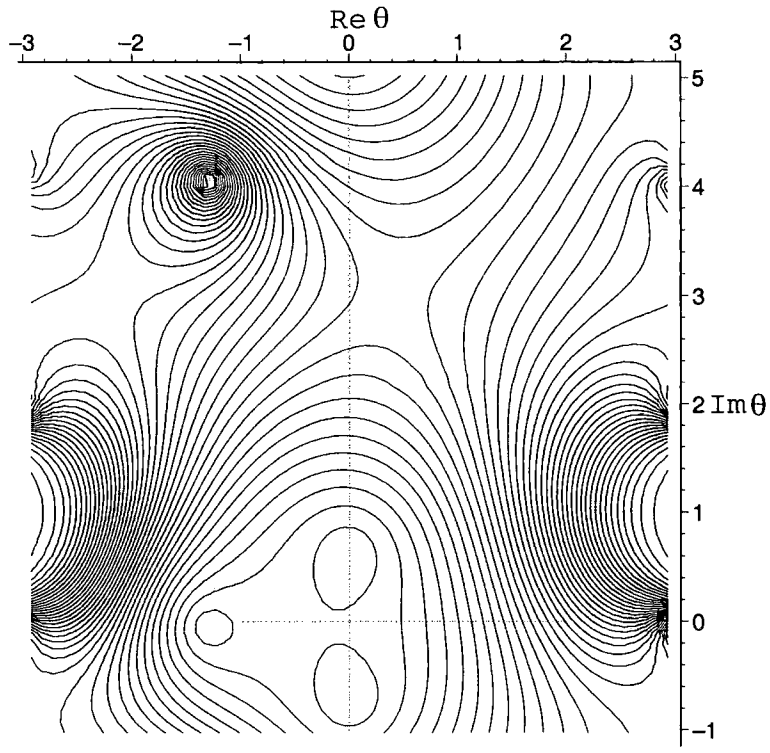

Figure 2.13: Contour plot of $1 + e^{f(\theta)}$ at $r = 0.1$ and $\alpha = 0.825\pi$ at $\xi = 2$. The axes are marked in units of $\pi/2$.

The point denoted R is the root that has been there all along but H and S are new holes. More importantly S must be a special hole since $\Im m f(\theta)$ is increasing at that point. The source term for such objects at positions h and s is

$$g(\theta) = -\ln S_0(\theta - h) + 2 \ln S_0(\theta - s)\,, \tag{2.60}$$

which does not agree with our result (2.57). However this is simply resolved. We were not sufficiently careful when calculating the residue terms and failed to use a continuous branch for the logarithm at $-h_1$. Correcting for this gives the correct source term (2.60) where we now identify $h = h_1$ and $s = -h_1$.

Now we try to solve the equation (2.57) with the new source term (2.60), and subject to the constraint (2.58). Unfortunately the iteration still fails to converge although we now believe the equations are correct and this problem is a numerical artifact. The branch of the logarithm chosen by Fortran is fixed and attempts to correct this 'by hand' have so far been unsuccessful. This problem with the specials has also been discussed in [76] and is currently under further investigation [1].

We can however make some progress if we consider the kink limit of the equation. In the limit $r \to 0$ the function f splits into a left and right kink as usual, but what happens to the two new holes? Their behaviour is rather simple: the left kink claims the special hole and the normal hole moves into the right kink. This is good news since the problem with the branch choice for the logarithm only occurs at the special hole. So, the equation $f_R(\theta)$ describing the right kink with source

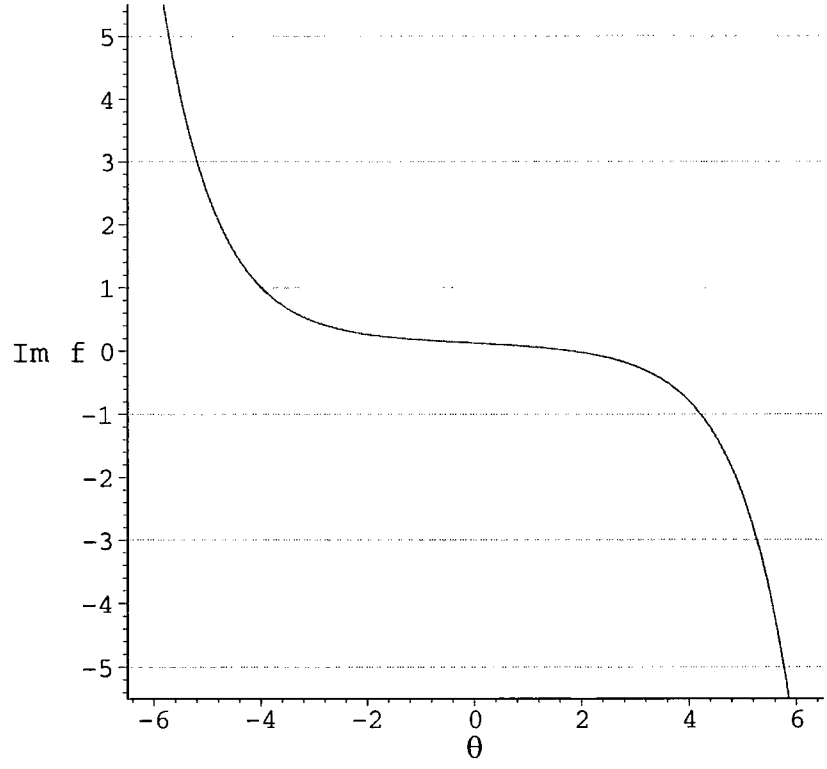

Figure 2.14: $\Im m(f(\theta)/\pi)$ at $\alpha = 0.05\pi$ and $r = 0.1$.

term $g(\theta) = -\ln S_0(\theta - h_1)$ should converge, and this is what we find numerically. Attempts to solve the left kink equation with the source term $g(\theta) = 2\ln S_0(\theta + h_1)$ fail as the equations do not converge due to the special hole.

We can predict possible values of α at which the NLIE fails to converge using the plateau value. The plateau which forms around $\theta = 0$ is equal to [50]

$$f = \frac{2\,i\,\alpha\xi}{\xi+1}\,, \tag{2.61}$$

and so we expect two new holes (although they do not have to be symmetrical) to appear when f is an integer multiple of $i\pi$. That is for the following values of α:

$$\alpha = \frac{\pi(\xi+1)}{2\xi}(2j-1) \quad , \quad j \in \mathbb{Z}\,. \tag{2.62}$$

This implies that at $\xi = 2$ new holes appear whenever $\alpha = \pi(3j/2-3/4)$. Note that these are exactly the values of α at which y zeros affect the TBA system. Intrigued by this similarity, we took a closer look at the positions of the zeros of the TBA functions, $X(\theta)$ and $Y(\theta)$, and the zeros of the function $1 + e^{f(\theta)}$. We were rather surprised to find very simple relations between the zero positions. Figures 2.17, 2.18 and 2.19 show contour plots of the functions $X(\theta)$, $Y(\theta)$ and $1 + e^{f(\theta)}$ in the complex θ-plane. Concentric circles indicate positions of either zeros or, for the latter function only, points where the function is infinite.

The dashed lines on Figure 2.17 indicate the real part of the positions of two pairs of X zeros. For later reference we label the lines as having real part $-b, -a, a, b$

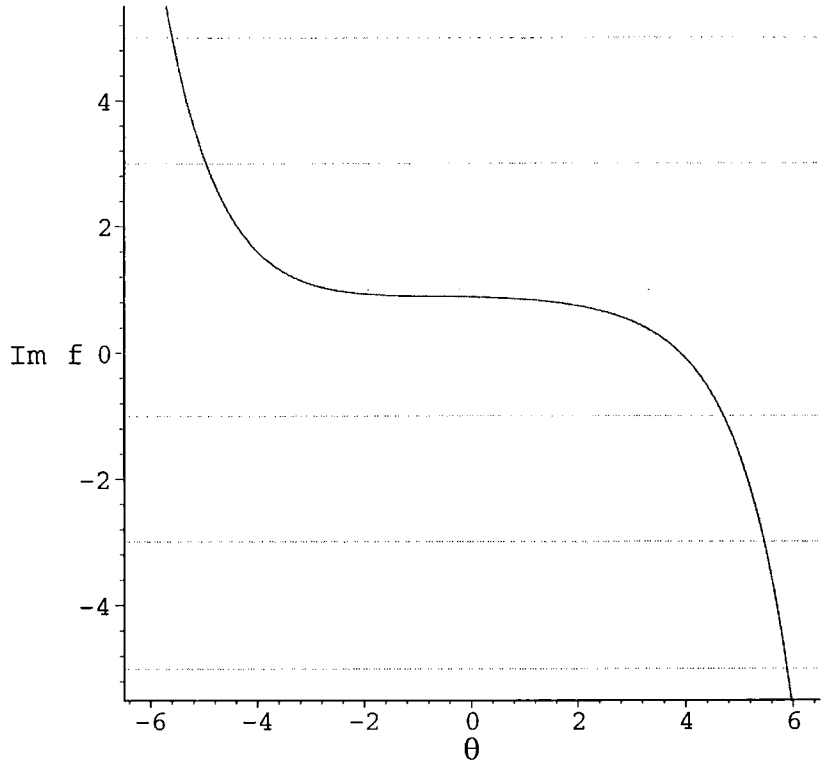

Figure 2.15: $\Im m(f(\theta)/\pi)$ at $\alpha = 0.725\pi$ and $r = 0.1$.

where $0 < a < b$. Similarly on Figure 2.18, but using a solid line, we have indicated the real part of the positions of a single pair of Y zeros. Turning now to the plot in Figure 2.19 we note that the solid lines match up exactly with a pair of zeros of $1+e^{f(\theta)}$. The same is not exactly true for the X zeros, but if we only mark the lines at $-a$ and b, then we find these also pass through zeros of $1 + e^{f(\theta)}$. In fact, each line seems to pass through two zeros: one on the real axis and one with imaginary part 2π. However, the three dimensional version of the plot indicates the concentric circles along the imaginary line 2π are points where $1 + e^{f(\theta)}$ is infinite and not zero.

In a similar way we can exactly match further pairs of Y zeros with zeros of $1+e^{f(\theta)}$. Furthermore, if the X zeros are at positions $\ldots, -d, -c, -b, -a, a, b, c, d, \ldots$, then by plotting just the lines at $\ldots, -c, -a, b, d, \ldots$ we match the remaining zeros of $1 + e^{f(\theta)}$.

What is the explanation underlying the relations between the zero structure of these functions? Recall that the method of derivation of each equation is very different. The derivation of the NLIE starts from the related lattice model, whereas the TBA is defined from the (conjectured) scattering amplitudes. Both methods are known to yield exactly the same value of the central charge for the ground-state. The TBA equations are known for many models, but there are very few equations of NLIE type so it would be rather important to be able to derive one equation from the other. A deeper understanding of the underlying structure of the equations may be a step towards this goal.

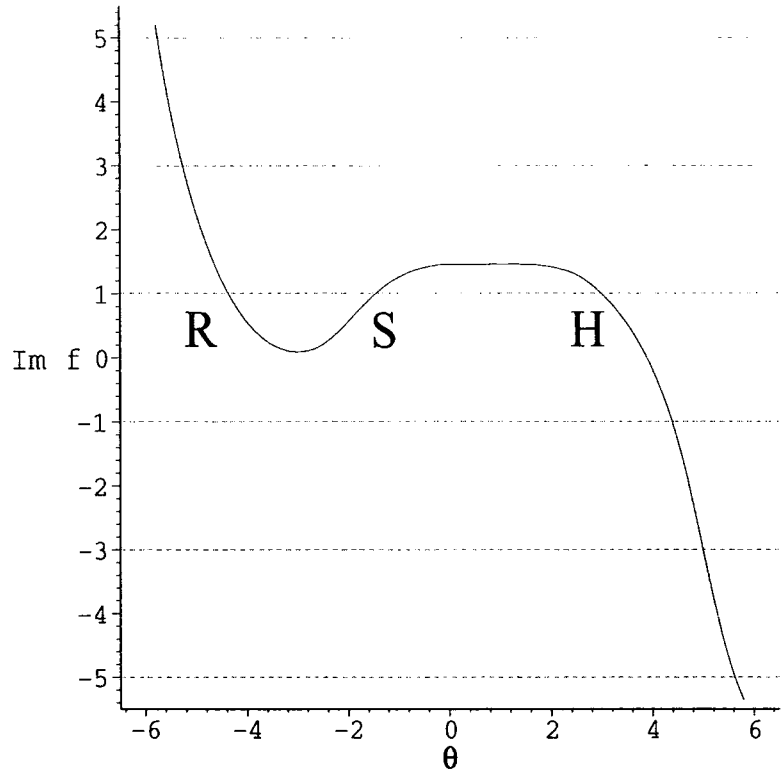

Figure 2.16: $\Im m(f(\theta)/\pi)$ at $\alpha = 0.8\pi$ and $r = 0.1$.

In the next section, we use the functional equations introduced in Section 1.5 to establish relations between the TBA system and NLIEs. The relations found between the various zeros are not just a curiosity: we find we can actually relate all the various functions in the game. This ultimately provides a method of calculating $f(\theta)$ when the iteration of the NLIE (2.55) fails to converge, but unfortunately only for the kink equations.

2.2 Relations between the equations

In this section we will show how the relationships between the zeros of the TBA and NLIE functions found numerically in the last section, all follow from functional relations satisfied by the $\mathbf{T}$ and $\mathbf{Q}_\pm$ operators of integrable quantum field theory. In Section 1.5 we introduced two different functional equations: the fusion relations (1.148) involving just the $\mathbf{T}$ operators and the $\mathbf{T}$–$\mathbf{Q}_\pm$ functional relations (1.155) relating the $\mathbf{Q}_\pm$ operators to $\mathbf{T}_{\frac{1}{2}}$. The first of these sets of relations led to equations of TBA type for the eigenvalues of the operators, whilst the second led to the single NLIE describing the ground-state energy of the sine-Gordon model.

To establish our result we need to take a rather indirect route: the T–Q formalism is defined only for the attractive regime of the sine-Gordon model, and in addition the resulting nonlinear integral equations are those in which the conformal

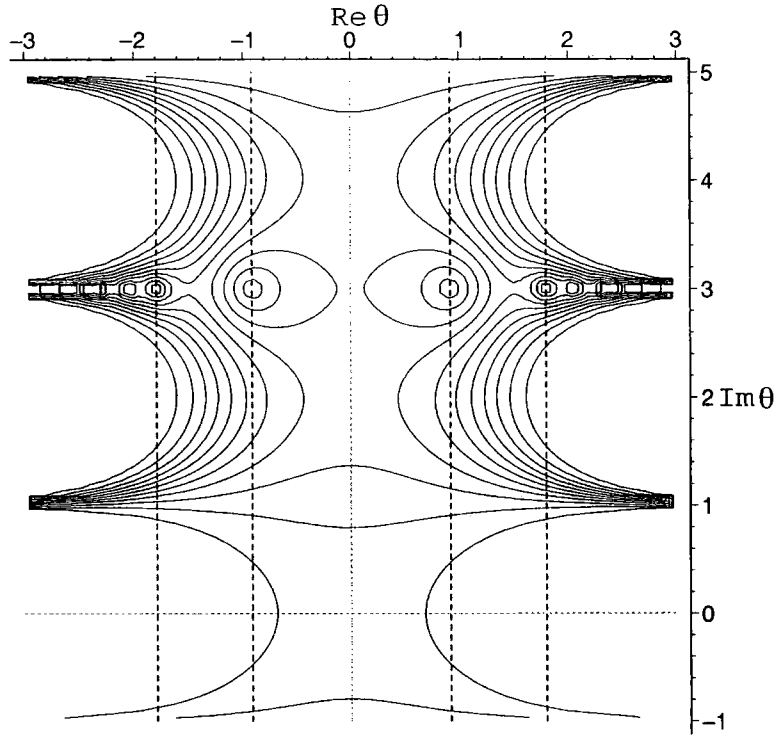

Figure 2.17: Contour plot of $X(\theta)$ at $r = 0.6$ and $\alpha = 0.58\pi$ at $\xi = 2$. The dashed lines indicate the positions of the first two pairs of X zeros. The axes are marked in units of $\pi/2$.

limit has been taken. We start by considering the equations at $\xi = 1/2$ where the functional relations introduced in Section 1.5 do hold. We use the relations to relate the zero structure of the functions at this value of ξ. We then propose relations that hold at $\xi = 2$, guided by both the numerical results and the duality mentioned in Section 1.4.1, which relates the Y-systems of the sine-Gordon model at these two points.

For both the attractive and repulsive points we also write down the form of the equations that hold for the massive models, and back up our conjectures with some numerics.

2.2.1 T-system at N=3

The $\mathbf{T}$ operators for a conformal field theory with central charge less than one were introduced in Section 1.5.1. For a general CFT there an infinite number of $\mathbf{T}$ operators and the fusion relations they satisfy are also infinite in number. However, if β^2 (related to the central charge via (1.144)) is such that $q^N = \exp(i\pi\beta^2 N) = \pm 1$, then the fusion relations truncate. When $\xi = 2$, equation (1.108) implies $\beta^2 = 1/3$ and so taking N to be 3 we have $q^3 = 1$. The fusion relations (1.148) therefore truncate to three equations involving the operators $\mathbf{T}_0 = \mathbb{1}$, $\mathbf{T}_{\frac{1}{2}}$ and $\mathbf{T}_1$. The

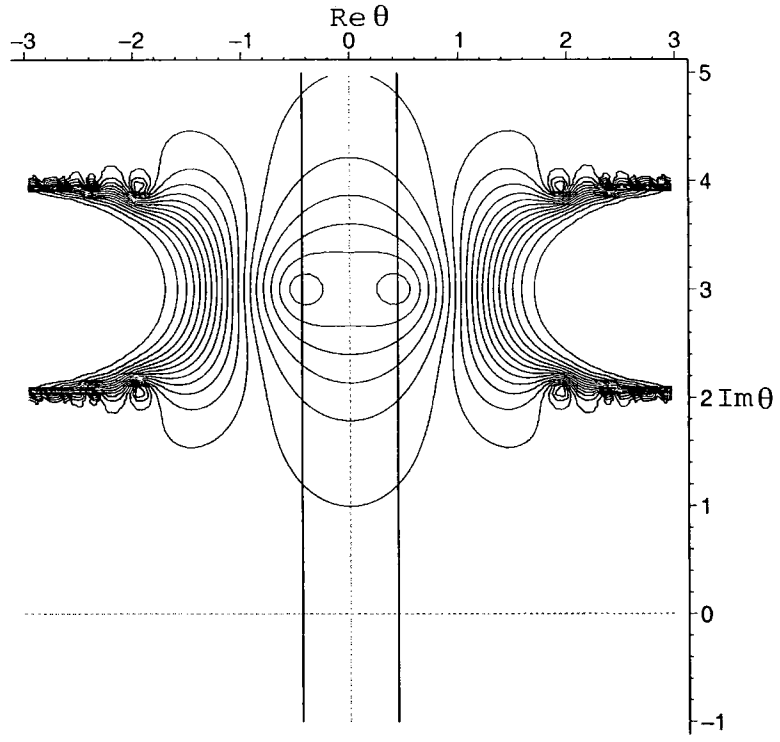

Figure 2.18: Contour plot of $Y(\theta)$ at $r = 0.6$ and $\alpha = 0.58\pi$ at $\xi = 2$. The vertical solid lines indicate the position of the first pair of Y zeros. The axes are marked in units of $\pi/2$.

dictionary (1.152) relates the eigenvalues of these operators to the D_3 Y-system via

$$\begin{aligned} Y_0(\theta) &= 0\,, \\ Y_{\frac{1}{2}}(\theta) &= T_1(\lambda)\,, \\ \overline{Y}(\theta) &= T_{\frac{1}{2}}(\lambda)\,, \end{aligned} \tag{2.63}$$

with $\lambda = \exp(2\theta/3)$ and $q = \exp(i\pi/3)$. To match our notation for the $\xi = 2$ Y-system we set $Y_{\frac{1}{2}} = X$, $\overline{Y} = Y$ and $\alpha = 2\,i\pi N$. The Y-system follows from the fusion relations (1.148)

$$X(\theta + i\pi/4)X(\theta - i\pi/4) = (1 + e^{i\alpha}Y(\theta))(1 + e^{-i\alpha}Y(\theta))\,, \tag{2.64}$$

$$Y(\theta + i\pi/4)Y(\theta - i\pi/4) = 1 + X(\theta)\,. \tag{2.65}$$

Setting $X(\theta) = e^{\varepsilon_1(\theta)}$ and $Y(\theta) = e^{\varepsilon_2(\theta)}$, the corresponding TBA equations are [1]

$$\varepsilon_1(\theta) = \sqrt{2}\,r\cosh\theta + \int \frac{d\theta'}{2\,\pi}\,\varphi_{11}(\theta - \theta')\,L_1(\theta') + \int \frac{d\theta'}{2\,\pi}\,\varphi_{12}(\theta - \theta')\,L_2(\theta') \tag{2.66}$$

$$\varepsilon_2(\theta) = r\cosh\theta + \int \frac{d\theta'}{2\pi}\,\varphi_{12}(\theta - \theta')\,L_1(\theta') + \int \frac{d\theta'}{2\pi}\,\varphi_{22}(\theta - \theta')\,L_2(\theta')\,, \tag{2.67}$$

where

$$L_1(\theta) = \ln(1 + e^{-\varepsilon_1(\theta)}) \tag{2.68}$$

$$L_2(\theta) = \ln(1 + e^{i\alpha - \varepsilon_2(\theta)})(1 + e^{-i\alpha - \varepsilon_2(\theta)}) \tag{2.69}$$

[1] These are the equations for the massive model. For the conformal case we must replace $r\cosh\theta$ by $\exp\theta$ in both the pseudoenergy equations and additionally replace $\cosh\theta$ with $2\exp\theta$ in $E(r)$.

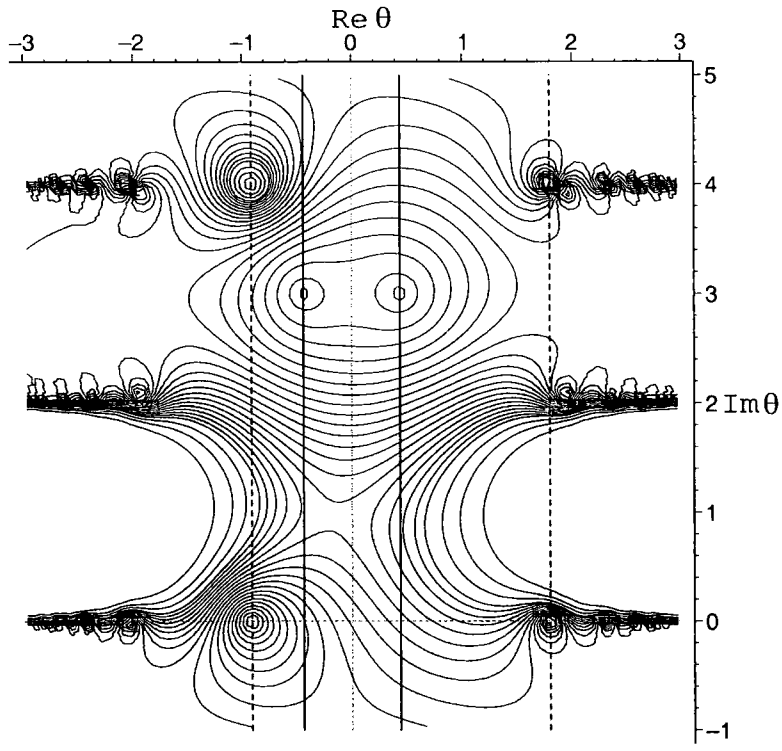

Figure 2.19: Contour plot of $1+e^{f(\theta)}$ at $r = 0.6$ and $\alpha = 0.58\pi$ at $\xi = 2$. The vertical solid lines indicate the position of a pair of zeros and the dashed lines indicate the positions of singlets. The axes are marked in units of $\pi/2$.

and the kernel functions are given by

$$\varphi_{11}(\theta) = \frac{2}{\cosh\theta} \tag{2.70}$$

$$\varphi_{12}(\theta) = \frac{2\sqrt{2}\,\cosh\theta}{2\,\cosh^2\theta - 1} \tag{2.71}$$

$$\varphi_{21}(\theta) = \frac{1}{\cosh\theta}\,. \tag{2.72}$$

The finite-size energy depends on both of the pseudoenergy functions and can be calculated using

$$E(r) = -M \int \frac{d\theta}{2\pi} \cosh\theta \left(L_2(\theta) + \sqrt{2}\, L_1(\theta)\right)\,. \tag{2.73}$$

2.2.2 Zero positions

Before proceeding to the kink equations, we plot the massive TBA functions $X(\theta)$ and $Y(\theta)$, and the function $1 + e^{f(\theta)}$ at $\xi = 1/2$. The results, shown in Figures 2.20, 2.21 and 2.22, suggest the Y zeros exactly match with zeros of $1 + e^{f(\theta)}$, whilst the X zeros must again be shared out between the left and right halves of the complex plane. In contrast to the behaviour at $\xi = 2$, the zeros must be shared out between the left and right halves of the complex plane in exactly the opposite way. That is if the TBA X zeros have real part at $\ldots, -d, -c, -b, -a, a, b, c, d, \ldots$, then the zeros of $1 + e^{f(\theta)}$ are at $\ldots, -d, -b, a, c, \ldots$.

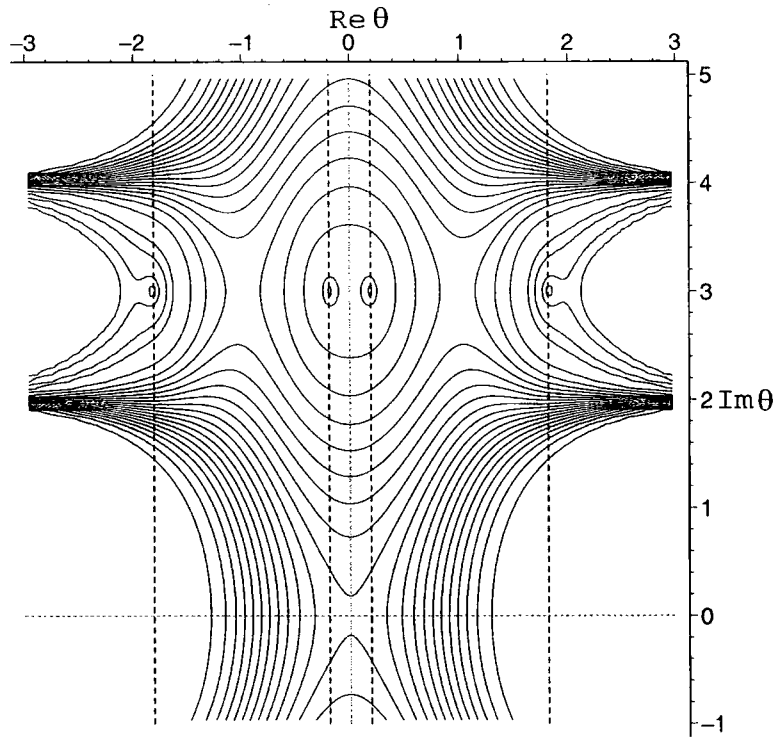

Figure 2.20: Contour plot of $X(\theta)$ at $r = 0.7$ and $\alpha = 0.95\pi$ at $\xi = 1/2$. The dashed lines indicate the positions of the first two pairs of X zeros. The axes are marked in units of $\pi/4$.

The kink functions

When the conformal limit of the TBA equations is taken, the zeros in the right half of the plane slide off towards infinity and become the right kink functions. Due to the symmetry of the TBA functions the leftmost zeros behave in an analogous way. The left and right kink functions are related via

$$X_L(\theta,\alpha) = X_R(-\theta,\alpha) \quad , \quad Y_L(\theta,\alpha) = Y_R(-\theta,\alpha) \; . \tag{2.74}$$

so we concentrate on just the right kink. When the conformal limit is taken, the zeros of the function $1+e^{f(\theta)}$ become part of either the right or left kink functions by heading towards plus or minus infinity respectively, However, for almost all values of α, $f(\theta)$ is not an even function of θ and the functions $f_L(\theta)$ and $f_R(\theta)$ will be different.

The exact relation between the zeros is pinned down using the $T-Q$ relation (1.158). We need to write it in terms of the functions $a_\pm$, which by comparing the equations (1.175) and (1.136) are related to the kink functions $f_{R/L}$ via

$$a_+(\theta,\alpha) = e^{f_R(\theta,\alpha)} \; , \tag{2.75}$$

$$a_-(\theta,\alpha) = e^{-f_L(-\theta,\alpha)} \; . \tag{2.76}$$

Since the functions $a_\pm(\theta,\alpha)$ are related via analytic continuation in α

$$a_+(\theta,\alpha) = a_-(\theta,-\alpha) \tag{2.77}$$

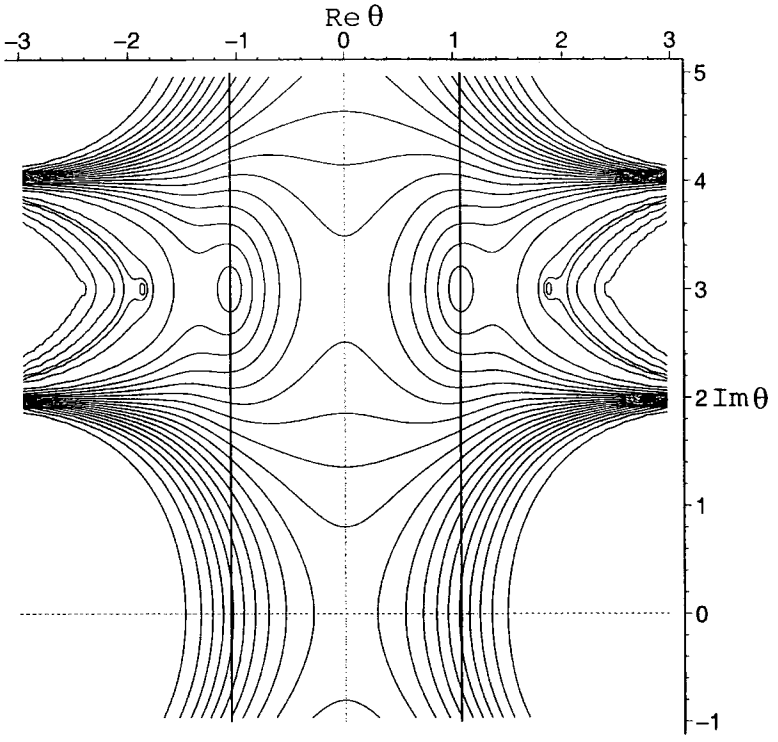

Figure 2.21: Contour plot of $Y(\theta)$ at $r = 0.7$ and $\alpha = 0.95\pi$ at $\xi = 1/2$. The vertical solid lines indicate the position of the first pair of Y zeros. The axes are marked in units of $\pi/4$.

we may restrict $\alpha > 0$.

The T–Q relation written in terms of $a_\pm(\lambda)$ is

$$T(\lambda)A_\pm(\lambda) = e^{\mp 2i\pi P} A_\pm(q^{-1}\lambda)(1 + a_\pm(\lambda))\,. \tag{2.78}$$

Suppose θ_k is a zero of $1+a_\pm(\theta)$. Now set $\theta = \theta_k$ in (2.78) so that the right hand side is zero. Since both T and $A_\pm$ are entire functions, it follows that either $T(\theta_k) = 0$ or $A_\pm(\theta_k) = 0$. We use this to split the set of zeros $\{\theta_k\}$ of $1 + a_\pm(\theta)$ into two subsets:

$$\begin{aligned} &\text{Type I}: && T(y_j) &&= 0\,, \\ &\text{Type II}: && A_\pm(x_i) &&= 0\,. \end{aligned} \tag{2.79}$$

We now match each type of zero with a zero of the TBA equations. The notation has already given away the relation between the Type I zeros and the TBA zeros: the dictionary (2.63) identifies $T(\lambda)$ with $Y(\theta)$ so (2.79) implies

$$Y(y_j) = 0 \quad \Longleftrightarrow \quad 1 + a_\pm(y_j) = 0\,. \tag{2.80}$$

The relation between the Type II zeros and the TBA X zeros is more subtle. This is expected since the plots indicated that the X zeros have to be split into two sets. We establish the connection using a further functional relation between the **T** and **Q** operators. This relation is given by the eigenvalue equivalent of equation (1.179). We set $N = 3$, replace T_1 with $Y_{\frac{1}{2}} = X(\theta)$ and change from the variable λ

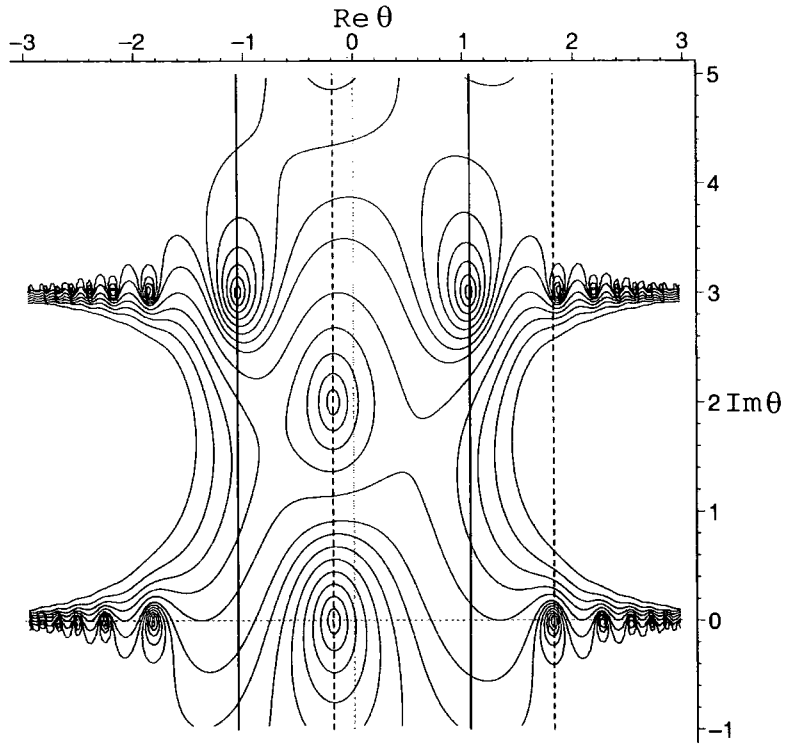

Figure 2.22: Contour plot of $1+a(\theta)$ at $r = 0.7$ and $\alpha = 0.95\pi$ at $\xi = 2$. The vertical solid lines indicate the position of a pairs of zeros and the dashed lines indicate the positions of singlets. The axes are marked in units of $\pi/4$.

to θ so that (1.179) becomes

$$X(\theta - 3i\pi/4) = \frac{\sin(\frac{3\xi\alpha}{1+\xi})}{\sin(\frac{\xi\alpha}{1+\xi})} A_+(\theta) A_-(\theta) \,. \tag{2.81}$$

We deduce that each θ_k such that $X(\theta \pm 3i\pi/4) = 0$ [2] is also a zero of either $A_+(\theta)$ or $A_-(\theta)$. Equivalently, by (2.78), each zero must correspond to either a zero of $1 + a_+(\theta)$ or $1 + a_-(\theta)$.

When the twist α is zero, the functions $a_\pm$ coincide and it is not necessary to split the X zeros into two sets. However, at nonzero α, the twist combined with the Y-system (2.65) allows us to pin down to which of the functions $a_\pm$ each X zero actually corresponds.

The Y-system implies that the zeros satisfying $X(x_i + 3i\pi/4) = 0$ must also satisfy

$$0 = \left(1 + e^{i\alpha} Y\left(x_i + i\pi/2\right)\right)\left(1 + e^{-i\alpha} Y\left(x_i + i\pi/2\right)\right) \,. \tag{2.82}$$

We split the full set of X zeros $\{x_i\}$ into two subsets $\{x_+\}, \{x_-\}$ according to which factor of (2.82) they cause to be zero:

$$\begin{aligned} X(x_+ + 3i\pi/4) = 0 \iff Y\left(x_+ + i\pi/2\right) = -e^{-i\alpha} \,, \\ X(x_- + 3i\pi/4) = 0 \iff Y\left(x_- + i\pi/2\right) = -e^{i\alpha} \,. \end{aligned} \tag{2.83}$$

[2] the sign is unimportant since the TBA equations are $3i\pi/2$ periodic in θ

This combined with (2.81) leads us to conjecture the following

$$\begin{aligned} A_+(x_+) = 0 &\iff 1 + a_+(x_+) = 0 \,, \\ A_-(x_-) = 0 &\iff 1 + a_-(x_-) = 0 \,. \end{aligned} \tag{2.84}$$

So pulling everything we have learnt in this section together we have

$$\boxed{\begin{aligned} Y(y_j) = 0 &\iff 1+a_\pm(y_j) = 0 \\ Y(x_\pm + i\pi/2) = -e^{\mp i\alpha} &\iff 1+a_\pm(x_\pm) = 0 \,. \end{aligned}}$$

The massive model

The above relations easily generalise to the massive model as loosely speaking each of the massive functions ($Y(\theta), X(\theta)$ and $f(\theta)$) are made from gluing a left and right kink together in the central region. All of the TBA zeros now appear in pairs, but the zeros of $1 + e^{f(\theta)}$ fall into two types: some in pairs (Type I) and some alone (Type II). We assume that the T–Q relation continues to hold for r dependent functions T,a and A with small and large as being related as before (1.167). We mark the zeros with a small bar to remind us that these now belong to the functions describing the massive model. Using the T–Q relation we again split the zeros of $1 + a(\theta)$ into two types:

$$\begin{aligned} \text{Type I}: &\quad T(\pm\bar{y}_j) = 0 \,, \\ \text{Type II}: &\quad A(\bar{x}_i) = 0 \,. \end{aligned} \tag{2.85}$$

The Type II zeros $\{\bar{x}\}$ are singlets and we need to further divide them into two sets depending upon whether they live in the left or right half of the complex θ-plane:

$$\{\bar{x}\} = \{\bar{x}_- : \Im m(\bar{x}_-) < 0\} \cup \{\bar{x}_+ : \Im m(\bar{x}_+) > 0\} \tag{2.86}$$

Then we claim the following holds

$$\boxed{\begin{aligned} Y(\pm\bar{y}_j) = 0 &\iff 1+a(\pm\bar{y}_j) = 0 \\ Y(\bar{x}_\pm + i\pi/2) = -e^{\mp i\alpha} &\iff 1+a_\pm(\bar{x}_\pm) = 0 \,. \end{aligned}}$$

These relations are in agreement with the plots shown in Figures 2.20, 2.21 and 2.22.

2.2.3 Direct relations between the functions

In the last section we pinned down the zero structure of both sets of functions for $\xi = 1/2$ in the attractive regime. In this section we again use the functional relations satisfied by the $\mathbf{T}$ and $\mathbf{Q}_\pm$ operators to find direct relations between the TBA and NLIE functions.

Again we use the relation (1.179) between $\mathbf{T}$ and $\mathbf{Q}_\pm$. We replace $\mathbf{Q}_\pm$ with $\mathbf{A}_\pm$ using (1.157) and consider the resulting eigenvalue equation:

$$T_{\frac{N}{2}-\frac{1}{2}}(\lambda) = e^{2i\pi pN}\frac{\sin(2\pi pN)}{\sin(2\pi p)}A_+(\lambda q^{\frac{N}{2}})A_-(\lambda q^{\frac{N}{2}})\,. \tag{2.87}$$

We shift $\lambda \to q^{\pm 1-N/2}\lambda$ and construct a fraction using the T functions

$$\frac{T_{\frac{N}{2}-\frac{1}{2}}(q^{1-N/2}\lambda)}{T_{\frac{N}{2}-\frac{1}{2}}(q^{-1-N/2}\lambda)} = \frac{A_+(q\,\lambda)\;A_-(q\,\lambda)}{A_+(q^{-1}\lambda)\;A_-(q^{-1}\lambda)} = a_+(\lambda)a_-(\lambda)\,, \tag{2.88}$$

and then set $N = 3$ and replace T with X according to (1.152). We now have a formula directly relating the functions:

$$\frac{X(\theta - i\pi/4)}{X(\theta + i\pi/4)} = a_+(\theta,\alpha)a_-(\theta,\alpha)\,. \tag{2.89}$$

A further useful relation can be found by taking the T–Q relation (2.78) at $q^{\pm 1/2}\lambda$

$$T_{\frac{1}{2}}(q^{\frac{1}{2}}\lambda)A_\pm(q^{\frac{1}{2}}\lambda) = e^{\mp 2\pi\, ip}A_\pm(q^{-\frac{1}{2}}\lambda)(1 + a_\pm(q^{\frac{1}{2}}\lambda)) \tag{2.90}$$

$$T_{\frac{1}{2}}(q^{-\frac{1}{2}}\lambda)A_\pm(q^{-\frac{1}{2}}\lambda) = e^{\mp 2\pi\, ip}A_\pm(q^{-\frac{3}{2}}\lambda)(1 + a_\pm(q^{-\frac{1}{2}}\lambda))\,. \tag{2.91}$$

Multiplying these equations yields

$$T_{\frac{1}{2}}(q^{\frac{1}{2}}\lambda)T_{\frac{1}{2}}(q^{-\frac{1}{2}}\lambda) = e^{\mp 4\pi\, ip}\frac{A_\pm(q^{-\frac{3}{2}}\lambda)}{A_\pm(q^{\frac{1}{2}}\lambda)}\left(1 + a_\pm(q^{\frac{1}{2}}\lambda)\right)\left(1 + a_\pm(q^{-\frac{1}{2}}\lambda)\right)\,. \tag{2.92}$$

Note that the left hand side forms part of the fusion relations at $j = 1/2$:

$$T_{\frac{1}{2}}(q^{\frac{1}{2}}\lambda)T_{\frac{1}{2}}(q^{-\frac{1}{2}}\lambda) = 1 + T_1(\lambda)\,. \tag{2.93}$$

We replace the left hand side with (2.93), and use the definition of $a_\pm(\lambda)$ (1.167) to yield

$$1 + T_1(\lambda) = a_\pm^{-1}(q^{-\frac{1}{2}}\lambda)\left(1 + a_\pm(q^{\frac{1}{2}}\lambda)\right)\left(1 + a_\pm(q^{-\frac{1}{2}}\lambda)\right)\,. \tag{2.94}$$

We set $N = 3$, replace T_1 with X and change to the variable θ to find

$$X(\theta) = a_\pm^{-1}(\theta - i\pi/4) + a_\pm^{-1}(\theta - i\pi/4)\,a_\pm(\theta + i\pi/4) + a_\pm(\theta + i\pi/4)\,. \tag{2.95}$$

Substituting this equation into the left hand side of (2.89) yields

$$a_+(\theta,\alpha)a_-(\theta,\alpha) = \frac{a_\pm^{-1}(\theta - i\pi/2) + a_\pm^{-1}(\theta - i\pi/2)\,a_\pm(\theta) + a_\pm(\theta)}{a_\pm^{-1}(\theta) + a_\pm^{-1}(\theta)\,a_\pm(\theta + i\pi/2) + a_\pm(\theta + i\pi/2)}\,. \tag{2.96}$$

This relation between the functions $a_\pm(\theta)$ and $a_\mp(\theta)$ holds for all values of α. Therefore we can use (2.96) to calculate $a_\mp(\theta)$ for free, once we have calculated $a_\pm(\theta)$. We will use this idea later for the model at $\xi = 2$.

Massive relations

Numerically we find the relations between the functions for the massive model take the form

$$\frac{X(\theta-i\pi/4,\alpha)}{X(\theta+i\pi/4,\alpha)} = a(\theta,\alpha)a^{-1}(-\theta,\alpha) = a(\theta,\alpha)a(\theta,-\alpha)\ , \tag{2.97}$$

and

$$a(\theta,\alpha)a(\theta,-\alpha) = \frac{a^{-1}(\theta-i\pi/2,\pm\alpha) + a^{-1}(\theta-i\pi/2,\pm\alpha)\,a(\theta,\pm\alpha) + a(\theta,\pm\alpha)}{a^{-1}(\theta,\pm\alpha) + a^{-1}(\theta,\pm\alpha)\,a(\theta+i\pi/2,\pm\alpha)+a(\theta+i\pi/2,\pm\alpha)}\ . \tag{2.98}$$

2.2.4 Extension of results to $\xi = 2$

We have used the functional relations to show how the singularity structure of the two types of NLIEs are intrinsically tied together at $\xi = 1/2$. Since we wish to use these ideas at $\xi = 2$ we need to modify the relations. A hint comes from the duality between the Y systems at these two points. The duality procedure implies the $\xi = 2$ Y system (2.14) is obtained from the $\xi = 1/2$ system (2.65) by replacing Y with $1/Y$ and sending $i\pi/4 \to i\pi/2$. However, we have defined the pseudoenergies differently: $X(\theta) = \exp(-\varepsilon_1(\theta))$ at $\xi = 2$ whereas the analogous relation at $\xi = 1/2$ is $X(\theta) = \exp(\varepsilon_1(\theta))$. Thus the duality transformation in our notation involves sending $i\pi/4 \to i\pi/2$.

We conjecture the relations between the zero positions for the kink functions are

$$\begin{array}{rcl} Y(y_j) = 0 & \Longleftrightarrow & 1 + a_\pm(y_j) = 0 \\ Y\left(x_\pm + i\pi\right) = -e^{\pm 2i\alpha} & \Longleftrightarrow & 1 + a_\pm(x_\pm) = 0 \end{array}$$

In contrast to the attractive regime we note that the sign of α must be reversed for the repulsive regime. These same relations hold for the massive equations as well: just replace $a_\pm(\theta)$ with $a(\theta)$ and consider x_+/x_- to be the zeros of $1 + e^{f(\theta)}$ in the right/left half of the complex plane. The above relations are in agreement with the suggestions from Figures (2.17),(2.18) and (2.19), and numerical checks also back up the above.

We can also write down exact relations between the functions along the lines of the equations (2.89) and (2.96). These are

$$\frac{X(\theta+i\pi/2)}{X(\theta-i\pi/2)} = a_+(\theta)a_-(\theta) \tag{2.99}$$

and

$$a_+(\theta,\alpha)a_-(\theta,\alpha) = \frac{a_\pm^{-1}(\theta+i\pi) + a_\pm^{-1}(\theta+i\pi)\,a_\pm(\theta) + a_\pm(\theta)}{a_\pm^{-1}(\theta) + a_\pm^{-1}(\theta)\,a_\pm(\theta-i\pi) + a_\pm(\theta-i\pi)}\ . \tag{2.100}$$

Now we can make use of our findings. We can use (2.100) to calculate $a_-(\theta)$ whenever the direct iteration of the equation fails to converge, provided we calculate

$a_+(\theta)$ first. In Table 2.2 we compare the value of $a_-(\theta)$ calculated using three different methods:

A : By directly iterating the NLIE.

B : Calculating the TBA function $X(\theta)$ and $a_+(\theta)$ then using formula (2.99).

C : Calculating $a_+(\theta)$ and then using formula (2.100).

Method	$\Re ea_-(\theta)$	$\Im ma_-(\theta)$
A	2.3072542827776	-2.0569510831190
B	2.3072542827768	-2.0569510831102
C	2.3072542827031	-2.0569510831973

Table 2.2: Comparison of various methods of calculating $a_-(\theta)$ at $\xi = 2$ for $\theta = 0.2 - i0.3$ at $\alpha = 0.2\pi$

2.3 Summary

In this chapter we have studied the sine-Gordon model at $\xi = 2$ in the repulsive regime. Using the idea of analytic continuation in the twist parameter α, we proposed TBA equations describing the spin-zero excited states of the theory. The next step was to check these results against a further type of NLIE also proposed to describe such states.

We then made a little progress towards further understanding the connections between these methods of calculating the finite-size energy of the sine-Gordon model by establishing relations between the zero positions of the various functions.

Chapter 3

Flows between conformal field theories

In the previous chapter we discussed the real coupled sine-Gordon model as an example of a perturbed conformal theory with a massive particle spectrum. This model also describes massless perturbations provided the coupling is continued to imaginary values, as mentioned in Chapter 1. Interpolating flows between minimal models are the subject of this chapter. The imaginary coupled sine-Gordon model provides a set of examples since it reproduces the flows between minimal models perturbed by ϕ_{13}. However, the primary field ϕ_{13} is not the only possible choice of operator with which we can perturb the minimal models. The fields ϕ_{21} and ϕ_{15} also produce integrable perturbations of $\mathcal{M}_{pq}$ [12, 77] provided the operator is relevant for that particular choice of p and q. Examples of flows between minimal models perturbed by these operators have been found by Martins [57], and they provide part of the motivation for this chapter. These are perturbations of the nonunitary minimal models $\mathcal{M}_{p,2p-1}$ and $\mathcal{M}_{p,2p+1}$ by the operators ϕ_{21} and ϕ_{15} respectively. The predicted trajectories are:

$$\mathcal{M}_{p,2p-1} + \phi_{21} \rightarrow \mathcal{M}_{p-1,2p-1} \; ; \tag{3.1}$$

$$\mathcal{M}_{p,2p+1} + \phi_{15} \rightarrow \mathcal{M}_{p,2p-1} \; . \tag{3.2}$$

From this we see that the flows can be chained together to form a single sequence, along which the perturbing operator alternates between ϕ_{21} and ϕ_{15}. The flows were further studied by Ravanini et al. in [61]. For each trajectory they proposed a set of TBA equations describing the evolution of the effective central charge from the ultraviolet to the infrared.

In this chapter we propose further sequence of flows for which the perturbing operator alternates in the same way. We find the sequence (3.1) and (3.2) is picked out by the monotonicity of the effective central charge as a function of r. More surprisingly, we discover $c_{\text{eff}}(r)$ undergoes a number of oscillations as it interpolates

between its short and long distance limits in all other cases.

In contrast to the TBA method used to study (3.1) and (3.2) in [61], we express $c_{\text{eff}}(r)$ in terms of a single nonlinear integral equation that describes infinitely-many different perturbed conformal field theories, each being picked out by an appropriate choice of certain parameters. The equation given in [34] is one example of a NLIE describing massive perturbations. Al.B. Zamolodchikov [52] proposed the only known example of such an equation describing massless flows by modifying the massive equation [34]. In Section 3.3 we use similar methods to modify the nonlinear integral equation proposed in [78] to describe massive ϕ_{12}, ϕ_{21} and ϕ_{15} perturbations of the minimal models. The modified equation enables the promised new sequences of flows to be studied.

We begin by reviewing Zamolodchikov's ideas before obtaining our NLIE in Section 3.3. In further sections the predicted flows are subjected to analytical and numerical checks before returning to comment on some features of the ϕ_{13} flows.

3.1 The imaginary coupled sine-Gordon model

Zamolodchikov's modification of the NLIE [34] enables flows between minimal models induced by the operator ϕ_{13} to be studied. The modification relies on elements of the corresponding massless scattering theory of the imaginary coupled sine-Gordon (ISG) model, so this is where we begin.

The imaginary coupled sine-Gordon model is obtained from (1.107) by the substitution $\lambda \to i\lambda$:

$$\mathcal{A}_{\text{ISG}} = \tfrac{1}{2}\int (\partial_\mu \phi)^2 \, d^2x - i\lambda \int \cos\beta \ \phi \ d^2x \,. \tag{3.3}$$

It will be more convenient to work with the parameter $\zeta = \beta^2/(8\pi - \beta^2)$ rather than the coupling constant β. As previously mentioned in Section 1.6, perturbative renormalisation group studies for $\zeta \gg 1$ indicate the imaginary coupled sine-Gordon model describes a massless interpolating trajectory from the model having parameter ζ at the ultraviolet point to an infrared point with parameter $\zeta - 1$.

The arguments used to demonstrate integrability are independent of the nature of the coupling constant, so the ISG model is integrable. The idea of scattering between massless particles is not entirely clear, but since the model is integrable one can hope that it will be possible to ignore any subtleties and implement the usual S-matrix technology regardless. This was the approach adopted in [79] and also by Al.B. Zamolodchikov in [52]. Thus we assume that n-particle scattering amplitudes always reduce to products of two-particle S-matrix elements. The massless scattering theory proposed in [79] involves right and left moving charged doublets $R, \bar{R}$ and

$L, \bar{L}$. As usual the momenta is parameterised using the rapidity variable θ via

$$p_R = \tfrac{1}{2} M e^{\theta}, \quad p_L = -\tfrac{1}{2} M e^{-\theta}. \tag{3.4}$$

Since the model has no mass scale, M no longer corresponds to the lightest mass in the theory. Instead it corresponds to the intercept scale.

The $R-R$ and $L-L$ scattering amplitudes are described by exactly the same amplitudes as the sine-Gordon scattering (1.117) provided we make the substitution $\zeta \to \zeta - 1$ (the notation ξ was used earlier, but we reserve this symbol for later use):

$$S_{LL}{}_{ss}^{ss} = S_{RR}{}_{ss}^{ss} = S, \tag{3.5}$$

$$S_{LL}{}_{\bar{s}s}^{\bar{s}s} = S_{RR}{}_{\bar{s}s}^{\bar{s}s} = S_R, \tag{3.6}$$

$$S_{LL}{}_{s\bar{s}}^{\bar{s}s} = S_{RR}{}_{s\bar{s}}^{\bar{s}s} = S_T. \tag{3.7}$$

The remaining amplitudes are

$$S_{RL}{}_{ss}^{ss} = S_{LR}{}_{ss}^{ss} = -\tilde{S}_0(\theta,\zeta) \cosh\left(\frac{i\pi - \theta}{\zeta - 1}\right), \tag{3.8}$$

$$S_{RL}{}_{\bar{s}s}^{\bar{s}s} = S_{LR}{}_{\bar{s}s}^{\bar{s}s} = \tilde{S}_0(\theta,\zeta) \cosh\left(\frac{\theta}{\zeta - 1}\right), \tag{3.9}$$

$$S_{RL}{}_{s\bar{s}}^{\bar{s}s} = \tilde{S}_0(\theta,\zeta) \sinh\left(\frac{i\pi}{\zeta - 1}\right), \tag{3.10}$$

$$S_{LR}{}_{s\bar{s}}^{\bar{s}s} = -\tilde{S}_0(\theta,\zeta) \sinh\left(\frac{i\pi}{\zeta - 1}\right), \tag{3.11}$$

with

$$\tilde{S}_0(\theta,\zeta) = \frac{1}{\cosh\left(\frac{i\pi-\theta}{\zeta-1}\right)} \exp\left(-\frac{i}{2}\int \frac{dk}{k} \sin(k\theta) \frac{\sinh(\frac{k\pi}{2})}{\sinh(\frac{(\zeta-1)k\pi}{2}) \cosh(\frac{k\pi}{2})}\right). \tag{3.12}$$

The NLIE (1.136) encodes the finite-volume ground-state energy of the massive sine-Gordon model for a continuous range of the coupling β, and at general 'twist' α. The equation is defined in terms of a single function $f(\theta)$, and depends upon the kernel function $\varphi(\theta)$ which is related to the soliton-soliton scattering amplitude $S(\theta)$ via

$$\varphi(\theta) = -\frac{i}{2\pi} \frac{d}{d\theta} \log S(\theta). \tag{3.13}$$

Rather than deriving the integral equations directly from the massless scattering amplitude, Zamolodchikov took a slightly easier route and conjectured them guided by the form of the massive nonlinear integral equation. Later in [52], he claims to have derived them directly from the Bethe ansatz equations [80] for the lattice model.

Zamolodchikov introduced two analytic functions $f_R(\theta)$ and $f_L(\theta)$ and coupled them together using kernels related to the massless scattering amplitudes. We will

only need the kernels related to the $R-R$ and $R-L$ diagonal scattering amplitudes $S_{RR}{}^{ss}_{ss}$ and $S_{RL}{}^{ss}_{ss}$:

$$\phi(\theta) = -\frac{i}{2\pi}\frac{d}{d\theta}\log S_{RR}{}^{ss}_{ss}(\theta) \tag{3.14}$$

$$= \int_{-\infty}^{\infty}\frac{dk}{2\pi}e^{ik\theta}\frac{\sinh(\frac{\pi}{2}(\zeta-2)k)}{2\cosh(\frac{\pi}{2}k)\sinh(k\frac{\pi}{2}(\zeta-1))}\,, \tag{3.15}$$

and

$$\chi(\theta) = -\frac{i}{2\pi}\frac{d}{d\theta}\log S_{RL}{}^{ss}_{ss}(\theta) \tag{3.16}$$

$$= -\int_{-\infty}^{\infty}\frac{dk}{2\pi}e^{ik\theta}\frac{\sinh(\frac{\pi}{2}k)}{2\cosh(\frac{\pi}{2}k)\sinh(k\frac{\pi}{2}(\zeta-1))}\,. \tag{3.17}$$

The following coupled equations were proposed to describe the massless ϕ_{13} perturbations

$$\begin{aligned} f_R(\theta) &= -i\frac{r}{2}e^{\theta} + \frac{i\pi\zeta\alpha}{\zeta-1} \\ &+ \int_{\mathcal{C}_1}\phi(\theta-\theta')\ln(1+e^{f_R(\theta')})\,d\theta' - \int_{\mathcal{C}_2}\phi(\theta-\theta')\ln(1+e^{-f_R(\theta')})\,d\theta' \\ &+ \int_{\mathcal{C}_1}\chi(\theta-\theta')\ln(1+e^{-f_L(\theta')})\,d\theta' - \int_{\mathcal{C}_2}\chi(\theta-\theta')\ln(1+e^{f_L(\theta')})\,d\theta' \end{aligned} \tag{3.18}$$

$$\begin{aligned} f_L(\theta) &= -i\frac{r}{2}e^{-\theta} - \frac{i\pi\zeta\alpha}{\zeta-1} \\ &+ \int_{\mathcal{C}_2}\phi(\theta-\theta')\ln(1+e^{f_L(\theta')})\,d\theta' - \int_{\mathcal{C}_1}\phi(\theta-\theta')\ln(1+e^{-f_L(\theta')})\,d\theta' \\ &+ \int_{\mathcal{C}_2}\chi(\theta-\theta')\ln(1+e^{-f_R(\theta')})\,d\theta' - \int_{\mathcal{C}_1}\chi(\theta-\theta')\ln(1+e^{f_R(\theta')})\,d\theta' \end{aligned} \tag{3.19}$$

The integration contours can be found in Figure 1.5 and r is a dimensionless quantity related to the finite-size of the cylinder: $r = MR$. The effective central charge is replaced by

$$\begin{aligned} c_{\text{eff}}(r) = \frac{3ir}{2\pi^2}\Big[&\int_{\mathcal{C}_1}e^{\theta}\ln(1+e^{f_R(\theta)})\,d\theta - \int_{\mathcal{C}_2}e^{\theta}\ln(1+e^{-f_R(\theta)})\,d\theta \\ &+ \int_{\mathcal{C}_2}e^{-\theta}\ln(1+e^{f_L(\theta)})\,d\theta - \int_{\mathcal{C}_1}e^{-\theta}\ln(1+e^{-f_L(\theta)})\,d\theta\,.\Big] \end{aligned} \tag{3.20}$$

In the UV and IR limits the effective central charge becomes

$$\begin{aligned} c_{ISG}(r=0) &= 1 - \frac{6\zeta}{\zeta+1}\alpha^2 \\ c_{ISG}(r=\infty) &= 1 - \frac{6\zeta}{\zeta-1}\alpha^2\,. \end{aligned} \tag{3.21}$$

We mentioned in Chapter 1 the fact that the sine-Gordon NLIE also describes the minimal models $\mathcal{M}_{p,q}$ perturbed by ϕ_{13}. In the same way we expect the new

NLIE to describe the massless ϕ_{13} perturbation of a minimal model $\mathcal{M}_{p,q}$. This can be achieved by simply setting the kernel parameter ζ to $p/(q-p)$ and the twist α to $1/p$. The effective central charge prediction, at both the UV and IR points (3.21), agrees with the pattern of massless ϕ_{13} flows (1.182) described in Section 1.6.

Numerical results were presented in [52] for the zero twist ($c_{\text{eff}}(0) = c_{\text{eff}}(\infty) = 1$) case, but in Section 3.5 we confirm that, with a suitable nonzero value of α, the massless ϕ_{13} perturbations of minimal models are also obtained, with results that agree with the perturbative picture. As we have already mentioned, TBA equations are not known for the nonunitary minimal models so the nonlinear integral equation has yielded some new information.

3.2 The ZMIK model

We turn now to the main tool in our search for flows between minimal models perturbed by relevant operators other than ϕ_{13}. A nonlinear integral equation describing finite-size effects in the $a_2^{(2)}$ model was recently conjectured in [78]. In a similar way to the sine-Gordon model this model is expected to describe ϕ_{12} , ϕ_{21} and ϕ_{15} perturbations of minimal models on the imposition of a suitably-chosen twist [81–83]. The NLIE describes only the massive model but we propose a modification in the hope of describing the massless interpolating flows induced by the perturbing operators ϕ_{21} and ϕ_{15}.

Depending upon the context, the $a_2^{(2)}$ related model is associated with various names: Tzitzéica–Izergin–Korepin–Bullough–Dodd–Zhiber–Mikhailov–Shabat. For brevity we will refer to it as the ZMIK model. The action is

$$\mathcal{A}_{ZMIK} = \int (\partial_\mu \phi)^2 \, d^2x + \frac{m^2}{\gamma^2} \int \left(\exp(i\sqrt{8\gamma}\phi) + 2\exp(-i\sqrt{2\gamma}\phi) \right) d^2x \qquad (3.22)$$

where γ is the coupling constant.

The NLIE conjectured [78] to describe the effective central charge of the massive ZMIK model is defined via a single function $f(\theta)$:

$$f(\theta) = i\pi\alpha - ir\sinh\theta + \int_{\mathcal{C}_1} \varphi(\theta-\theta') \ln(1+e^{f(\theta')}) \, d\theta' - \int_{\mathcal{C}_2} \varphi(\theta-\theta') \ln(1+e^{-f(\theta')}) \, d\theta' , \qquad (3.23)$$

where the contours $\mathcal{C}_1$ and $\mathcal{C}_2$ are as in Figure 1.5 and r is equal to MR. The kernel

$$\varphi(\theta) = -\int_{-\infty}^{\infty} \frac{dk}{2\pi} \frac{e^{ik\theta} \sinh(\frac{\pi}{3}k) \cosh(\frac{\pi}{6}k(1-2\xi))}{\cosh(\frac{\pi}{2}k) \sinh(k\frac{\pi}{3}\xi)} \qquad (3.24)$$

is equal to $i/2\pi$ times the logarithmic derivative of the scalar factor in the S-matrix of the ZMIK model. The effective central charge is given by

$$c_{\text{eff}}(r) = \frac{3ir}{\pi^2} \left(\int_{\mathcal{C}_1} \sinh\theta \, \ln(1+e^{f(\theta)}) \, d\theta - \int_{\mathcal{C}_2} \sinh\theta \, \ln(1+e^{-f(\theta)}) \, d\theta \right) . \qquad (3.25)$$

The parameter ξ is related to the $a_2^{(2)}$ coupling γ as $\xi = \gamma/(2\pi - \gamma)$ while α corresponds to the twist. To obtain massive ϕ_{12}, ϕ_{21} and ϕ_{15} perturbations of a minimal model $\mathcal{M}_{p,q}$, the values of ξ and α must be chosen as follows [78]:

$$\phi_{12} \quad : \quad \xi = \frac{1}{\frac{2q}{p}-1} \quad , \quad \alpha = 2/p \quad , \quad p < 2q \; ; \tag{3.26}$$

$$\phi_{21} \quad : \quad \xi = \frac{1}{\frac{2p}{q}-1} \quad , \quad \alpha = 2/q \quad , \quad p > q/2 \; ; \tag{3.27}$$

$$\phi_{15} \quad : \quad \xi = \frac{1}{\frac{q}{2p}-1} \quad , \quad \alpha = 1/p \quad , \quad p < q/2 \; . \tag{3.28}$$

In each case, the inequality delimits the region of the (p, q)-plane within which ξ is positive, and the corresponding perturbation is relevant. Standard manipulations of (3.25) using the ultraviolet limit of (3.23) provide the value of the effective central charge in the UV limit:

$$c_{\text{eff}}(0) = 1 - \frac{3\xi}{\xi+1}\alpha^2 \; . \tag{3.29}$$

Plugging in the values of ξ and α prescribed by (3.26),(3.27) and (3.28), this always equals $1-6/pq$ (the effective central charge of a minimal model), but the subsequent terms in the small r expansion of $c_{\text{eff}}(r)$ will differ, as expected given the different perturbations being described.

Zamolodchikov's modification [52] of the massive NLIE made use of elements of the corresponding massless scattering theory. Unfortunately we cannot do the same for the ZMIK model, since a description of the massless scattering in terms of an S-matrix is not yet known. Instead we follow the results of [52], and substitute the single equation (3.23) with two equations describing hypothetical left and right movers. In this way we hope to seek a massless modification of the NLIE (3.23) which will interpolate between an ultraviolet theory with parameter ξ and an infrared theory with parameter $\xi-1$. This behaviour agrees with the previously-known flows since the formulae (3.27) and (3.28) indicate the massive versions of the perturbations (3.1) and (3.2) have $\xi = 2p - 1$ and $\xi = 2p$ respectively.

3.3 The ZMIK NLIE

We are now ready to propose a NLIE describing the massless ϕ_{12}, ϕ_{21} and ϕ_{15} perturbations of minimal models using [52] as a guide. We begin by writing down a set of coupled nonlinear integral equations for two analytic functions $f_R(\theta)$ and $f_L(\theta)$:

$$\begin{aligned} f_R(\theta) \; &= -i\frac{r}{2}e^{\theta} + i\pi\alpha' \\ &\quad + \int_{C_1} \phi(\theta-\theta') \ln(1+e^{f_R(\theta')})\, d\theta' - \int_{C_2} \phi(\theta-\theta') \ln(1+e^{-f_R(\theta')})\, d\theta' \end{aligned}$$

$$+\int_{\mathcal{C}_1}\chi(\theta-\theta')\ln(1+e^{-f_L(\theta')})\,d\theta'-\int_{\mathcal{C}_2}\chi(\theta-\theta')\ln(1+e^{f_L(\theta')})\,d\theta' \quad (3.30)$$

$$\begin{aligned} f_L(\theta) &= -i\frac{r}{2}e^{-\theta}-i\pi\alpha' \\ &+\int_{\mathcal{C}_2}\phi(\theta-\theta')\ln(1+e^{f_L(\theta')})\,d\theta'-\int_{\mathcal{C}_1}\phi(\theta-\theta')\ln(1+e^{-f_L(\theta')})\,d\theta' \\ &+\int_{\mathcal{C}_2}\chi(\theta-\theta')\ln(1+e^{-f_R(\theta')})\,d\theta'-\int_{\mathcal{C}_1}\chi(\theta-\theta')\ln(1+e^{f_R(\theta')})\,d\theta' \quad (3.31) \end{aligned}$$

The expression (3.25) for the effective central charge is replaced with

$$\begin{aligned} c_{\text{eff}}(r) &= \frac{3ir}{2\pi^2}\Big[\int_{\mathcal{C}_1}e^{\theta}\ln(1+e^{f_R(\theta)})\,d\theta-\int_{\mathcal{C}_2}e^{\theta}\ln(1+e^{-f_R(\theta)})\,d\theta \\ &+\int_{\mathcal{C}_2}e^{-\theta}\ln(1+e^{f_L(\theta)})\,d\theta-\int_{\mathcal{C}_1}e^{-\theta}\ln(1+e^{-f_L(\theta)})\,d\theta\Big]\,, \end{aligned} \quad (3.32)$$

where the contours are as before.

We have not specified the kernels functions ϕ and χ , but by considering the UV and IR limits of the equations we are able to fix them. It is useful at this point to consider these limits. The connections between the massive and massless models are shown in Figure 3.1. A model $M_{p,q}$ can be perturbed in two directions: one resulting in a further minimal model $M_{p',q'}$ in the IR, and the other a massive model with $c_{\text{eff}}=0$. If the ultraviolet limit of the NLIE describing either of the resulting models is taken, then the original CFT should be recovered.

We first consider the behaviour of the equations in the IR limit. In the far infrared, $r\to\infty$ and the interaction between the two functions becomes negligible resulting in the two equations (3.30) and (3.31) decoupling. The result is two copies of the UV limit of (3.23), with the kernel $\varphi(\theta)$, given by (3.24), substituted by $\phi(\theta)$. Since the IR destination is to be the model at $\xi-1$, this suggests we should take $\phi(\theta)$ to be the massive kernel (3.24) with the substitution $\xi\to\xi-1$:

$$\phi(\theta)=-\int_{-\infty}^{\infty}\frac{dk}{2\pi}\frac{e^{ik\theta}\sinh(k\frac{\pi}{3})\cosh(\frac{\pi}{6}k(3-2\xi))}{\cosh(\frac{\pi}{2}k)\sinh(k\frac{\pi}{3}(\xi-1))}\,. \quad (3.33)$$

This is similar to the imaginary coupled sine-Gordon NLIE. In the ISG case, the kernel was related to the massive scattering amplitude with the proviso that the parameter ζ became $\zeta-1$.

To find $\chi(\theta)$ we consider the UV behaviour of the new system. As remarked above this should coincide with the UV limit of the massive system (3.23). As $r\to 0$, the solution to (3.30), (3.31) splits into a pair of kink systems, centered at $\theta=\pm\ln(1/r)$. We focus on one of them by replacing θ by $\theta-\ln(1/r)$, and keeping this variable finite as the limit $r\to 0$ is taken. The exponential term in (3.30) is replaced by $-\frac{i}{2}e^{\theta}$, while to leading order the exponential in (3.31) can be neglected. Furthermore, the integration contours in any integral involving f_L may now be moved across the real θ axis since the singularities in $\ln(1+e^{\pm f_L(\theta)})$

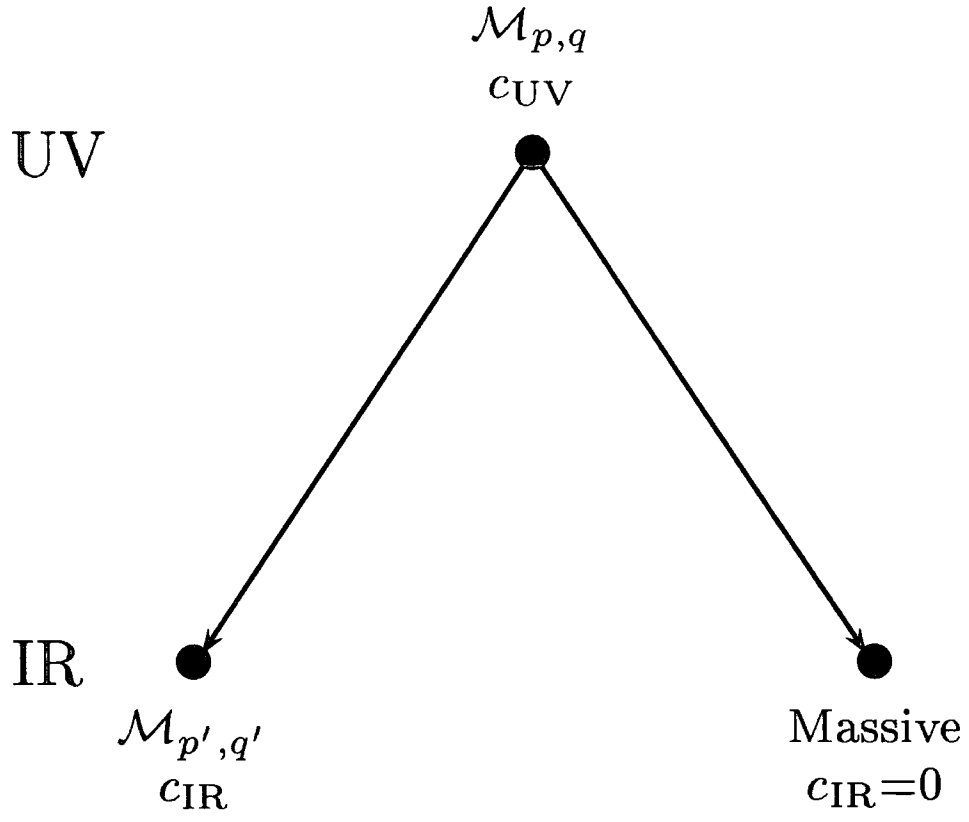

Figure 3.1: The two possible behaviours (massive and massless) of a minimal model perturbed by a relevant operator.

(previously-found on the real axis) are pushed to $-\infty$. We thus shift $\mathcal{C}_2$ down to coincide with $\mathcal{C}_1$ in all such integrals, and take $\mathcal{C}_1$ to be the line $\Im m\,\theta = -\eta$, with η a suitably-small real number.

For $f_R(\theta)$ the singularities do not disappear, but using the reality properties of f_R, $[f_R(\theta)]^* = -f_R(\theta^*)$, we rewrite the integrations above and below the axis in terms of the imaginary part of a single integration along $\mathcal{C}_1$. The final set of equations reads

$$\begin{aligned} f_R(\theta) &= -\tfrac{i}{2}e^{\theta} + i\pi\alpha' + 2i\int_{-\infty}^{\infty}\phi(\theta-(\theta'-i\eta))\Im m(\ln(1+e^{f_R(\theta'-i\eta)}))\,d\theta' \\ &\quad - \int_{-\infty}^{\infty}\chi(\theta-(\theta'-i\eta))f_L(\theta'-i\eta)\,d\theta' \qquad (3.34) \\ f_L(\theta) &= -i\pi\alpha' + \int_{-\infty}^{\infty}\phi(\theta-(\theta'+i\eta))f_L(\theta'+i\eta)\,d\theta' \\ &\quad - 2i\int_{-\infty}^{\infty}\chi(\theta-(\theta'-i\eta))\Im m(\ln(1+e^{f_R(\theta'-i\eta)}))\,d\theta' \,. \qquad (3.35) \end{aligned}$$

We now take the Fourier transform of (3.34) and (3.35) yielding

$$\begin{aligned} \mathcal{F}[f_R(\theta)+\tfrac{i}{2}e^{\theta}] &= 2i\,\pi^2\alpha'\delta(k) + 2\,i\,\tilde{\phi}(k)\,\tilde{L}_R(k) - \tilde{\chi}(k)\,\tilde{f}_L(k) \qquad (3.36) \\ (1-\tilde{\phi}(k))\,\tilde{f}_L(k) &= -2i\,\pi^2\alpha'\delta(k) - 2\,i\,\tilde{\chi}(k)\,\tilde{L}_R(k) \qquad (3.37) \end{aligned}$$

where $\tilde{L}_R(k)$ denotes the transform of $\Im m(\ln(1+e^{f_R(\theta'-i\eta)}))$ and the exponential term in (3.34) has been taken to the left hand side to ensure the existence of the transform. Inserting (3.37) into (3.36) we obtain

$$\mathcal{F}[f_R(\theta)+\tfrac{i}{2}e^{\theta}] = 2i\,\pi^2\alpha'\,\delta(k)\left(1+\frac{\tilde{\chi}(k)}{1-\tilde{\phi}(k)}\right) - 2\,i\,\tilde{L}_R(k)\left(\tilde{\phi}(k)+\frac{\tilde{\chi}(k)^2}{1-\tilde{\phi}(k)}\right) . \quad (3.38)$$

The Fourier transform of the kink limit of the massive equation (3.23) is

$$\mathcal{F}[f(\theta)+\tfrac{i}{2}e^{\theta}] = 2i\,\pi^2\alpha\,\delta(k) - 2\,i\,\tilde{L}_R(k)\,\tilde{\varphi}(k) . \quad (3.39)$$

Since these should match we find

$$\tilde{\varphi}(k) = \tilde{\phi}(k) + \frac{\tilde{\chi}(k)^2}{1-\tilde{\phi}(k)} \quad (3.40)$$

and

$$\alpha = \alpha'\left(1+\frac{\tilde{\chi}(0)}{1-\tilde{\phi}(0)}\right) . \quad (3.41)$$

After substituting the explicit expressions for φ and ϕ in (3.40) we can solve for χ and then invert the Fourier transform, with the result

$$\chi(\theta) = -\int_{-\infty}^{\infty}\frac{dk}{2\pi}\,\frac{e^{ik\theta}\sinh(\frac{\pi k}{3})\cosh(\frac{\pi k}{6})}{\cosh(\frac{\pi k}{2})\sinh(\frac{\pi k}{3}(\xi-1))} \quad (3.42)$$

and, from (3.41),

$$\alpha' = \alpha\frac{\xi}{(\xi-1)} . \quad (3.43)$$

Since (3.40) involves only $\chi(k)^2$ we have made a choice of sign when taking the square root. We took the negative sign since only then do the values taken by $c_{\text{eff}}(\infty)$, when flowing from a minimal model $\mathcal{M}_{p,q}$, always assume the form $1-6/p'q'$, as has to be the case if the infrared destination of the flow is to be another minimal model. It is possible that the flows found for the other sign choice also have an interpretation in some other context, but, as we are primarily interested in flows to minimal models, we do not explore this question here.

3.3.1 The new flows

In this section we examine the NLIEs a little more closely and deduce the IR minimal models to which they interpolate. This, when combined with the UV knowledge, allows a general pattern of sequences of flows to be established. The simplest sequence turns out to be the previously-found flows (3.1) and (3.2).

By construction, the new massless system exhibits the same ultraviolet central charge as the corresponding massive system:

$$c_{\text{eff}}(0) = 1 - \frac{3\xi}{(\xi+1)}\alpha^2. \quad (3.44)$$

In addition, we suppose that the recipe for choosing ξ and α (3.26), (3.27) and (3.28) also holds for the massless perturbations. In the next section this will be subjected to some more detailed checks. For now we just note that this agrees with the neat mapping of the kink limit of the equation onto that of the massive model.

Before going further we should mention one immediate difficultly with our NLIE: our convention $p < q$ for the coprime pair p, q means that the value assigned to ξ by (3.26) for ϕ_{12} perturbations is less than 1. The same is true for ϕ_{15} perturbations of $\mathcal{M}_{p,q}$ whenever $q > 4p$. This is not a problem for the massive perturbations, but the massless kernel $\phi(\theta)$ has a pole at $\theta = \frac{2}{3}(\xi-1)\pi i$, which crosses the real θ axis as ξ dips below 1. In addition, the formula (3.43) clearly has a pole at ξ=1. These sort of problems could perhaps be overcome by analytic continuation, but we will stick to values of ξ where this does not occur. Thus in the rest of this chapter we will focus solely on the ϕ_{21} and ϕ_{15} perturbations, found via equations (3.27) and (3.28) respectively, and additionally restrict the ϕ_{15} perturbations to models $\mathcal{M}_{p,q}$ with $q < 4p$.

In the infrared the massless system mimics a massive system with ξ replaced by $\xi-1$ and α replaced by $\alpha' = \alpha\,\xi/(\xi-1)$, and so

$$c_{\text{eff}}(\infty) = 1 - \frac{3(\xi-1)}{\xi}(\alpha')^2 = 1 - \frac{3\xi}{(\xi-1)}\alpha^2. \tag{3.45}$$

This begs the question to which minimal model does $c_{\text{eff}}(\infty)$ correspond? Consider first the perturbation of $\mathcal{M}_{p,q}$ by ϕ_{21}. We must impose that $p > q/2$ for it to be relevant. Substituting the requisite values of ξ and α (taken from (3.27)) into (3.44) and (3.45) we find:

$$\mathcal{M}_{p,q} + \phi_{21} \;:\quad p > q/2\,, \quad c_{\text{eff}}(0) = 1 - \frac{6}{pq}\,, \quad c_{\text{eff}}(\infty) = 1 - \frac{6}{(q-p)q}\,. \tag{3.46}$$

Similarly, for the ϕ_{15} perturbations we have

$$\mathcal{M}_{p,q} + \phi_{15} \;:\quad p < q/2\,, \quad c_{\text{eff}}(0) = 1 - \frac{6}{pq}\,, \quad c_{\text{eff}}(\infty) = 1 - \frac{6}{p(4p-q)}\,. \tag{3.47}$$

We note that the infrared limiting values of the effective central charges are all consistent with the destinations of the flows being minimal models. In fact had the opposite sign choice for $\chi(\theta)$ been taken in (3.42), the values of $c_{\text{eff}}(\infty)$ for the ϕ_{21} and ϕ_{15} perturbations would have been $1 - 6(q-p)/(qp^2)$ and $1 - 6(4p-q)/(pq^2)$ respectively, neither of which coincide with an effective central charge for a minimal model.

The UV value of the effective central charge c_{eff} depends on both the central charge c of the CFT and the scaling dimension $d = h + \bar{h}$ of the primary field of smallest dimension via

$$c_{\text{eff}}(0) = c - 12\,d\,. \tag{3.48}$$

Thus a knowledge of c_{eff} alone is not enough to uniquely identify a nonunitary minimal model, and so the destinations cannot be totally fixed using this information. Moreover, there are cases in which even the knowledge of the full $c_{\text{eff}}(r)$ is not sufficient to identify the model or models involved, and this was first noted in [84]. The 'type II conjecture' explicitly equates the effective central charges of the following models:

$$\mathcal{M}_{p,q}+\phi_{15} \quad \leftrightarrow \quad \mathcal{M}_{q/2,2p}+\phi_{21} \quad \leftrightarrow \quad \mathcal{M}_{2p,q/2}+\phi_{12} \qquad (p=2n+1,\ q=2m)\ . \tag{3.49}$$

The second equivalence is just a question of labelling, but the first is much less trivial. The conjecture originally came from a comparison of the massive models $\mathcal{M}_{5,6}+\phi_{21}$ with $\mathcal{M}_{3,10}+\phi_{15}$, and $\mathcal{M}_{6,7}+\phi_{12}$ with $\mathcal{M}_{3,14}+\phi_{15}$. The original TBA paper by Al.B. Zamolodchikov [19] noted that, even though the S-matrices were different, the same TBA equations described both $\mathcal{M}_{5,6}+\phi_{21}$ (the scaling Lee-Yang model) and $\mathcal{M}_{3,10}+\phi_{15}$ (the 3-state Potts model). Similarly, the S-matrices are different for the models $\mathcal{M}_{6,7}+\phi_{12}$ and $\mathcal{M}_{3,14}+\phi_{15}$, but the same TBA equations provide the ground-state energy for both of these models. The 'type II conjecture' was based on these cases and the equivalence of the ultraviolet central charge of the models (3.49). However, the massive NLIE (3.23) confirms the equivalence, since the recipe (3.26)–(3.28) predict exactly the same values of ξ and α, assuming the correctness of the equations. The NLIEs describing the massless theories are parameterised according to essentially the same recipe and so will be subject to similar ambiguities.

In spite of these provisos, the forms taken by the results (3.46) and (3.47) make for some obvious conjectures for the IR destinations, and these will receive further support by both analytical and numerical means. Such checks will never resolve type II ambiguities, so for these cases the conjectures are better motivated by the belief that the pattern observed in other cases should hold in complete generality. Taking into account the '$p<q$' labelling convention for a minimal model $\mathcal{M}_{p,q}$, the ϕ_{15} case splits into two and we have the following predictions for massless perturbations of general minimal models:

$$\mathcal{M}_{p,q}+\phi_{21} \quad \to \quad \mathcal{M}_{q-p,q} \quad (\ p<q<2p)\ , \tag{3.50}$$

$$\mathcal{M}_{p,q}+\phi_{15} \quad \to \quad \mathcal{M}_{p,4p-q} \quad (2p<q<3p)\ , \tag{3.51}$$

$$\mathcal{M}_{p,q}+\phi_{15} \quad \to \quad \mathcal{M}_{4p-q,p} \quad (3p<q<4p)\ . \tag{3.52}$$

There is only a single flow on this list from any given minimal model: when ϕ_{21} is relevant, ϕ_{15} is irrelevant, and vice versa. Note also that the case (3.52) can only occur as the last member of a sequence: for $3p<q<4p$, ξ lies between 1 and 2 and the next step would therefore involve a value of ξ less than 1, and we have already decided to exclude such cases.

On setting $q = 2p - 1$ in (3.50) and $q = 2p + 1$ in (3.51) the previously-known flows (3.1) and (3.2) are reproduced. This is not the only sequence, and we can see the general pattern more clearly if we define an 'index' $I = 2p - q$, and rephrase (3.50) and (3.51) as

$$\mathcal{M}_{p,2p-I} + \phi_{21} \;\to\; \mathcal{M}_{p-I,2p-I}\ , \qquad (\xi, \alpha') = (\tfrac{2p}{I} - 1, \tfrac{1}{p-I})\ , \tag{3.53}$$

$$\mathcal{M}_{p,2p+I} + \phi_{15} \;\to\; \mathcal{M}_{p,2p-I}\ , \qquad (\xi, \alpha') = (\tfrac{2p}{I}, \tfrac{2}{2p-I})\ . \tag{3.54}$$

So we have found, as promised, further sequences of flows where the perturbing operator alternates between ϕ_{21} and ϕ_{15}.

In all cases $I(\mathrm{IR}) = -I(\mathrm{UV})$; the flows (3.1) and (3.2) make up the unique sequence with $|I| = 1$. For $|I| > 1$, there may be more than one sequence, with flows sharing the same value of $|I|$ interlacing each other. The number of different sequences with index $\pm I$ is restricted by the constraint that the pair of integers labelling a minimal model must always be coprime. Therefore the number of different sequences is given by the Euler φ-function $\varphi(|I|)$, equal to the number of integers less than $|I|$ which are coprime to $|I|$ (so for $n = 1 \ldots 6$, $\varphi(n) = 1, 1, 2, 2, 4, 2$). The index measures the distance from the line $q = 2p$ across which the relevance and irrelevance of the fields ϕ_{21} and ϕ_{15} swap over. All of this is perhaps best seen pictorially, and in Figure 3.2 some of the predicted flows are plotted, superimposed on a grid of the minimal models $\mathcal{M}_{p,q}$. The horizontal arrows of length $|I|$ correspond to ϕ_{21} perturbations, while the vertical arrows, of length $2|I|$, are ϕ_{15} perturbations.

3.4 Numerical results

As a first check on our results we evaluated the effective central charge numerically for a number of members of the $|I| = 1$ series, and made a comparison with the results from the massless TBA equations discussed in [61]. In [61] such TBA equations were written in a 'universal' form of the kind first described in [27] and briefly mentioned in Chapter 1. For numerical work it is more convenient to write the equations in the following way:

$$\varepsilon_a(\theta) = \nu_a(\theta) - \sum_{b=1}^{n} (l_{ab}^{(A_n)} - \delta_{ab}) \int_{-\infty}^{\infty} K(\theta - \theta') \ln(1 + e^{-\varepsilon_b(\theta')})\, d\theta'\ , \tag{3.55}$$

$$c_{\mathrm{eff}}(r) = \frac{3}{\pi^2} \sum_{a=1}^{n} \int_{-\infty}^{\infty} \nu_a(\theta) \ln(1 + e^{-\varepsilon_a(\theta)})\, d\theta \tag{3.56}$$

where $n \equiv \xi - 3$ is integer and $l_{ab}^{(A_n)}$ is the incidence matrix of the A_n Dynkin diagram (see Figure 3.9). The driving terms are given by

$$\nu_a(\theta) = \frac{r}{2}(e^{\theta}\delta_{a,1} + e^{-\theta}\delta_{a,n})\ , \tag{3.57}$$

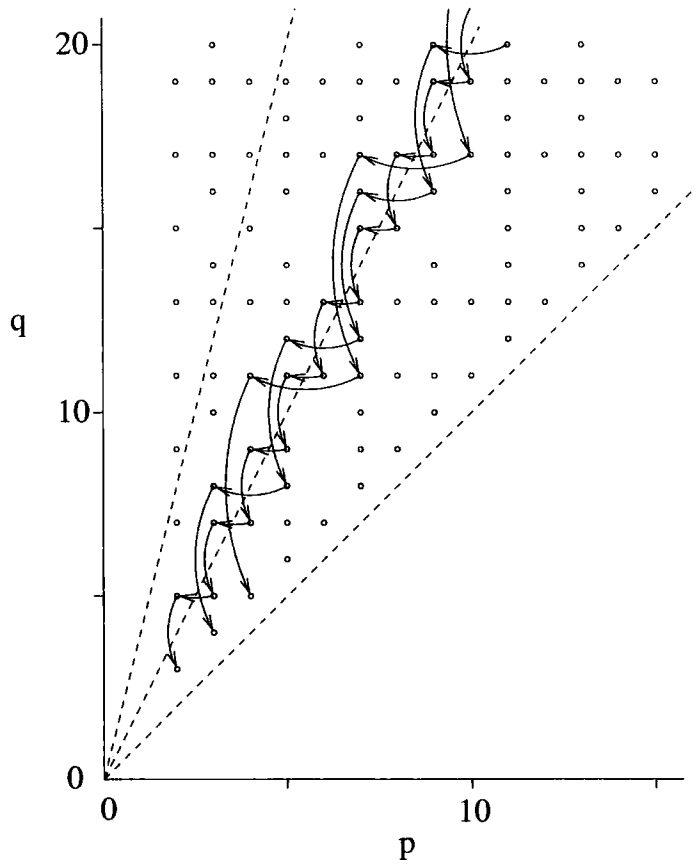

Figure 3.2: The grid of minimal models $\mathcal{M}_{p,q}$ and a selection of the predicted flows showing the unique sequences with $|I| = 1$ and $|I| = 2$, and one of the two sequences with $|I| = 3$. Also shown are the lines $q{=}p$, $q{=}2p$ and $q{=}4p$.

and the kernel function is

$$\mathcal{K}(\theta) = \frac{\sqrt{3}}{\pi} \frac{\sinh 2\theta}{\sinh 3\theta} \quad . \tag{3.58}$$

The agreement between the NLIE and the TBA is extremely good, and is illustrated in Table 3.1 and Figure 3.3.

Satisfied that our NLIE correctly matches the previously-known flows, we turned to the new families with index $|I| > 1$. Figure 3.4 shows the (unique) series with $|I| = 2$, Figure 3.5 one of the two possible series with $|I| = 3$ and Figure 3.6 a series with $|I| = 6$. For all of these flows the effective central charge initially increases from its UV value, oscillates as the system size is increased, before finally flowing to the predicted IR fixed point. This perhaps-surprising behaviour is in contrast to the $|I| = 1$ series where all of the flows are monotonic. We will discuss this further at the end of Section 3.4.2.

3.4.1 Perturbation theory

The claims of the last section can be put on a more secure footing by taking a closer look at the behaviour of the effective central charges at small and large r. If the

Model	(ξ, α')	r	TBA	NLIE
$\mathcal{M}_{3,5} + \phi_{21}$	$(5, \frac{1}{2})$	0.01	0.59996121217228	0.59996121217225
		0.02	0.59986582853966	0.59986582853967
$\mathcal{M}_{3,7} + \phi_{15}$	$(6, \frac{2}{5})$	0.01	0.71421869185983	0.71421869185981
		0.02	0.71408433022934	0.71408433022935
$\mathcal{M}_{4,7} + \phi_{21}$	$(7, \frac{1}{3})$	0.01	0.78560676745058	0.78560676745059
		0.02	0.78543110694683	0.78543110694684
$\mathcal{M}_{4,9} + \phi_{15}$	$(8, \frac{1}{3})$	0.01	0.83317811607441	0.83317811607433
		0.02	0.83296826731142	0.83296826731135

Table 3.1: Comparison of $c_{\text{eff}}(r)$ calculated using the TBA equations and the NLIE for some of the flows with index $|I| = 1$.

NLIE do provide the effective central charge for these perturbed minimal models, then the ground state energy predictions must agree with conformal perturbation theory about the ultraviolet point. This must be equally true for perturbations about the infrared point.

For the comparison we will need the leading asymptotics of the kernels $\phi(\theta)$ (3.33) and $\chi(\theta)$ (3.42) as $\theta \to -\infty$. That of ϕ can be found from the residues of the poles in the integrand of (3.33) at $k = -i$ and $k = -3i/(\xi-1)$, and is:

$$\phi(\theta) \sim -\frac{\sqrt{3}\sin(\frac{\pi}{3}\xi)}{\pi\sin(\frac{\pi}{3}(\xi-1))}e^{\theta} + \frac{3\sin(\frac{\pi}{(\xi-1)})\cos(\frac{\pi}{2(\xi-1)})}{\pi(\xi-1)\cos(\frac{3\pi}{2(\xi-1)})}e^{3\theta/(\xi-1)} + \ldots, \quad \theta \to -\infty \ . \tag{3.59}$$

Similarly χ has poles in the integrand at $k = -i$ and $k = -3i(\xi-1)$, and its leading asymptotic is

$$\chi(\theta) \sim -\frac{3}{2\pi\sin(\frac{\pi}{3}(\xi-1))}e^{\theta} - \frac{3\sin(\frac{\pi}{(\xi-1)})\cos(\frac{\pi}{2(\xi-1)})}{\pi(\xi-1)\cos(\frac{3\pi}{2(\xi-1)})}e^{3\theta/(\xi-1)} + \ldots, \quad \theta \to -\infty \ . \tag{3.60}$$

We begin with some results in the infrared followed by more exact results in the ultraviolet region.

IR results

We first analyse the NLIE as $r \to \infty$, to see whether its behaviour is compatible with the claimed infrared destinations of the massless flows. In spite of the fact that conformal perturbation theory about the infrared fixed point is not renormalisable, there are a number of unambiguous predictions against which the equation can be checked. The key ideas are set out in [45, 85], and are further discussed in, for example, [54, 62, 63].

In general, the infrared model will be described by an action of the form

$$S = S^*_{\text{IR}} + \mu_1 \int \psi \ d^2x + \mu_2 \int T\bar{T}\, d^2x + (\text{further terms}) \tag{3.61}$$

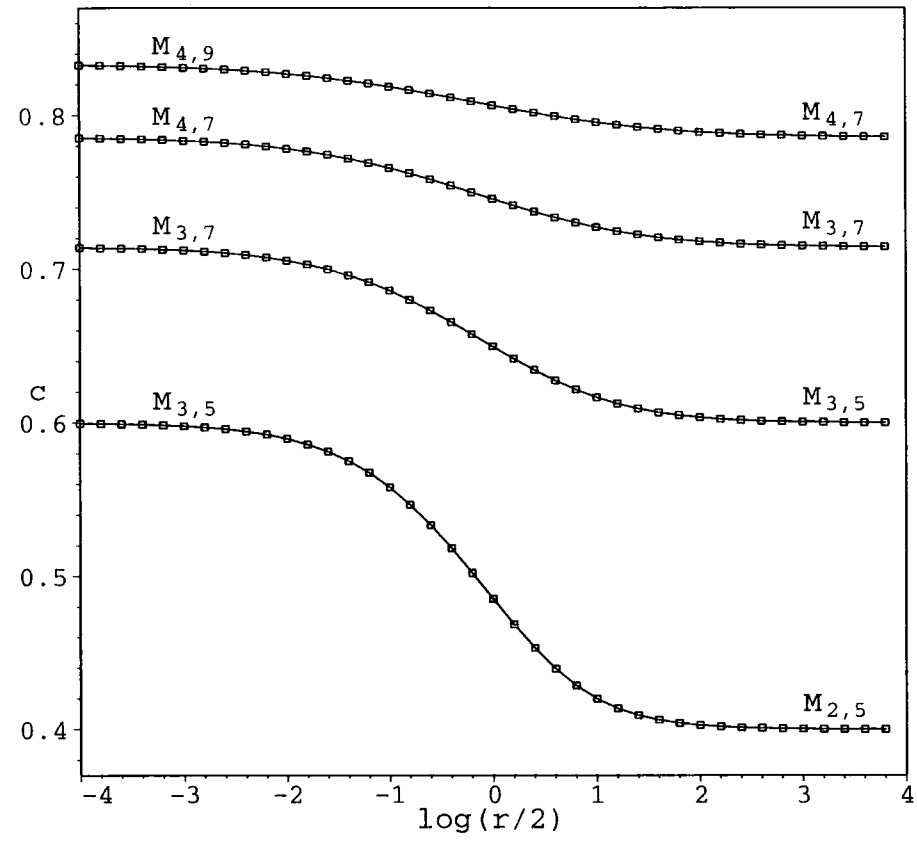

Figure 3.3: TBA (boxes) and NLIE data (solid lines) for the 'diagonal' sequence with $|I| = 1$.

where $S^*_{\rm IR}$ is the action, and ψ one of the (irrelevant) primary fields of the infrared conformal field theory and T the holomorphic component of the stress energy tensor. ψ might be absent, in which case the only operators attracting the flow to the IR fixed point would be the descendents of the identity; $T\bar{T}$ being the least irrelevant example. In principle there can be an infinite number of higher dimensional further terms in (3.61) corresponding to descendents of ψ and $T\bar{T}$ and further families of irrelevant operators belonging to the IR CFT.

On dimensional grounds, the couplings μ_1 and μ_2 are related to the single cross-over scale M as

$$\mu_1 = \kappa_1 M^{2-2h} \quad , \quad \mu_2 = \kappa_2 M^{-2} \; , \tag{3.62}$$

with κ_1 and κ_2 dimensionless constants and h the conformal dimension of ψ. The first perturbing term in (3.61) yields a series in $\mu_1 R^{2-2h} = \kappa_1 r^{2-2h}$ if all powers of μ_1 contribute, or $\mu_1^2 R^{4-4h} = \kappa_1^2 r^{4-4h}$ if only even powers appear, as happens when ψ is odd under some symmetry of $S^*_{\rm IR}$.

If we consider just the action of the second perturbing term of (3.61), its contribution to the full effective central charge can be developed in a perturbative expansion

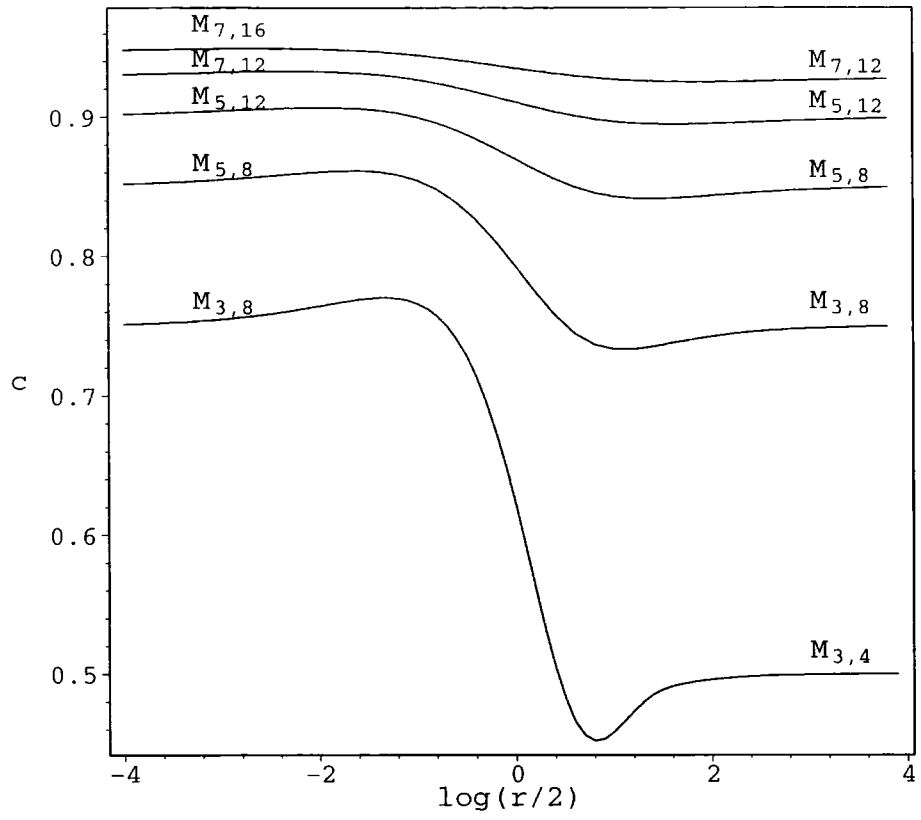

Figure 3.4: The sequence of nonunitary flows with $|I| = 2$.

as

$$c_{\text{eff}}(r) = c_{\text{eff}}(\infty) + 24\pi \sum_{n=1}^{\infty} \frac{(-4\pi^2\mu_2)^n}{n!R^n} \int \prod_{j=2}^{n} |z_j|^2 d^2 z_j \, |\langle \tau(1)\tau(z_2)\ldots\tau(z_n)\rangle_c|^2 \,, \tag{3.63}$$

where $\langle \tau(1)\tau(z_2)\ldots\tau(z_n)\rangle_c$ is the connected correlation function of the n operators $\tau(z) = T(z) - \frac{c}{24z^2} I$. This results in a series in $\mu_2 R^{-2} = \kappa_2 r^{-2}$, the first terms of which were found explicitly in [85]:

$$c_{\text{eff}}(r) = c_{\text{eff}}(\infty) - \frac{\pi^3 c_{\text{eff}}(\infty)^2}{6} \kappa_2 \, r^{-2} + \frac{\pi^6 c_{\text{eff}}(\infty)^3}{18} \kappa_2^2 \, r^{-4} + (\text{further terms}) \,. \tag{3.64}$$

Putting everything together gives $c_{\text{eff}}(r)$ the following large-r expansion:

$$\begin{aligned} c_{\text{eff}}(r) \;\sim\; & c_{\text{eff}}(\infty) + (\text{a series in } \kappa_1 r^{2-2h} \text{ or } \kappa_1^2 r^{4-4h}) \\ & - \frac{\pi^3 c_{\text{eff}}(\infty)^2}{6} \kappa_2 \, r^{-2} + \frac{\pi^6 c_{\text{eff}}(\infty)^3}{18} \kappa_2^2 \, r^{-4} + (\text{further terms}) \end{aligned} \tag{3.65}$$

These first corrections to $c_{\text{eff}}(\infty)$ should be good at least up to the order at which the 'further terms' cut in. We have very little control over these omitted terms and, as this series is only expected to be asymptotic, we cannot expect very high accuracy. Nevertheless, it allows for some useful comparisons with results from the NLIE obtained both analytically and numerically.

By considering the large r behaviour of the NLIE we can identify the operator ψ attracting each flow into the infrared CFT. When r is large, the nontrivial behaviours

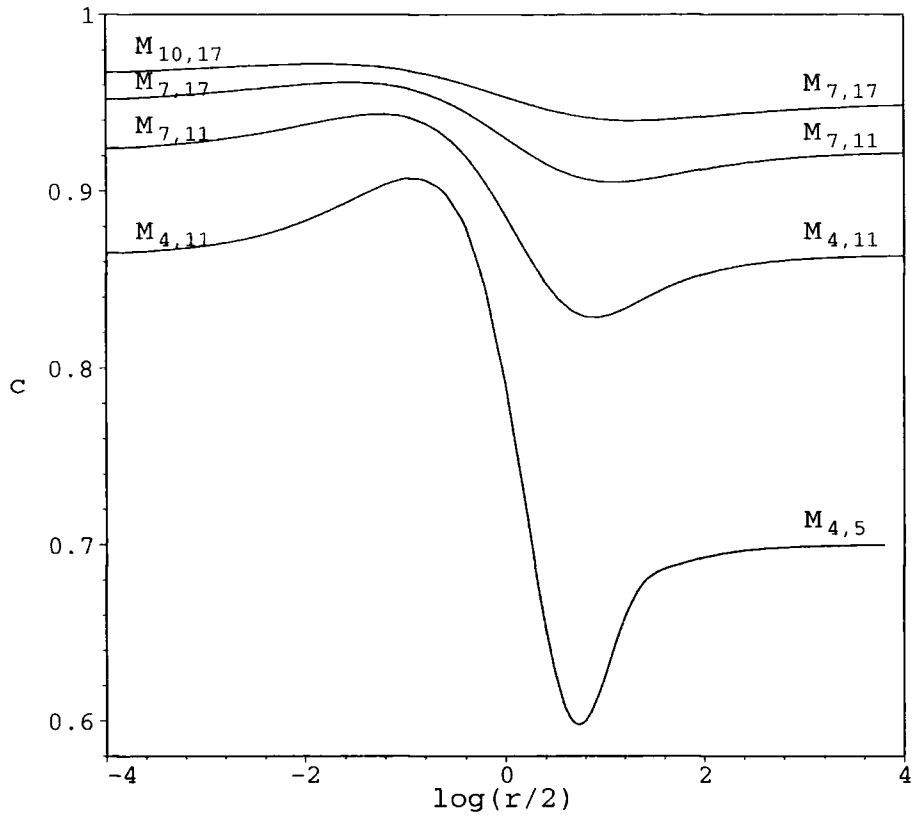

Figure 3.5: One of the two sequences with $|I| = 3$.

of the functions f_L and f_R appearing in (3.30) and (3.31) are concentrated in 'kink' regions near $\theta = -\ln r$ and $\theta = \ln r$ respectively. So long as the contours $\mathcal{C}_1$ and $\mathcal{C}_2$ are kept a finite distance from the real θ-axis, the functions $\ln(1 + e^{\pm f_L})$ and $\ln(1 + e^{\pm f_R})$ appearing in these equations are doubly-exponentially suppressed in the central zone between the kinks. So the principal interaction between equations (3.30) and (3.31), and hence the principal correction to $c_{\text{eff}}(r)$, comes from the exponential tail of the kernel function $\chi(\theta)$, given by (3.60).

We can consider the effects of the two terms in (3.60) separately since we may vary ξ to prevent the exponentials powers becoming equal and resulting in 'resonance' effects. We first consider the second term of (3.60), decaying as $e^{3\theta/(\xi-1)}$ as $\theta \to -\infty$. Inserted into (3.30) and considered iteratively, corrections to $f_R(\theta)$ as a series in $r^{-6/(\xi-1)}$ will be generated. Feeding through into $c_{\text{eff}}(r)$, these corrections can be matched against the κ_1 terms in (3.65), allowing h, the conformal dimension of the field ψ, to be extracted:

$$h = \frac{\xi+2}{\xi-1} \quad \text{or} \quad h = \frac{2\xi+1}{2\xi-2} \tag{3.66}$$

depending on the symmetry of ψ (even or odd respectively). Inserting the value of ξ at the ultraviolet point, given by (3.27) and (3.28), we can then compare h with the Kac formula

$$h_{ab} = \frac{(bp'-aq')^2 - (p'-q')^2}{4p'q'} \tag{3.67}$$

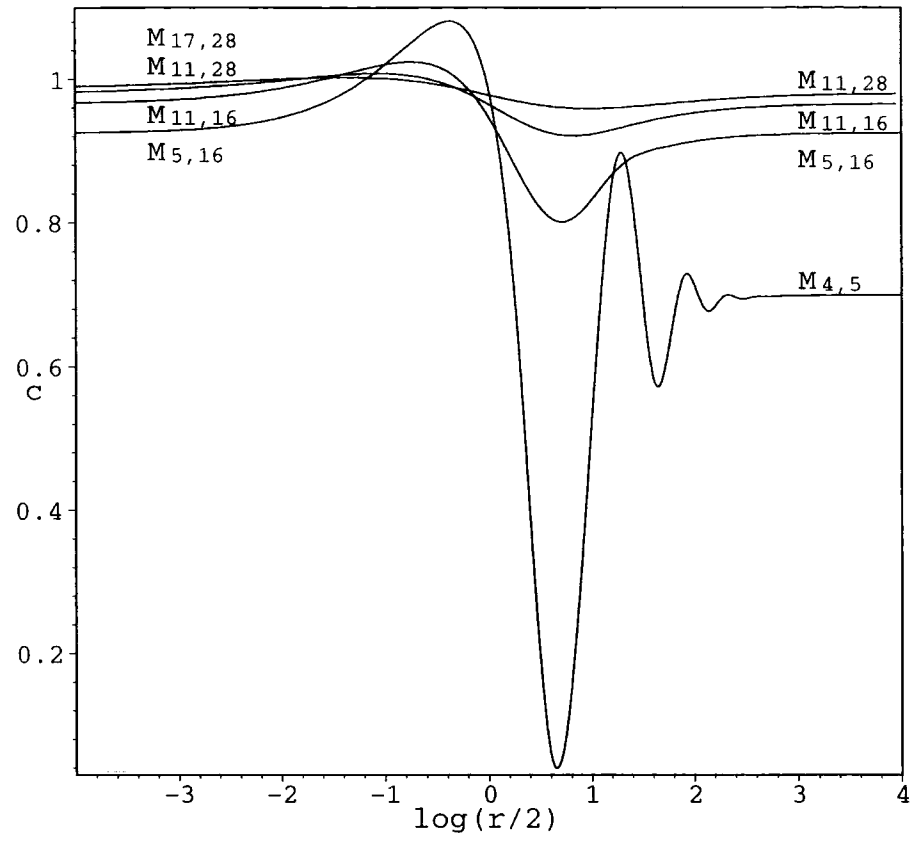

Figure 3.6: One of the sequences with $|I| = 6$.

at the appropriate (IR) values of p' and q'. This leads us to conjecture the following pattern of arriving operators ψ:

$$\mathcal{M}_{p,q} + \phi_{21} \;\to\; \mathcal{M}_{q-p,q} \quad (\; p < q < 2p) \qquad \text{arriving via } \phi_{21}\ , \tag{3.68}$$

$$\mathcal{M}_{p,q} + \phi_{15} \;\to\; \mathcal{M}_{p,4p-q} \quad (2p < q < 3p) \qquad \text{arriving via } \phi_{15}\ , \tag{3.69}$$

$$\mathcal{M}_{p,q} + \phi_{15} \;\to\; \mathcal{M}_{4p-q,p} \quad (3p < q < 4p) \qquad \text{arriving via } \phi_{51}\ . \tag{3.70}$$

In making these identifications we took account of the fact that ϕ_{21} is an odd operator, while ϕ_{15} is even.

Exactly the same line of argument starting from the e^{θ} term in (3.60) reveals a further series of corrections to c_{eff} as powers of r^{-2}, perfectly adapted to match the $T\bar{T}$ terms in (3.65). However this time it is possible to say more, by observing that the effect of this part of $\chi(\theta)$ on equations (3.30) and (3.31) can be reabsorbed into a shift of r by a constant, and furthermore that this constant can be expressed in terms of $c(r)$. This allows the first few terms of the iterative expansion to be found exactly. The same idea was used in [63] to extract IR asymptotics from various massless TBA systems; in the current context we find

$$c_{\text{eff}}(r) \sim c_{\text{eff}}(\infty) - \frac{\pi c_{\text{eff}}(\infty)^2}{\sin\frac{\pi}{3}(\xi-1)} r^{-2} + \frac{2\pi^2 c_{\text{eff}}(\infty)^3}{\sin^2\frac{\pi}{3}(\xi-1)} r^{-4} + \dots \tag{3.71}$$

Matching r^{-2} terms in (3.65) and (3.71) gives the exact relation

$$\kappa_2 = \frac{6}{\pi^2 \sin\frac{\pi}{3}(\xi-1)} \,. \tag{3.72}$$

Plugging this result into the coefficient of the r^{-4} term in (3.65) we find complete agreement with (3.71). This provides a nontrivial check on the IR behaviour of the massless NLIE.

We have to be careful whenever $\xi-1$ is an integer multiple of 3, since the coefficients in (3.71) will be formally infinite. Nevertheless, we can still make a prediction for the r^{-2} term: the expansion related to the operator ψ also contributes at this order for these particular values of ξ and may cancel the singularity. A contribution proportional to r^{-2} comes from the term of order $\mu_1^{(2-2h)k}$ (ψ odd) or $\mu_1^{(4-4h)k}$ (ψ even) for some integer k. In each case, whether the operator is even or odd is immaterial as ξ is related to k via $\xi = 3k+1$ so that a single calculation suffices to cover both cases. The additional term from the expansion related to ψ has the potential to cancel the pole in the r^{-2} term leaving a residual finite contribution to (3.71). We can find this by evaluating

$$\lim_{\xi\to 3k+1}\left[\frac{-\pi\, c_{\text{eff}}(\infty)^2}{\sin\frac{\pi}{3}(\xi-1)}\left(r^{-2} - r^{\frac{-6k}{\xi-1}}\right)\right] \tag{3.73}$$

with the result that the contribution to c_{eff} should be modified to

$$\frac{6(-1)^k c_{\text{eff}}(\infty)^2}{\xi-1} r^{-2}\ln r \qquad (k\in\mathbb{N}) \,. \tag{3.74}$$

We performed some numerical fits on the IR data by solving the NLIE and calculating $c_{\text{eff}}(r)$ for values of r between 40 and 2000. After subtracting the exactly known value of $c_{\text{eff}}(\infty)$, the data was fitted against a series of the form

$$c_{\text{eff}}(r) - c_{\text{eff}}(\infty) = \sum_{k_1=1}^{n_1} c_{k_1} r^{(2-2h)k_1} + \sum_{k_2=1}^{n_2} c_{k_2} r^{-2k_2} \tag{3.75}$$

where the truncation levels n_1 and n_2 were chosen to give the best possible fits, and whenever $\xi-1$ was an integer multiple of 3 we also included a term of the form $r^{-2}\ln r$. Our results are summarised in Table 3.2. Accuracy was fairly low due to the asymptotic nature of the series, but, where relevant, we have also included the predicted ('exact') values of coefficients, which were obtained from equations (3.71) and (3.74).

UV results

The situation in the ultraviolet is in many respects much simpler. Conformal perturbation theory gives direct access to a function $c_{\text{pert}}(r)$, related to the ground-state energy (1.81) as

$$E(M,R) = -\frac{\pi}{6R} c_{\text{pert}}(r) \,. \tag{3.76}$$

Model	$c_{\text{eff}}(r)-c_{\text{eff}}(\infty)$
$\mathcal{M}_{3,5}+\phi_{21}$	$0.58041577\,r^{-2}+0.000061\,r^{-3}+1.66\,r^{-4}+0.12\,r^{-\frac{9}{2}}+\ldots$
Exact	$0.58041579\,r^{-2}+1.6844\,r^{-4}$
$\mathcal{M}_{3,7}+\phi_{15}$	$1.30591\,r^{-2}+1.65488\,r^{-\frac{12}{5}}+\ldots$
Exact	$1.30593\,r^{-2}$
$\mathcal{M}_{4,7}+\phi_{21}$	$0.51029\,\ln(r)\,r^{-2}-0.68683\,r^{-2}+\ldots$
Exact	$0.51020\,\ln(r)\,r^{-2}$
$\mathcal{M}_{7,11}+\phi_{21}$	$-6.8516\,r^{-2}+8.8213\,r^{-\frac{9}{4}}+\ldots$
Exact	$-6.8510\,r^{-2}$
$\mathcal{M}_{5,8}+\phi_{21}$	$-1.1253\,\ln(r)\,r^{-2}+1.3757\,r^{-2}+\ldots$
Exact	$-1.125\ \ln(r)\,r^{-2}$
$\mathcal{M}_{6,17}+\phi_{15}$	$-2.32081\,r^{-2}+12.85\,r^{-4}-1.527\,r^{\frac{-30}{7}}+\ldots$
Exact	$-2.32082\,r^{-2}+12.56\,r^{-4}$

Table 3.2: Comparison of the infrared expansion of $c_{\text{eff}}(r)-c_{\text{eff}}(\infty)$ for various models against the exact coefficients.

Note that c_{pert} contains a bulk part which must be subtracted before comparisons can be made with the NLIE. For a theory perturbed by a relevant primary operator ϕ with scaling dimensions $(h_{\text{UV}}, h_{\text{UV}})$, c_{pert} has the expansion [19,23]

$$c_{\text{pert}}(r) = c(0) + \sum_{n=1}^{\infty} C_n (\lambda R^y)^n \tag{3.77}$$

and, in contrast to the situation in the IR, the series is expected to have a finite radius of convergence. Here $y = 2-2h_{\text{UV}}$, λ is the coupling and the coefficients C_n are given in terms of the connected correlation functions of the perturbing field on the plane as

$$C_n = \frac{12\,(-1)^n}{n!\,(2\pi)^{yn-1}} \int \prod_{j=2}^{n} \frac{d^2 z_j}{|z_j|^y} \langle V(0)\phi(1,1)\phi(z_2,\bar{z}_2)\ldots\phi(z_n,\bar{z}_n)V(\infty)\rangle_{\text{c}}\,, \tag{3.78}$$

where V creates the CFT ground-state on the cylinder. This is the state with lowest conformal dimension, and for a general minimal model $\mathcal{M}_{p,q}$ it corresponds to the field $\phi_0 \equiv \phi_{ab}$ with a and b integers satisfying $bp - aq = 1$. Only for the unitary models $\mathcal{M}_{p,p+1}$ does it coincide with the conformal vacuum ϕ_{11}.

We are interested in ϕ_{15} and ϕ_{21} as the perturbing operator ϕ. As mentioned above ϕ_{21} is odd, so only the even coefficients C_{2n} are nonzero for this case. By dimensional arguments λ must be related to the crossover scale M as

$$\lambda = \kappa M^y \tag{3.79}$$

with κ a dimensionless constant. It follows that (3.77) is a series in r^y for the ϕ_{15} perturbations, and r^{2y} for the ϕ_{21} perturbations.

The effective central charge calculated using the NLIE is expected to expand as

$$c_{\text{eff}}(r) = c_{\text{eff}}(0) + B(r) + \sum_{n=1}^{\infty} c_n r^{yn} \tag{3.80}$$

for some value of y, where $B(r)$ corresponds to the bulk part. The NLIEs are periodic in the θ variable:

$$f_R\,(\theta + 2\,i\,\pi(\xi{+}1)/3) = f_R(\theta) \quad , \quad f_L\,(\theta + 2\,i\,\pi(\xi{+}1)/3) = f_L(\theta) \tag{3.81}$$

and so these functions can be expanded in powers of $e^{\frac{3\theta}{\xi+1}}$. As mentioned in Chapter 1 this suggests that the effective central charge will be a series in $r^{6/(1+\xi)}$. So, if ξ is chosen according to (3.27) or (3.28), the ultraviolet conformal dimensions and scaling dimensions $y = 2{-}2h_{\text{UV}}$ are

$$\phi_{21} \quad : \; h_{\text{UV}} = \frac{2\,\xi{-}1}{2\,\xi{+}2} \qquad y = \frac{3}{\xi{+}1} \tag{3.82}$$

$$\phi_{15} \quad : \; h_{\text{UV}} = \frac{\xi{-}2}{\xi{+}1} \qquad y = \frac{6}{\xi{+}1}\,. \tag{3.83}$$

Recall that all the odd terms are zero for the ϕ_{21} case [78] so that the perturbative expansion (3.77) is matched in both cases. Before we can make a direct comparison between c_{pert} and c_{eff} we must calculate the irregular bulk term $B(r)$. Fortunately, it can be obtained exactly from the NLIE using a small generalisation of arguments used in [19] and [34]. The term we need is given by the behaviour as $r \to 0$ of

$$2\,\frac{3ir}{2\pi^2}\Big[\int_{\substack{c_2\\>0}} e^{-\theta}\frac{d}{d\theta}\ln(1{+}e^{f_L(\theta)})\,d\theta - \int_{\substack{c_1\\>0}} e^{-\theta}\frac{d}{d\theta}\ln(1{+}e^{-f_L(\theta)})\,d\theta\Big]\,, \tag{3.84}$$

where the '>0' indicates that only those parts of the contours $\mathcal{C}_1$ and $\mathcal{C}_2$ with positive real part should be taken, and the symmetry between f_L and f_R was used to trade the first two integrals in (3.32) for the prefactor 2. Consider the $r \to 0$ limit of (3.30) and (3.31) in the region $0 \ll \Re e\,\theta \ll \ln(1/r)$, where the driving term $-i\frac{r}{2}e^{-\theta}$ in (3.31) can be dropped. Take the derivative of these equations with respect to θ, and extract the contributions to the convolutions proportional to e^{θ} using (3.59) and (3.60). These should cancel either against the remaining driving term or between themselves to ensure that the functions f_L and f_R have no such dependency. This leads to the equations

$$\begin{aligned}
i\frac{r}{2} \;=& -\frac{\sqrt{3}\sin(\frac{\pi}{3}\xi)}{\pi\sin(\frac{\pi}{3}(\xi{-}1))}\Big[\int_{\substack{c_1\\>0}} e^{-\theta'}\frac{d}{d\theta'}\ln(1{+}e^{f_R(\theta')})\,d\theta' - \int_{\substack{c_2\\>0}} e^{-\theta'}\frac{d}{d\theta'}\ln(1{+}e^{-f_R(\theta')})\,d\theta'\Big] \\
& -\frac{3}{2\pi\sin(\frac{\pi}{3}(\xi{-}1))}\Big[\int_{\substack{c_1\\>0}} e^{-\theta'}\frac{d}{d\theta'}\ln(1{+}e^{-f_L(\theta')})\,d\theta' - \int_{\substack{c_2\\>0}} e^{-\theta'}\frac{d}{d\theta'}\ln(1{+}e^{f_L(\theta')})\,d\theta'\Big]\,; \\
0 \;=& -\frac{\sqrt{3}\sin(\frac{\pi}{3}\xi)}{\pi\sin(\frac{\pi}{3}(\xi{-}1))}\Big[\int_{\substack{c_2\\>0}} e^{-\theta'}\frac{d}{d\theta'}\ln(1{+}e^{f_L(\theta')})\,d\theta' - \int_{\substack{c_1\\>0}} e^{-\theta'}\frac{d}{d\theta'}\ln(1{+}e^{-f_L(\theta')})\,d\theta'\Big] \\
& -\frac{3}{2\pi\sin(\frac{\pi}{3}(\xi{-}1))}\Big[\int_{\substack{c_2\\>0}} e^{-\theta'}\frac{d}{d\theta'}\ln(1{+}e^{-f_R(\theta')})\,d\theta' - \int_{\substack{c_1\\>0}} e^{-\theta'}\frac{d}{d\theta'}\ln(1{+}e^{f_R(\theta')})\,d\theta'\Big]\,.
\end{aligned}$$

Solving for the integrals needed for the evaluation of (3.84), we find

$$B_{massless}(r) = -\frac{3}{\pi}\frac{\sin(\frac{\pi}{3}\xi)\sin(\frac{\pi}{3}(\xi-1))}{\sin(\pi\xi)}r^2 \ . \tag{3.85}$$

We can analyse the massive equation (3.23) in a similar way and predict

$$B_{massive}(r) = -\frac{\sqrt{3}\sin(\frac{\pi}{3}\xi)}{2\,\pi\sin(\frac{\pi}{3}(\xi+1))}r^2 \ . \tag{3.86}$$

The denominator of (3.85) is zero whenever $\xi-1$ or ξ is an integer multiple of 3, but an application of L'Hôpitals rule shows that

$$B_{massless}(r)\Big|_{\xi=3n \text{ or } \xi=3n+1} = -\frac{\sqrt{3}}{2\,\pi}r^2 \ . \tag{3.87}$$

The formula (3.85) does have a pole when $\xi+1$ is an integer multiple of 3. Since the overall result remains finite this infinity should cancel against one of the terms in the regular expansion of c_{pert}, leaving a logarithmic contribution to the final result just like the IR calculation in Section 3.4.1 (for more details of these kind of cancellations see for example [63, 86, 87]). The calculation might again appear to split into two cases: the term proportional to r^2 in the perturbative expansion occurs at an order n which depends both on the dimension and on the 'parity' of the perturbing operator: $n = 2/y$ for ϕ_{15}, and $1/y$ for ϕ_{21}. However from (3.82) and (3.83) we see that $n = (\xi+1)/3$ in both cases and they can be treated simultaneously. The logarithm is found by evaluating

$$\lim_{\xi\to 3n-1} -\frac{3\sin(\frac{\pi}{3}\xi)\sin(\frac{\pi}{3}(\xi-1))}{\pi\sin(\pi\xi)}\left(r^2 - r^{2n\frac{3}{\xi+1}}\right) \tag{3.88}$$

which yields

$$B_{massless}(r)\Big|_{\xi=3n-1} = (-1)^n\frac{3}{2\,\pi^2\,n}r^2\ln r \ . \qquad (n\in\mathbb{N}) \tag{3.89}$$

Similarly, and for exactly the same values of ξ, logarithms arise in the bulk term related to the massive perturbations. This time we must evaluate

$$\lim_{\xi\to 3n-1} -\frac{\sqrt{3}\sin(\frac{\pi}{3}\xi)}{2\pi\sin(\frac{\pi}{3}(\xi+1))}\left(r^2 - r^{2n\frac{3}{\xi+1}}\right) \tag{3.90}$$

and in these cases we find

$$B_{massive}(r)\Big|_{\xi=3n-1} = \frac{3}{2\,\pi^2\,n}r^2\ln r \ . \qquad (n\in\mathbb{N}) \tag{3.91}$$

This seems to leave the coefficient of the r^2 term unknown, but one piece of information can be extracted, which will be used in Section 3.4.3. The logarithm can be traced back to a divergence in the perturbative integral defining the term C_n, and so providing the same regularisation scheme is used for both flow directions, the

perturbative contributions should cancel upon taking their sum or difference. The remaining finite contribution can be found directly from (3.85) and (3.86):

$$\Big(B_{massless}(r) \pm B_{massive}(r)\Big)\Big|_{\xi=3n-1} = \pm\frac{\sqrt{3}}{4\,\pi}\,r^2 \qquad (n \in \mathbb{N}) \tag{3.92}$$

where the plus signs should be chosen if n is odd and the minus signs if n is even.

We used an iterative method to solve the NLIEs (3.30) and (3.31), and calculated $c_{\text{eff}}(r)$ to high accuracy. The resulting data was fitted against a series of the form

$$c_{\text{eff}}(r) - c_{\text{eff}}(\infty) - B(r) = \sum_{n=1}^{n_3} c_n r^{yn} \tag{3.93}$$

where the exact values of the ultraviolet central charge and the relevant bulk term have been subtracted off. The cutoff n_3 was chosen to give the best possible estimates of the perturbative coefficients c_n. Before we can make a comparison with CPT, we must also fix the value of κ. For the massive systems this was determined exactly in [14,88], and it turns out, numerically at least, that the same relationship between λ and M holds in the massless cases, apart from a factor of either -1 or i.

The relationship between massive and massless ϕ_{21} and ϕ_{15} perturbations was clarified in [61]. The first massless flows found were related to the massive flows by flipping the sign of the coupling constant λ: $\lambda \to -\lambda$, and this is the behaviour exhibited for the ϕ_{15} perturbations. However, for the odd operator ϕ_{21} this change will have no effect since the expansion of c_{eff} is in powers of λ^{2y}. The solution, proposed in [61] for the $|I| = 1$ series, is that the models are instead related via the following transformation: $\lambda \to i\lambda$. We fully expect these results to continue to hold for the new flows, and so the expansion coefficients of c_{eff} in the massive and massless directions should be related. Whether we are considering the odd or even operator, the CPT coefficients C_n are the same for both flow directions so, provided the mass and the crossover scales M are equal, we expect

$$\phi_{15}: \qquad c_n = (-1)^n\,\tilde{c}_n\,, \tag{3.94}$$

$$\phi_{21}: \qquad c_{2n} = (-1)^n\,\tilde{c}_{2n}\,, \tag{3.95}$$

where the symbols $\tilde{c}_n$ are the expansion coefficients obtained using the massive NLIE (3.23). Tables 3.3, 3.4, 3.5 and 3.6 present the first few perturbative coefficients for the models $\mathcal{M}_{3,8}$, $\mathcal{M}_{4,11}$ $\mathcal{M}_{5,8}$ and $\mathcal{M}_{7,11}$ perturbed in both massless and massive directions. The relative signs of the coefficients confirm relations (3.94) and (3.95). Similar results were obtained for the models $\mathcal{M}_{5,12}$ and $\mathcal{M}_{3,10}$ perturbed by ϕ_{15}, and the models $\mathcal{M}_{3,4}$ and $\mathcal{M}_{3,5}$ perturbed by ϕ_{21}. All this provides strong support for the claim that, modulo the bulk terms, the results from the massive and massless integral equations are related by analytic continuation in the parameter λ.

n	$\tilde{c}_n$ (massive)	c_n (massless)
0	3/4	3/4
1	-0.2397699953	0.239769950
2	0.0338727	0.0338717
3	-0.001757	0.00176
4	-0.000177	-0.00019

Table 3.3: Comparison of massive and massless UV coefficients for $\mathcal{M}_{3,8}+\phi_{15}$.

n	$\tilde{c}_n$ (massive)	c_n (massless)
0	19/22	19/22
1	-0.393148695201	0.393148695201
2	0.0166115829	0.0166115834
3	-0.001225836	0.001225827
4	-0.00003425	-0.00003422
5	0.0000116	-0.000012

Table 3.4: Comparison of massive and massless UV coefficients for $\mathcal{M}_{4,11}+\phi_{15}$.

n	$\tilde{c}_n$ (massive)	c_n (massless)
0	0.85	0.85
2	-0.1128538069088	0.1128538069085
4	0.1607667041	0.1607667048
6	0.003799534	-0.003799535
8	-0.0009586	-0.0009585
10	-0.0001554	0.0001554

Table 3.5: Comparison of massive and massless UV coefficients for $\mathcal{M}_{5,8}+\phi_{21}$.

n	$\tilde{c}_n$ (massive)	c_n (massless)
0	71/77	71/77
2	-0.1595765857	0.1595765856
4	0.09745855	0.09745859
6	0.0011733	-0.0011734
8	-0.00068	-0.00067
10	0.000012	-0.000011

Table 3.6: Comparison of massive and massless UV coefficients for $\mathcal{M}_{7,11}+\phi_{21}$.

Model	κ^2_{num}	κ^2
$\mathcal{M}_{5,12}$	0.012665147953	0.012665147955 ...
$\mathcal{M}_{7,16}$	0.0247653386712	0.0247653469711 ...
$\mathcal{M}_{4,11}$	-0.06407485530	-0.06407485531 ...
$\mathcal{M}_{7,17}$	0.0092588732986	0.0092588732985 ...
$\mathcal{M}_{10,23}$	0.02340788397	0.0234078837 ...
$\mathcal{M}_{3,10}$	-0.0188367	-0.0188368 ...

Table 3.7: Comparison of exact and numerical values of κ^2 for ϕ_{15} perturbed models.

A further check on the ϕ_{15} perturbations can be made since we can find the value of κ directly from the expansion of c_{eff}. The first term in the perturbative expansion (3.77) is simply given by

$$C_1 = -12\,(2\pi)^{(1-y)} C_{\phi_0\,\phi_{15}\,\phi_0}\,. \tag{3.96}$$

The operator product coefficient $C_{\phi_0\,\phi_{15}\,\phi_0}$ between the perturbing operator ϕ_{15} and the ground-state ϕ_0 can be found in [89]. Comparing (3.77) and (3.80) at order $n = 1$, we have the relation

$$\kappa = \frac{c_1}{C_1}\,. \tag{3.97}$$

With this formula and the coefficient c_1, found using the massless NLIEs, we estimated κ^2 numerically for a number of models. Table 3.7 reports the results, and compares them with the exact expression for κ^2 for (massive) ϕ_{15} perturbations given in [88]:

$$\lambda^2 = \frac{4^2\,(\xi-1)^2\;\gamma\left(\frac{2+\xi}{2(1+\xi)}\right)\;\gamma\left(\frac{5\xi}{2(1+\xi)}\right)}{\pi^2\;(2-3\xi)^2\;(2-\xi)^2\;\gamma^2\left(\frac{3+\xi}{1+\xi}\right)}\left[\frac{M\;\Gamma\left(\frac{\xi+1}{3}\right)}{\sqrt{3}\;\Gamma\left(\frac{1}{3}\right)\;\Gamma\left(\frac{\xi}{3}\right)}\right]^{\frac{12}{\xi+1}} \tag{3.98}$$

where $\gamma(x) = \frac{\Gamma(x)}{\Gamma(1-x)}$ and M is the mass of the lightest kink. The relation given in [88] was in terms of $\xi^{\text{FLZZ}} = \frac{p}{q-p}$ and m, the mass of the lightest breather, related to M as $m = 2M\,\sin(\frac{\pi}{3}\xi)$. The agreement is clearly very good. Note that κ^2 is sometimes negative – these are cases where, in the normalisations of [89], $C_{\phi_0\,\phi_{15}\,\phi_0}$ turns out to be purely imaginary.

3.4.2 Non-monotonic behaviour

We were rather surprised to find that $c_{\text{eff}}(r)$ was a non-monotonic function of r for all of the flows we studied. The expectation that the functions would be purely monotonic came about because this is the behaviour seen in all previous cases of interpolating flows including the $|I| = 1$ flows. In addition, there had been some notion of a c_{eff} theorem analogous to A.B. Zamolodchikov's c-theorem [90] for flows between unitary minimal models. The theorem states that for unitary minimal

models one can define a function which is equal to the central charge at the conformal points and never increases as r tends to infinity. For unitary minimal models $c(r) = c_{\text{eff}}(r)$ plays the rôle of such a function and, as we have seen, the central charge *is* a monotonic function of r. The idea had been that for the nonunitary models the same would be true, with $c(r)$ replaced by $c_{\text{eff}}(r)$. However our results clearly indicate that this does not hold.

The new question to ask is what is so special about the $|I| = 1$ flows? We can mention one reason why, exceptionally, $c_{\text{eff}}(r)$ should be a monotonic function of r for these flows. The behaviour of a flow is determined at small r by the first nonzero term in the perturbative expansion. Thus whether c_{eff} initially increases or decreases will typically be determined by the sign of $C_1\lambda$ (ϕ_{15}) or $C_2\lambda^2$ (ϕ_{21}). In particular, if C_1 (respectively C_2) is nonzero then for one sign of λ (or λ^2), c_{eff} will initially increase, leading to an immediate violation of the 'c_{eff}-theorem', and a flow which must be non-monotonic if $c_{\text{eff}}(\infty)$ is to be less than $c_{\text{eff}}(0)$. But for the model $\mathcal{M}_{3,5} + \phi_{21}$, the first coefficient C_2 was calculated to be zero in [61]. In this case the asymptotic UV behaviour is instead controlled by $C_4\lambda^4$ and this permits c_{eff} to decrease initially for both (massless and massive) signs of λ^2. A similar calculation for the other models in the $|I| = 1$ series finds C_1 (ϕ_{15}) or C_2 (ϕ_{21}) to be zero and thus, as in the first model, all of the flows are able to be monotonic. A numerical fit of the data for models higher up in the series confirms these coefficients are zero within our numerical accuracy. For all other sequences of models such vanishings of C_1 or C_2 do not occur, forcing at least one of each pair of massive and massless flows to be non-monotonic. One remaining mystery is why it should always be the *massless* flow which is non-monotonic.

3.4.3 Further curiosities

The $|I| = 1$ sequence of flows was found in [57] via an associated staircase model, and the final step of this staircase interpolates in the infrared to a massive model with $c_{\text{eff}} = 0$. It turns out that the NLIE also reproduces this behaviour: even though the operator ϕ_{15} is not a member of the Kac table for $\mathcal{M}_{2,5}$, (3.51) formally predicts a further flow, to a theory with $c_{\text{eff}} = 0$:

$$\mathcal{M}_{2,5} + \phi_{15} \to \mathcal{M}_{2,3} \,. \tag{3.99}$$

There is nothing to stop us using the massless NLIE (3.30, 3.31) and the ϕ_{15} recipe (3.28) to compute an effective central charge for this flow. Interestingly when we do this our numerical results shows that c_{eff} has an exponential behaviour in the infrared, as would be expected for a massive, rather than a massless, flow. Furthermore, comparing c_{eff} (massless) with that of the massive flow $\mathcal{M}_{2,5} + \phi_{15}$ calculated using (3.23) and (3.28), we find the effective central charges match exactly at all

values of r. They also turn out to coincide with the results from the more standard massive flow $\mathcal{M}_{25} + \phi_{12}$, computed using (3.23) and (3.26). This means that the flow is at least physically reasonable, since ϕ_{12} is the single relevant primary field in $\mathcal{M}_{2,5}$. However, it remains a curiosity that the same flow can be found from three different nonlinear integral equations. A sample of our numerical results is shown in Table 3.8. Note that this example shows that the straightforward prediction of scaling dimensions based on periodicity arguments is not always correct: for $\mathcal{M}_{2,5} + \phi_{15}$ one would have expected a series in $r^{6/5}$ for $c_{\text{eff}}(r)$, whereas in fact the expansion is in powers of $r^{12/5}$.

r	$\mathcal{M}_{2,5} + \phi_{15}$ (massless)	$\mathcal{M}_{2,5} + \phi_{15}$ (massive)	$\mathcal{M}_{2,5} + \phi_{12}$ (massive)
0.01	0.39997512539833	0.39997512539839	0.39997512539863
0.2	0.39254149935036	0.39254149935037	0.39254149935054

Table 3.8: Comparison of effective central charge for the three a priori different models.

As mentioned in Section 3.3.1 there is only one possible flow from each minimal model. However if we compare the infrared destinations of (3.51) and (3.52) we see it is possible for two different ultraviolet models, both perturbed by ϕ_{15}, to flow to the same infrared fixed point, one attracted via the irrelevant operator ϕ_{15} and the other via ϕ_{51}. Figure 3.7 illustrates two such flows. As previously-noted, the sequence attracted by ϕ_{51} necessarily stops at this model, but the other sequence may continue to flow down further.

For some models, the predictions of the flows (3.68)–(3.70) must be treated with caution, as we were unable to check them explicitly. Examples are the minimal models $\mathcal{M}_{p,q}$ perturbed by ϕ_{15} when p and q are related as $4p-q=1$. For these cases the twist α' is equal to 2, and a trivial shift of $f_{L/R}(\theta)$ leaves a system with $\alpha'=0$. This prevents us from tuning in a straightforward way onto the required ultraviolet model: numerically, the massless NLIE simply recovers a flow from $c_{\text{eff}}(0) = 1$ to $c_{\text{eff}}(\infty) = 1$.

We also observe that (3.50) formally predicts the following flows from unitary minimal models:

$$\mathcal{M}_{p,p+1} + \phi_{21} \to \mathcal{M}_{1,p}\ , \quad (\xi, \alpha') = (\tfrac{p}{p+1}, 1)\ . \tag{3.100}$$

However it is not clear what is meant by $\mathcal{M}_{1,p}$, and our numerical results indicate that while these flows behave as expected for small r, at some intermediate scale $c_{\text{eff}}(r)$ appears to have a discontinuity. Based on the Ising model case (see below) we suspect there may be a square root singularity, and this may or may not be linked to α' being equal to 1. Also, by the type II equivalence, a similar phenomenon occurs for the models $\mathcal{M}_{p,4p-2}$ perturbed by ϕ_{15}.

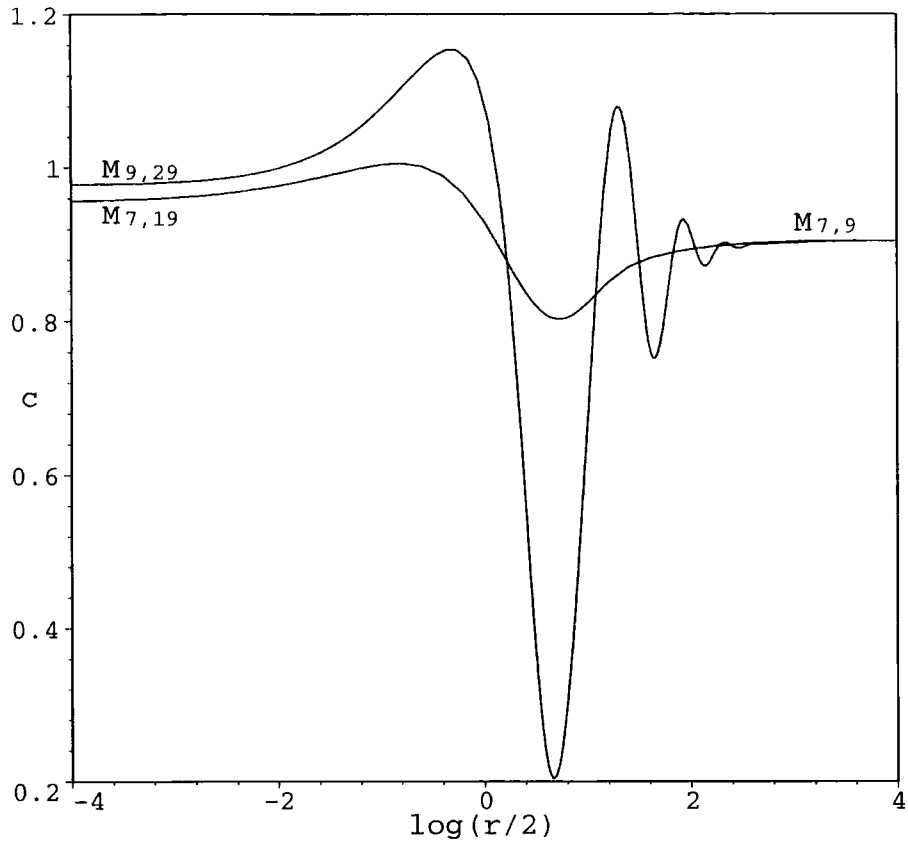

Figure 3.7: Two different flows to the same IR point. $\mathcal{M}_{7,9}$: $\mathcal{M}_{9,29} + \phi_{15}$ attracted via ϕ_{51} , and $\mathcal{M}_{7,19} + \phi_{15}$ attracted via ϕ_{15} .

In one case a detailed check on these exceptional flows can be made with relative ease: the Ising model $\mathcal{M}_{3,4}$ perturbed by ϕ_{21}. For real coupling λ, an exact expression for the (massive) effective central charge can be extracted from the ground-state energy (2.2) given in Chapter 2. We can make an exact prediction for c_{eff} in the massless case by suitably modifying the massive formula: we send $r \to ir$ in the perturbative expansion, swap the logarithmic bulk term for that of the massless model (3.85), and find the coefficient of the r^2 term using (3.92). The exact result is:

$$c_{\text{eff}}^{\text{massless}}(r) = \frac{1}{2} - \frac{3r^2}{2\pi^2}\left[\ln r - \frac{1}{2} - \ln\pi + \gamma_E + \frac{\pi}{2\sqrt{3}}\right] + \frac{6}{\pi}\sum_{k=1}^{\infty}\left(\sqrt{(2k-1)^2\pi^2 - r^2} - (2k-1)\pi + \frac{r^2}{2\,(2k-1)\pi}\right) \quad (3.101)$$

This formula predicts a square root singularity at $r{=}\pi$ which prevents a smooth interpolating flow to the far infrared, but we can at least match against the NLIE for values of r out to this point. As Table 3.9 and Figure 3.8 show, our numerical results agree well with the exact formula (3.101); although the accuracy decreases as the branch point is approached.

r	$c_{\text{eff}}^{NLIE}(r)$	$c_{\text{eff}}^{exact}(r)$
0.0001	0.500000014242146	0.500000014242144
0.6	0.535668551455508	0.535668551455511
1.1	0.49940046725090	0.49940046725085
1.4	0.4131296597211	0.4131296597212
1.8	0.18775453205	0.18775453226

Table 3.9: Comparison of exact and numerical values for c_{eff} for the ϕ_{21} perturbation of $\mathcal{M}_{3,4}$.

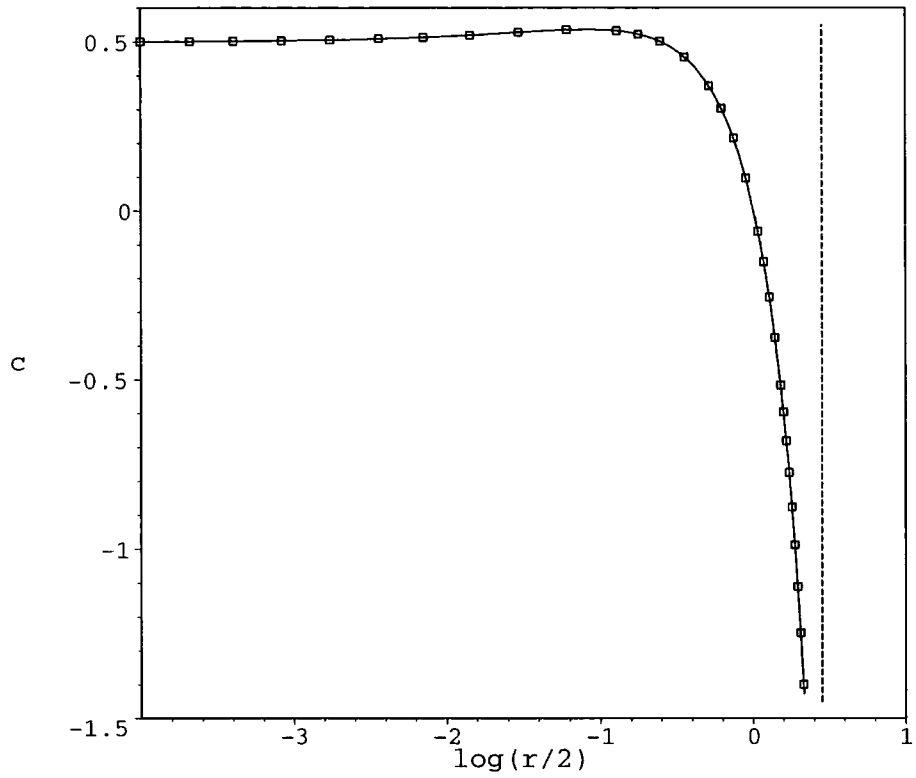

Figure 3.8: NLIE data (boxes) and exact values for $c_{\text{eff}}(r)$ (solid line) for the ϕ_{21} perturbation of the Ising model. The vertical dashed line corresponds to $r = \pi$.

3.4.4 Massive and massless TBA equations

We have already mentioned that no TBA equations are known for the massless flows with $|I| > 1$. This puzzle can be highlighted by looking at some cases where the corresponding massive TBA system *can* be conjectured.

We consider three families of massive systems found in the 'ADET' class of models (mentioned in Chapter 1) and classified in [58]. The first set is obtained from (3.55) simply by replacing the driving term (3.57) by

$$\nu_a(\theta) = r\,\delta_{a,1}\cosh\theta\ . \tag{3.102}$$

This gives the massive flows corresponding to the $|I| = 1$ massless flows, and is the only set for which TBA equations are known for both the massive *and* massless perturbations.

For the second set, we continue to use the driving term (3.102), but replace $l_{ab}^{(A_n)}$ with $l_{ab}^{(T_n)}$ (the incidence matrix of the 'tadpole' graph $T_n = A_{2n}/\mathbb{Z}_2$), letting 1 label the node furthest from the 'tadpole' node (see Figure 3.9). In [91] these systems were identified with the models $\mathcal{M}_{n+2,2n+2} + \phi_{21}$ for n odd and $\mathcal{M}_{n+1,2n+4} + \phi_{15}$ for n even. We note here that these are precisely the models in the $|I| = 2$ series. The massless NLIE predicts, in addition to these previously-known massive flows, the existence of interpolating flows ($n \to n-1$) within this family.

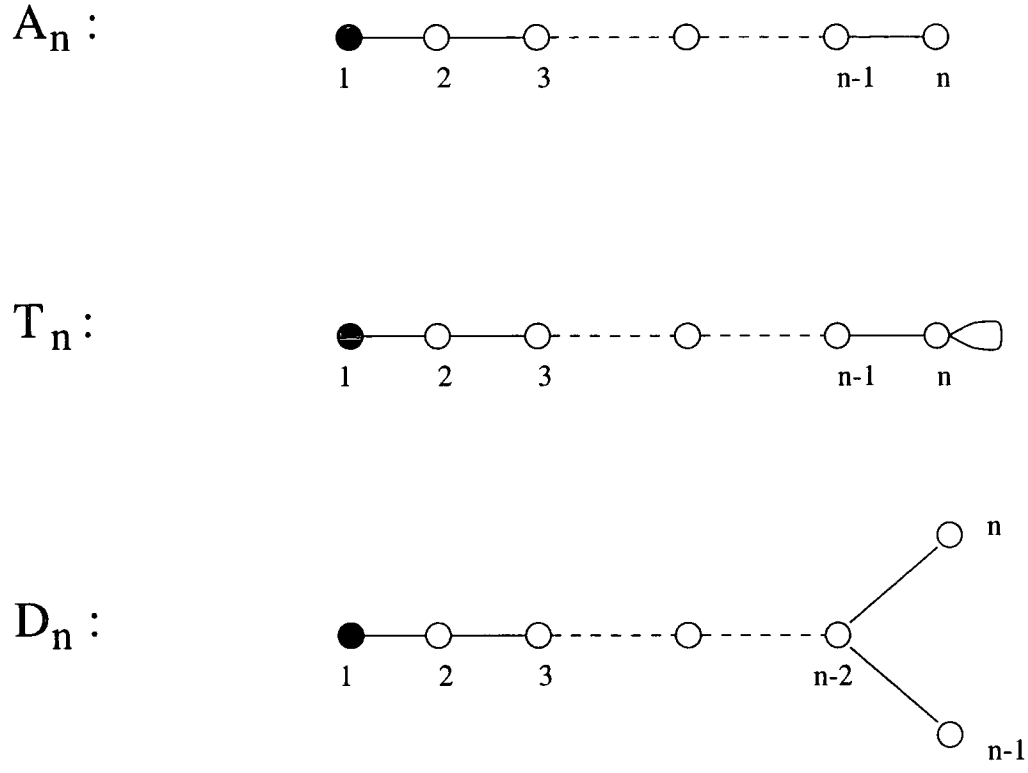

Figure 3.9: The A_n, T_n and D_n graphs, indicating in each case the node to which the driving term $r\cosh\theta$ in the massive TBA system should be attached.

The final family of massive TBA equations is obtained by replacing the A_n incidence matrix with the D_n one. For these cases we must be wary of the type II conjecture, and for each TBA system there are two possible identifications:

$$A_n^+ \equiv \mathcal{M}_{2n-1,2+4n} + \phi_{15} \quad \text{and} \quad A_n^- \equiv \mathcal{M}_{1+2n,4n-2} + \phi_{21} \ . \tag{3.103}$$

The sets $A_n^\pm$ correspond, in the ultraviolet, to the two series of models with index $|I| = 4$. Turning to the massless flows implied by the NLIE, there is a further ambiguity in the infrared destinations. However, the general pattern of (3.50), (3.51) and (3.68)–(3.70) suggests

$$A_n^\pm \to A_{n-1}^\mp \ . \tag{3.104}$$

We have checked the low-lying members of each family of massive TBA equations against the massive NLIE (3.23), finding agreement to our numerical accuracy

(about 14 digits) in each case. However, returning to the question of finding massless versions of these equations, we observe a key difference between the first family and the other two: as is clear from Figure 3.9, the graphs for the $|I| = 1$ systems have a $\mathbb{Z}_2$ symmetry which is in general absent from those for $|I| = 2$ or 4 (the single exception occurs when $|I| = 4$, $n = 4$). The trick that allowed us to move between massive and massless systems for $|I| = 1$ by swapping the ν's defined in (3.102) for those defined in (3.57) relied completely on this symmetry. This '$\mathbb{Z}_2$ trick' was first employed in [45]; more generally, the nodes '1' and 'n' could be replaced by any pair of nodes related by a $\mathbb{Z}_2$ graph symmetry. To the best of our knowledge, all massless TBA systems that have been discovered to date are related to massive systems in essentially this way. Thus if the T_n and D_n TBA systems do have associated massless versions, they are likely to be of a somewhat different nature to all previously-encountered examples.

The $|I| = 4$, $n = 4$ system might appear to offer a counterexample, since the exceptional symmetry of its graph does allow a massless version of the massive TBA to be constructed. However this equation turns out not to reproduce the massless NLIE. For example, for the massless TBA $c_{\text{eff}}(\infty) = 5/7$, which identifies the IR destination of the flow as $\mathcal{M}_{3,7}$ rather than the $\mathcal{M}_{7,10}$ or $\mathcal{M}_{5,14}$ found by the NLIE. Furthermore, the short-distance expansion of $c_{\text{eff}}(r)$ turns out to be inconsistent with the massless TBA flow being related to the massive one by analytic continuation of the coupling λ – rather, it is the flow produced by the massless NLIE which has this property. This failure of the $\mathbb{Z}_2$ trick to produce the analytically-continued massless flow can be put into a more general context. Recall from Section 1.3.1 that TBA equations have associated Y-systems, and that these entail a periodicity: $Y_a(\theta) = Y_a(\theta + iP)$ for certain functions $Y_a(\theta)$, where P depends on the particular Y-system. Suppose that a diagram symmetry relates nodes a and $\tilde{a}$ for this system. Then it can be argued that the associated massive and massless TBA equations will be related by analytic continuation if $Y_a(\theta) = Y_{\tilde{a}}(\theta + iP/2)$, and not otherwise. In particular, for systems related to the ADET diagrams, such a property holds if and only if the nodes a and $\tilde{a}$ are 'conjugate', where conjugation acts on TBA diagrams in the same way as charge conjugation acts on the particles in an affine Toda field theory [25,92]. For the D_n diagrams, the fork nodes are related by charge conjugation for n odd, but not for n even. This matches the above observation that the massive and massless D_4-related systems are not related by continuation in λ.

TBA equations describing the massive ϕ_{13} perturbations of the nonunitary minimal models $\mathcal{M}_{p,q}$ for general p and q have been proposed in [93]. Apart from the unitary series, $q = p+1$, the proposed equations do not possess the necessary symmetry to use the '$\mathbb{Z}_2$ trick' to find the TBA equations for the massless models.

3.5 ϕ_{13} perturbations of nonunitary minimal models

In this section we comment on some features of massless ϕ_{13} perturbations which are revealed when similar methods are used. We define an index $J = q - p$ [46], and set $\zeta = p/J$ and $\alpha = 1/p$. The flow from ζ to $\zeta - 1$ is

$$\mathcal{M}_{p,p+J} + \phi_{13} \to \mathcal{M}_{p-J,p} \qquad \text{attracted via } \phi_{31} \ . \tag{3.105}$$

Again, the number of sequences for each J is given by the Euler φ-function, $\varphi(J)$. Figure 3.10 shows some of the possible sequences.

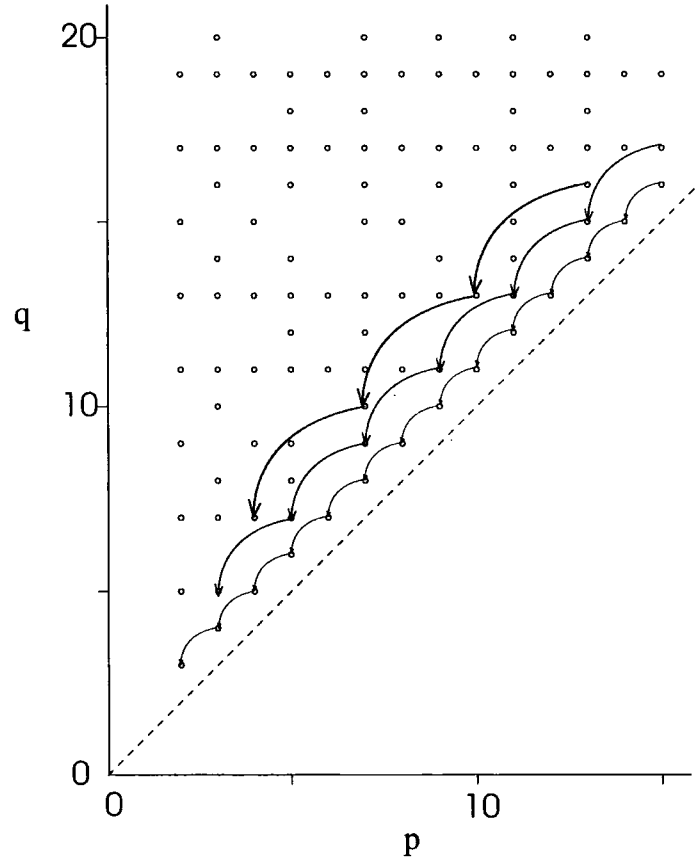

Figure 3.10: The grid of minimal models $\mathcal{M}_{p,q}$ and a selection of the predicted flows induced by ϕ_{13} perturbations. We show the unique sequences with $|J| = 1$ and $|J| = 2$ and one of the two sequences with $|J| = 3$. The line q=p is also shown.

We now use the pair of massless NLIEs ((3.18), (3.19)) found by Al.B. Zamolodchikov [52] to study these flows. However, just as in the $a_2^{(2)}$ case, we cannot access all possible minimal models via this equation. The kernel $\phi(\theta)$ (3.15) has a pole at $i\pi(\zeta - 1)$ which crosses the real θ axis as ζ falls below 1. As before, this could probably be overcome using analytic continuation, but for now we choose $\zeta > 1$, requiring $2p > q$, to prevent such problems occurring. We also find a set of models, $\mathcal{M}_{p,2p-1} + \phi_{13}$, where $\alpha' = 1$ and the would-be IR model is $\mathcal{M}_{1,p}$. Numerically we

find c_{eff} suffers some sort of discontinuity at an intermediate scale for these flows, just as in the ZMIK case.

Solving the massless equations (3.18) and (3.19) for the unitary cases ($J = 1$), we find that results from the TBA equations of [45] are matched to high accuracy[1]. The results for $J > 1$ are perhaps more interesting, since TBA systems for these nonunitary flows are not known. Just as for the ϕ_{21}/ϕ_{15} flows with $|I| > 1$, the monotonicity property is lost. Typical cases are illustrated in Figures 3.11 and 3.12.

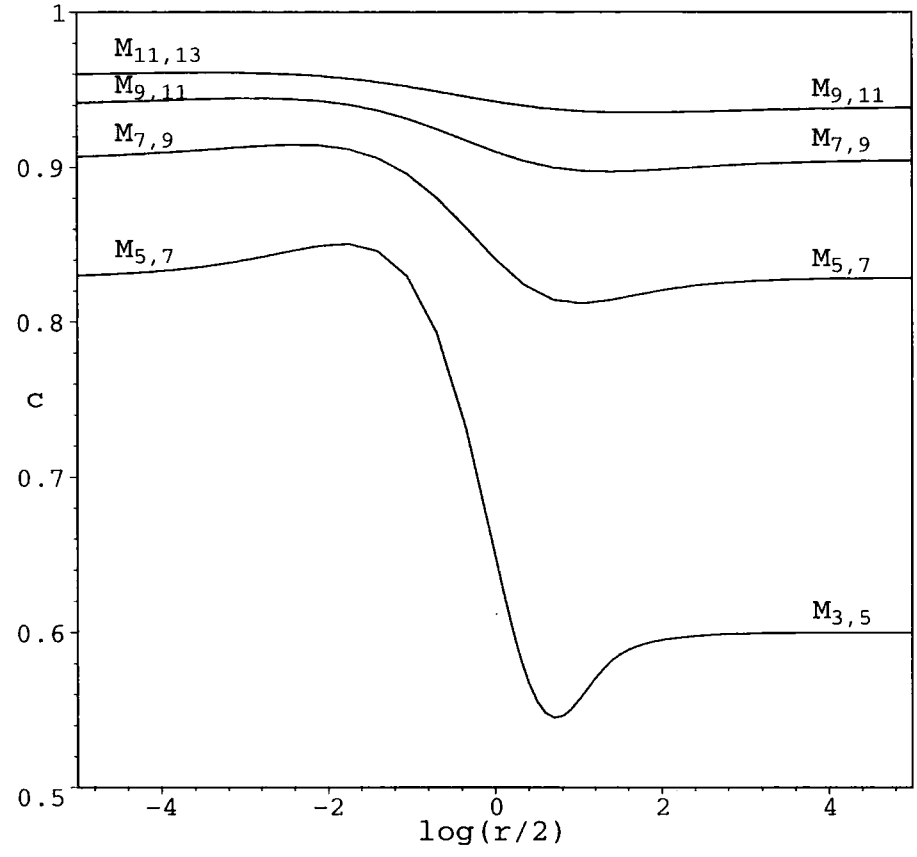

Figure 3.11: One of the $J = 2$ nonunitary ϕ_{13} perturbed flows calculated using the NLIE of [52].

3.6 Summary

Using a simple nonlinear integral equation we have been able to study a number of interpolating flows and fit them into sequences. The simplest example of such a sequence being the flows found in [57, 61]. One of the most unexpected features to emerge was the consistent failure of the effective central charge to be a monotonic function of the system size. Taking into account the full set of minimal models, both unitary and nonunitary, we see that for massless flows a monotonic behaviour of $c_{\text{eff}}(r)$ is very much the exception rather than the rule.

[1]This has also been checked by Al.B. Zamolodchikov [94]

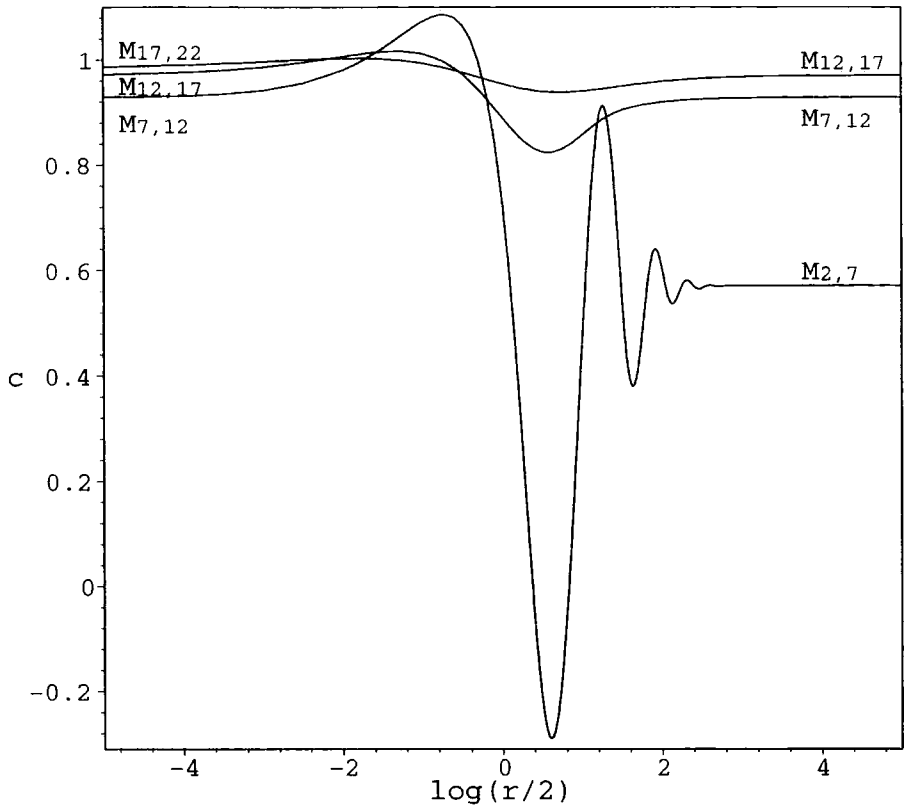

Figure 3.12: One of the nonunitary ϕ_{13} perturbed flows with index $J = 5$ calculated using the NLIE of [52].

Some of these new flows have recently appeared in connection with character identities found by Warnaar [95] using q-trinomial coefficients. The sequences that appeared in this context are equivalent to our sequences labelled by the index $I = 5$ ending at $M_{3,4}$, the $I = 6$ sequence ending at $M_{4,5}$ and the $I = 7$ sequence ending at $M_{5,6}$. It will be interesting to see if more of our sequences appear in this context.

Chapter 4

Spectral problems

In Chapter 1 we discussed two different sets of functional relations: the Y-systems related to the integral equations of TBA type and the $T-Q$ relation which led to a further nonlinear integral equation. These functional relations and related integral equations continue to be of fundamental importance in this chapter. In a new direction of research, Dorey and Tateo [96] have shown how objects normally seen in integrable quantum field theory also arise in the study of the spectra of ordinary differential equations (ODEs).

This rather unexpected connection began with a relation between the spectral determinants of one of the most basic equations in quantum mechanics, the Schrödinger equation with a simple potential term, and the T-systems of integrable quantum field theories. The T-systems are related to the Y-systems encoded on A_{n-1} (or equivalently $SU(n)$) Dynkin diagrams. A more general potential allowed a connection to be made between further spectral determinants and certain eigenvalues of the $\mathbf{Q}_{\pm}$-operators. This work was based on the quantum Wronskian functional relation (1.156) satisfied by these operators. In both cases the eigenvalues of the ordinary differential equation are found using nonlinear integral equations.

These ideas were quickly followed up by the authors of [97, 98], and in [99] the $\mathbf{T}$-operators were also related to spectral determinants. Now that the $\mathbf{T}$ and $\mathbf{Q}$-operators had been found on the ODE side, a natural question to ask was 'is there an equivalent of the $\mathbf{T}-\mathbf{Q}$ relation?' The answer, found in [99], requires a detour into spectral theory of second-order ordinary differential equations defined in the complex x-plane. Solutions of such equations can be studied in sectors of the complex plane. A particular eigenvalue problem is then defined by specifying two such sectors, and finding eigenvalues such that solutions of the ODE decay exponentially in both sectors simultaneously. For ODEs defined in the complex plane there are therefore a number of different eigenvalue problems depending upon the choice of sectors.

Within any particular sector there will be solutions that tend to zero as x tends to infinity, technically known as *subdominant*, and others that tend to infinity, known

as *dominant*. Two solutions with differing asymptotic behaviour in a sector must be linearly independent and so form a basis for all solutions of the ODE. Solutions between different sectors are related by functions known as Stokes multipliers and these 'connection' problems provide the answer to the above question. The **T−Q** functional relation is seen to be equivalent to the relation between solutions of the ODE in different sectors of the complex plane.

Generalisations of these ideas to higher order differential equations began in [78] where certain third-order differential equations were mapped onto the $SU(3)$ Bethe ansatz systems. Independent work by Suzuki [100] provided some support for the idea that general $SU(n)$ BA systems may be found by considering n^{th} order differential equations. However, this paper did not treat the completely general case as the form of the potential term was restricted and the role of a particularly important generalisation of the Baxter $T-Q$ system to $n > 2$ was not elucidated.

After reviewing the ideas mentioned above, this chapter extends the correspondence between integrable quantum field theories and ordinary differential equations by considering n^{th} order equations. We find the $SU(n)$ related BA systems and derive nonlinear integral equations for the associated spectral problems. This work can be found in [3] and briefly mentioned in [4]. Some of the aspects of the problem are also discussed in [101].

4.1 The Schrödinger equation and $SU(2)$

The one dimensional Schrödinger equation with potential term $V(x) = |x|^{2M}$ is defined for x on the real line as

$$\left(-\frac{d^2}{dx^2} + V(x)\right)\psi(x) = E_k\psi(x) \ . \tag{4.1}$$

The potential is confining so the spectrum $\{E_k\}$ is discrete and the energy levels are all distinct. The case $M = 1$ corresponds to the simple harmonic oscillator and its eigenvalues, initially calculated by Heisenberg in 1925, are simply given by $E_k = 2k+1$. Unfortunately exact formulae are not known for the eigenvalue problem when $M \neq 1$. However, progress has been made analytically and numerically, much of it in recent years, by various means. For example, the asymptotic values of the eigenvalues can be estimated using the Bohr-Sommerfield approximation

$$b_0(E_k)^{\mu} \sim 2\pi(k+1/2) \quad , \quad k \to \infty \tag{4.2}$$

where

$$\mu = \frac{M+1}{2M} \quad , \quad b_0 = \frac{\pi^{1/2}\Gamma\left(\frac{1}{2M}\right)}{M\,\Gamma\left(\frac{3}{2}+\frac{1}{2M}\right)} \ . \tag{4.3}$$

An alternative way of treating the eigenvalues is to encode them into spectral functions. One example is the spectral determinant: this is an entire function which

has its zeros exactly at the positions of the eigenvalues E_k. It is defined by

$$D_M(E) = D_M(0) \prod_{k=0}^{\infty} \left(1 - \frac{E}{E_k}\right) . \tag{4.4}$$

The key fact, found by Voros [102, 103], is that the spectral determinants satisfy certain functional relations. These result in exact quantisation conditions for the eigenvalues which although non-trivial can be solved numerically. This is not the avenue we wish to follow here, rather we focus on the functional relations themselves.

The case $M = 2$ corresponds to the quartic oscillator and the spectral determinants of this problem satisfy [102]

$$D(j^{-1}E)D(E)D(jE) = D(j^{-1}E) + D(E) + D(jE) + 2 \tag{4.5}$$

where $j = \exp(2\,i\pi/3)$. Dorey and Tateo [96] noticed that a similar relation arises in TBA studies of the massive quantum field theory related to the Lie algebra A_3. The relevant TBA equations are those given in Section 2.2.1, provided the twist α is now set to zero. We rewrite the Y-system (2.65) in terms of $t = \exp(4\theta/3)$ as

$$X(e^{-i\pi/3}t)X(e^{i\pi/3}t) = (1 + Y(t))^2 \tag{4.6}$$

$$Y(e^{-i\pi/3}t)Y(e^{i\pi/3}t) = 1 + X(t)\,, \tag{4.7}$$

which upon substituting (4.7) into (4.6) gives a relation formally similar to (4.5)

$$Y(e^{-2\pi i/3}t)Y(t)Y_1(e^{2\pi i/3}t) = Y(e^{-2\pi i/3}t) + Y(t) + Y(e^{2\pi i/3}t) + 2\,. \tag{4.8}$$

The analytic properties of the functions D and Y match provided we consider the massless limit of the TBA equations. Then setting $r = b_0$ and $t = E$, the function $D(E)$ can be identified with $Y(t)$. The eigenvalues of the quartic oscillator can now be found to high accuracy by solving the TBA equations (2.67) and then searching for the zeros of $Y(t)$.

The connection also extends to integer values of M greater than 2, where the functional relations satisfied by the spectral determinant are more complicated [102]. This time the spectral determinant should be identified with the function $T_M(\theta)$ of the A_{2M-1} model. This was conjectured in [96] and a proof found by Suzuki in [98]. (An alternative proof can be found in [99].) The T-system

$$T_a\,(\theta - i\,\pi/2M)\,T_a\,(\theta + i\,\pi/2M) = 1 + \prod_{b=1}^{r} T_b(\theta)^{l_{ab}} \tag{4.9}$$

is related to the Y-system via $Y_a(\theta) = \prod_{b=1}^{r} T_b(\theta)^{l_{ab}}$ where l_{ab} is the incidence matrix of the A_{2M-1} Dynkin diagram. This agrees with the quartic oscillator case since $T_2(\theta) = Y_1(\theta)$ when $M = 2$, and our notation for the A_3 Y-system equated $Y_1(\theta)$ with $Y(\theta)$.

Voros also found functional relations for the spectral determinants when M is allowed to be half-integer [103]. The equations simplify if the spectral determinant is written as two subdeterminants $D(E) = D^+(E)D^-(E)$ where the eigenvalues are split according to the parity of their associated eigenfunctions. Decomposing the subdeterminants as

$$D_M^{\pm}(E) = D_M^{\pm}(0) \prod_{k \atop \text{odd}}^{\text{even}} \left(1 - \frac{E}{E_k^{\pm}}\right) \tag{4.10}$$

they satisfy [102]

$$\Omega^{1/2} D^+(\Omega^{-1}E)D^-(\Omega E) - \Omega^{-1/2} D^+(\Omega E)D^-(\Omega^{-1}E) = 2i \tag{4.11}$$

where $\Omega = \exp(i\pi/(M+1))$. This functional equation can be mapped onto the 'quantum Wronskian' relation (1.156) satisfied by the $\mathbf{Q}_{\pm}$-operators, which were introduced in Chapter 1. The relation is more transparent if the $\mathbf{Q}_{\pm}$-operators are replaced with the related $\mathbf{A}_{\pm}$-operators using (1.157)

$$q^{2p/\beta^2}\mathbf{A}_+(q^{1/2}\lambda)\mathbf{A}_-(q^{-1/2}\lambda) - q^{-2p/\beta^2}\mathbf{A}_+(q^{-1/2}\lambda)\mathbf{A}_-(q^{1/2}\lambda) = 2i\sin(2\pi p)\ . \tag{4.12}$$

Applying this operator equation to the vector $|p\rangle$ (an eigenstate of $\mathbf{Q}_{\pm}(\lambda)$), it becomes a functional equation for the eigenvalues $A_{\pm}(\lambda, p)$. These are identified with the spectral determinants via

$$A_{\pm}\left(\lambda, p = \beta^2/4\right) = \alpha^{\mp} D_M^{\mp}\left(\lambda^2/\nu^2\right) \tag{4.13}$$

where the proportionality coefficients are found by comparing the known asymptotics of the two functions. The constants are found to be

$$\begin{aligned} \nu &= (2M+2)^{-1/2\mu}\Gamma\left(\frac{1}{2\mu}\right)^{-1} \\ \beta^2 &= 1/(M+1) \\ p &= 1/(4M+4) \\ \alpha^{\pm} &= \sqrt{\pi}\,(2M+2)^{\mp 1/4\mu}\,\Gamma\left(\frac{1}{2} \pm \frac{1}{4\mu}\right)^{-1}\ . \end{aligned} \tag{4.14}$$

The identification (4.13) means the problem of finding the eigenvalues $\{E_k\}$ now amounts to finding the zeros of the $A_{\pm}(\lambda)$ functions. But we already know from the discussion in Chapter 1 that this is easily done with the help of the nonlinear integral equation for the massless twisted sine-Gordon model (1.136). The equation takes the form

$$\begin{aligned} \ln a_{\pm}(\theta) &= -\frac{1}{2} i b_0 \mu^{-2\mu} e^{\theta} + i\,\alpha_{\pm} + \int_{\mathcal{C}_1} d\theta'\, \varphi(\theta-\theta') \ln(1 + a(\theta')) \\ &\qquad - \int_{\mathcal{C}_2} d\theta'\, \varphi(\theta-\theta') \ln(1 + a^{-1}(\theta')) \end{aligned} \tag{4.15}$$

with $\lambda = \exp(\theta/2\mu)$ and twist $\alpha_{\pm} = \pm\pi/2$.

The $T-Q$ relation, written in terms of $a_\pm(\lambda)$ (2.78), implies the zeros of $1+a_\pm(\lambda)$ correspond to either zeros of $T(\lambda)$ or $A_\pm(\lambda)$. The inequality $\mp 2p > -\beta^2$ means that all of the zeros of $A_\pm(\lambda)$ lie on the positive real axis of the λ^2-plane whereas the $T(\lambda)$ zeros lie on the negative real axis. Thus a search for the zeros of $1 + a_\pm(\lambda)$ along the positive segment of the real axis provides the eigenvalues of the Schrödinger problem at both integer and half-integer values of M. In fact the correspondence was conjectured to hold for all values of $M > 1$ [96]. This was explicitly checked at $M = 15/8$ and $M = 7/8$ [96] and subsequently proved in [97,99].

The initial mapping only worked for one specific value of the twist. The authors of [97] quickly realised that all values of the twist could be obtained if the Schrödinger equation was generalised to include an angular momentum term. The relevant equation is

$$\left(-\frac{d^2}{dx^2} + x^{2M} + l(l+1)/x^2\right)\psi(x) = E_k\psi(x) \ , \tag{4.16}$$

and the identification (4.13) becomes

$$A_\pm\left(\lambda, p = (2l+1)\beta^2/4\right) = \alpha^{\mp} D_M^{\mp}\left(\lambda^2/\nu^2\right) \ . \tag{4.17}$$

The modification of the NLIE is achieved by replacing $\alpha_\pm = \pm\pi/2$ with $\alpha_\pm = \pm\pi(l+1/2)$.

The correspondence between objects in integrable quantum field theory and ordinary differential equations actually goes much deeper. In addition to the **Q**-operators and the quantum Wronskian relation, further mathematical structures found in integrable QFT are found in the theory of ordinary differential equations. The rôle of the **T**$-$**Q** relation on the ODE side of the correspondence was found in [99]. The authors of this paper also found an explanation for the rôle of the **T**-operators and the fusion relations they satisfy. We now review the ideas contained in [99], since their generalisations form the bulk of the work in this chapter.

4.1.1 Stokes multipliers

A detailed study of the properties of solutions to second-order ODEs defined in the complex plane can be found in [104]. Here we simply state the necessary result for the Schrödinger equation with angular momentum term (4.16). There exists a solution $y(x, E)$ to (4.16) that is an entire function of (x, E, l) (although there may be a branch point in $\psi(x)$ at $x = 0$) with asymptotic behaviour

$$y \sim \frac{1}{2i}\, x^{-M/2} \exp\left(-\frac{1}{M+1} x^{M+1}\right) \tag{4.18}$$

as x tends to infinity in the sector

$$|\arg x| < \frac{3\pi}{2(M+1)} \ . \tag{4.19}$$

This information uniquely characterises $y(x, E, l)$. We also denote $\mathcal{S}_k$ to be the sector of the complex plane satisfying

$$\left|\arg x - \frac{2k\pi}{2(M+1)}\right| < \frac{\pi}{2(M+1)} \,. \tag{4.20}$$

Figure 4.1 shows three of the Stokes sectors when M is taken to be just greater than 2.

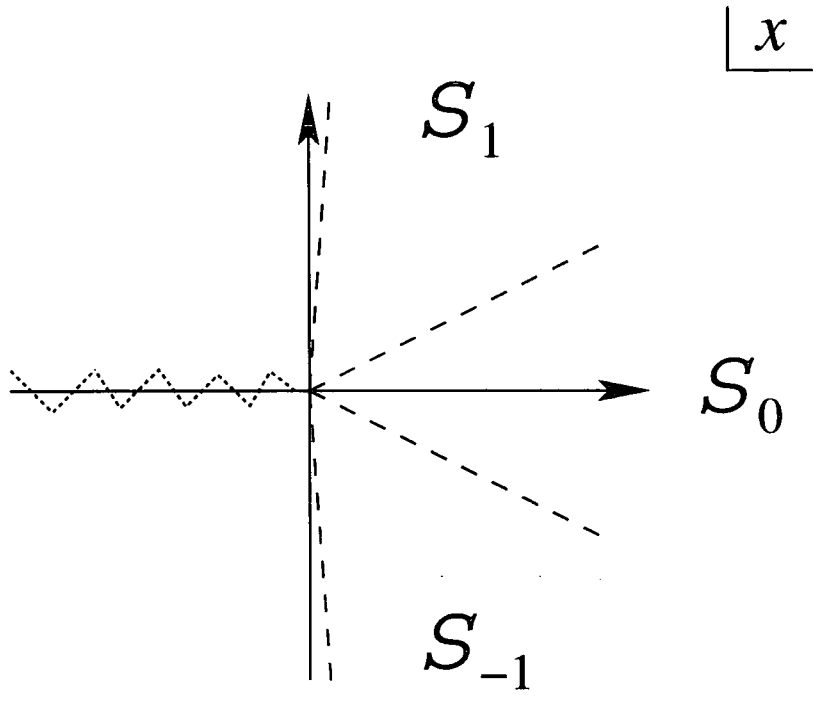

Figure 4.1: Stokes sectors for the ODE (4.16) with $M > 2$.

Other solutions are constructed by considering

$$y_k = y_k(x, E, l) = \omega^{k/2} y(\omega^{-k} x, \omega^{-2Mk} E, l) \quad , \quad \omega = e^{\frac{\pi i}{M+1}} \,. \tag{4.21}$$

Plugging y_k into (4.16) confirms it is a solution of the ODE provided k is an integer. The asymptotic behaviour follows from (4.18)

$$y_k \sim \frac{1}{2i} \omega^{-M(1+k)/2} \exp\left(-\frac{1}{M+1} \omega^{-k(M+1)} x^{M+1}\right) . \tag{4.22}$$

We now compare the asymptotic behaviour (4.22) of y_k and y_{k+1} in the sector $\mathcal{S}_k$ and find that y_k is a subdominant solution whereas y_{k+1} is dominant. Thus, we have found a basis (actually, many bases) of solutions $\{y_k, y_{k+1}\}$ for the second-order ODE. We expand y_{-1} in terms of the basis $\{y_0, y_1\}$ as

$$y_{-1}(x, E, l) = C(E, l) y(x, E, l) + \tilde{C}(E, l) y_1(x, E, l) \tag{4.23}$$

where the Stokes multipliers C and $\tilde{C}$ are entire functions of E and l. Taking the Wronskian [1] of both sides with $y_1(x,E,l)$ or $y_0(x,E,l)$ and rearranging we find

$$C = \frac{W^{(2)}_{-1,1}}{W^{(2)}_{0,1}} \quad , \quad \tilde{C} = \frac{W^{(2)}_{-1,0}}{W^{(2)}_{0,1}} \, . \tag{4.24}$$

Using the asymptotic behaviour (4.22) in the sector $\mathcal{S}_0$ we find the Wronskian $W^{(2)}_{0,1}$ is equal to 1. Wronskians with different arguments are related via $W^{(2)}_{k_1+1,k_2+1}(E) = W^{(2)}_{k_1,k_2}(\omega^{-2M}E)$, and so (4.24) implies $\tilde{C} = -1$.

We now rewrite (4.23) in terms of the basic solution $y(x,E,l)$. Our goal is to find a match with the $T-Q$ relation, which is a function of E only. The first idea might be to set $x = 0$ in (4.23), but this will only work if $l(l+1)$ is exactly zero. The problem is that if this quantity is negative, that is $-1 < l < 0$, then $y(x=0,E,l)$ is identically zero, while if it is positive then $y(x=0,E,l)$ will be infinite almost everywhere. This is because any solution of the ODE is a linear combination of solutions ψ^+ and ψ^- which behave as x^{l+1} and x^{-l} as $x \to 0$. The resolution of this problem [97,99] is to make use of these two further solutions of the ODE and their behaviour as $x \to 0$. We define ψ^+ by the asymptotic

$$\psi^+(x,E,l) \sim x^{l+1} + O(x^{l+3}) \, . \tag{4.25}$$

This asymptotic only uniquely determines ψ^+ if $\Re e\, l > -3/2$ since the other solution ψ^-, which behaves as x^{-l}, may dominate outside this region. In the ODE (4.16) l only appears in the combination $l(l+1)$ so we can continue l to $-1-l$ and define the other solution as

$$\psi^-(x,E,l) \equiv \psi^+(x,E,-1-l) \, . \tag{4.26}$$

As before we define further functions $\psi^\pm_k$ that are also solutions of (4.16)

$$\psi^\pm_k \equiv \psi^\pm_k(x,E,l) = \omega^{k/2}\psi^\pm(\omega^{-k}x, \omega^{-2Mk}E, l) \, . \tag{4.27}$$

We find by considering the limit $x \to 0$ that

$$\psi^\pm_k(x,E,l) = \omega^{\mp k(l+1/2)}\psi^\pm(x,E,l) \, . \tag{4.28}$$

The next step is to take the Wronskian of the Stokes relation (4.23) with $\psi^\pm$. We define

$$D^\mp(E,l) = W^{(2)}[y(x,E,l), \psi^\pm(x,E,l)] \tag{4.29}$$

so that the result can be written

$$C(E,l)D^\pm(E,l) = \omega^{\mp(1/2+l)}D^\mp(\omega^{2M}E,l) + \omega^{\pm(1/2+l)}D^\mp(\omega^{-2M}E,l) \tag{4.30}$$

[1] The Wronskian of two functions $y_{k_1}(x)$ and $y_{k_2}(x)$ is defined to be $W^{(2)}_{k_1,k_2} = y_{k_1}(x)y'_{k_2}(x) - y_{k_2}(x)y'_{k_1}(x)$. Furthermore, provided both the functions are solutions of the same Schrödinger equation, the Wronskian will be independent of x, and it vanishes if and only if the two functions are linearly dependent.

where we have used

$$W^{(2)}[y_k, \psi^{\pm}](E, l) = \omega^{\pm k(l+1/2)} W^{(2)}[y, \psi^{\pm}](w^{2kM} E, l) \,. \tag{4.31}$$

For convenience we rewrite the arguments of the functions $D^{\pm}(E, l)$ using the relation $\omega^{2(M+1)} = 1$:

$$C(E, l) D^{\pm}(E, l) = \omega^{\mp(1/2+l)} D^{\mp}(\omega^{-2} E, l) + \omega^{\pm(1/2+l)} D^{\mp}(\omega^{2} E, l) \,, \tag{4.32}$$

and we are ready to map this onto the T–Q relation. To make the comparison easier, we again quote the result of applying the $\mathbf{T}$–$\mathbf{Q}_{\pm}$ operator equation to the vector $|p\rangle$. The result, written in terms of the $A_{\pm}$ eigenvalues and explicitly including the p dependence, is

$$T(\lambda, p) A_{\pm}(\lambda, p) = e^{\pm 2\pi i p} A_{\pm}(q\lambda, p) + e^{\mp 2\pi i p} A_{\pm}(q^{-1}\lambda, p) \,. \tag{4.33}$$

Comparing this equation with (4.32) we see that they have the same form provided $\omega = q$ and $\omega^{l+1/2} = e^{2\pi i p}$. This boils down to the relations (4.14) found earlier and confirms the identification between the functions $D^{\pm}$ and $A^{\mp}$ (4.13). In addition, the rôle of the T eigenvalues on the ODE side of the correspondence has emerged. Comparing the above functional equations and using the asymptotics of the functions the following identification can be made

$$\begin{aligned} T(\lambda, p = \beta^2/4) &= C\left(\frac{\lambda^2}{\nu^2}\right) \\ &= W^{(2)}_{-1,1}\left(\frac{\lambda^2}{\nu^2}\right) \end{aligned} \tag{4.34}$$

where the last line follows from (4.24). Furthermore, it is argued in [99] that the function T is also a spectral determinant of an eigenvalue problem. The relation (4.34) implies T is proportional to the Wronskian of two solutions of (4.16): y_{-1} and y_1. Thus T is zero if and only if the Wronskian is zero, which in turn only holds if and only if y_{-1} and y_1 are linearly dependent. So we have two solutions decaying simultaneously in the sectors $\mathcal{S}_{-1}$ and $\mathcal{S}_1$ and this constitutes the definition of an eigenvalue problem, with the zeros of T coinciding with the zeros of the spectral determinant.

Finally, evaluating (4.32) at a zero E_k of $D^{-}(E, l)$, we have

$$\omega^{2l+1} \frac{D^{-}(\omega^2 E_k, l)}{D^{-}(\omega^{-2} E_k, l)} = -1 \,, \tag{4.35}$$

since $C(E, l)$ is entire. Now we make use of the product representation for the spectral determinants (4.10) and find

$$\omega^{2l+1} \prod_{j=1}^{\infty} \frac{(E_j - \omega^2 E_k)}{(E_j - \omega^{-2} E_k)} = -1 \,, \tag{4.36}$$

which is a set of $SU(2)$ Bethe ansatz equations.

4.2 Generalisation to $SU(n)$

The initial third-order differential equation considered in [78] had one free parameter M and was simply given by

$$\left(\frac{d^3}{dx^3} + x^{3M} - E\right)\psi(x) = 0 \ . \tag{4.37}$$

This was mapped onto an $SU(3)$ BA system at a specific set of values for the twist parameters. The full BA system has two free parameters, corresponding to twists, which are missing in the initial ODE. The solution, found in [78], was to enlarge the set of equations to those of the form

$$\left(\frac{d^3}{dx^3} - G\left(\frac{1}{x^2}\frac{d}{dx} - \frac{1}{x^3}\right) + \frac{L}{x^3} + x^{3M} - E\right)\psi(x) = 0 \tag{4.38}$$

with additional parameters G and L.

This combined with the most general $SU(2)$ equation (4.16), tends to suggest that the $SU(n)$ twists should be associated with the addition of terms homogeneous with $\frac{d^n}{dx^n}$, of the form

$$A_k x^{-k}\frac{d^{n-k}}{dx^{n-k}} \quad , \quad k = 2 \ldots n \ . \tag{4.39}$$

It is always possible to eliminate the $k = 1$ term by redefining ψ, and we will assume that this has done. We define the general n^{th} order differential equation to be

$$\left((-1)^{n+1}\frac{d^n}{dx^n} + \frac{A_2}{x^2}\frac{d^{n-2}}{dx^{n-2}} + \frac{A_3}{x^3}\frac{d^{n-3}}{dx^{n-3}} + \ldots + \frac{A_n}{x^n} + x^{nM} - E\right)\psi(x) = 0 \tag{4.40}$$

with $n-1$ free parameters $\{A_2, A_3, \ldots, A_n\}$ which exactly matches the number of twists in an $SU(n)$ BA system. The equation studied in [100] corresponds to setting all of the A_k to zero and restricting nM to be an integer. For our current purposes the variables $\{A_k\}$ turn out to be rather inconvenient, and we now give an alternative parameterisation of the ODE which will turn out to simplify the subsequent discussion.

4.2.1 The ordinary differential equation

First, define a general homogeneous differential operator of degree one by setting

$$D(g) = \left(\frac{d}{dx} - \frac{g}{x}\right) \ . \tag{4.41}$$

Useful properties of this operator are

$$D(g)^\dagger = -D(-g) \ , \tag{4.42}$$

$$D(g_2 - 1)D(g_1) = D(g_1 - 1)D(g_2) \ . \tag{4.43}$$

The first of these relates the operator to its adjoint, while the second expresses a form of commutativity. Now, given a vector $\mathbf{g} = \{g_0, g_1, \ldots g_{n-1}\}$, set

$$D(\mathbf{g}) = D(g_{n-1} - (n-1))\, D(g_{n-2} - (n-2)) \ldots D(g_1 - 1)\, D(g_0)\ . \tag{4.44}$$

This is a homogeneous differential operator of order n; by the 'commutativity' property it depends on the components $\{g_0 \ldots g_{n-1}\}$ of $\mathbf{g}$ in a symmetrical manner. From now on we also impose

$$\sum_{i=0}^{n-1} g_i = \frac{n(n-1)}{2} \tag{4.45}$$

to ensure the vanishing of the term in $D(\mathbf{g})$ proportional to $x^{-1}\frac{d^{n-1}}{dx^{n-1}}$. Finally, we record one more property of $D(\mathbf{g})$ which will be useful later: its indicial polynomial (see for example [105]) is

$$f(\lambda) = \prod_{i=0}^{n-1}(\lambda - g_i)\ . \tag{4.46}$$

With these ingredients in place, the more convenient way to write (4.40) is as follows

$$\Big((-1)^{n+1}D(\mathbf{g}) + P(x,E)\Big)\psi(x) = 0\ , \qquad P(x,E) = x^{nM} - E\ . \tag{4.47}$$

The parameters $\{g_0, g_1, \ldots, g_{n-1}\}$ can be related to the set $\{A_2, A_3, \ldots, A_n\}$, but as the relations are not needed in the following we do not quote them here. However, to tie in with the $SU(3)$ case (4.38), we note that the parameters G and L are related to $\mathbf{g} = \{g_0, g_1, g_2\}$ via

$$\begin{aligned} G &= g_0g_1 + g_0g_2 + g_1g_2 - 2\,, \\ L &= 2 - g_0g_1g_2 - (g_0g_1 + g_0g_2 + g_1g_2)\,. \end{aligned} \tag{4.48}$$

4.2.2 The fundamental system of solutions

A number of important properties of the solutions of the n^{th} order ODE are needed and, generalising the $SU(2)$ case, we take our cue from the approach of [104] to second-order ODEs. We claim that (4.47) has a solution $y(x, E, \mathbf{g})$ such that:

- $y(x, E, \mathbf{g})$ is an entire function of $(x, E, \mathbf{g})$, modulo a possible branch point at the origin of the complex x-plane.
- the asymptotic behaviour as $|x| \to \infty$ in the sector $|\arg x| < (n+1)\pi/n(M+1)$ is

$$\frac{d^p y}{dx^p} \sim (-1)^p\, \frac{x^{(1-n+2p)M/2}}{i^{(n-1)/2}\sqrt{n}} \exp\left(-x^{M+1}/(M+1)\right) \tag{4.49}$$

for $p = 0, 1, \ldots$. The asymptotic changes for $M < 1/(n-1)$; more generally the behaviour can be found from the WKB-like formula

$$y \sim P(x,E)^{-(n-1)/2n} \exp\Big(-\int^x P(t,E)^{1/n} dt\Big), \tag{4.50}$$

and details of the extension in the n=2 case can be found in [99].

• y is uniquely characterised by the asymptotic (4.49) for $p = 0$ and x real.

These properties were proved in [104] for n=2, $nM\in\mathbb{Z}$, and $D(\mathbf{g})=\frac{d^2}{dx^2}$. The paper [100] contains some discussion for the general n case with the restricted potential term mentioned above. We do not attempt a proof here for the general n^{th} order ODE (4.47).

We now construct a basis of solutions for the ODE, just as is done for the $SU(2)$ case in Section 4.1.1, by considering the functions

$$y_k(x, E, \mathbf{g}) = \omega^{(n-1)k/2}\, y(\omega^{-k}x, \omega^{-nMk}E, \mathbf{g}) \quad , \qquad \omega = e^{2\pi i/n(M+1)} . \tag{4.51}$$

Substituting (4.51) into (4.47), we find that y_k is a solution of the differential equation provided $k \in \mathbb{Z}$. If sectors $\mathcal{S}_k$ are defined as

$$\mathcal{S}_k : \qquad \left|\arg x - \frac{2k\pi}{n(M+1)}\right| < \frac{\pi}{n(M+1)} , \tag{4.52}$$

then as $x \to \infty$ in $\mathcal{S}_{k-\frac{n}{2}} \cup \mathcal{S}_{k-\frac{n}{2}+1} \cup \ldots \cup \mathcal{S}_{k+\frac{n}{2}}$, (4.49) implies the asymptotic behaviour is

$$\frac{d^p y_k}{dx^p} \sim (-1)^p \omega^{-k(1-n+2p)(M+1)/2} \frac{x^{(1-n+2p)M/2}}{i^{(n-1)/2}\sqrt{n}} \exp\left(-\omega^{-k(M+1)}x^{M+1}/(M+1)\right) . \tag{4.53}$$

Up to a constant multiple, y_k is the unique solution to (4.47) which is subdominant in $\mathcal{S}_k$.

We mentioned earlier the use of the terminology dominant and subdominant to describe the possible asymptotic behaviour of the solutions of a second-order differential equation. The pattern becomes much more complicated when we consider an n^{th} order differential equation. In general, there will be n different behaviours for solutions at large $|x|$ corresponding to the n roots of unity. The possible behaviours are

$$y \sim \frac{x^{(1-n)M/2}}{i^{(n-1)/2}\sqrt{n}} \exp\left(e^{\frac{2\pi iq}{n}} x^{M+1}/(M+1)\right) \quad , q = 0, \ldots, n-1 \tag{4.54}$$

and, depending on the sector, more than one of these solutions will tend to zero. Following [78], we associate the adjective subdominant to the solution which tends to zero fastest in a given sector.

We can establish the linear independence of a set of solutions using Wronskians, and, as they will play an important role in the following, we first setup some notation. Generalising the Wronskian of two functions, we define the Wronskian of m functions $f_1(x), \ldots, f_m(x)$ as

$$W^{(m)}[f_1, f_2, \ldots f_m] = \text{Det} \begin{bmatrix} f_1 & f_2 & \cdots & f_m \\ f_1' & f_2' & \cdots & f_m' \\ \vdots & \vdots & & \vdots \\ f_1^{[m-1]} & f_2^{[m-1]} & \cdots & f_m^{[m-1]} \end{bmatrix} \tag{4.55}$$

where $f_i^{[p]}(x) = \frac{d^p}{dx^p} f_i(x)$. We also set

$$W^{(m)}_{k_1,k_2,\ldots k_m} = W^{(m)}[y_{k_1}, y_{k_2}, \ldots y_{k_m}]\,, \tag{4.56}$$

and we will give a special status to those Wronskians whose arguments are successive integers

$$W^{(m)}_k = W^{(m)}_{k,k+1,k+2,\ldots k+m-1}\,. \tag{4.57}$$

Note that $W^{(1)}_k = y_k$, and that (generalising (4.51))

$$W^{(m)}_{k_1+k,k_2+k,\ldots\, k_m+k}(x,E,\mathbf{g}) = \omega^{m(n-m)k/2} W^{(m)}_{k_1,k_2,\ldots\, k_m}(\omega^{-k}x, \omega^{-nMk}E, \mathbf{g})\,. \tag{4.58}$$

For an n^{th} order ODE with vanishing $(n-1)^{\text{th}}$ order term, as is true of our case by (4.45), it is standard that all n-fold Wronskians $W^{(n)}[f_1, \ldots f_n]$ are independent of x, and vanish if and only if the solutions $f_1, \ldots f_n$ are linearly dependent. In particular, (4.53) can be used as $|x| \to \infty$ in $\mathcal{S}_{k-1/2} \cup \mathcal{S}_{k+1/2}$ to show that $W^{(n)}_k = 1$, and so, for each $k \in \mathbb{Z}$, the functions $\{y_k, y_{k+1}, \ldots, y_{k+n-1}\}$ are linearly independent, and furnish a basis of solutions to (4.47).

4.2.3 Stokes multipliers and functional relations

We generalise (4.23) by expanding y_0 in terms of the basis provided by the set $\{y_1, y_2, \ldots, y_n\}$:

$$\sum_{k=0}^{n} (-1)^k C^{(k)}(E,\mathbf{g})\, y_k(x,E) = 0\,, \tag{4.59}$$

where $C^{(0)}(E,\mathbf{g}) = 1$ and the constants $C^{(k)}(E,\mathbf{g})$, $k > 0$ are entire functions of both E and $\mathbf{g}$ and again called Stokes multipliers.

We can find explicit formulae for the Stokes multipliers by taking suitable Wronskians: this is the analogue of the method used in Section 4.1.1 for the $SU(2)$ case. We begin by taking the Wronskian of (4.59) with all the functions of the basis apart from y_k

$$[W^{(n)} \sum_{k=0}^{n} (-1)^k C^{(k)}(E,\mathbf{g})\, y_k(x,E), y_0, \ldots, y_{k-1}, y_{k+1}, \ldots, y_n] = 0\,. \tag{4.60}$$

Most of the terms vanish by antisymmetry and we are left with the simple relation

$$C^{(k)}(E,\mathbf{g}) = W^{(n)}_{01\ldots\hat{k}\ldots n}(E,\mathbf{g}) \tag{4.61}$$

where the hat $(\hat{k})$ indicates that the corresponding index is to be omitted and we used $W^{(n)}_1 = 1$. Clearly, $C^{(n)} = W^{(n)}_0 = 1$. We now relate $C^{(1)}$ to the 'privileged' Wronskians $W^{(m)}_k$. This discussion can be generalised to the other Stokes multipliers; however they will not be needed in the following.

For general p, consider the determinants

$$0 = \mathrm{Det}\begin{bmatrix} y_0^{[i]} & y_1^{[i]} & \dots & y_p^{[i]} \\ y_0 & y_1 & \dots & y_p \\ y_0' & y_1' & \dots & y_p' \\ \vdots & \vdots & & \vdots \\ y_0^{[p-1]} & y_1^{[p-1]} & \dots & y_p^{[p-1]} \end{bmatrix} \tag{4.62}$$

with $i = 0, 1, \dots p-2$. Expanding the first row of each using Cramer's rule, we have

$$0 = \sum_{k=0}^{p} (-1)^k \begin{bmatrix} y_k \\ y_k' \\ \vdots \\ y_k^{[p-2]} \end{bmatrix} W^{(p)}_{01\dots\hat{k}\dots p} \,. \tag{4.63}$$

Now form a $(p-1)\times(p-1)$ matrix with the RHS of (4.63) as the first column, and the vectors $\mathbf{v}_j = [y_j, y_j', \dots y_j^{[p-2]}]^t$, $j = 2, 3 \dots p-1$ as the remainder. Taking its determinant yields the following Plücker-type relation (see for example [106]):

$$0 = W^{(p-1)}_{02\dots p-1} W^{(p)}_{12\dots p} - W^{(p-1)}_{12\dots p-1} W^{(p)}_{02\dots p} + (-1)^p W^{(p-1)}_{p2\dots p-1} W^{(p)}_{01\dots p-1} \,. \tag{4.64}$$

Rearranging, and supplementing the notation (4.57) with the convention $W_k^{(0)} = 1$ $\forall k$ this becomes

$$\frac{W^{(p)}_{02\dots p}}{W_1^{(p)}} = \frac{W^{(p-1)}_{02\dots p-1}}{W_1^{(p-1)}} + \frac{W_2^{(p-1)}}{W_1^{(p-1)}} \frac{W_0^{(p)}}{W_1^{(p)}} \,. \tag{4.65}$$

Repeatedly substituting this relation into itself until $W_k^{(0)}$ is reached we find

$$\frac{W^{(p)}_{02\dots p}}{W_1^{(p)}} = \sum_{m=0}^{p-1} \frac{W_2^{(m)}}{W_1^{(m)}} \frac{W_0^{(m+1)}}{W_1^{(m+1)}} \,. \tag{4.66}$$

Since $C^{(1)} = W^{(n)}_{02\dots n}$, we can set $p = n$ and multiply (4.66) through by $\prod_{j=0}^{n} W_1^{(j)}$ to find a functional relation between the Stokes multiplier $C^{(1)}$ and the Wronskians $W_k^{(m)}$

$$C^{(1)} \prod_{j=0}^{n} W_1^{(j)} = \sum_{m=0}^{n-1} \left(\prod_{j=0}^{m-1} W_1^{(j)} \right) W_2^{(m)} W_0^{(m+1)} \left(\prod_{j=m+2}^{n} W_1^{(j)} \right) \,. \tag{4.67}$$

4.2.4 Bethe ansatz equations

A standard set of BA equations depend only on the twist parameter and the energy, and so equation (4.67) is not quite ready to be mapped onto them yet since it depends on x as well as E and $\mathbf{g}$. The simplest idea used in [99] and also for the first ODE considered in [78], is to set x to zero. This will only work at exceptional values of the g_i since in general the differential operator $D(\mathbf{g})$ has a (regular) singularity at

$x = 0$. Instead, motivated by the general $SU(2)$ case [97, 99] we expand $y(x, E, \mathbf{g})$ as

$$y(x, E, \mathbf{g}) = W_0^{(1)}(x, E, \mathbf{g}) = \sum_{i=0}^{n-1} D_{[i]}^{(1)}(E, \mathbf{g})\, \chi_i(x, E, \mathbf{g}) \tag{4.68}$$

where the χ_i form an alternative basis of solutions to (4.47), fixed by the demand that they have the simplest possible behaviours near the origin:

$$\chi_i \sim x^{g_i} + O(x^{g_i+n}), \qquad x \to 0. \tag{4.69}$$

(Recall that the g_i are the roots of the indicial polynomial (4.46).) Strictly speaking the asymptotic (4.69) does not always suffice to pin down *all* of the χ_i. Assume, until further notice, that the g_i's are ordered as

$$\Re e(g_0) < \Re e(g_1) < \ldots < \Re e(g_{n-1}). \tag{4.70}$$

Then χ_0 is certainly uniquely determined by (4.69), and the $\chi_{i>0}$ can be defined by a process of analytic continuation from this solution, just as is done for the Schrödinger equation in Section 4.1.1. This idea will be used in Section 4.3.2 below.

An expansion for $W_0^{(m)}(x, E, \mathbf{g})$ follows from substituting (4.68) into (4.56). The result will contain the functions $\chi_i(\omega^{-k}x, \omega^{-nMk}E, \mathbf{g})$ as well as the $\chi_i(x, E, \mathbf{g})$. However, all of these functions are solutions to the initial ODE, and by considering their behaviour near $x = 0$ we find

$$\chi_i(\omega^{-k}x, \omega^{-nMk}E, \mathbf{g}) = \omega^{-kg_i}\chi_i(x, E, \mathbf{g}). \tag{4.71}$$

Therefore the m-fold Wronskians $W_0^{(m)}$ have expansions of the form

$$W_0^{(m)}(x, E, \mathbf{g}) = \sum_{0 \le j_1 < j_2 < \ldots < j_m \le n-1} D_{[j_1 j_2 \ldots j_m]}^{(m)}(E, \mathbf{g})\, W^{(m)}[\chi_{j_1}, \chi_{j_2} \ldots \chi_{j_m}](x, E, \mathbf{g}). \tag{4.72}$$

Using (4.71), (4.68) and (4.56), the coefficients $D_{[j_1 j_2 \ldots j_m]}^{(m)}(E, \mathbf{g})$ can be expressed as sums of products of the $D_{[i]}^{(1)}(\omega^{-nMk}E, \mathbf{g})$. This leads to relations which generalise the 'quantum Wronskians' of [38]. However, for current purposes we treat the coefficients with different values of m as independent functions.

We will initially focus on the dominant terms of the expansions (4.72). The ordering (4.70) implies these are

$$W_0^{(m)}(x, E, \mathbf{g}) \sim D_{[01\ldots m-1]}^{(m)}(E, \mathbf{g})\, x^{\beta_m + m(n-m)/2}, \qquad x \to 0 \tag{4.73}$$

where in order to simplify subsequent calculations we set

$$\beta_m = \sum_{j=0}^{m-1} g_j - m(n-1)/2. \tag{4.74}$$

Substituting (4.72) into (4.67) an x-independent equation is found by extracting the coefficient of the leading power: x^α, $\alpha = \sum_{j=0}^{n}(\beta_j + j(n-j)/2)$. Shifting E to $\omega^{nM}E$ and setting

$$\begin{aligned} D^{(m)}(E,\mathbf{g}) &= D^{(m)}_{[01\ldots m-1]}(E,\mathbf{g})\,, \quad D^{(m)}_k(E,\mathbf{g}) = D^{(m)}(\omega^{-nMk}E,\mathbf{g})\,, \\ T^{(1)}(E,\mathbf{g}) &= C^{(1)}(\omega^{nM}E,\mathbf{g})\,, \end{aligned} \tag{4.75}$$

the final result can be written as

$$T^{(1)}\prod_{j=0}^{n}D_0^{(j)} = \sum_{m=0}^{n-1}\left(\prod_{j=0}^{m-1}D_0^{(j)}\right)\omega^{-\beta_m}D_1^{(m)}\,\omega^{\beta_{m+1}}D_{-1}^{(m+1)}\left(\prod_{j=m+2}^{n}D_0^{(j)}\right). \tag{4.76}$$

This functional equation generalises the $SU(2)$ $T-Q$ relation (1.155) with the rôle of the eigenvalues of the Q (or A in [38]) operators being played by the functions $D^{(j)}$.

We can now derive an initial set of BA equations for the zeroes $E = F_k^{(m)}$ of the functions $D^{(m)}(E)$. (For the next few equations we will leave the dependence of all functions on $\mathbf{g}$ implicit.) The LHS of (4.76) vanishes if we set $E = F_k^{(m)}$, as do all but the terms with superscript $m-1$ and m on the RHS. If we assume that there are no further vanishings, then the following set of coupled equations for the $\{F_k^{(m)}\}$ follow from equating the remaining two terms:

$$\frac{D^{(m-1)}(\omega^{-nM}F_k^{(m)})}{D^{(m-1)}(F_k^{(m)})}\,\frac{D^{(m)}(\omega^{nM}F_k^{(m)})}{D^{(m)}(\omega^{-nM}F_k^{(m)})}\,\frac{D^{(m+1)}(F_k^{(m)})}{D^{(m+1)}(\omega^{nM}F_k^{(m)})} = -\omega^{-2\beta_m+\beta_{m-1}+\beta_{m+1}} \tag{4.77}$$

where $k = 1, 2, \ldots, \infty$. These form a system of Bethe ansatz equations (BAE) of $SU(n)$ type (see, for example, equation (3.32) of [107]). We wish to use functions which are real on the real axis of the complex E-plane and so we make one more definition

$$D^{(m)}(E,\mathbf{g}) = A^{(m)}(\omega^{-nM(m-1)/2}E,\mathbf{g})\,, \quad F_k^{(m)} = \omega^{nM(m-1)/2}E_k^{(m)}\,. \tag{4.78}$$

Then the BAE (4.77) become

$$\frac{A^{(m-1)}(\omega^{-nM/2}E_k^{(m)})}{A^{(m-1)}(\omega^{nM/2}E_k^{(m)})}\,\frac{A^{(m)}(\omega^{nM}E_k^{(m)})}{A^{(m)}(\omega^{-nM}E_k^{(m)})}\,\frac{A^{(m+1)}(\omega^{-nM/2}E_k^{(m)})}{A^{(m+1)}(\omega^{nM/2}E_k^{(m)})} = -\omega^{-2\beta_m+\beta_{m-1}+\beta_{m+1}}\,. \tag{4.79}$$

We can write these equations in a compact form using the Cartan matrix C_{mt} of the $SU(n)$ Dynkin diagram [2]:

$$\prod_{t=1}^{n-1}\omega^{C_{mt}\beta_t}\,\frac{A^{(t)}(\omega^{\frac{nM}{2}C_{mt}}E_k^{(m)})}{A^{(t)}(\omega^{-\frac{nM}{2}C_{mt}}E_k^{(m)})} = -1\,, \qquad k = 1, 2, \ldots, \infty\,. \tag{4.80}$$

[2]The Cartan matrix is related to the incidence matrix of a Dynkin digram via $C_{mt} = 2\delta_{mt} - l_{mt}$.

We can also write these equations solely in terms of the $\{E_j^{(m)}\}$ using the Hadamard factorization theorem, provided we first establish the order of the functions $A^{(m)}(E)$. We can adapt the WKB treatment of the $SU(2)$ case [99] to show the function $A^{(1)}(E,\mathbf{g}) = D_{[0]}^{(1)}(E,\mathbf{g})$ has the large $|E|$ asymptotic

$$\ln A^{(1)}(E,\mathbf{g}) \sim \kappa(nM,n)(-E)^{\mu}, \qquad |E| \to \infty\,,\ |\arg(-E)| < \pi\,, \tag{4.81}$$

where

$$\mu = \frac{(M+1)}{nM}\,, \quad \kappa(a,b) = \frac{\Gamma\left(1+\frac{1}{a}\right)\Gamma\left(1+\frac{1}{b}\right)\sin(\frac{\pi}{b})}{\Gamma\left(1+\frac{1}{a}+\frac{1}{b}\right)\sin(\frac{\pi}{b}+\frac{\pi}{a})}\,. \tag{4.82}$$

Thus $A^{(1)}(E,\mathbf{g})$ has order μ and we claim the functions $A^{(m)}(E,\mathbf{g})$ for general m are also of this order. This follows from plugging the asymptotic (4.81) into the explicit expansion of the $D_{[i]}^{(m)}$ in terms of the $D_{[i]}^{(1)}$, where we have assumed the $D_{[i]}^{(1)}$ also have the asymptotic (4.81). This piece of information is sufficient for the moment, but for the NLIE we need a more precise result on the actual large E asymptotics of all the functions. A direct calculation proved difficult as many of the leading terms inside the Wronskians cancelled, but indirect evidence suggested the following:

$$\ln A^{(m)}(E,\mathbf{g}) \sim \frac{\sin(\pi m/n)}{\sin(\pi/n)}\kappa(nM,n)(-E)^{\mu}\ ,\quad |\arg(-E)| < \pi\,. \tag{4.83}$$

We back up this claim in Section 4.3.3 when we carry out numerical checks for the "soluble" case $M = 1/n$. In addition, (4.83) has a $\mathbb{Z}_2$ symmetry which matches that of the spectral determinants to be discussed in Section 4.3.1.

For $M > 1/(n-1)$ the order μ of the functions $A^{(m)}(E,\mathbf{g})$ is less than one, and so the Hadamard factorization theorem implies we may write

$$A^{(m)}(E,\mathbf{g}) = A^{(m)}(0,\mathbf{g})\prod_{j=1}^{\infty}\Big(1-\frac{E}{E_j^{(m)}}\Big)\quad,\quad m=1,\ldots,n-1\,, \tag{4.84}$$

where the actual values of the normalisation constants $A^{(m)}(0,\mathbf{g})$ are irrelevant for the following. Substituting (4.84) into (4.80) yields

$$\prod_{t=1}^{n-1}\omega^{C_{mt}\beta_t}\prod_{j=1}^{\infty}\left(\frac{E_j^{(t)}-\omega^{\frac{nM}{2}C_{mt}}E_k^{(m)}}{E_j^{(t)}-\omega^{-\frac{nM}{2}C_{mt}}E_k^{(m)}}\right) = -1\,,\qquad k=1,2,\ldots\,. \tag{4.85}$$

This is an $SU(n)$ type Bethe ansatz system for the infinite set of zeros $\{E_k^{(m)}\}$.

4.3 The nonlinear integral equation

The next task is to find a nonlinear integral equation for the spectral functions $A^{(m)}(E)$. We will then be able to use the solution of the NLIE to calculate the zero positions $\{E_k^{(m)}\}$.

We begin by defining the function

$$a^{(m)}(E,\mathbf{g}) = \prod_{t=1}^{n-1} \omega^{-C_{mt}\beta_t} \frac{A^{(t)}(\omega^{-\frac{nM}{2}C_{mt}}E,\mathbf{g})}{A^{(t)}(\omega^{\frac{nM}{2}C_{mt}}E,\mathbf{g})} \tag{4.86}$$

so that setting $E = E_k^{(m)}$ in (4.80) implies

$$a^{(m)}(E_k^{(m)},\mathbf{g}) = -1 \quad , \quad m = 1,\ldots,n-1 \ . \tag{4.87}$$

Each of these functions can be associated to the m^{th} node of the $SU(n) \equiv A_{n-1}$ Dynkin diagram.

We will follow the ideas of [34, 38, 78] (another approach can be found in [35]) and turn this infinite set of equations (4.87) for the unknown zeros $\{E_k^{(m)}\}$ into a finite set of coupled nonlinear integral equations. First we write $\ln a^{(m)}$ as an infinite sum over the zeroes $E_k^{(m)}$ of $A^{(m)}$ using the product representation (4.84):

$$\ln a^{(m)}(E,\mathbf{g}) = \sum_{t=1}^{n-1} \ln \omega^{-C_{mt}\beta_t} + \sum_{t=1}^{n-1}\sum_{j=1}^{\infty} \ln \frac{E_j^{(t)} - \omega^{-\frac{nM}{2}C_{mt}}E}{E_j^{(t)} - \omega^{\frac{nM}{2}C_{mt}}E} \ . \tag{4.88}$$

Following the method introduced in Section 1.5.2 we define the functions

$$F_{mt}(E) = \ln \frac{1-\omega^{-\frac{nM}{2}C_{mt}}E}{1-\omega^{\frac{nM}{2}C_{mt}}E} \ . \tag{4.89}$$

We now make two important assumptions about the locations of the points $E_k^{(m)}$: we assume they all lie on the positive real axis of the complex E-plane, and that these are the only points in some narrow strip about this axis at which $a^{(m)}(E,\mathbf{g})$ is equal to -1. We expect that these will hold for some range of the parameters $\mathbf{g}$ including the choice $\mathbf{g} = \{0,1,\ldots,n-1\}$. For this choice of $\mathbf{g}$, the solution of the resulting ODE can be found directly using Fourier transforms; more details can be found in Section 4.3.3. Plots of the solutions in the complex plane confirm the above assumptions about the locations of the zeros of $1 + a^{(m)}(E,\mathbf{g})$ for this particular choice of $\mathbf{g}$.

Now we use Cauchy's Theorem to replace the sum over the zeros in (4.88) by an integral along a contour $\mathcal{C}$ which goes from $+\infty$ to 0 above the real axis, encircles the origin and returns to ∞ below the real axis:

$$\ln a^{(m)}(E,\mathbf{g}) = \frac{-2\pi i}{n(M+1)} \sum_{t=1}^{n-1} C_{mt}\,\beta_t + \sum_{t=1}^{n-1} \int_{\mathcal{C}} \frac{dE'}{2\pi i} F_{mt}(E/E')\partial_{E'} \ln(1 + a^{(t)}(E',\mathbf{g})) \ . \tag{4.90}$$

(This is where we needed the assumptions about the zero positions.) After a variable change $E = \exp(\theta/\mu)$, we define (with a mild abuse of notation) $\ln a^{(m)}(\theta) \equiv \ln a^{(m)}(e^{\theta/\mu},\mathbf{g})$, integrate by parts and use the property $[a^{(m)}(\theta)]^* = a^{(m)}(\theta^*)^{-1}$ to

find

$$\ln a^{(m)}(\theta) - \sum_{t=1}^{n-1} \int_{-\infty}^{\infty} d\theta' R_{mt}(\theta-\theta') \ln a^{(t)}(\theta') \;=\; \frac{-2\pi i}{n(M+1)} \sum_{t=1}^{n-1} C_{mt}\,\beta_t$$
$$- 2i \sum_{t=1}^{n-1} \int_{-\infty}^{\infty} d\theta' R_{mt}(\theta-\theta') \Im m \ln(1+a^{(t)}(\theta'-i0)) \;. \quad (4.91)$$

Here

$$R_{mt}(\theta) \;=\; \frac{i}{2\pi}\partial_\theta F_{mt}(e^{\theta/\mu}) \;=\; \frac{i}{2\pi}\partial_\theta \ln \frac{\sinh\left(\frac{n\theta}{2(\xi+1)} - \frac{i\pi C_{mt}}{2(\xi+1)}\right)}{\sinh\left(\frac{n\theta}{2(\xi+1)} + \frac{i\pi C_{mt}}{2(\xi+1)}\right)} \quad (4.92)$$

where $\xi = 1/M$. We solve the equations (4.91) for $\ln a^{(m)}(\theta)$ using Fourier transforms. The transformed equations can be written in a compact form as

$$\sum_{t=1}^{n-1} (\delta_{mt} - \tilde{R}_{mt}(k)) \mathcal{F}[\ln\, a^{(t)}](k) \;=\; -\frac{4i\pi^2\delta(k)}{n(M+1)} \sum_{t=1}^{n-1} C_{mt}\,\beta_t$$
$$- 2i \sum_{t=1}^{n-1} \tilde{R}_{mt}(k) \Im m \mathcal{F}[\ln(1+a^{(t)})](k) \quad (4.93)$$

where the non-vanishing entries of $\tilde{R}_{mt}(k)$ (see Appendix A) are

$$\tilde{R}_{<mt>}(k) = \frac{\sinh(\frac{\pi}{n}\xi k)}{\sinh(\frac{\pi}{n}(1+\xi)k)} \;,\quad \tilde{R}_{mm}(k) = \frac{\sinh(\frac{\pi}{n}(1-\xi)k)}{\sinh(\frac{\pi}{n}(1+\xi)k)} \;, \quad (4.94)$$

and the notation $< mt >$ implies that the nodes m and t are connected on the Dynkin diagram of $SU(n)$. We now apply the inverse matrix $(\mathbb{1} - \tilde{R}(k))^{-1}$ to (4.93) to find

$$\mathcal{F}[\ln\, a^{(m)}](k) \;=\; -\frac{4i\pi^2\delta(k)}{n(M+1)} \sum_{r,t=1}^{n-1} (\mathbb{1} - R(k))^{-1}_{mr}\, C_{rt}\,\beta_t$$
$$+2i \sum_{r,t=1}^{n-1} (\mathbb{1} - R(k))^{-1}_{mr}\, R_{rt}(k) \Im m \mathcal{F}[\ln(1+a^{(t)})](k) \;. \quad (4.95)$$

We transform back and rewrite the imaginary parts in terms of values above and below the real axis to obtain a set of coupled NLIEs for the functions $a^{(m)}(\theta)$, $m = 1, \ldots, n-1$. The contours $\mathcal{C}_1$ and $\mathcal{C}_2$ run from $-\infty$ to $+\infty$, just below and just above the real θ-axis (these contours are shown in Figure 1.5):

$$\ln a^{(m)}(\theta) = \quad i\pi\alpha_m(\mathbf{g}) - ib_0 M_m\, e^{\theta}$$
$$+ \sum_{t=1}^{n-1} \left(\int_{\mathcal{C}_1} d\theta' \varphi_{mt}(\theta-\theta') \ln(1+a^{(t)}(\theta')) - \int_{\mathcal{C}_2} d\theta' \varphi_{mt}(\theta-\theta') \ln(1+\frac{1}{a^{(t)}(\theta')}) \right) . \quad (4.96)$$

The driving terms $ib_0 M_n e^{\theta}$ arise from zero modes, which can be traced to the poles of $(\mathbb{1} - \tilde{R}(k))^{-1}$ at $k = i$. For large θ, the convolution term of (4.96) becomes doubly

exponentially suppressed and can be neglected; in this limit the twist term $i\pi\alpha_m(\mathbf{g})$ can also be dropped. Thus the asymptotic behaviour is dominated by

$$\ln a^{(m)}(\theta) \sim -ib_0 M_m\, e^{\theta} \ . \tag{4.97}$$

This combined with the large E asymptotic (4.83) fixes the constants to be:

$$b_0 = 2\sin(\pi\mu)\kappa(nM,n) \ , \qquad M_m = \frac{\sin(\pi m/n)}{\sin(\pi/n)} \ . \tag{4.98}$$

Now we need to find the expressions for the kernel and twist factors

$$\varphi_{mt}(\theta) \ = \ \mathcal{F}^{-1}\left[\left(\mathbb{1} - (\mathbb{1} - \tilde{R}(k))^{-1}\right)_{mt}\right](\theta) \ , \tag{4.99}$$

$$\alpha_m(\mathbf{g}) \ = \ -\frac{2\pi}{n(M+1)} \sum_{r,t=1}^{n-1} \Big(\mathbb{1} - \tilde{R}(0)\Big)^{-1}_{mr} C_{rt}\,\beta_t \ . \tag{4.100}$$

These can be written more explicitly with the help of the 'deformed' Cartan matrix, which reduces to the normal Cartan matrix as $k \to 0$:

$$C_{mt}(k) = \begin{cases} 2 & m = t, \\ \frac{-1}{\cosh(\frac{\pi k}{n})} & < mt > \end{cases} \ , \tag{4.101}$$

and its inverse

$$C^{-1}_{tm}(k) = C^{-1}_{mt}(k) = \frac{\coth(\frac{\pi}{n}k)\sinh(\frac{\pi}{n}(n-m)k)\sinh(\frac{\pi}{n}t\,k)}{\sinh(\pi k)} \qquad (m \geq t) \ . \tag{4.102}$$

By (4.94), the non-vanishing off-diagonal and diagonal elements of $\tilde{R}(k)$ are related by $2\tilde{R}_{<mt>}(k) = (1-\tilde{R}_{mm}(k))/\cosh(\frac{\pi k}{n})$, and so

$$\delta_{mt} - \tilde{R}_{mt}(k) = \frac{1}{2} C_{mt}(k)(1 - \tilde{R}_{mm}(k)) \ , \tag{4.103}$$

where

$$1 - \tilde{R}_{mm}(k) = \frac{2\sinh(\frac{\pi}{n}\xi k)\cosh(\frac{\pi}{n}k)}{\sinh(\frac{\pi}{n}(1+\xi)k)} \ . \tag{4.104}$$

Plugging relations (4.103) and (4.104) into (4.100) and (4.99) we obtain

$$\begin{aligned} \varphi_{mt}(\theta) \ &= \ \int_{-\infty}^{\infty} \frac{dk}{2\pi}\, e^{ik\theta}\Big(\delta_{mt} - \frac{\sinh(\frac{\pi}{n}(1+\xi)k)}{\sinh(\frac{\pi}{n}\xi k)\cosh(\frac{\pi}{n}k)} C^{-1}_{mt}(k)\Big) \ , \\ \alpha_m(\mathbf{g}) \ &= \ -\frac{2}{n}\,\beta_m \, . \end{aligned} \tag{4.105}$$

The final NLIEs exactly match the massless versions of the equations found in [108, 109]. Their notivation differs from ours and is closer to that of Destri and de Vega's work on the sine-Gordon model [34,110]. Solvable lattice models with affine Lie algebra symmetry $\hat{A}_n$ are considered, and NLIEs derived from the associated nested Bethe ansatz equations. Taking the scaling limit in an analogous way to

that described for the sine-Gordon model in Chapter 1 gives the continuum NLIEs (4.96).

The eigenvalues of $y(0, E, \mathbf{g})$ satisfy (4.87) and so they can be found by searching along the real axis for the zeros of $1 + a^{(1)}(\theta)$. We can estimate the positions of the zeros predicted from the NLIE using the large θ asymptotic (4.97). At a zero θ_p, (4.87) implies

$$\ln a^{(1)}(\theta_p) = i\pi(2p-1) \quad , \quad p \in \mathbb{N} \, . \tag{4.106}$$

Replacing the LHS with (4.97) we have

$$-ib_0 M_1 e^{\theta_p} + i\pi\alpha_1(\mathbf{g}) = i\pi(2p-1) \tag{4.107}$$

and the approximate eigenvalues are then given by

$$E_p = e^{\theta_p/\mu} = \left[\frac{\pi}{2\sin(\pi\mu)\kappa(nM,n)}\Big(2p-1+\alpha_1(\mathbf{g})\Big)\right]^{\frac{nM}{M+1}} \quad , \quad p = 1, 2, \ldots \, . \tag{4.108}$$

4.3.1 Symmetry properties

The $SU(n)$ Dynkin diagram has an evident $\mathbb{Z}_2$ symmetry which swaps nodes m and $n-m$. This symmetry is also respected by the BAE so long as the twists α_m and α_{n-m} are transformed at the same time. We expect the symmetry to also be apparent in the differential equation, but how is not immediately obvious. The first node of the Dynkin diagram is associated with the basic solution $y(x, E, \mathbf{g})$ while its partner, the $(n-1)^{\text{th}}$ node, is associated with an $(n-1)$-fold Wronskian $W_0^{(n-1)}(x, E, \mathbf{g})$. We expect these should be related in some way. A clue to this puzzle is provided by the $n = 3$ case [78], where the Wronskian $W_0^{(2)}(x, E, \mathbf{g})$ is shown to be a solution of the adjoint equation. [3] This general property of third-order differential equations was originally observed in [111] and it easily generalises to higher order ODEs. We show below how the Wronskian of $n-1$ solutions of an n^{th} order ODE automatically provides a solution to the adjoint equation.

For general n, the factorised form (4.44) of $D(\mathbf{g})$ for the differential operator proves hard to work with and we suppose instead that (4.47) has been rewritten as

$$\frac{d^n}{dx^n}\psi + B_2(x)\frac{d^{n-2}}{dx^{n-2}}\psi + B_3(x)\frac{d^{n-3}}{dx^{n-3}}\psi + \ldots + (-1)^{n+1}P(x,E)\,\psi \;=\; 0\,. \tag{4.109}$$

The relation between the previous description of the ODE (4.47) and the coefficients $B_i(x)$ is unimportant in the following.

Now consider $n-1$ solutions to this equation, gathered together into a vector as $\mathbf{f} = (f_1, f_2, \ldots f_{n-1})$. We create an $(n-1) \times (n-1)$ square matrix whose i^{th}

[3] Suppose $\sum_{k=0}^{n} p_k(x) y^{[n-k]}(x) = 0$ is a linear homogeneous ordinary differential equation of n^{th} order with real coefficients. Then its adjoint is given by $\sum_{k=0}^{n} (-1)^{n-k} (p_k(x) y(x))^{[n-k]} = 0$.

row, denoted $\mathbf{f}^{[a_i]}$, is given by differentiating the components of $\mathbf{f}$, a_i times. The determinant of this matrix will be denoted $V[a_1, a_2, \ldots a_{n-1}]$. Using this notation the Wronskian of $f_1, f_2 \ldots f_{n-1}$ is

$$W^{(n-1)}[f_1, f_2, \ldots f_{n-1}](x, E, \mathbf{g}) = V[0, 1, \ldots, n-2]\,. \tag{4.110}$$

The differential of a determinant is simply equal to a sum of determinants in which each row has been differentiated. In our notation this is

$$\frac{d}{dx} V[a_1, a_2, \ldots a_{n-1}] = \sum_{k=1}^{n-1} V[a_1, \ldots a_{k-1}, a_k{+}1, a_{k+1}, \ldots a_{n-1}]\,. \tag{4.111}$$

Differentiating (4.110) once, all but one term vanishes by antisymmetry and we find

$$\frac{d}{dx} W^{(n-1)} = V[0, 1, \ldots n{-}4, n{-}3, n{-}1]\,. \tag{4.112}$$

Differentiating again we have two nonzero terms

$$\frac{d^2}{dx^2} W^{(n-1)} = V[0, 1, \ldots n{-}4, n{-}2, n{-}1] + V[0, 1, \ldots n{-}4, n{-}3, n]\,. \tag{4.113}$$

The last term can be rewritten using (4.109) to substitute for $\mathbf{f}^{[n]}$:

$$V[0, 1, \ldots n{-}4, n{-}3, n] = -B_2(x) V[0, 1, \ldots n{-}4, n{-}3, n{-}2] = -B_2(x) W^{(n-1)}. \tag{4.114}$$

(Again, all other terms vanish by antisymmetry.) Thus

$$\Big(\frac{d^2}{dx^2} + B_2(x)\Big) W^{(n-1)} = V[0, 1, \ldots n{-}4, n{-}2, n{-}1]\,. \tag{4.115}$$

We now repeat this procedure. Differentiate both sides of (4.115) gives

$$\Big(\frac{d^3}{dx^3} + \frac{d}{dx} B_2(x)\Big) W^{(n-1)} = V[0, 1, \ldots n{-}5, n{-}3, n{-}2, n{-}1] + V[0, 1, \ldots n{-}4, n{-}2, n]\,. \tag{4.116}$$

Again we replace $\mathbf{f}^{[n]}$ using (4.109) to rewrite the last term as

$$V[0, 1, \ldots n{-}4, n{-}2, n] = -B_3(x) V[0, 1, \ldots n{-}4, n{-}2, n{-}3] = B_3(x) W^{(n-1)}\,. \tag{4.117}$$

Substituting this into (4.116) we now have

$$\Big(\frac{d^3}{dx^3} + \frac{d}{dx} B_2(x) - B_3(x)\Big) W^{(n-1)} = V[0, 1, \ldots n{-}5, n{-}3, n{-}2, n{-}1]\,. \tag{4.118}$$

Differentiating both sides of (4.118) will again result in two terms on the RHS. The second of these can be rewritten using (4.109), but this time yields $-B_4(x) W^{(n-1)}$ instead of $+B_3(x) W^{(n-1)}$ as the one non-vanishing contribution. Taking this over onto the LHS and continuing to differentiate, one finally finds that $W^{(n-1)}$ satisfies

$$\Big(\frac{d^n}{dx^n} + \frac{d^{n-2}}{dx^{n-2}} B_2(x) - \frac{d^{n-3}}{dx^{n-3}} B_3(x) + \ldots - P(x, E)\Big) W^{(n-1)} = 0\,, \tag{4.119}$$

which is indeed (up to an overall sign) the equation adjoint to (4.109). Now we can return to the factorised form of $D(\mathbf{g})$, take its adjoint using (4.42), and rewrite (4.119) as:

$$\Big((-1)^{n+1}D(\mathbf{g}^\dagger) + (-1)^n P(x,E)\Big)W^{(n-1)}(x,E,\mathbf{g}) = 0\ , \quad P(x,E) = x^{nM} - E\ , \tag{4.120}$$

with

$$\mathbf{g}^\dagger = \{g_0^\dagger, g_1^\dagger, \dots\ g_{n-1}^\dagger\}\ , \qquad g_j^\dagger = n-1-g_{n-1-j}\ . \tag{4.121}$$

For n even this is the original ODE (4.47), modulo the swap to the 'conjugate' set of parameters $\mathbf{g}^\dagger$. For n odd, the term $P(x,E)$ has been replaced by $-P(x,E)$. However, the conventions adopted in the definition (4.51) mean that the 'half-shifted' functions $y_{k+1/2}(x,E,\mathbf{g})$ ($k \in \mathbb{Z}$) themselves solve (4.47) with P replaced by $-P$. Taking an $(n-1)$-fold Wronskian of these functions and repeating the above discussion, the minus signs cancel. In particular, this means that whether n is even or odd we have

$$\Big((-1)^{n+1}D(\mathbf{g}^\dagger) + P(x,E)\Big)W^{(n-1)}_{1-n/2}(x,E,\mathbf{g}) = 0\ . \tag{4.122}$$

This is exactly the equation solved by the $y_k(x,E,\mathbf{g}^\dagger)$ and since these functions both satisfy the same equation, they must be proportional. We can fix the proportionality constant by comparing the asymptotics of $y_k(x,E,\mathbf{g}^\dagger)$ and $W^{(n-1)}_{1-n/2}(x,E,\mathbf{g})$ as $|x| \to \infty$ in $\mathcal{S}_0$. This establishes the formula

$$W^{(n-1)}_{1-n/2}(x,E,\mathbf{g}) = y(x,E,\mathbf{g}^\dagger)\,, \tag{4.123}$$

and shows that the $(n-1)$-fold Wronskian is (up to a shift in its arguments) just a basic solution to another ODE, and thus demonstrates that the relation between the first and last nodes is indeed reflected in the properties of the differential equation. The spectral functions corresponding to the remaining nodes on the Dynkin diagram can now be obtained either as m-fold Wronskians of the $W^{(n-1)}_{k+1/2}$, or as $(n-m)$-fold Wronskians of the y_k, and the diagram symmetry should be reflected in the equality of the results of the two calculations. Keeping the normalisation of the y's as in (4.53), the necessary identity is the following:

$$W^{(n-m)}_{m-1} = W^{(m)}[W^{(n-1)}_0, W^{(n-1)}_1, \dots, W^{(n-1)}_{m-1}]\,. \tag{4.124}$$

While we do not have a general proof, for $m = 2$ this result follows from the Jacobi identity (cf. for example equation (2.20) of [107]) and the fact that $W^{(n)} = 1$. This case is also equivalent to a formula due to Frobenius [112], see also [113].

We know the explicit forms of the differential equations associated with the first and last nodes of the $SU(n)$ Dynkin diagram, but we can also enquire what are the

ODEs for the remaining nodes. We can make a small amount of progress towards answering this question using the following fourth-order ODE as an example:

$$\Big(-\frac{d^4}{dx^4} + P(x,E)\Big)\psi = 0 \quad , \quad P(x,E) = x^{4M} - E\,. \tag{4.125}$$

The middle node of the $SU(4)$ Dynkin diagram is associated with the Wronskian of two solutions of (4.125). We denote the solutions f_1 and f_2 and use the notation introduced above to write the Wronskian as

$$W^{(2)}[f_1, f_2](x,E) = V[0,1]\,. \tag{4.126}$$

Differentiating both sides once we have

$$\frac{d}{dx}W^{(2)} = V[0,2] \tag{4.127}$$

where the other term has vanished by antisymmetry. Differentiating again the nonzero terms are

$$\frac{d^2}{dx^2}W^{(2)} = V[1,2] + V[0,3]\,. \tag{4.128}$$

Again we differentiate to find

$$\frac{d^3}{dx^3}W^{(2)} = V[1,3] + (V[1,3] + V[0,4]) = 2V[1,3] \tag{4.129}$$

where we used (4.125) to substitute for $\mathbf{f}^{[4]}$:

$$V[0,4] = P(x,E)\,V[0,0] = 0\,. \tag{4.130}$$

Differentiating we have

$$\frac{d^4}{dx^4}W^{(2)} = 2V[2,3] - 2P(x,E)\,W^{(2)}\,, \tag{4.131}$$

and we have again used (4.125) to write

$$V[1,4] = P(x,E)V[1,0] = -P(x,E)\,W^{(2)}\,. \tag{4.132}$$

Finally we differentiate for a fifth time to find

$$\frac{d^5}{dx^5}W^{(2)} = 2V[2,4] - 2\frac{d}{dx}P(x,E)\,W^{(2)} - 2P(x,E)\,\frac{d}{dx}W^{(2)}\,. \tag{4.133}$$

We use (4.125) to substitute for $\mathbf{f}^{[4]}$ in $V[2,4]$ yielding $-P(x,E)V[0,2]$. We now rewrite this using (4.127) and substitute into (4.133). Rearranging we have found a fifth-order differential equation for $W^{(2)}$:

$$\Big(\frac{d^5}{dx^5} + 4P(x,E)\frac{d}{dx} + 2\frac{d}{dx}P(x,E)\Big)W^{(2)}(x,E) = 0\,. \tag{4.134}$$

Explicitly this is

$$\frac{d^5}{dx^5}W^{(2)}(x,E) + 4(x^{4M} - E)\frac{d}{dx}W^{(2)}(x,E) + 8Mx^{4M-1}W^{(2)}(x,E) = 0\,. \tag{4.135}$$

A search along the real axis for the zeros of the function $1 + a^{(2)}(\theta)$ should yield the eigenvalues of this differential equation. In Section 4.3.3 we will check this conjecture using a simple linear potential.

It should be possible to use a similar method to find the differential equations satisfied by the spectral functions associated to the central nodes of the $SU(n)$ $n > 5$ Dynkin diagrams.

4.3.2 Analytic continuation

The x-independent functional relation generalising the $T-Q$ relation (4.76) came from the dominant term of the expansion of $W_0^{(m)}(x, E, \mathbf{g})$ (4.72). However, which term is dominant depends on the ordering (4.70) of the g_i's. Moreover, the NLIE will be sensitive to any changes since it depends on the BA twist $\alpha(\mathbf{g})$ rather than the parameters $\mathbf{g}$. On the other side, the commutativity property (4.43) of the operator $D(g)$ ensures that shuffling the g_i leaves the ODE unchanged. Using this invariance, we find that analytic continuation between different twists corresponding to the same ODE allows access to the other terms $D^{(1)}_{[i]}(E, \mathbf{g})$ $(i \neq 1)$ of the expansion (4.72).

We start by finding the explicit expression for the coefficients $D^{(1)}_{[i]}$. We take the Wronskian of the expansion (4.68) with all of the χ_k functions $(k = 0, 1, \ldots, n-1)$ apart from χ_i. Everything on the RHS apart from the term with coefficient $D^{(1)}_{[i]}$ will be zero by antisymmetry and rearranging we have

$$D^{(1)}_{[i]}(E, \mathbf{g}) = (-1)^i \frac{W^{(n)}[W_0^{(1)}(x, E, \mathbf{g}), \chi_0, \ldots \chi_{i-1}, \chi_{i+1}, \ldots \chi_{n-1}]}{W^{(n)}[\chi_0, \ldots \chi_{n-1}]} \,. \tag{4.136}$$

The explicit form of the denominator can be found by evaluating the Wronskian as $x \to 0$ using (4.69). (Recall that the Wronskian of n independent solutions of an n^{th} order ODE is x independent.) We find

$$W^{(n)}[\chi_0, \ldots \chi_{n-1}] = \prod_{j=0, i=j+1}^{n-1} (g_j - g_i) \,. \tag{4.137}$$

Now if the parameters are analytically continued from

$$\mathbf{g} = \{g_0, \ldots g_i, \ldots g_j, \ldots g_{n-1}\} \tag{4.138}$$

to

$$\mathbf{g}' = \{g_0, \ldots g_j, \ldots g_i, \ldots g_{n-1}\} \tag{4.139}$$

the effect upon the set of χs is to swap χ_i with χ_j. This implies

$$D^{(1)}_{[i]}(E, \mathbf{g}') = D^{(1)}_{[j]}(E, \mathbf{g}) \,, \qquad D^{(1)}_{[j]}(E, \mathbf{g}') = D^{(1)}_{[i]}(E, \mathbf{g}) \,, \tag{4.140}$$

and the other $D^{(1)}_{[k]}(E, \mathbf{g})$ remain unchanged. This continues to be true if we also permute the remaining g_k (k not equal to i or j), and we will use this idea in

Section 4.3.3. So long as the property (4.45) is preserved at all points of the continuation, the NLIE will hold throughout. At the end of the continuation the ODE will have returned to its original form, but the NLIE will have undergone a nontrivial monodromy, since the twists will have changed. The NLIE describing $D^{(1)}_{[1]}(E,\mathbf{g})$ is defined with α in terms of $\mathbf{g} = \{g_0, g_1, \ldots, g_{n-1}\}$. So an NLIE describing $D^{(1)}_{[i]}(E,\mathbf{g})$ can be found by continuing the twist parameter α to α' via the transformation $g_0 \to g_i$, with the remaining g_k being allowed to permute amongst themselves. In fact, a number of different NLIEs can be obtained, depending on the permutation chosen.

4.3.3 Linear potential

This idea of analytic continuation can be illustrated using a set of special choices for the vector $\mathbf{g}$ for which the resulting differential operator $D(\hat{\mathbf{g}})$ is equal to $\frac{d^n}{dx^n}$. This happens if we let $\hat{\mathbf{g}}$ be a vector with distinct components g_j taking values in the set $\{0, 1, \ldots (n-1)\}$; there are $n!$ different $\hat{\mathbf{g}}$. We use the notation $\hat{\mathbf{g}}_i$ to indicate g_0 has been fixed to be equal to i, leaving the remaining components free. In this particularly simple case, the functions (4.136) become

$$D^{(1)}_{[i]}(E,\hat{\mathbf{g}}_i) = \frac{1}{i!}\frac{d^i}{dx^i} y(0,E,\hat{\mathbf{g}}_i) \; . \tag{4.141}$$

The direct treatment of previous sections only allowed us to discuss $D^{(1)}_{[0]} = y(0,E,\hat{\mathbf{g}})$, but, according to the continuation idea just described, the NLIEs should also encode information about the higher derivatives $y^{[i]}$. We can check this numerically by setting $M = 1/n$, which results in the linear potential $P(x,E) = x - E$. This simple ODE is

$$\left((-1)^{n+1}\frac{d^n}{dx^n} + x - E\right) y(x,E,\hat{\mathbf{g}}_i) = 0 \tag{4.142}$$

and, as in [78] for the $n = 3$ case, is solvable by a complex Fourier transform. The choice of M lies outside the range $M > 1/(n-1)$, but we find that the NLIE continues to hold, just as in previous examples [78, 96]. If we write $y(x,E,\hat{\mathbf{g}}_i) = \mathcal{A}(x-E)$, then the ODE becomes

$$(-1)^{n+1}\frac{d^n\mathcal{A}(x)}{dx^n} + x\mathcal{A}(x) = 0 \; . \tag{4.143}$$

Fourier transforming (4.143), the solution of the resulting first-order ODE can be transformed back to give the following normalised solution

$$\mathcal{A}(x) = \frac{1}{i^{(n-1)/2}\sqrt{2\pi}} \int_\Gamma dp \; e^{-ipx + \frac{(ip)^{n+1}}{n+1}} \; . \tag{4.144}$$

To ensure the integral is convergent the contour must follow a path in the lower half complex plane that starts at $|x| = \infty$ along the ray $\arg(x) = -\frac{\pi}{2} - \frac{\pi}{n+1}$ and ends along $\arg(x) = -\frac{\pi}{2} + \frac{\pi}{n+1}$. The contour Γ is illustrated in Figure 4.2.

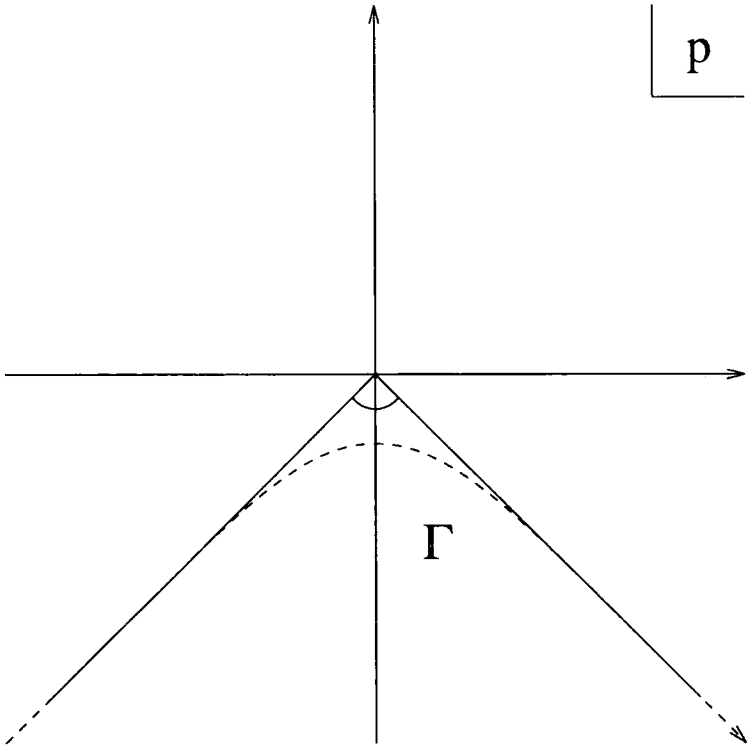

Figure 4.2: The integration contour for the solution (4.144) of the linear potential case.

We used the program Mathematica to search for the first nine zeros of (4.144) with $n = 3, 4$ and 5, and found that all of the zeros lie on the negative real axis. Taking derivatives of (4.144), we find this is also true for the zeros of the functions $\mathcal{A}'(x), \mathcal{A}''(x), \ldots, \mathcal{A}^{[n-1]}(x)$ and so the zeros of $y^{[i]}(0, E, \hat{\mathbf{g}}_\mathbf{i})$ are real and positive. This backs up the assumption, made in Section 4.3, that all of the eigenvalues lie on the positive real axis of the complex E-plane.

We numerically iterated the NLIE (4.96) until the solution converged and then searched for the zeros of $1 + a^{(1)}(\theta, \hat{\mathbf{g}}_\mathbf{0})$ along the real axis. The agreement with the zeros of $y(0, E, \hat{\mathbf{g}}_\mathbf{0})$ is very good and shown in Tables C.1 and C.5 for the fourth and fifth-order ODEs. In addition, using the idea of analytic continuation from $\mathbf{g}_0$ to $\mathbf{g}_1$, $\mathbf{g}_2 \ldots$ we were able to find the zeros of $y'(0, E, \hat{\mathbf{g}}), \ldots, y^{[n-1]}(0, E, \hat{\mathbf{g}})$. The results shown in Appendix C compare the positions of the zeros found using the NLIE with the 'exact' values found by solving (4.144) for the fourth and fifth-order ODEs; the agreement is to about 15dp.

A further comparison can be made by estimating the positions of the zeros of $\mathcal{A}(x)$ and its derivatives via a saddle-point treatment of (4.144). We consider the stationary points of the exponent of the integral in (4.144) for large negative x. These are given by

$$p_k = -i\, e^{\frac{i\pi}{n}(1+2k)}\, |x|^{\frac{1}{n}} \quad , \quad k = 0, \ldots, n-1\,, \tag{4.145}$$

and the contribution from each point can be considered separately. We expand the

exponent of the integral about p_k, and drop the terms of third or greater order. The quadratic term contributes to a pure Gaussian integral and so we find that each p_k provides the following contribution to (4.144)

$$\frac{|x|^{\frac{1-n}{2n}}}{i^{(n-1)/2}\sqrt{n}}\, e^{\frac{n}{n+1}|x|^{\frac{n+1}{n}} e^{\frac{i\pi}{2n}(1+2k)}+i\sigma}\,, \tag{4.146}$$

where the phase σ is the direction of steepest descent from the stationary point. Along the integration contour Γ, the largest contribution to (4.144) is found near p_0 and p_{n-1}. The respective phases are $(n-1)\pi/2n$ and $(1-n)\pi/2n$. The sum of these contributions yields an approximate formula for $\mathcal{A}(-|x|)$:

$$\mathcal{A}(-|x|) \sim \frac{|x|^{\frac{1-n}{2n}}}{i^{(n-1)/2}\sqrt{n}} \left(e^{\frac{n}{n+1}|x|^{\frac{n+1}{n}} e^{\frac{i\pi}{n}} - \frac{i\pi(n-1)}{2n}} + e^{\frac{n}{n+1}|x|^{\frac{n+1}{n}} e^{-\frac{i\pi}{n}} + \frac{i\pi(n-1)}{2n}} \right) \tag{4.147}$$

which we may rewrite as

$$\mathcal{A}(-|x|) \sim \frac{2\,|x|^{\frac{1-n}{2n}}}{i^{(n-1)/2}\sqrt{n}}\, e^{\frac{n}{n+1}|x|^{\frac{n+1}{n}} \cos\frac{\pi}{n}} \cos\left(\frac{n}{n+1}|x|^{\frac{n+1}{n}} \sin\frac{\pi}{n} - \frac{\pi(n-1)}{2\,n} \right)\,. \tag{4.148}$$

Differentiating (4.148) m times the dominant behaviour for large negative x is

$$\begin{aligned} \mathcal{A}^{[m]}(-|x|) \;\sim\; & (-1)^m \frac{2\,|x|^{\frac{2\,m+1-n}{2\,n}}}{i^{(n-1)/2}\sqrt{n}}\, e^{\frac{n}{n+1}|x|^{\frac{n+1}{n}} \cos\frac{\pi}{n}} \times \\ & \cos\left(\frac{n}{n+1}|x|^{\frac{n+1}{n}} \sin\frac{\pi}{n} - \frac{\pi(n-1)}{2\,n} + \frac{\pi m}{n} \right)\,. \end{aligned} \tag{4.149}$$

The approximate positions of the zeros of the m^{th} derivative, found by setting $\mathcal{A}^{(m)}(x) = 0$, are given by

$$x = -\left[\frac{\pi(n+1)}{2\,n \sin\frac{\pi}{n}} \left(2p - \frac{2\,m+1}{n} \right) \right]^{\frac{n}{n+1}}\,, \quad n = 1, 2, \ldots\,, \tag{4.150}$$

which agrees with the approximation found directly from the NLIE (4.96). The tables in appendix C also contain a column showing the approximate zero positions predicted using (4.150).

During the numerical calculations we occasionally found the NLIE (4.96) fails to converge. Generally this happens whenever there is a breakdown in one or other of the two assumptions necessary for the derivation of the NLIE in its simplest form, made at the beginning of Section 4.3. We assumed that all of the zeros $E_k^{(m)}$ lie on the positive real axis and our calculations using (4.144) indicate this is certainly true for the $E_k^{(1)}$. The results found using the NLIE agree with this, and in the cases that converged we were able to confirm that all of the eigenvalues $E_k^{(m)}$ for $m > 1$ are also real and positive.

It must therefore be the second assumption which sometimes fails. This happens when points appear on the positive real axis of the complex E-plane, not in the set $\{E_k^{(m)}\}$, at which the functions $a^{(m)}$ take the value -1. We can say when such a

point may have appeared by considering the values taken by $\ln a^{(m)}(\theta)$ at $\pm\infty$. All of the functions $\ln a^{(m)}(\theta)$ with $\alpha(\mathbf{g}) = 0$ resemble a kink function interpolating from $\ln a^{(m)}(-\infty)$ to $\ln a^{(m)}(\infty) = -\infty$, with shape similar to that depicted in Figure 4.3. The left plateau $\ln a^{(m)}(-\infty)$ is a continuous function of $\alpha(\mathbf{g})$. As this parameter varies the plateau value may cross one of the dashed lines in the plot indicating the odd multiples of π. Thus there will be a point θ_i where for some integer r $\ln a^{(m)}(\theta_i) = i\pi(2r+1)$, and the second assumption fails to hold.

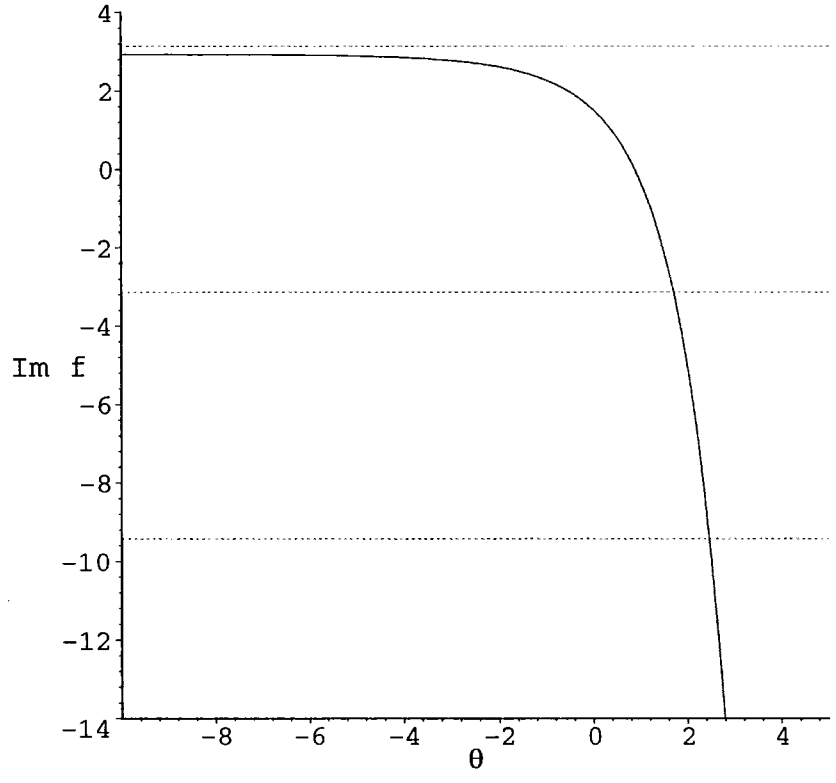

Figure 4.3: $\Im m f(\theta) = \Im m \ln a(\theta)$ for real θ. The dashed lines are at odd multiples of π.

The plateau values follow from plugging $\theta = -\infty$ into the NLIE (4.96) and integrating. The resulting 'stationary' equations are easily solved and we find

$$\ln a^{(m)}(-\infty) = \frac{i\pi\xi}{1+\xi}\sum_{t=1}^{n-1} C_{mt}\alpha_t(\mathbf{g}) \tag{4.151}$$

where C_{mt} is the ordinary Cartan matrix. Thus if

$$\left|\frac{\xi}{1+\xi}\sum_{t=1}^{n-1} C_{mt}\alpha_t(\mathbf{g})\right| \geq \pi \tag{4.152}$$

we should be aware that an extra zero may have appeared. For $n = 2$ these points turn out to be zeroes of $T(E)$, and the necessary modification of the NLIE was discussed in [76].

For the fourth-order differential equation the choice $\hat{\mathbf{g}}_\mathbf{i}$ gave a convergent NLIE for each $i = 1, 2, 3$. Turning now to $n = 5$, the choice $\hat{\mathbf{g}}_\mathbf{2} = \{2, 1, 0, 3, 4\}$ implies

$\ln a^{(3)}(-\infty) = i\pi$. The second assumption no longer holds, and as expected the NLIE fails to converge. However this is not the only possible choice for $\hat{\mathbf{g}}_2$, since we may permute all but the first parameter. We find the choice $\{2,0,1,3,4\}$ gives a convergent NLIE, and the zeros of y'' are easily found.

Using the permutation trick, we found the convergence problem can be avoided in most cases. One exception is n=3. The two choices for $\hat{\mathbf{g}}_1$ are $(1,0,2)$ and $(1,2,0)$, and for neither of these did the NLIE converge. This is to be expected since (4.151) predicts that $\ln a^{(2)}(-\infty)$ is equal to $i\pi$ and $-i\pi$ for these choice of $\hat{\mathbf{g}}_1$. Despite this fact, an extrapolation of the zero positions found at nearby values of $\mathbf{g}$ allowed a comparison with the results of the complex Fourier transform. We found that the zeroes of $y'(0,E,\hat{\mathbf{g}})$ were indeed reproduced. Note that in this case the zeroes of $y(0,E,\hat{\mathbf{g}})$ and $y''(0,E,\hat{\mathbf{g}})$ can be found from an NLIE which respects the $SU(3)$ diagram symmetry [78], but that to find the zeroes of $y'(0,E,\hat{\mathbf{g}})$, we are forced to use an integral equation which breaks this symmetry. Figure 4.4 shows the movement of the first five zeros of $1+a^{(1)}(\theta)$ as a function of g_0 during the analytic continuation $\hat{\mathbf{g}}_0$ to $\hat{\mathbf{g}}_1$. We have fixed $g_2 = 2$ and, since the sum $g_0+g_1+g_2$ must equal 3, set $g_1 = 1-g_0$ and varied g_0 between 0 and 1. As g_0 approaches 1 the iteration of the NLIE breaks down, and for these values we instead show, using broken lines, the extrapolation to the exact zeros. Figure 4.5 shows the movement of the first five zeros of $1+a^{(2)}(\theta)$ for the convergent continuation $\hat{\mathbf{g}}_0$ to $\hat{\mathbf{g}}_2$. This time we set $g_1 = 1, g_2 = 2-g_0$ and again varied g_0 between 0 and 1.

The ordinary differential equation related to the spectral function associated to the middle node of the $SU(4)$ Dynkin digram was found in Section 4.3.1. We test this conjecture by considering the linear potential $P(x,E) = x-E$ and set $W^{(2)}(x,E,\hat{\mathbf{g}}_0) = \mathcal{W}(x-E)$ so that the ODE (4.134) becomes

$$\frac{d^5}{dx^5}\mathcal{W}(x) + 2\mathcal{W}(x) + 4x\frac{d}{dx}\mathcal{W}(x) = 0\,. \tag{4.153}$$

The solution, found using Fourier transforms, is

$$\mathcal{W}(x) = C\int_\Gamma dp\,\frac{e^{-ipx+\frac{ip^5}{20}}}{\sqrt{p}}\,, \tag{4.154}$$

where C is the normalisation constant. Table C.10 in Appendix C compares the eigenvalues found by solving $1+a^{(2)}(\theta)=0$ with the exact results from a numerical treatment (using Mathematica) of (4.154).

4.3.4 Duality

For the case of the Schrödinger equation, $n=2$, a duality transformation can be defined which relates wavefunctions with a confining potential ($M>0$) to those with a singular potential ($-1<M<0$). The solutions and the spectrum of the

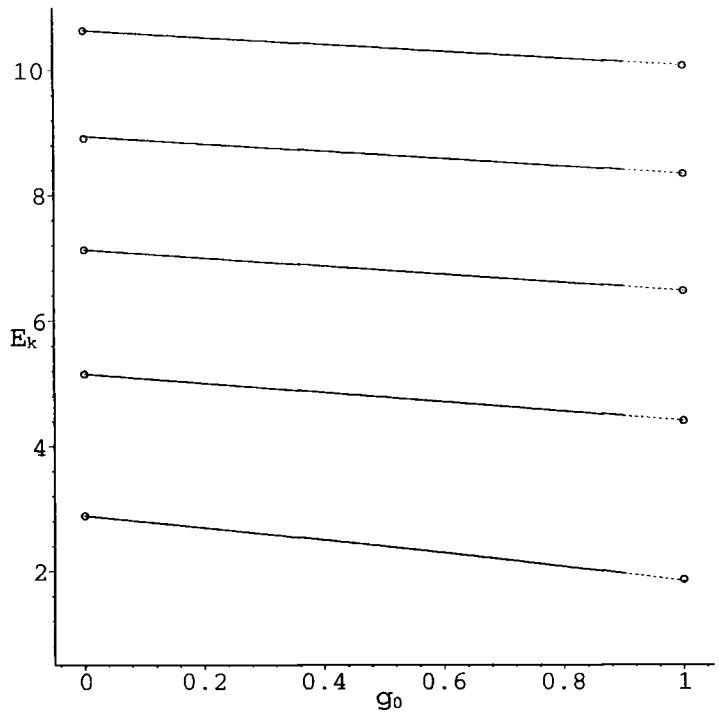

Figure 4.4: The movement of the first five zeros (solid lines) of $1 + a^{(1)}(\theta)$ during the continuation $\hat{\mathbf{g}}_0$ to $\hat{\mathbf{g}}_1$. The extrapolation (broken lines) is shown as well as the exact values (circles).

dual ODEs are simply related. The same phenomenon was observed in the third-order problem [78] and this duality also extends to the n^{th} order problem. We show this by carrying out a (generalised) Langer [114] transformation

$$z = \ln x\,, \quad y(x) = e^{(n-1)z/2} u(z)\,. \tag{4.155}$$

The use of the operators $D(g)$ and $D(\mathbf{g})$ makes this task very simple, since the relation

$$\left(\frac{d}{dx} - \frac{g}{x}\right) e^{\frac{p-1}{2}z(x)} f(z(x)) = e^{\frac{p-3}{2}z} \left(\frac{d}{dz} + \frac{p-1}{2} - g\right) f(z) \tag{4.156}$$

allows exponentials of z to be passed successively through the factors of $D(\mathbf{g})$, resulting in the transformed equation

$$\left[(-1)^{n+1}\left(\frac{d}{dz} - \gamma_{n-1}\right) \cdots \left(\frac{d}{dz} - \gamma_1\right)\left(\frac{d}{dz} - \gamma_0\right) + e^{n(1+M)z} - Ee^{nz}\right] u(z) = 0 \tag{4.157}$$

where $\gamma_i = g_i - (n-1)/2$. To find an ODE with a potential $\tilde{M} = -M/(M+1)$ lying between 0 and 1, we exchange the rôle of the exponentials in (4.157) via the transformation $z \to \frac{z}{M+1} + \ln \frac{M+1}{E^{1/n}}$. In this way we obtain

$$\left[(-1)^{n+1}\left(\frac{d}{dz} - \frac{\gamma_{n-1}}{M+1}\right) \cdots \left(\frac{d}{dz} - \frac{\gamma_1}{M+1}\right)\left(\frac{d}{dz} - \frac{\gamma_0}{M+1}\right) - \tilde{E}e^{nz} - e^{\frac{nz}{M+1}}\right] u(z) = 0\,, \tag{4.158}$$

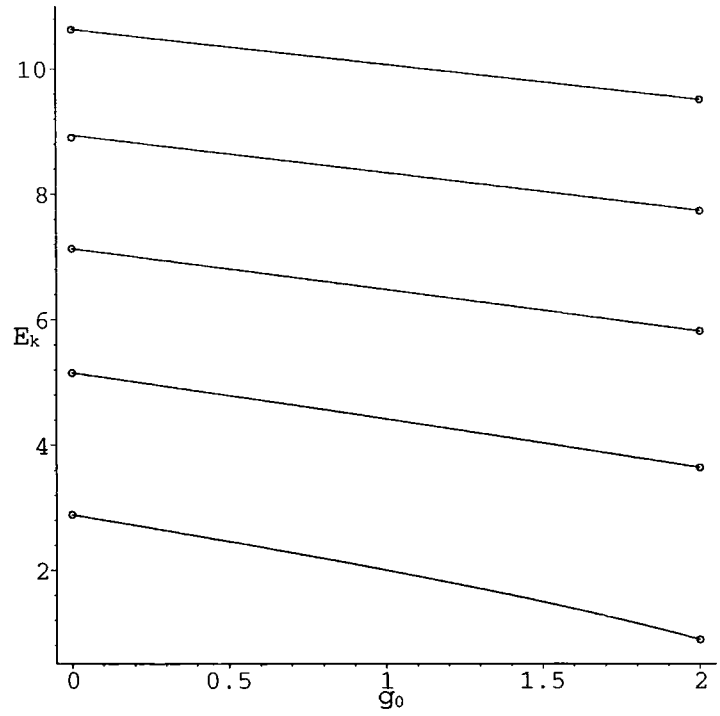

Figure 4.5: The movement of the first five zeros of of $1 + a^{(2)}(\theta)$ during the continuation $\hat{\mathbf{g}}_0$ to $\hat{\mathbf{g}}_2$. The circles denote the exact zeros.

where $\tilde{E} = -\frac{(M+1)^{nM}}{E^{M+1}}$. We now reverse the Langer transformation, so that (4.47) becomes

$$\Big((-1)^{n+1}D(\tilde{\mathbf{g}}) + P(x,\tilde{E})\Big)\tilde{y}(x) = 0\ , \qquad P(x,\tilde{E}) = -x^{-\frac{nM}{M+1}} - \tilde{E}\ . \tag{4.159}$$

where

$$\tilde{\mathbf{g}} = \{\tilde{g}_0, \tilde{g}_1, \ldots, \tilde{g}_{n-1}\}\ , \qquad \tilde{g}_i = \frac{g_i + M(n-1)/2}{M+1}\ . \tag{4.160}$$

(Observe that the property (4.45) is preserved by this transformation.) The solutions of the dual ODEs are explicitly related via

$$\tilde{y}(x,\tilde{E},\tilde{\mathbf{g}}) = (M+1)^{(1-n)/2}E^{(n-1)/2n}x^{(n-1)M/2(M+1)}\,y((M+1)E^{-1/n}x^{1/(M+1)},E,\mathbf{g})\ . \tag{4.161}$$

Thus the differential operator $D(\mathbf{g})$ transforms very simply under duality, and the treatment of the earlier sections also applies to a large class of further equations with M in the range $-1 < M < 0$.

4.4 Summary

In this chapter we have extended the correspondence between integrable quantum field theories and ordinary differential equations by considering a general n^{th} order ordinary differential equation. One of the main results was finding a neat way to encode the $n-1$ twists on the ODE side of the correspondence. This lead us naturally

to a generalisation of the $SU(2)$ $T-Q$ functional relation and the associated $SU(n)$ Bethe ansatz systems.

We derived nonlinear integral equations for the spectral problem of the basic solution $y(x, E, \mathbf{g})$. We also discussed how the twist parameters can be analytically continued so that the eigenvalues corresponding to other spectral problems can be found using the same NLIE. Our claims were backed up with some numerical evidence from two simple examples: the fourth and fifth-order ODEs with a linear potential.

Chapter 5

Outlook

Nonlinear integral equations of various kinds have been the main tool throughout this thesis. Initially such equations were used to study the finite-size effects of integrable quantum field theories, but as demonstrated in Chapter 4, they have more recently been employed in a new context related to eigenvalue problems of n^{th} order ordinary differential equations.

Extending the work on $SU(2)$ and $SU(3)$ we demonstrated the existence of an $SU(n)$ structure inside a certain set of n^{th} order ODEs. The result was a set of $n-1$ coupled nonlinear integral equations from which the eigenvalues of the ordinary differential equation were obtained. For $n = 2$ and $n = 3$ these equations are the ultraviolet limit of the NLIEs which describe finite-size effects in the massive sine-Gordon and ZMIK model respectively. The NLIEs found for larger values of n can also be related to perturbed conformal field theories [108, 109] , and in fact a relationship has been claimed with the affine Toda field theories with imaginary coupling constant [115]. One direction for future work is to implement some of the ideas in Chapter 3 for these A_n related systems. It would be interesting to see if the resulting 'massless' nonlinear integral equations also exhibit the nonmonotonic behaviour demonstrated by the equations related to $a_2^{(2)}$ and $a_1^{(1)}$. In addition, further study of the massless scattering theory for the A_2 related model, and beyond, is warranted since the corresponding S-matrices and spectrum are currently unknown. A further unsolved problem is to generalise the NLIEs to describe the excited state energies of these massless models, and the ideas contained in Chapter 2 may help towards this aim.

The correspondence between Bethe ansatz systems and ordinary differential equations has so far been studied for A_n. However this is not the only Lie algebra that has appeared naturally in the context of integrable systems; there are also the simply laced cases D_n, E_6, E_7 and E_8. The next step would be to extend the correspondence to include the integrable quantum field theories related to these algebras.

Chapter 2 demonstrated the ability of nonlinear integral equations, with suitable modifications, to also describe the excited states of integrable models. So far the NLIEs arising in connection with ordinary differential equations have always been those describing the ground state energy, but it seems likely that the excited state equations should also have partners on the ODE side.

The T and Q functions and the related functional equations underpin many of the results in this thesis and their further study is necessary if we wish to understand the underlying mathematical structures related to the integrability of models.

We hope to have shown in this thesis that the study of finite-size effects has a wide range of applications, and also provides tools to study areas of previously unrelated mathematics. We expect the interconnections will allow new links to be made and further mathematical structures studied.

Appendix A

Fourier conventions

Throughout this thesis we use the following conventions for the Fourier transform of a function $f(\theta)$:

$$\tilde{f}(k) = \mathcal{F}[f(\theta)] = \int_{-\infty}^{\infty} f(\theta)\, e^{-i\theta k}\, d\theta \tag{A.1}$$

with corresponding inverse

$$f(\theta) = \mathcal{F}^{-1}[\tilde{f}(k)] = \frac{1}{2\pi} \int_{-\infty}^{\infty} \tilde{f}(k)\, e^{i\theta k}\, dk\ . \tag{A.2}$$

In Chapters 1 and 4 we also need the following formulae

$$i\partial_\theta \ln \frac{\sinh(h\theta + i\pi\tau)}{\sinh(h\theta - i\pi\tau)} = \frac{2h\sin(2\pi\tau)}{\cosh(2h\theta) - \cos(2\pi\tau)} \tag{A.3}$$

and

$$\int \frac{d\theta}{2\pi} e^{-ik\theta} \frac{2h\sin(2\pi\tau)}{\cosh(2h\theta) - \cos(2\pi\tau)} = \frac{\sinh((1-2\tau)\frac{\pi k}{2h})}{\sinh(\frac{\pi k}{2h})}\ . \tag{A.4}$$

Appendix B

The sine-Gordon plots

In this appendix we plot the TBA functions for the sine-Gordon model with parameter $\xi = 2$ and $r = 0.01$. The axes are marked in units of $\pi/2$. The figures show contour plots of the functions $G_1(\theta) = |1 + X(\theta)|/(1 + |1 + X(\theta)|)$ and $G_2(\theta) = |1 + 2\cos\alpha\, Y(\theta) + Y^2(\theta)|/(1 + |1 + 2\cos\alpha\, Y(\theta) + Y^2(\theta)|)$ in the complex θ-plane; the concentric circles indicate the points at which $1 + X(\theta)$ and $1 + 2\cos\alpha\, Y(\theta) + Y^2(\theta)$ are equal to zero. The plots show the movement of the zeros as α varies from 0 to just greater than π. Figures 2.7 and 2.10 summarise the behaviour of the singularities which cross the integration contours.

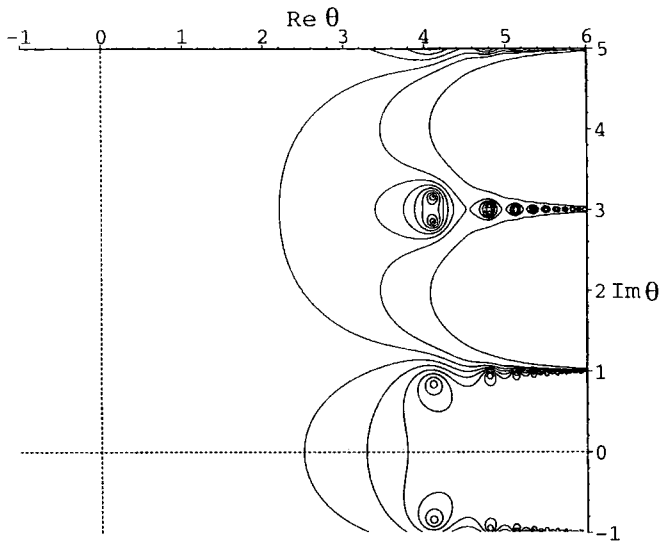

Figure B.1: $G_1(\theta, \alpha = 0)$

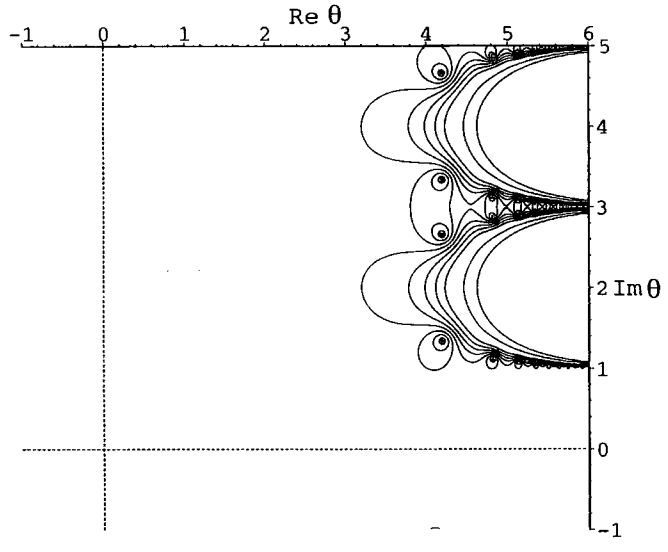

Figure B.2: $G_1(\theta, \alpha = 0.475\pi)$

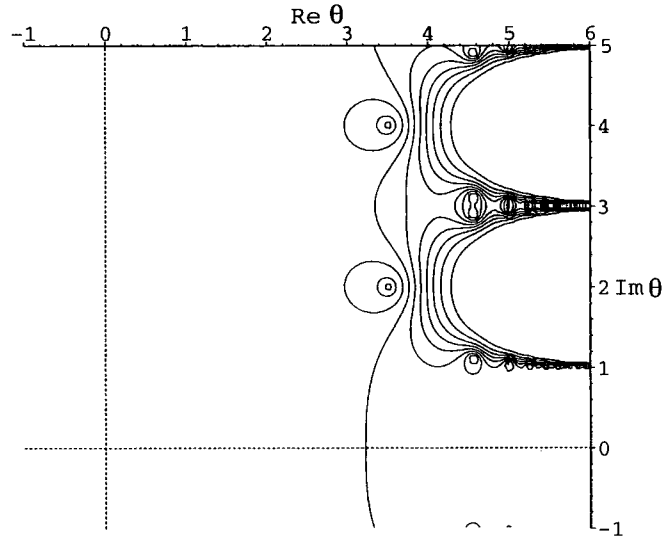

Figure B.3: $G_1(\theta, \alpha = 0.59\pi)$

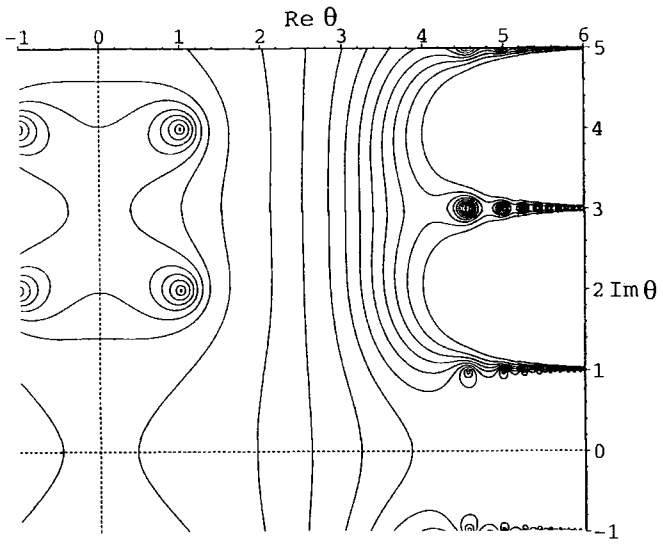

Figure B.4: $G_1(\theta, \alpha = 0.725\pi)$

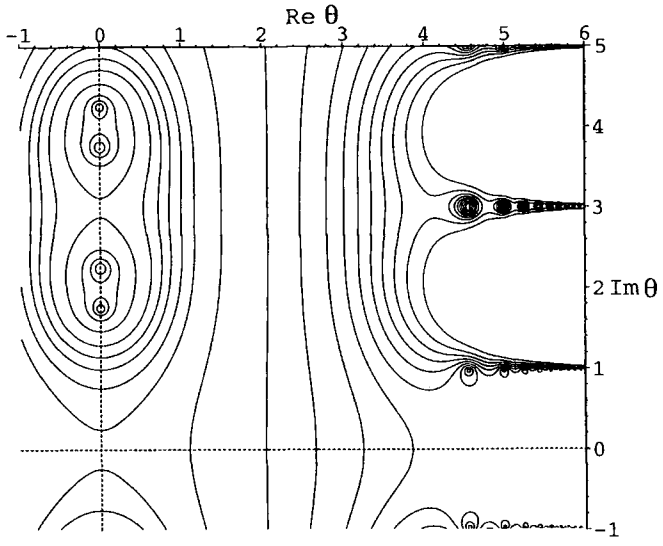

Figure B.5: $G_1(\theta, \alpha = 0.735\pi)$

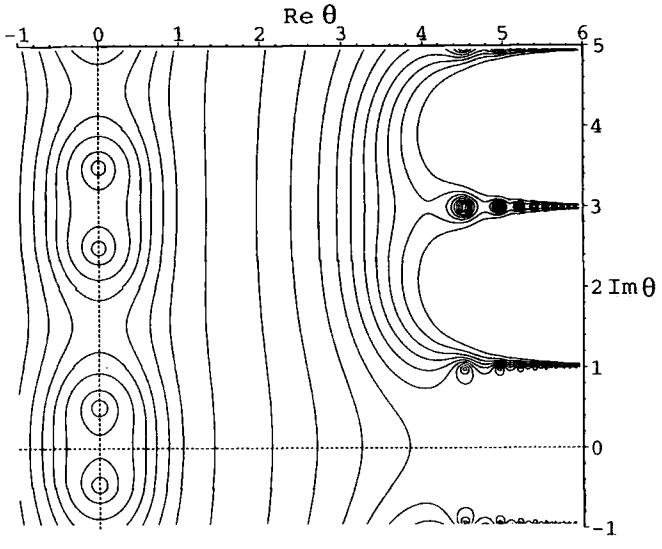

Figure B.6: $G_1(\theta, \alpha = 0.755\pi)$

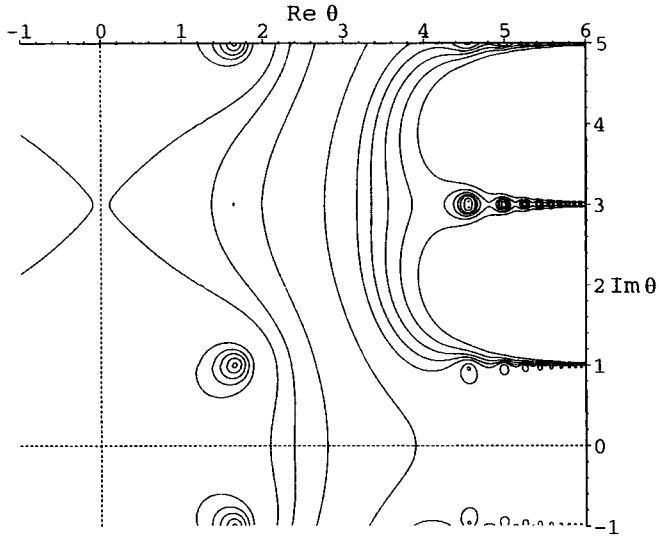

Figure B.7: $G_1(\theta, \alpha = 0.8\pi)$

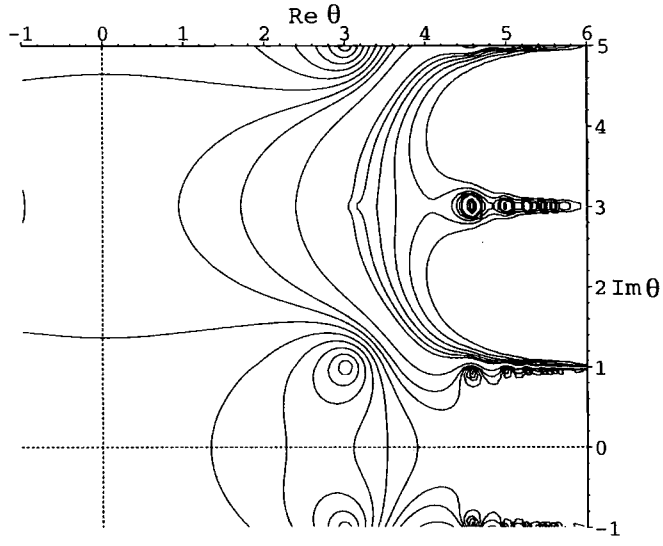

Figure B.8: $G_1(\theta, \alpha = 0.9995\pi)$

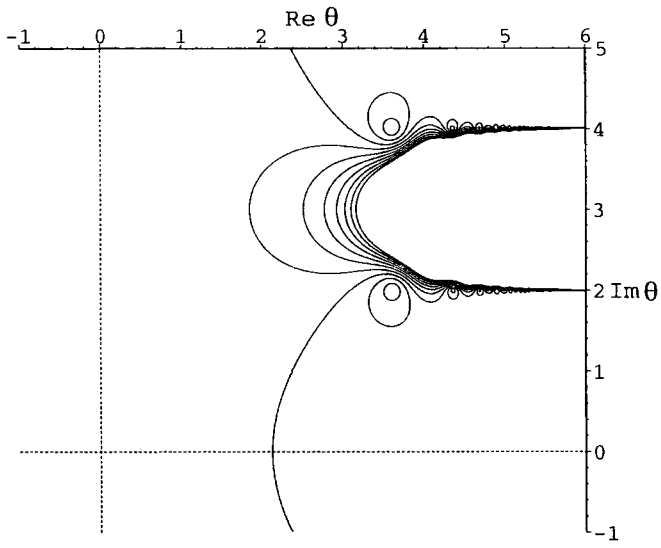

Figure B.9: $G_2(\theta, \alpha = 0.475\pi)$

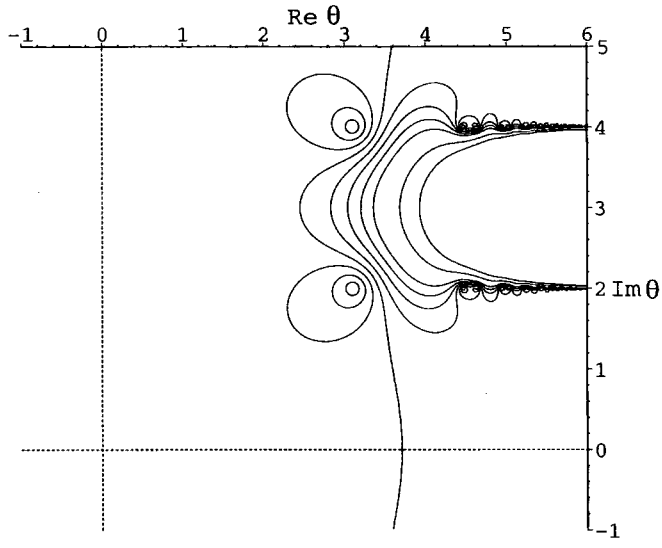

Figure B.10: $G_2(\theta, \alpha = 0.725\pi)$

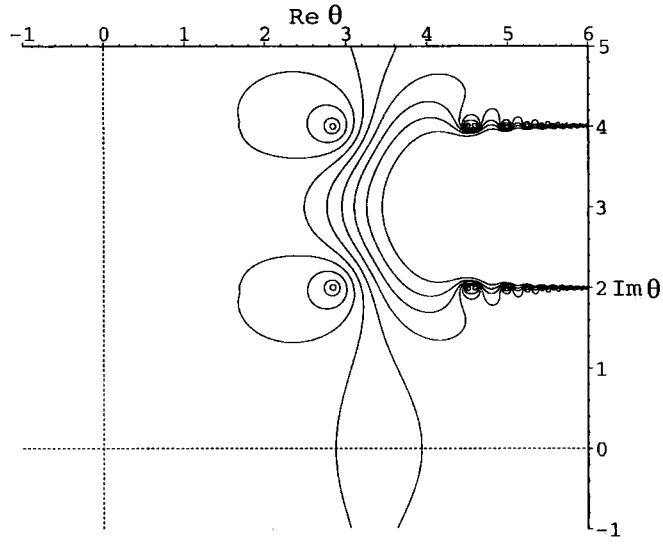

Figure B.11: $G_2(\theta, \alpha = 0.8\pi)$

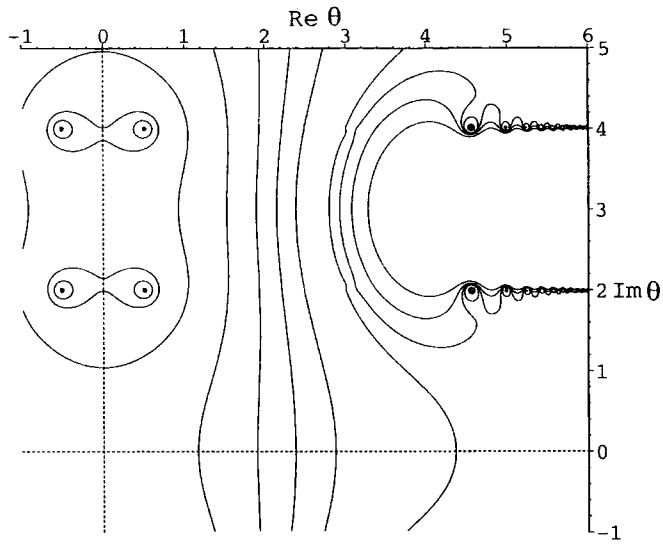

Figure B.12: $G_2(\theta, \alpha = 0.995\pi)$

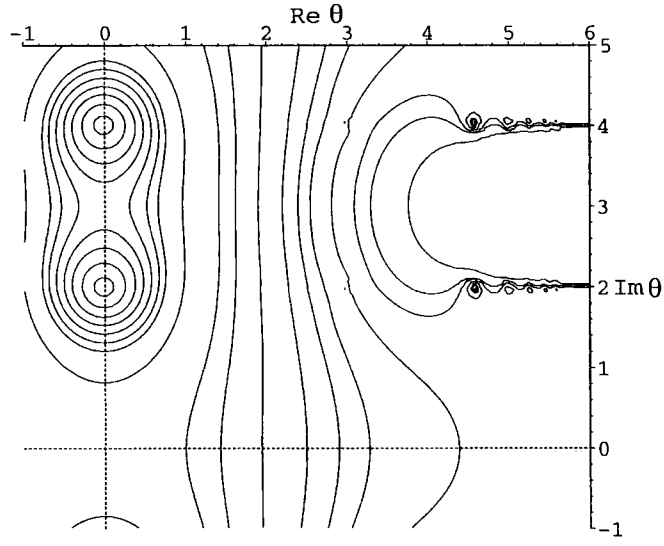

Figure B.13: $G_2(\theta, \alpha = 0.9995\pi)$

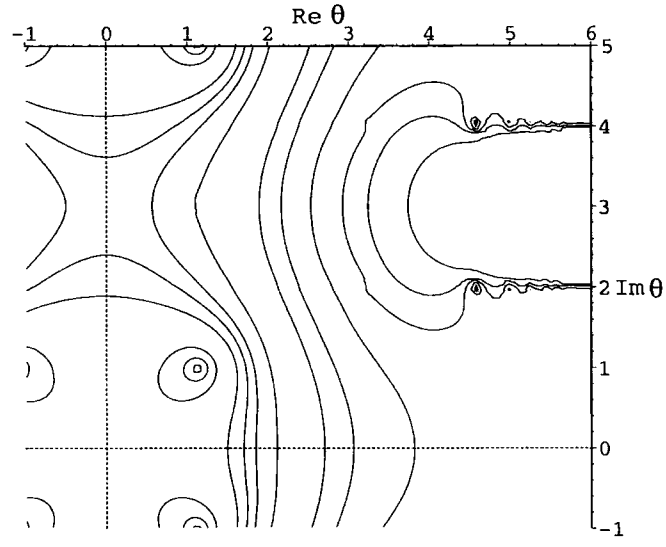

Figure B.14: $G_2(\theta, \alpha = 1.0025\pi)$

Appendix C

Numerical Results

The following tables compare the positions of the zeros of $\mathcal{A}(-x)$ and its derivatives found using three different methods. We calculate the exact solution from the formula (4.144) using Mathematica, numerically iterate the NLIE (4.96) and then search for the solutions of $1 + a^{(m)}(\theta) = 0$ for real θ, and finally we find the approximate positions using the saddle point formula (4.150). The tables present the results for the fourth and fifth order ODEs (4.47).

Table C.10 contains the eigenvalues of the fifth order differential equation (4.134) associated with the second node of the $SU(4)$ Dynkin diagram.

k	E_k (exact)	E_k (WKB)	E_k (NLIE)
1	3.590768483607046	3.54214	3.590768483607042
2	6.535508534650583	6.51720	6.535508534650583
3	9.184913585056730	9.17424	9.184913585056734
4	11.65605567904067	11.6487	11.65605567904068
5	14.00269367721830	13.9971	14.00269367721831
6	16.25488893482446	16.2505	16.25488893482445
7	18.43163123598472	18.4279	18.43163123598472
8	20.54591529506557	20.5428	20.54591529506559
9	22.60714755193681	22.6044	22.60714755193681

Table C.1: Zeros of $\mathcal{A}(-x)$ for $SU(4)$.

k	E_k (exact)	E_k (WKB)	E_k (NLIE)
1	2.643390050530237	2.70622	2.643390050530245
2	5.802227360903837	5.81222	5.802227360903833
3	8.525450780911227	8.53028	8.525450780911221
4	11.04042534551858	11.0434	11.04042534551857
5	13.41770040646422	13.4199	13.41770040646421
6	15.69318114446193	15.6948	15.69318114446193
7	17.88855933869047	17.8892	17.88855933869046
8	20.01829166137255	20.0194	20.01829166137254
9	22.09266066724255	22.0936	22.09266066724255

Table C.2: Zeros of $\mathcal{A}'(-x)$ for $SU(4)$.

k	E_k (exact)	E_k (WKB)	E_k (NLIE)
1	1.734075176483602	1.79839	1.734075176483640
2	5.063665746126293	5.08513	5.063665746126325
3	7.863342180451495	7.87391	7.863342180451512
4	10.42306919991221	10.2987	10.42306919991221
5	12.83144410688622	12.8363	12.83144410688622
6	15.13048659289235	15.1343	15.13048659289236
7	17.34468306388243	17.3477	17.34468306388243
8	19.48999241054207	19.4925	19.48999241054208
9	21.57759355396265	21.5798	21.57759355396267

Table C.3: Zeros of $\mathcal{A}''(-x)$ for $SU(4)$.

k	E_k (exact)	E_k (WKB)	E_k (NLIE)
1	0.854738972707337	0.74677	0.854738972707348
2	4.325536146898128	4.33093	4.325536146898143
3	7.199659112335162	7.20355	7.199659112335170
4	9.804415961378657	9.80708	9.804415961378663
5	12.24415079820764	12.2461	12.24415079820764
6	14.56694316777623	14.5685	14.56694316777623
7	16.80009457472668	16.8013	16.80009457472668
8	18.96108312777428	18.9621	18.9610831277743
9	21.06199506770279	21.0629	21.06199506770279

Table C.4: Zeros of $\mathcal{A}'''(-x)$ for $SU(4)$.

k	E_k (exact)	E_k (WKB)	E_k (NLIE)
1	4.361832679545867	4.30988	4.361832679545953
2	8.054407705768769	8.03320	8.054407705768822
3	11.43951647946485	11.4268	11.43951647946490
4	14.63562731810256	14.6268	14.63562731810260
5	17.69795469023313	17.6912	17.69795469023315
6	20.65781224235028	20.6525	20.65781224235030
7	23.53518630595816	23.5308	23.53518630595816
8	26.34386269731433	26.3401	26.34386269731434
9	29.09388489711714	29.0906	29.09388489711713

Table C.5: Zeros of $\mathcal{A}(-x)$ for $SU(5)$.

k	E_k (exact)	E_k (WKB)	E_k (NLIE)
1	3.456159834276373	3.49549	3.456159834276479
2	7.316474858986602	7.32207	7.316474858986646
3	10.76384671608901	10.7662	10.76384671608906
4	13.99753875066087	13.9989	13.99753875066089
5	17.08641174794345	17.0873	17.08641174794345
6	20.06660576373530	20.0673	20.06660576373532
7	22.96035975383073	22.9609	22.96035975383075
8	25.78268708279861	25.7831	25.78268708279861
9	28.54437115652793	28.5447	28.54437115652792

Table C.6: Zeros of $\mathcal{A}'(-x)$ for $SU(5)$.

k	E_k (exact)	E_k (WKB)	E_k (NLIE)
1	2.569521688226928	2.64079	2.569521688227008
2	6.576774353479521	6.59684	6.576774353479530
3	10.08711618336288	10.0974	10.08711618336288
4	13.35871947664098	13.3654	13.35871947664097
5	16.47431877918114	16.4792	16.47431877918111
6	19.47496173602145	19.4792	19.47496173602143
7	22.38517186820524	22.3883	22.38517186820521
8	25.22120493208898	25.2238	25.22120493208896
9	27.99459203505789	27.9968	27.99459203505786

Table C.7: Zeros of $\mathcal{A}''(-x)$ for $SU(5)$.

k	E_k (exact)	E_k (WKB)	E_k (NLIE)
1	1.699240579386870	1.72529	1.699240579387166
2	5.837067469655661	5.85528	5.837067469655795
3	9.409720072821775	9.41964	9.409720072821885
4	12.71933452235401	12.7259	12.71933452235413
5	15.86176468928719	15.8666	15.86176468928731
6	18.88293517925482	18.8867	18.88293517925492
7	21.80965981427642	21.8129	21.80965981427653
8	24.65944291301730	24.6621	24.65944291301738
9	27.44456753361847E	27.4470	27.44456753361854

Table C.8: Zeros of $\mathcal{A}'''(-x)$ for $SU(5)$.

k	E_k (exact)	E_k (WKB)	E_k (NLIE)
1	0.843270447809549	0.69065	0.843270447809785
2	5.098501785523339	5.09426	5.098501785523439
3	8.732036642256688	8.73196	8.732036642256784
4	12.07954735580031	12.0799	12.07954735580044
5	15.24883828837857	15.2492	15.24883828837869
6	18.29058121393539	18.2909	18.29058121393551
7	21.23386086711533	21.2342	21.23386086711542
8	24.09742778388938	24.0978	24.09742778388948
9	26.89431772359141	26.8946	26.89431772359146

Table C.9: Zeros of $\mathcal{A}''''(-x)$ for $SU(5)$.

k	E_k (exact)	E_k (NLIE)
1	3.094010291318771	3.094010291318791
2	5.226889777373171	5.226889777373144
3	7.209847266593714	7.209847266593725
4	9.066331743254636	9.066331743254635
5	10.83331896596270	10.83331896596270
6	12.53143797888895	12.53143797888896
7	14.17410051629643	14.17410051629643
8	15.77061699016209	15.77061699016210
9	17.32779194012912	17.32779194012914

Table C.10: Zeros of $\mathcal{A}(-x)$ for $SU(4)$ Second node.

Bibliography

[1] P.E. Dorey, C. Dunning, G. Takacs and F. Ravanini, 'Level crossing and spectral flow in the finite-volume Sine-Gordon model', In preparation.

[2] P. Dorey, C. Dunning and R. Tateo, 'New families of flows between two-dimensional conformal field theories', Nucl. Phys. B578 (2000) 699–727

[3] P. Dorey, C. Dunning and R. Tateo, 'Differential equations for general $SU(n)$ Bethe Ansatz systems', J. Phys. A33 (2000) 8427–8442 `hep-th/008039`

[4] P.E. Dorey, C. Dunning and R. Tateo, 'Ordinary Differential Equations and Integrable Models', JHEP Proceedings PRHEP-tmr 2000/034 Nonperturbative Quantum Effects 2000. `hep-th/0010148`

[5] J. Cardy, *Scaling and Renormalization in Statistical Physics*, (Cambridge University Press 1996)

[6] K.G. Wilson, 'Renormalization group and critical phenomena. 1. Renormalization group and the Kadanoff scaling picture', Phys. Rev. B4 (1971) 3174–3183

[7] A.M. Polyakov, 'Conformal symmetry of critical fluctuations', JETP Lett. 12 (1970) 381–383

[8] A.A. Belavin, A.M. Polyakov and A.B. Zamolodchikov, 'Infinite conformal symmetry in two-dimensional quantum field theory', Nucl. Phys. B241 (1984) 333–380

[9] P. Di Francesco, P. Mathieu and D. Sénéchal, 'Conformal Field Theory', (Springer 1998)

[10] H.W.J. Blöte, J.L. Cardy and M.P Nightingale, 'Conformal invariance, the central charge, and universal finite size amplitudes at criticality', Phys. Rev. Lett. 56 (1986) 742–745

[11] C. Itzykson, H. Saleur and J.B. Zuber, 'Conformal invariance of nonunitary two-dimensional models', Europhys. Lett. 2 (1986) 91–96

[12] A.B. Zamolodchikov, 'Integrable field theory from conformal field theory', Adv. Stud. in Pure Maths. 19 (1989) 641–674

[13] J.L. Cardy and G. Mussardo, 'S-matrix of the Yang-Lee Singularity in two dimensions', Phys. Lett B225 (1989) 275–278

[14] V.A. Fateev, 'The exact relations between the coupling constant and the masses of particles for the integrable perturbed conformal field theories', Phys. Lett. B234 (1994) 45–51

[15] S. Parke, 'Absence of particle production and factorization of the S-matrix in (1+1)-dimensional models', Nucl. Phys. B174 (1980) 166–185

[16] A.B. Zamolodchikov and Al.B. Zamolodchikov, 'Factorized S matrices in two dimensions as the exact solutions of certain relativitic field models', Ann. of Phys. 120 (1979) 253–291

[17] P.E. Dorey, 'Exact S-matrices', `hep-th/9810026`

[18] C.N. Yang and C.P. Yang, 'Thermodynamics of one-dimensional systems of bosons with repulsive delta funtion interaction', J. Math. Phys. 10 (1969) 1115–1122

[19] Al.B. Zamolodchikov, 'Thermodynamic Bethe Ansatz in relativistic models: Scaling 3-state Potts and Lee-Yang models', Nucl. Phys. B342 (1990) 695–720

[20] T.R. Klassen and E. Melzer, 'Purely elastic scattering theories and their ultraviolet limits', Nucl. Phys. B338 (1990) 485–528

[21] M.J. Martins, 'Scaling nonunitary models with degenerate ground state: thermodynamic Bethe ansatz approach', Phys. Lett. B257 (1991) 317–321

[22] P. Christe and M.J. Martins, 'Ultraviolet behaviour of the integrable off critical nonunitary series $M(3/Q)$', Mod. Phys. Lett A5 (1990) 2189–2195

[23] T.R. Klassen and E. Melzer, 'The thermodynamics of purely elastic scattering theories and conformal perturbation theory', Nucl. Phys. B350 (1991) 635–689

[24] A.E. Arinshtein, V.A. Fateev and Al.B. Zamolodchikov, 'Quantum S matrix of the (1+1)-dimensional Todd Chain', Phys. Lett. B76 (1979) 389–392

[25] H.W. Braden, E. Corrigan, P.E. Dorey and R. Sasaki, 'Affine Toda field theory and exact S-matrices', Nucl. Phys. B338 (1990) 689–746

[26] P. Christe and G. Mussardo, 'Integrable systems away from criticality: the Toda field theory and S matrix of the tricritical Ising model', Nucl. Phys. B330 (1990) 465

[27] Al.B. Zamolodchikov, 'On the thermodynamic Bethe ansatz equations for the reflectionless ADE scattering theories', Phys. Lett. B253 (1991) 391–394

[28] R.F. Dashen, B. Hasslacher, and A. Neveu, 'The particle spectrum in model field theories from semiclassical functional integral techniques', Phys. Rev. D11 (1975) 3242–3450

[29] M. Takahashi and M. Suzuki, 'One-dimensional anisotropic Heisenberg model at finite temperature', Prog. Theor. Phys. 48 (1972) 2187–2209

[30] R. Tateo, 'The sine-Gordon model as $\frac{SO(n)_1 \times SO(n)_1}{SO(n)_2}$ perturbed coset theory and genrelizations', Int. J. Mod. Phys. A10 (1995) 1357–1376

[31] R. Tateo, 'New functional dilogarithm identities and sine-Gordon Y-systems', Phys. Lett. B355 (1995) 157–164

[32] V.A. Fateev and Al.B. Zamolodchikov, 'Integrable perturbations of $\mathbb{Z}_N$ parafermion models and the $O(3)$ sigma model', Phys. Lett. B271 (1991) 91–100

[33] P. Fendley and H. Saleur, '$N = 2$ Supersymmetry, Painleve III and exact scaling functions in 2D polymers', Nucl. Phys. B388 (1992) 609–626

[34] C. Destri and H.J. de Vega, 'New thermodynamic Bethe ansatz equations without strings', Phys. Rev. Lett. 69 (1992) 2313–2317;
— 'Unified approach to thermodynamic Bethe ansatz and finite size corrections for lattice models and field theories', Nucl. Phys. B438 (1995) 413–454

[35] A. Klümper, M.T. Batchelor and P.A. Pearce, 'Central charges of the 6- and 19-vertex models with twisted boundary conditions', J. Phys. A24 (1991) 3111–3133

[36] R. Baxter, *Exactly solved models in statistical mechanics* (Academic Press 1982)

[37] V.V. Bazhanov, S.L. Lukyanov and A.B. Zamolodchikov, 'Integrable Structure of Conformal Field Theory, Quantum KdV Theory and Thermodynamic Bethe Ansatz', Commun. Math. Phys. 177 (1996) 381–398

[38] V.V. Bazhanov, S.L. Lukyanov and A.B. Zamolodchikov, 'Integrable Structure of Conformal Field Theory 2. Q-operator and DDV equation', Commun. Math. Phys. 190 (1997) 247–278

[39] V.V. Bazhanov, S.L. Lukyanov and A.B. Zamolodchikov, 'Integrable Quantum Field theories in finite volume: Excited state energies', Nucl. Phys. B489 (1997) 487–531

[40] B.L. Feigin and D.B. Fuchs, 'Representations of the Virasoro algebra', Topology. Proceedings, Leningrad 1982 Eds (L.D. Fadeev and A.A. Mal'cev).

[41] V.V. Bazhanov, S.L. Lukyanov and A.B. Zamolodchikov, 'Integrable Structure of Conformal Field Theory 3. The Yang-Baxter relation', Commun. Math. Phys. 200 (1999) 297–324

[42] E.C. Titchmarsh, 'The theory of functions', (OUP 1932)

[43] A.B. Zamolodchikov, 'Renormalization group and perturbation theory about fixed points in two-dimensional field theory', Sov. J. Nucl. Phys. 46 (1987) 1090–1096

[44] A.W.W. Ludwig and J.L. Cardy, 'Perturbative evaluation of the conformal anomaly at new critical points with application to random systems', Nucl. Phys. B285 (1987) 687–718

[45] Al.B. Zamolodchikov, 'From tricritical Ising to critical Ising by Thermodynamic Bethe Ansatz', Nucl. Phys. B358 (1991) 524–546

[46] M. Lässig, 'New hierarchies of multicriticality in two-dimensional field theory', Phys. Lett. B278 (1992) 439–442

[47] C. Ahn, 'RG flows of non-unitary minimal CFTs', Phys. Lett. B294 (1992) 204–208

[48] F.A. Smirnov, 'Reductions of the sine-Gordon model as a perturbation of minimal models of conformal field theory', Nucl. Phys. B337 (1990) 156–180

[49] A. LeClair, 'Restricted sine-Gordon theory and the minimal conformal series', Phys. Lett. B230 (1989) 103–107

[50] D. Fioravanti, A. Mariottini, E. Quattrini and F. Ravanini, 'Excited state Destri-De Vega equation for sine-Gordon and restricted sine-Gordon models', Phys. Lett. B390 (1997) 243–251, `hep-th/96080911`

[51] P. Fendley, H. Saleur and Al.B. Zamolodchikov, 'Massless flows I: the sine-Gordon and $O(n)$ models', Int. J. Mod. Phys. A8 (1993) 5717–5750, `hep-th/9304050`

[52] Al.B. Zamolodchikov, 'Thermodynamics of imaginary coupled sine-Gordon. Dense polymer finite-size scaling function', Phys. Lett. B335 (1994) 436–443

[53] Al.B. Zamolodchikov, 'TBA equations for integrable perturbed $SU(2)_k \times SU(2)_l/SU(2)_{k+l}$ coset models', Nucl. Phys. B366 (1991) 122–132

[54] T.R. Klassen and E. Melzer, 'Spectral flow between conformal field theories in 1+1 dimensions', Nucl. Phys. B370 (1992) 511–550

[55] M.J. Martins, 'The thermodynamic Bethe ansatz for deformed WA_{N-1} conformal field theories', Phys. Lett. B277 (1992) 301–305

[56] F. Ravanini, 'Thermodynamic Bethe ansatz for $G_k \times G_l/G_{k+l}$ coset models perturbed by their $\phi_{1,1,adj}$ operator', Phys. Lett. B282 (1992) 73–79

[57] M.J. Martins, 'Renormalization group trajectories from resonance factorized S matrices', Phys. Rev. Lett. 69 (1992) 2461–2464, hep-th/9205024;
— 'Exact resonance A-D-E S-matrices and their renormalization group trajectories', Nucl. Phys. B394 (1993) 339–355

[58] F. Ravanini, R. Tateo and A. Valleriani, 'Dynkin TBAs', Int. J. Mod. Phys. A8 (1993) 1707–1727

[59] V.A. Fateev, E. Onofri and Al.B. Zamolodchikov, 'Integrable deformations of the $O(3)$ sigma model. The sausage model', Nucl. Phys. B406 (1993) 521–565

[60] P. Fendley and K. Intriligator, 'Exact N=2 Landau-Ginzburg flows', Nucl. Phys. B413 (1994) 653–674

[61] F. Ravanini, M. Stanishkov and R. Tateo, 'Integrable perturbations of CFT with complex parameter: The $\mathcal{M}_{3/5}$ model and its generalizations', Int. J. Mod. Phys. A11 (1996) 677–698

[62] G. Feverati, E. Quattrini and F. Ravanini, 'Infrared behaviour of massless integrable flows entering the minimal models from ϕ_{31}', Phys. lett. B374 (1996) 64–70, hep-th/9512104

[63] P. Dorey, R. Tateo and K.E. Thompson, 'Massive and massless phases in self-dual $\mathbb{Z}_N$ spin models: some exact results from the thermodynamic Bethe ansatz', Nucl. Phys. B470 (1996) 317–368, hep-th/9601123

[64] R. Tateo, 'The sine-Gordon model as $SO(N)_1 \times SO(N)_1/SO(N)_2$ perturbed coset theory and generalisation', Int. J. Mod. Phys. A10 (1995) 1357–1376

[65] P. Dorey and R. Tateo, 'Excited states by analytic continuation of TBA equations', Nucl. Phys B482 (1996) 639–659

[66] C.M. Bender and T.T. Wu, Anharmonic oscillator', Phys. Rev 194 (1969) 1231–1260

[67] P. Dorey and R. Tateo, 'Excited states in some simple perturbed conformal field theories', Nucl. Phys. B515 (1998) 575–623

[68] V.P. Yurov and A.B. Zamolodchikov, 'Truncated conformal space approach to scaling Lee-Yang model', Int. J. Mod. Phys. A5 (1990) 3221–3246

[69] Al.B. Zamolodchikov, 'Mass scale in the sine-Gordon model and its reductions', Int. J. Mod. Phys. A10 (1995) 1125–1150

[70] P. Fendley, 'Excited-state energies and supersymmetric indices', Adv. Theor. Math. Phys. (1998) 210–236

[71] A. Klümper and P.A. Pearce, 'Analytical calculations of Scaling Dimensions: Tricritical Hard Square and Critical Hard Hexagons', J. Stat. Phys. 64 (1991) 13–76;;

— 'Conformal weights of RSOS lattice models and their fusion hierachies', J. Phys. A183 (1992) 304–350

[72] C. Destri and H.J. de Vega, 'Nonlinear integral equation and excited states scaling functions in the sine-Gordon model', Nucl. Phys. B504 (1997) 621–664

[73] G. Feverati, F. Ravanini and G. Takacs, 'Truncated Conformal Space at $c = 1$, Nonlinear Integral Equation and Quantisation Rules for Multi-Soliton States', Phys. Lett. B430 (1998) 264–273

[74] G. Feverati, F. Ravanini and G. Takacs, 'Nonlinear Integral Equation and Finite Volume Spectrum of Sine-Gordon Theory', Nucl. Phys. B540 (1999) 543–586

[75] G. Feverati, F. Ravanini and G. Takacs, 'Scaling functions in the odd charge sector of sine-Gordon/massive Thirring theory', Phys. Lett. B444 (1998) 442–450

[76] G. Feverati, F. Ravanini and G. Takacs, 'Nonlinear integral equation and finite volume spectrum of minimal models perturbed by $\phi_{1,3}$', Nucl. Phys. B570 (2000) 615–643, `hep-th/9909031`

[77] P.E. Dorey, 'The exact S-matrix of affine Toda field theories', *Degree Thesis, Durham 1990*

[78] P. Dorey and R. Tateo, 'Differential equations and integrable models: the $SU(3)$ case', Nucl. Phys. B571 (2000) 583–606, `hep-th/9910102`

[79] P. Fendley, H. Saleur and Al.B. Zamolodchikov, 'Massless flows II: the exact S-matrix approach', Int. J. Mod. Phys. A8 (1993) 5751–5778, `hep-th/9304051`

[80] H. Saleur and S. Skorik, 'Solution of the Thirring model with imaginary mass and massless scattering', Phys. Lett. B336 (1994) 205–212

[81] F.A. Smirnov, 'Exact S-matrices for ϕ_{12}-Perturbated minimal models of conformal field theory', Int. J. Mod. Phys. A6 (1991) 1407–1428

[82] M.J. Martins, 'Constructing an S matrix from the truncated conformal approach data', Phys. Lett. B262 (1991) 39–44

[83] G. Takacs, 'A new RSOS restriction of the Zhiber-Mikhailov-Shabat model and $\Phi_{(1,5)}$ perturbations of nonunitary minimal models', Nucl. Phys. B489 (1997) 532–556, `hep-th/9604098`

[84] H. Kausch, G. Takacs and G. Watts, 'On the relation between $\phi_{(1,2)}$ and $\phi_{(1,5)}$ perturbed minimal models', Nucl. Phys. B489 (1997) 557–579, hep-th/9605104

[85] Al.B. Zamolodchikov, 'Thermodynamic Bethe Ansatz for RSOS scattering theories', Nucl. Phys. B358 (1991) 497–523

[86] D.A. Huse and M.E. Fisher, 'The decoupling point of the axial next-nearest-neighbour Ising model and marginal crossover', J. Phys. C15 (1982) L585–595

[87] J.L. Cardy and G. Mussardo, 'Universal properties of self-avoiding walks from two-dimensional field theory', Nucl. Phys. B410 (1993) 451–493, hep-th/9306028

[88] V. Fateev, S. Lukyanov, Al.B. Zamolodchikov and A.B. Zamolodchikov, 'Expectation values of local fields in Bullough-Dodd model and integrable perturbed conformal field theories', Nucl. Phys. B516 (1998) 652–674

[89] Vl.S. Dotsenko and V.A. Fateev, 'Operator algebra of two-dimensional conformal theories with central charge $c \leq 1$', Phys. Lett. B154 (1985) 291–295

[90] A.B. Zamolodchikov, ' "Irreversibility" of the flux of the renormalization group in a 2-D field theory', JETP Lett. 43 (1986) 730–732

[91] E. Melzer, 'Supersymmetric analogs of the Gordon-Andrews identities, and related TBA systems', hep-th/9412154

[92] P. Dorey, 'Root systems and purely elastic S-matrices', Nucl. Phys. B358 (1991) 654–676

[93] C. Ahn and S. Nam, 'Thermodynamic Bethe ansatz equations for perturbed minimal conformal field theories', Phys. Lett. B271 (1991) 329–336

[94] Al.B. Zamolodchikov, private communication

[95] S. O. Warnaar, 'Refined q-trinomial coefficients and character identities', math.QA/0005123

[96] P. Dorey and R. Tateo, 'Anharmonic oscillators, the thermodynamic Bethe ansatz and nonlinear integral equations', J. Phys. A32 (1999) L419–L425

[97] V.V. Bazhanov, S.L. Lukyanov and A.B. Zamolodchikov, 'Spectral determinants for Schrödinger equation and Q-operators of Conformal Field Theory', hep-th/9812247

[98] J. Suzuki, 'Anharmonic Oscillators, Spectral Determinant and Short Exact Sequence of $U_q(\widehat{sl}_2)$', J. Phys. A32 (1999) L183–L188

[99] P. Dorey and R. Tateo, 'On the relation between Stokes multipliers and the $T-Q$ system of conformal field theory', Nucl. Phys. B563 (1999) 573–602

[100] J. Suzuki, 'Functional relations in Stokes multipliers and Solvable Models related to $U_q(A_n^{(1)})$', J. Phys. A33 (2000) 3507–3522 quant-ph/0003066

[101] J. Suzuki, 'Stokes multipliers, Spectral Determinants and $T-Q$ relations', nlin-sys/0009006

[102] A. Voros, 'Spectral Zeta Functions', Adv. Stud. Pure Math. 21 (1992) 327–358

[103] A. Voros, 'Exact quantisation condition for anharmonic oscillators (in one dimension)', J. Phys. A27 (1994) 4653–4661

[104] P.-F. Hsieh and Y. Sibuya, 'On the asymptotic integration of second order linear ordinary differential equations with polynomial coefficients', J. Math. Analysis and Applications 16 (1966) 84–103;
— Y. Sibuya, *Global Theory of a second-order linear ordinary differential operator with polynomial coefficient*, (Amsterdam: North-Holland 1975)

[105] Earl A. Coddington and Norman Levinson, *Theory of Ordinary Differential Equations*, (McGraw-Hill 1955)

[106] J. Harris, *Algebraic Geometry*, (Springer-Verlag 1992)

[107] I. Krichiver, O. Lipan, P. Wiegmann and A. Zabrodin, 'Quantum Integrable Models and Discrete Classical Hirota Equations', Commun. Math. Phys. 199 (1997) 267–304, hep-th/9604080

[108] A. Mariottini, 'Ansatz di Bethe termodinamico ed equazione di Destri-de Vega in teorie di campo bidimensionali', *Degree thesis (in Italian), Bologna March 1996*

[109] P. Zinn-Justin, 'Nonlinear integral equations for complex Affine Toda models associated to simply laced Lie algebras', J. Phys. A31 (1998) 6747–6770

[110] C. Destri and H.J. de Vega, 'New approach to thermal Bethe ansatz', hep-th/9203064

[111] G.D. Birkhoff, 'On the solutions of ordinary linear homogeneous differential equations of the third order', Ann. Math. 12 (1910-11) 103–127

[112] G. Frobenius, Crelle (Journal fur die reine und angewandte Mathematik) Vol 77 (1874), 248

[113] M. Bôcher, 'On Wronskians of functions of a real variable', Bull. AMS Vol VIII, October 1901, 53–63

[114] R.E. Langer, 'On the connection formulas and the solutions of the wave equation', Phys. Rev. 51 (1937) 669–676

[115] T.J. Hollowood and P. Mansfield, 'Rational conformal field theories at, and away from, criticality as Toda field theories', Phys. Lett. B226 (1989) 73–79